Budapest University of Technology and Economics

Department of Networked Systems and Services
Laboratory of Acoustics and Studio Technologies

PhD Thesis

A Unified Wave Field Synthesis Framework

with Application for Moving Virtual Sources

Gergely Firtha

September 26, 2018

Gergely Firtha

A Unified Wave Field Synthesis Framework
with Application for Moving Virtual Sources

PhD Thesis, September 26, 2018
Supervisor: Péter Fiala

Budapest University of Technology and Economics
Laboratory of Acoustics and Studio Technologies
Department of Networked Systems and Services
Magyar Tudósok körútja 2.
1117 and Budapest

Contents

Nomenclature

$\mathbf{x}$	Position vector in Descartes coordinates: $\mathbf{x} = [x,\ y,\ z]^{\mathrm{T}}$
$\mathbf{v}$	General 3D vector in Descartes coordinates: $\mathbf{v} = [v_x,\ v_y,\ v_z]^{\mathrm{T}}$
$\lvert\mathbf{v}\rvert$	Length, or l^2 norm of vector: $\lvert\mathbf{v}\rvert = \sqrt{\sum_i v_i^2}$
$\hat{\mathbf{v}}$	Normalized vector, with unit length pointing into the direction of $\mathbf{v}$: $\hat{\mathbf{v}} = \frac{\mathbf{v}}{\lvert\mathbf{v}\rvert}$.
$\langle\mathbf{u}\cdot\mathbf{v}\rangle$	Inner product of vectors $\mathbf{u}$ and $\mathbf{v}$: $\langle\mathbf{u}\cdot\mathbf{v}\rangle = \sum_i u_i \cdot v_i = \mathbf{u}^{\mathrm{T}}\mathbf{v}$
$\mathbf{n}$	Normal vector of a surface, or contour
$\frac{\partial}{\partial x_i}$	Partial derivative of a function with respect variable x_i
$\frac{\mathrm{d}}{\mathrm{d}x_i}$	Total derivative of a function with respect argument x_i
$\nabla_{\mathbf{x}}$	Gradient operator. In Descartes-coordinates: $\nabla_{\mathbf{x}} f = \frac{\partial f}{\partial x}\mathbf{e}_x + \frac{\partial f}{\partial y}\cdot\mathbf{e}_y + \frac{\partial f}{\partial z}\cdot\mathbf{e}_z$, with $\mathbf{e}_{x,y,z}$ being unit vectors into x, y, z directions
$\nabla_{\mathbf{x}}\cdot$	Divergence operator. In Descartes-coordinates: $\nabla_{\mathbf{x}}\cdot f = \frac{\partial f}{\partial x} + \frac{\partial f}{\partial y} + \frac{\partial f}{\partial z}$
$\nabla^2_{\mathbf{x}}$	Laplacian operator. In Descartes-coordinates: $\nabla^2_{\mathbf{x}} f = \frac{\partial^2 f}{\partial x^2} + \frac{\partial^2 f}{\partial y^2} + \frac{\partial^2 f}{\partial z^2}$
$\frac{\partial}{\partial\mathbf{v}}$	Directional derivative of a function into the direction of vector $\mathbf{v}$: $\frac{\partial}{\partial\mathbf{v}} f = \langle\nabla_{\mathbf{x}} f\cdot\mathbf{v}\rangle$
$f'_{x_i}(\mathbf{x}_0)$	Shorthand for the partial derivative of function $f(\mathbf{x})$ with respect to variable x_i, taken at the evaluation point $\mathbf{x}_0$: $f'_{x_i}(\mathbf{x}_0) = \frac{\partial}{\partial x_i} f(\mathbf{x})\Big\rvert_{\mathbf{x}=\mathbf{x}_0}$
$f''_{x_i,x_j}(\mathbf{x}_0)$	Shorthand for the second partial derivative of function $f(\mathbf{x})$ with respect to variables x_i, x_j, taken at the evaluation point $\mathbf{x}_0$: $f''_{x_i,x_j}(\mathbf{x}_0) = \frac{\partial^2}{\partial x_i \partial x_j} f(\mathbf{x})\Big\rvert_{\mathbf{x}=\mathbf{x}_0}$
$\mathcal{F}_x\{\}$	Fourier transform of a function with respect to variable x
$\mathcal{F}^{-1}_{k_x}\{\}$	Inverse Fourier transform of a function with respect to variable k_x
$*_x$	Convolution of functions w.r.t. variable x: $f *_x g = \int_{-\infty}^{\infty} f(x - x_0) g(x_0)\mathrm{d}x_0$.

1 Introduction

1.1 Overview of spatial audio techniques

Spatial audio aims at the recreation of a sound scene containing sources of sound, termed as audio objects, in a sense that the human listener perceives the spatial characteristics of the desired acoustic environment [Zha+17]. *Sound field reproduction* achieves this by driving an arrangement of fix positioned loudspeakers, so that the superposition of the sound waves emerging from the individual loudspeakers generate the impression of the desired virtual audio object, present in the sound scene. Alternatively *binaural rendering* applies a headphone for the reproduction of localization cues for the human auditory system directly at the ears of the listener. These cues are triggered by the head-related transfer function (HRTF) including the interaural time and level differences (ITD and ILD), due the anthropometry of the listener, dynamic cues due to the movement of the listener's head and several environment scattering cues, which all are combined by the human brain, generating the perceived spatial impression [Bla83].

The present thesis considers only spatial audio by loudspeakers. In this case the general aim is the derivation of loudspeaker driving signals from a given source excitation signal in a manner that the reproduced field exhibits prescribed spatial characteristics, e.g. a specific apparent direction of arrival, or a prescribed apparent source width. In the following first a short overview is given on the different sound field reproduction approaches, classified according to the basic goal of reproduction.

Stereophony: Sound field reproduction has been the subject of excessive study and development over the second half of the XX. century, starting with the work of Blumlein, who introduced the first two-loudspeaker system in 1931 (along with the related recording, transmission and playback methodology) and thereby creating the basics of *stereophony* [Blu32; Ale00]. Blumlein's invention was first put to practice in the 1950's, and since then stereophony has risen to a huge commercial success. Modern stereophonic systems include the well-known Dolby stereo, 5.1, 7.1 systems, the 22.2 system of the NHK [Ham+05; Ham+11] or the currently state-of-the-art commercial spatial audio systems, the Dolby Atmos [Atm] and the DTS-X. While the first three systems ensured only 2D sound reproduction in the horizontal plane containing the listener's ears, recent systems introduced height information as well by adding height channels to the reproduction loudspeaker layout.

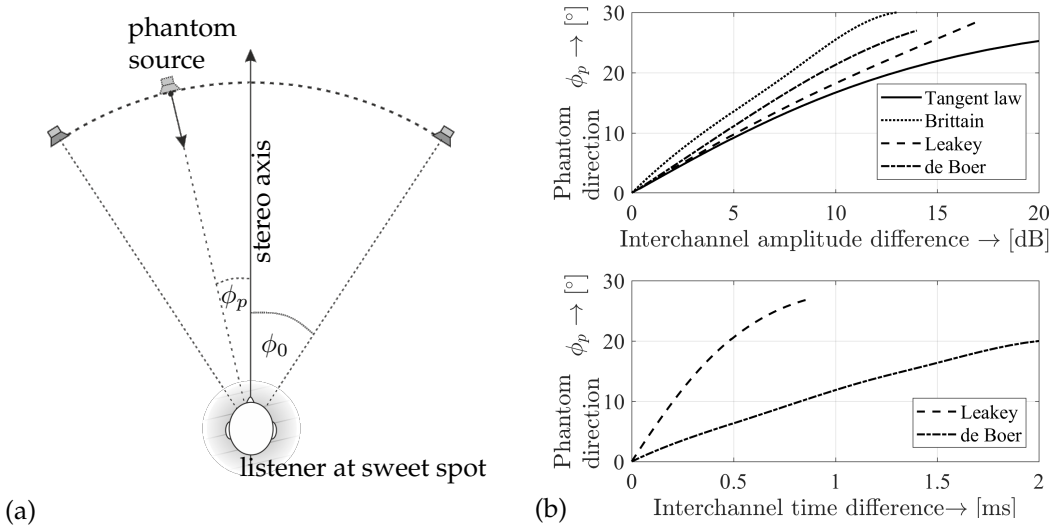

Figure 1.1. Typical two-channel stereophonic loudspeaker geometry (a) and exemplary interchannel amplitude and time differences (b) for the panning of the phantom source to be localized from the angular direction ϕ_p. The data are experimental results, as published by de Boer [Boe40] (measured for male speech signal), Brittain and Leakey (measured for speech signal, limited to 5 kHz) [BL56] and Leakey [Lea60] (measured for wide-band speech signal), while tangent law is a physical based analytically given curve.

Generally speaking—independently from the number of the speakers applied—stereophony generates the desired spatial impression by the recreation of some of the above localization cues at the listener position. Correct localization therefore can be ensured only over a limited listening area, termed as the *sweet spot*, being a central limitation of these techniques. Increasing the number of the loudspeakers allows only for a more precise reproduction of the target fields's spatial attributes (e.g. for a more accurate localization).

The source of the stereophonic signals may be either a recording of the sound scene to be reproduced, captured by a suitable microphone array [Lip85; WD99; WT17], or the signal of the audio objects present in the virtual sound scene, distributed among the loudspeakers applied for reproduction.

The latter approach requires an appropriate *panning law*, describing how the individual loudspeaker signals are obtained from the object source signal, ensuring that in the reproduced field the given audio object is perceived by the listener with desired spatial characteristics (e.g. object position, apparent width, etc.) [Pul01a; Pul01b]. Traditional stereophonic panning techniques included applying either interchannel intensity difference or time delay between the signals of the loudspeakers. These techniques are commonly referred to as *intensity stereophony/amplitude panning* and *time-based stereophony* respectively. Ultimately both approaches control the apparent virtual audio object's position by adjusting the interaural time difference between the listener's ears (meaning that even amplitude difference between the loudspeaker signals is converted to time difference at the ears).

Originally both interchannel amplitude and time differences, ensuring correct localization were defined based on experimental data [Boe40; BL56; Lip85; HW97; Rum01]. Later the physically motivated *sine law* [Bau61; RS07] and the *tangent law of panning*[Ben+85; RS07] emerged for the derivation of the required loudspeaker

gains, based on an analytical model of stereophonic reproduction. The latter one is discussed within the context of the introduced theoretical framework in the present thesis. Amplitude panning was extended towards 3D spatial audio by Vector Base Amplitude Panning (VBAP) introduced by Pulkki [Pul97], allowing the positioning of phantom/virtual sources in the 3D space by distributing its excitation signal between loudspeaker triplets [1].

Ambisonics: As an alternative for stereophony the theory of Ambisonics was introduced by Gerzon in the 1970's, proposing both a novel recording and reproduction system [Ger73] and later elaborating an objective evaluation methodology for Ambisonic type sound systems [Ger92]. Being an intermediate approach between stereophony and sound field synthesis, traditional Ambisonics aims at the reproduction of physical properties of a sound field in the proximity of a fixed listening position.

Generally speaking Ambisonics represents a sound field in terms of its orthogonal decomposition over a sphere, so that the sound scene to be reproduced is described and stored as coefficients of the orthogonal basis functions. The orthogonal basis for Ambisonics is given by the set of spherical harmonics. The so-called encoding step of Ambisonics format is therefore the decomposition of the sound field to be reproduced into a series of spherical harmonics up to a given order N, with the order defining the spatial resolution, and the size of the receiver zone for the representation [Ger85]. Ambisonics signals hence are time histories belonging to given spherical harmonic shapes.

Traditional Ambisonics considered only spherical harmonics up to the first order ($N = 1$) [Ger75], while modern microphone array designs allow the capturing of the sound field to be reproduced at a higher resolution with the technique termed as Higher Order Ambisonics (HOA, $N \geq 2$) [AW02; ME02; AG10]. Similarly to stereophony, besides measuring the target sound field at a predefined listener position, Ambisonics allows the rendering of virtual audio objects defined by a physical model: once a model for the spatial characteristics of the virtual audio object is available, spherical harmonic decomposition may be performed analytically resulting in Ambisonics coefficients up to an arbitrary order [AS08b; Ahr10].

Finally, at the reproduction, or decoding stage the loudspeaker signals for the actual loudspeaker layout are decoded from the spherical harmonics coefficients following some suitable decoding strategy [Dan00; Dan+03; Zot+12; ZF12]. Applying a decoding strategy that takes the actual reproduction loudspeaker characteristics into consideration is termed as Near-Field Compensated Higher Order Ambisonics (NFC-HOA) [Dan03].

Sound field synthesis: An important property of spherical harmonic decomposition of a given sound field around a fixed point is that increasing the decomposition order increases the area/volume at which the sound field is represented correctly, overcoming the sweet spot limitation of stereophony. This fact adumbrates the motiva-

[1] VBAP can be applied for loudspeaker pairs as well, in which case the formulation is equivalent with the tangent law of stereophony.

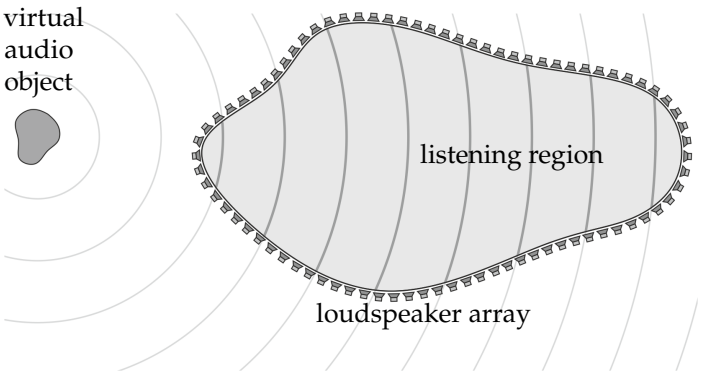

Figure 1.2. The general geometry for sound field synthesis: the goal of synthesis is to reproduce the physical properties of a virtual sound object, or primary source of sound inside a control region, bounded by a densely spaced loudspeaker ensemble.

tion behind physically based sound field reproduction methods, commonly referred to as *sound field synthesis techniques*, or *holophony*: once the physical properties of a desired sound field is reproduced over an extended listening area, it is inherently ensured that the listener perceives the desired perceptual properties [Spo+13]. Obviously, controlling the sound field over an extended region requires numerous loudspeakers, positioned on the boundary of the control region. Hence, these techniques are often referred to as *massive multichannel sound reproduction methods* [Spo+13; Zha+17].

Generally speaking, the sound field synthesis problem is an inverse problem: the synthesized sound field is described analytically in the form of an integral/summation of the individual loudspeakers' sound field, used for reproduction [Faz+08; Faz10; Ahr10; Ahr12]. In order to derive analytical loudspeaker signals this integral formulation has to be solved in an inverse manner for any target virtual sound field. The solution is available explicitly only in special geometries: for a spherical and circular arrangement of loudspeakers the direct solution is proven to coincide with NFC-HOA [WA01; Dan03; Pol05; Faz+08; AS08a; Faz10; AS11a], while for a theoretical infinite planar or linear distribution of loudspeakers the solution is known as the *Spectral Division Method (SDM)* [Faz10; AS10c; AS12; Ahr12]. NFC-HOA and SDM are therefore commonly referred to as the *explicit solution* for the sound field synthesis problem.

Besides NFC-HOA and SDM the most prominent, well-known sound field synthesis approach is Wave Field Synthesis, the main subject of the present dissertation. Wave Field Synthesis (WFS) aims to recreate the desired sound field—or more precisely the desired wavefront—by putting the Huygens-principle into practice: each reproduction loudspeaker acts as the source of a secondary wavefront, so that the resultant field of the entire speaker arrangement coincides with that of a virtual sound source [Ber+93; Ver97; Ahr12]. As WFS yields driving signals from the local behaviour of the virtual sound field at the position of the loudspeakers it is often termed as a *local solution* to the SFS problem. On the other hand the explicit solutions compute the driving signal for a single loudspeaker from the global description of the virtual field, therefore NFC-HOA and SDM are termed as *global solutions*. Furthermore, since WFS extracts the loudspeaker driving signals from an appropriate boundary integral representation of sound fields, containing the solution implicitly, WFS is referred to as an *implicit solution*.

Categorization of spatial audio techniques: As a summary of the foregoing the above described spatial audio techniques may be categorized based on the representation of the virtual sound scene to be reproduced [Spo+13]

- *Channel-based representation* is the most widely used method up to nowadays, storing and transmitting directly the driving signals of the loudspeakers used for reproduction. Traditional stereophonic methods like Dolby stereo, 5.1, 7.1 are commonly channel-based formats with the drawback of reproducing the desired spatial characteristics only by applying a predefined, often standardized loudspeaker layout.
- *Object-based representation* stores the desired virtual sound scene in terms of the virtual audio object properties: the time history of the individual auditory events along with their spatial characteristics as metadata (position, source width, etc.). Obviously, the decoding/reproduction stage requires the rendering of the loudspeaker driving signal for the actual loudspeaker layout, for which either VBAP, Wave Field Synthesis or simple stereophonic panning laws may be used.
- As a third possibility, *transform-based representation* stores the characteristics of the sound scene in terms of its coefficients for the expansion into orthonormal spatial basis functions. Similarly to the object-based case, a sophisticated decoding/rendering stage is required at the reproduction side in order to derive the driving signals for the loudspeaker arrangement, for which either NFC-HOA or the Spectral Division Method may be applied.

Due to the simplicity of the reproduction stage, up to the recent years commercially available technologies almost exclusively utilized channel-based representations, however in the recent years object-based reproduction techniques have started to gain more ground. Dolby Atmos and DTS-X are the first commercially successful object-based surround sound technologies, both realizing object-based stereophony [Atm]. As the next step, the 3D audio coding part of the latest MPEG-H coding standard allows for standardized encoding, transmission and decoding of spatial audio scenes [Her+15b; Her+15a]: the standard audio decoder is capable of decoding either channel-based, object-based, or transform-based representations of the desired audio scene. Object-based rendering is performed by Vector-based Amplitude Panning, while transform-based representation is realized by a standardized Higher-Order Ambisonics encoder and decoder.

Since several years Wave Field Synthesis based sound systems are available commercially with the introduction of the IOSONO and Sonic Emotion systems, even though that no complete unified WFS theory has been existed so far: previous WFS approaches deal with the reproduction of specific sound object models applying specific loudspeaker geometries with well-defined control regions. These limitations are overcome in the present thesis by presenting a generalized Wave Field Synthesis approach. In the following, first a brief overview on Wave Field Synthesis history is given, with highlighting the deficiencies of its theory that motivated the research, summarized in the present dissertation.

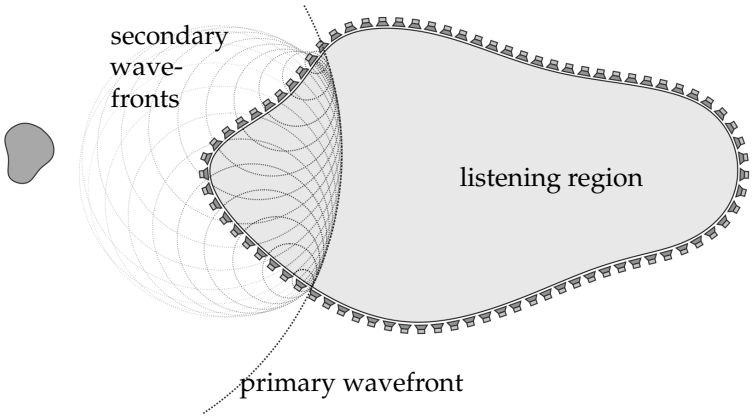

Figure 1.3. Reproduction of a primary wavefront based on the Huygens-principle.

1.2 Wave Field Synthesis history and motivation of the presented research:

Huygens' principle states that each point on a primary wavefront at a given time instant acts as the source of spherical wavelets and the sum of these secondary waves determine the form of the original wavefront at any subsequent time [Huy90]. Hence if secondary sources of sound are present in the space covering a part of the primary wavefront, then the primary field can be reconstructed as the sum of the secondary wavefronts. The idea of synthesizing wavefronts with loudspeakers based on the Huygens principle in order to reconstruct wavefields over an extended listening area dates back to the 1930's, to the concept of the *acoustic curtain* by Steinberg and Snow [SS34]. They intuitively stated that an auditory scene could be recorded, transmitted and reproduced by recording the sound scene with a large, densely spaced microphone array and playing back with the same amount of loudspeakers located in the same arrangement as the microphones, at the reproduction venue [2]. The concept is illustrated in Figure 1.3. Due to the obvious technical constraints of that time the concept has not been put into practical application until the 1980's.

The original theory of Wave Field Synthesis—often referred to as *traditional WFS*—evolved from the works of Berkhout et al. at the Technical University of Delft utilizing concepts, well-known in the field of seismic migration.The basis of WFS theory were the Rayleigh integrals, the mathematical form of the Huygens' principle, representing a sound field as the sum of spherical waves emerging from an infinite plane. Berkhout applied the stationary phase method (SPA) to the Rayleigh integrals in order to arrive at loudspeaker driving signals for a linear array of loudspeakers instead of the practically infeasible planar array. The original formulation provided driving signals for loudspeakers with dipole characteristics [Ber88; Ber+93]—soon extended for monopole loudspeakers as well [Ber92; Vog93; Vri+94; Sta97; Ver97; Bru04]—, reproducing the wavefront of a virtual spherical wave in the horizontal plane, containing the loudspeaker array. It was discussed that the dimensionality reduction performed by the SPA restricts the amplitude correct reproduction to a control curve in the plane

[2] In fact, Snow termed the acoustic curtain concept as an ideal stereophonic system [Sno53].

of synthesis, termed here as the reference curve [Son+98]. For traditional WFS this reference curve was usually chosen to be a reference line, parallel with the loudspeaker arrangement [Sta96; Sta97]. The theoretical framework of traditional WFS has been extended towards various aspects, including the consideration of loudspeaker directivity [Vri96; FF12], stochastic loudspeaker properties [FF13a; FF13b], application of curved arrays [Sta96], synthesis of extended and directive sources [Cor07; Baa08], the perceptual aspects of synthesis [Hul04; Wit+04; Str+04; Cor06; Wit07] or the inclusion of the reproduction room's effects to the WFS theory [Spo+03; CN03; Spo+04; Buc+04; Pet+05]. Traditional WFS was also the subject of various research projects, most notably the CARROUSO project, aiming at the integration of the technique into the MPEG-4 standard [Spo+01]. This endeavor was not realized eventually, but two "spin-off" companies of the project, the IOSONO and Sonic Emotion are still offering commercially available WFS systems nowadays.

The latest milestone in Wave Field Synthesis theory were the works of Spors et al., generalizing WFS towards the synthesis of an arbitrary analytically available sound field, applying an arbitrary shaped loudspeaker contour [RS07; Spo+08]. The presented loudspeaker driving signals allowed the synthesis of general 2-dimensional sound fields, ensuring amplitude correct synthesis at a single reference point, allowing the reproduction of complex virtual sound scenes, e.g. the field, generated by a moving sound source [AS08c; AS08d; AS11c]. The method however—since it derived driving signals from the 2D Rayleigh integral—failed to control the amplitude of general 3D sound fields. Furthermore, the exact connection between traditional and the latter *revisited WFS* formulations has not been known so far.

The present dissertation revisits the theoretical basics of Wave Field Synthesis. First, several high frequency acoustic concepts are introduced—e.g the local wavenumber vector and the local wavefront curvature—being beneficial for the deeper understanding of the results, concerning WFS. By using these concepts brief and physically illustrative loudspeakers driving signals are derived. These driving signals allow the reproduction of arbitrary two, or three-dimensional sound fields applying an arbitrary shaped ensemble of loudspeakers with the amplitude of the synthesized field optimized along an arbitrary reference curve. Hence, the presented theoretical framework includes previous WFS approaches as special cases.

The introduced high frequency concepts are well-known in the field of high frequency acoustics and ray acoustics. This indicates the important fact that WFS can be regarded as the ray tracing, or ray-based solution of the general sound field synthesis problem—which is a key message of the present work—, realizing the matching of the virtual source's and the secondary loudspeakers' wavefronts at the predefined reference positions [3]. This fact is also confirmed in the present thesis by showing that WFS is the high frequency, ray based approximation of the explicit, direct solution for the sound field synthesis problem. This connection of WFS techniques and the explicit SFS solution has been investigated only for particular virtual source models in the

[3] It should be noted that in some of the early works of Berkhout termed the technique as Wave Front Synthesis [Ber+92; Ber92] which terminology may be more expressive, reflecting the underlying physical interpretation of the approach.

related literature, e.g. for the case of a virtual spherical wave [SA10] and for a virtual plane wave [SS16].

Finally, as a complex application example for the presented framework the reproduction of moving virtual sources is investigated in details. The reproduction of moving sources has been the subject of studies since the early age of WFS theory, as an obvious need when dynamic sound scenes are to be synthesized. Early formulations attempted to synthesize the field of a moving point source by applying the traditional WFS driving signals with changing the virtual source position as the function of time. This approach however failed to properly recreate Doppler effect, leading to serious artifacts in the synthesized field as investigated in details by Franck et al. [Fra+07]. Ahrens et al. used the revisited WFS formulation in order to recreate the field of a moving source [AS08c; AS08d; Ahr12]. However, due to physical constrains of revisited WFS theory, it failed to control the amplitude of the synthesized source. In the present work the physically correct loudspeaker driving signals are presented for the synthesis of moving sources of sound, applying either WFS or the explicit solution.

With highlighting the related publications by the author, the thesis is structured as follows

- Chapter 2 gives an overview on basic acoustic concepts, required for dealing with the general sound field synthesis problem. Different descriptions of sound fields are discussed, including spectral integral and boundary integral representations.
- Chapter 3 introduces important high frequency concepts—the local wavenumber vector local wavefront curvature and the high frequency gradient approximation—which are later applied in order to explain results, concerning the *stationary phase approximation (SPA)* of integrals. The SPA is of central importance in the aspect of the present thesis: loosely speaking the present work discusses how integral representations can be manipulated by the SPA in order to extract the desired SFS driving signals from them. The application of the SPA to the different integral representations is discussed via examples. Some of the results in these examples—describing wave dynamics by investigating the sound field's phase function and its derivatives—are well-known in the field of ray acoustics, however the present thesis introduces a novel approach for their derivation, so far unknown in the related literature.
- Chapter 4 deals with the solution of the general sound field synthesis problem. By applying the SPA to the boundary integral representation of wavefields a unified Wave Field Synthesis framework is introduced, capable of the synthtesis of an arbitrary sound field applying arbitrary shaped loudspeaker ensembles, with optimizing the synthesis on a pre-defined reference curve [Fir+17; Sch+17]. The application of the presented concepts are illustrated with examples, highlighting how previous WFS approaches are included inherently in the present framework. By applying asymptotic approximation to the Spectral Division Method a novel SFS method is introduced, ensuring wavefront matching along a control curve requiring merely the virtual field measured at these control points [FF17a]. It is highlighted, that the proposed method is equivalent with WFS, indicating the general relation between the implicit and the explicit SFS methods

[Fir+18]. Finally, the effect of the discrete secondary source source distribution (instead of the theoretical continuous one) is discussed, and a novel anti-aliasing strategy is introduced [FF18a].

- As a detailed, complex example for the above theoretical results, in Chapter 5 the reproduction of moving virtual sources is investigated. By adapting the unified WFS theory to the analytical description of sources under motion, driving signals are presented for an arbitrary contour of loudspeakers [FF15b; FF16b; FF17b]. Besides Wave Field synthesis, the explicit solution is also presented, serving as a reference solution [FF14b; FF14a]. Finally, several practical aspects of synthesis are discussed, evolving at the practical application of the presented driving signals, e.g. numerical calculation of the presented analytical driving signals and the effects of the applied loudspeaker geometry [FF18b]. For this latter question the explicit solution—for which WFS constitutes a high frequency approximation similarly to the case of stationary sound scenes [FF15a]—is utilized to the analytical investigation of the evolving artifacts [FF16a].

2 Theory of wave propagation and radiation problems

In this chapter the basics of sound radiation theory are introduced. The section starts with discussing the physics of sound propagation and radiation by deriving the formulation and solution of the governing homogeneous and inhomogeneous wave equations. Various integral representations of sound fields are presented including spectral and boundary integrals.

2.1 The wave equation

Sound is a mechanical disturbance propagating in an elastic fluid, causing an alternation in the fluid's density and pressure, as well as displacement of the medium's particles. The propagation of the disturbance is described by the acoustic wave equation.

Consider a homogeneous, elastic fluid, modeled as an ideal gas with no viscosity. In the aspect of the present thesis it is appropriate to restrict the investigation to sound propagation solely in air at room temperature.

The domain of investigation $\Omega \in \mathbb{R}^n$ where sound waves propagate is termed *sound field* hereinafter. Within this thesis usually 3 dimensional problems are investigated ($n = 3$). The acoustical properties of the sound field are described by *dynamic field variables* in each point $\mathbf{x} \in \Omega$, at each time instant t: the vector variable *particle velocity* $\mathbf{v}(\mathbf{x}, t)$ and the scalar *instantaneous sound pressure* $p(\mathbf{x}, t)$ superimposed onto the static pressure $p_0 \approx 10^5$ Pa. The medium is quiescent, meaning that on average each particle is at rest with zero particle displacement (thus zero particle velocity) at the static pressure p_0. The presence of sound waves causes incremental change in the instantaneous pressure and the particle velocity.

In order to apply a linear model for sound propagation two assumptions are made. Since the traveling speed of thermal diffusion is small compared to the speed of sound, it is feasible to assume that heat exchange in the wave due to compression and expansion is negligible: the state changes are modeled as adiabatic. Furthermore the alternation of the instantaneous sound pressure is small compared to the static pressure, so the non-linear adiabatic state change characteristics can be linearized around p_0. This later assumption is fulfilled for pressure magnitudes below the threshold of pain of the human auditory system [GD04; Ahr12].

First the homogeneous wave equation is presented, valid for a *source-free domain*, describing merely the propagation characteristics of acoustic waves. For a more detailed derivation refer to [MI68; Ber93; Wil99; Bla00].

2.1.1 The homogeneous wave equation

The linear homogeneous wave equation may be derived by utilizing two fundamental physical principles.

- *The equation of motion:* By applying Newton's second law for an infinitesimal small volume of the fluid the connection between the particle velocity vector and the pressure field is established at each point at each time instant. The resulting *Euler's equation* states that the force acting on the volume due to variation in the spatial pressure distribution causes an acceleration of the volume:

$$\nabla_{\mathbf{x}}\, p(\mathbf{x},t) = -\rho_0 \frac{\partial}{\partial t}\mathbf{v}(\mathbf{x},t), \tag{2.1}$$

  where $\nabla_{\mathbf{x}}$ is the gradient operator and ρ_0 is the fluid's ambient density. In room temperature for the above given static pressure $\rho_0 = 1.18\ \mathrm{kg/m^3}$.

- *The gas law:* For adiabatic processes the change of state is governed by the relation

$$p\, V^{\gamma} = \mathrm{const}, \tag{2.2}$$

  with p and V being the pressured and volume of the fluid respectively and where $\gamma = C_P/C_V$ is the ratio of specific heats of the fluid with constant pressure and with constant volume. For air it is given as $\gamma = 1.4$. Linearization of (2.2) around the static state p_0, V_0 yields

$$\mathrm{d}p = p(\mathbf{x},t) = -\gamma\, p_0 \frac{\mathrm{d}V}{V_0}, \tag{2.3}$$

  where V_0 is the undisturbed volume. The relative change of volume $\mathrm{d}V/V_0$ may be expressed by the *divergence* of the particle displacement $\nabla_{\mathbf{x}} \cdot \mathbf{u}(\mathbf{x},t)$. Applying the definition of divergence and expressing the equation in terms of particle velocity yields

$$\frac{\partial}{\partial t} p(\mathbf{x},t) = -\gamma\, p_0\, \nabla_{\mathbf{x}} \cdot \mathbf{v}(\mathbf{x},t). \tag{2.4}$$

  This *continuity equation* states that the net flow of the fluid out of an infinitezimal volume results in decreased density and pressure inside the volume [AW05].

Taking the time derivative of equation (2.4) and the divergence of equation (2.1) the particle velocity may be eliminated. By using the *Laplace operator* $\nabla_{\mathbf{x}} \cdot \nabla_{\mathbf{x}} = \nabla_{\mathbf{x}}^2$ the scalar linear homogeneous wave equation is obtained for the sound pressure

Homogeneous wave eq.

$$\nabla_{\mathbf{x}}^2 p(\mathbf{x},t) - \frac{1}{c^2}\frac{\partial^2}{\partial t^2} p(\mathbf{x},t) = 0, \tag{2.5}$$

where $c \equiv \sqrt{\frac{\gamma p_0}{\rho_0}}$ is the speed of sound in the medium. For air in room temperature it is given as $c = 343.1\ \mathrm{m/s}$. The instantaneous pressure may also be eliminated in

a similar manner, resulting in the vector wave equation for each component of the particle velocity

$$\nabla_{\mathbf{x}}^2 \mathbf{v}(\mathbf{x},t) - \frac{1}{c^2}\frac{\partial^2}{\partial t^2}\mathbf{v}(\mathbf{x},t) = \mathbf{0}, \tag{2.6}$$

valid in curl-free media, where $\nabla_{\mathbf{x}}\,(\nabla_{\mathbf{x}}\,\cdot) = \nabla_{\mathbf{x}}^2$ holds. Besides the pressure and the velocity, acoustic fields are often described by the scalar *velocity potential* $\varphi(\mathbf{x},t)$, for which the acoustic wave equation also holds, and which is related to the other field variables as

$$\mathbf{v}(\mathbf{x},t) = \nabla_{\mathbf{x}}\,\varphi(\mathbf{x},t), \qquad p(\mathbf{x},t) = -\rho_0\frac{\partial}{\partial t}\varphi(\mathbf{x},t). \tag{2.7}$$

The wave equations fully describe the properties of acoustic wave propagation as long as the above made assumptions are fulfilled.

Equations (2.1) and (2.5) may be transformed into the angular frequency domain by performing a temporal Fourier transform according to (A.1). Applying the differentiation property of the Fourier transform to (2.1) yields the frequency domain Euler's equation

$$\nabla_{\mathbf{x}}\,P(\mathbf{x},\omega) = -\mathrm{j}\omega\rho_0\mathbf{V}(\mathbf{x},\omega), \tag{2.8}$$

Euler equation

relating the pressure distribution of a time-harmonic sound field to the harmonic velocity vector field. By taking the Fourier transform of the wave equation (2.5), the *homogeneous Helmholtz equation* is obtained:

$$\nabla_{\mathbf{x}}^2 P(\mathbf{x},\omega) + k^2 P(\mathbf{x},\omega) = 0, \tag{2.9}$$

Helmholtz equation

where k is the *acoustic wavenumber*, which is related to the temporal frequency through the linear *dispersion relation* $k = \frac{\omega}{c}$. Equation (2.9) must hold for every physically possible *steady-state* wave form with harmonic time-dependence for a source-free volume. In the aspect of the present thesis the time domain wave equation is rarely solved directly, therefore the general solution of the Helmholtz equation will be presented in the following.

2.1.2 The inhomogeneous wave equation

So far wave propagation in source-free volumes was investigated, without considering how these waves were generated. A simple scalar disturbance of the pressure field may be included into the wave equation resulting in the time domain *inhomogeneous wave equation*

$$\nabla_{\mathbf{x}}^2 p(\mathbf{x},t) - \frac{1}{c^2}\frac{\partial^2}{\partial t^2}p(\mathbf{x},t) = -s(\mathbf{x},t), \tag{2.10}$$

Inhomogeneous wave eq.

and by taking the Fourier transform with respect to time in the *inhomogeneous Helmholtz equation*

$$(\nabla_{\mathbf{x}}^2 + k^2)P(\mathbf{x},\omega) = -S(\mathbf{x},\omega). \tag{2.11}$$

Term $s(\mathbf{x},t)$ is referred to as the *load term*, and it describes the spatial extension and time history of the excitation.

To involve more physical source excitation models additional force source terms may be added to the equation of motion (2.1), or injected mass/volume terms may be included in the continuity equation (2.4). This results in the *general inhomogeneous wave equations* [Pie91; Kin+00; How07]

$$\nabla_{\mathbf{x}}^2 p(\mathbf{x},t) - \frac{1}{c^2}\frac{\partial^2}{\partial t^2} p(\mathbf{x},t) = -\rho_0 \frac{\partial}{\partial t} q(\mathbf{x},t) + \nabla_{\mathbf{x}} \cdot \mathbf{f}(\mathbf{x},t), \tag{2.12}$$

and

$$(\nabla_{\mathbf{x}}^2 + k^2) P(\mathbf{x},\omega) = -\mathrm{j}\omega\rho_0 Q(\mathbf{x},\omega) + \nabla_{\mathbf{x}} \cdot \mathbf{F}(\mathbf{x},\omega) \tag{2.13}$$

in the time and angular frequency domains, respectively, where $q(\mathbf{x},t)$ describes the rate of increase of fluid volume per unit volume [1] and $\mathbf{f}(\mathbf{x},t)$ represents a body force excitation. The first term is generated by sources that change the fluid volume, e.g. a pulsating sphere or a baffled dynamic loudspeaker. The latter force term is produced by sources moving through the fluid without any change in volume, e.g. unbaffled loudspeakers. A further third type of excitation term, as introduced by Lighthill, accounts for sounds, produced by turbulence resulting in quadrupole sound fields [Lig52; Lig54; Kin+00]. This third term is not investigated in the present thesis.

2.1.3 Boundary conditions

In order to obtain a particular solution of the wave equation the behaviour of waves, arriving at boundaries has to be known: the wavefield must satisfy prescribed boundary conditions. The general geometry is depicted in Figure 2.1 with an enclosing surface/contour denoted by $\partial\Omega$. If the domain of interest is the exterior of the enclosing boundary while the sources are inside the volume—or it is the vibrating boundary surface itself—the problem to be solved is termed an *exterior radiation problem*. On the other hand, if the aim is to determine the sound field inside a source-free volume—or the reflected field of a sound source inside a cavity—an *interior problem* must be solved.

The boundary conditions are typically prescribed pressure or particle velocity. Zero pressure or velocity on the boundary surface formulates *homogeneous boundary conditions*. Non-zero field variables on the other hand are termed *inhomogeneous boundary conditions*.

In the aspect of this thesis two types of boundary conditions are of interest:

- *Dirichlet boundary condition* prescribes the pressure measured on the boundary surface. The homogeneous Dirichlet boundary conditions are thus

$$P(\mathbf{x},\omega) = 0, \quad \forall \quad \mathbf{x} \in \partial\Omega. \tag{2.14}$$

  These types of boundaries are called *sound-soft* or *pressure release* boundaries, and are used to model e.g. the surface of the ocean for a wave propagating in the water [Zio95; Bla00].

[1] The volume injection term $q(\mathbf{x},t)$ can be modeled as a simple disturbance in the velocity potential i.e. satisfies equation $\nabla_{\mathbf{x}}^2\varphi(\mathbf{x},t) - \frac{1}{c^2}\frac{\partial^2}{\partial t^2}\varphi(\mathbf{x},t) = -q(\mathbf{x},t)$ [Jen+07].

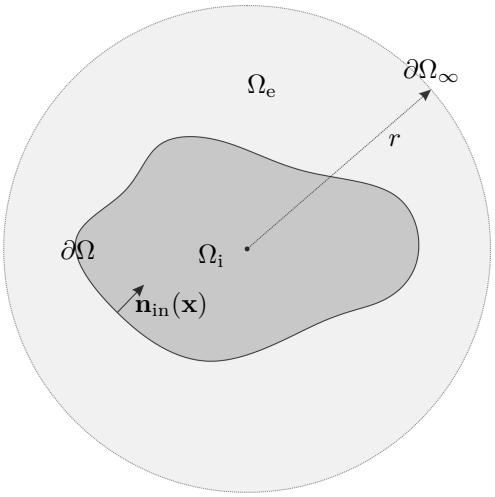

Figure 2.1. Geometry for the boundary conditions in general interior and exterior radiation problems. The Sommerfeld radiation condition can be derived in a mixed interior and exterior radiation problem by prescribing appropriate boundary conditions on the surface $\partial\Omega_\infty$ besides increasing its radius r to infinity, which ensures that no reflection may occur from this outer boundary surface.

The inhomogeneous Dirichlet boundary condition assumes a specific pressure distribution on the boundary surface:

$$P(\mathbf{x},\omega) = f_D(\mathbf{x},\omega), \quad \forall \quad \mathbf{x} \in \partial\Omega. \tag{2.15}$$

- *Neumann boundary condition* gives the normal derivative of the pressure on the boundary surface, i.e. prescribes the normal velocity of the surface. Homogeneous Neumann boundary condition are

$$\frac{\partial P(\mathbf{x},\omega)}{\partial \mathbf{n}} = 0, \quad \forall \quad \mathbf{x} \in \partial\Omega, \tag{2.16}$$

where $\mathbf{n}(\mathbf{x})$ is either the interior or exterior normal vector of the boundary surface, and $\frac{\partial}{\partial \mathbf{n}} P(\mathbf{x},\omega) = \langle \mathbf{n}(\mathbf{x}) \cdot \nabla_{\mathbf{x}} P(\mathbf{x},\omega) \rangle$. These type of boundaries are termed *sound hard*, or *rigid* boundaries, with the boundary condition ensuring that no incident wave can mobilize the boundary surface.

Inhomogeneous Neumann boundary conditions are given by

$$\frac{\partial P(\mathbf{x},\omega)}{\partial \mathbf{n}} = f_N(\mathbf{x},\omega), \quad \forall \quad \mathbf{x} \in \partial\Omega. \tag{2.17}$$

Vibrating surfaces (e.g. mounted loudspeakers, or baffled pistons) are most often modeled using these type of boundary conditions.

For radiation problems it is feasible to assume free field conditions, i.e. only outgoing waves are present in the sound field. This is ensured by the *Sommerfeld radiation condition* that excludes the non-physical solutions of the wave equation emerging from infinity. Mathematically it can be formulated by implying boundary condition on $\partial\Omega_\infty$ with r increased to infinity—as shown in Figure 2.1 [Sch92; Wil99]—reading as

$$\lim_{r\to\infty} r \left(\frac{\partial}{\partial r} P(\mathbf{x},\omega)\Big|_{\mathbf{x}\in\partial\Omega_\infty} + \mathrm{j}\frac{\omega}{c} P(\mathbf{x},\omega) \right) = 0, \quad \forall \quad \mathbf{x} \in \partial\Omega_\infty. \tag{2.18}$$

2.2 Solution of the homogeneous wave equation

2.2.1 Plane wave theory

Now the general solution of the homogeneous wave equation is discussed in Cartesian coordinate systems, leading to plane wave theory. The Descartes coordinate form of the Laplace-operator is given in the nomenclature. A common method for obtaining the general solution of the Helmholtz equation is the separation of variables [Dev12]: it is supposed that the solution of (2.9) can be written in the form of the product

$$P(\mathbf{x},\omega) = W(\omega)X(x)Y(y)Z(z). \tag{2.19}$$

Substituting it into (2.9) and dividing both sides by $W(\omega)X(x)Y(y)Z(z)$ yields

$$\underbrace{\frac{\mathrm{d}^2X(x)}{\mathrm{d}x^2}\frac{1}{X(x)}}_{-k_x^2} + \underbrace{\frac{\mathrm{d}^2Y(y)}{\mathrm{d}y^2}\frac{1}{Y(y)}}_{-k_y^2} + \underbrace{\frac{\mathrm{d}^2Z(z)}{\mathrm{d}z^2}\frac{1}{Z(z)}}_{-k_z^2} = -k^2. \tag{2.20}$$

Since each term contains a total derivative—being independent from any other variable—equality may hold only if each term is constant. These constant are denoted by k_x^2, k_y^2, k_z^2. Consequently each part of the equation leads to a simple eigenvalue problem, for which the eigenfunction solution is given by exponentials. Written e.g. for the x-variable:

$$\frac{\partial^2X(x)}{\partial x^2} = -k_x^2X(x) \quad \rightarrow \quad X(x) = A_1\mathrm{e}^{-\mathrm{j}k_xx} + A_2\mathrm{e}^{\mathrm{j}k_xx}. \tag{2.21}$$

The solutions may be substituted back into equation (2.19). In order to include every possible solution the general solution for the free field homogeneous Helmholtz equation is yielded by summation over all possible values of $k_x - k_y - k_z$ weighted by arbitrary constants. However, the variables are not independent. For a fixed temporal frequency their relation is described by the *dispersion relation*, resulting from (2.20)

$$k^2 = \left(\frac{\omega}{c}\right)^2 = k_x^2 + k_y^2 + k_z^2, \tag{2.22}$$

connecting the temporal and spatial frequencies. Through the present thesis k_y will be used as a dependent variable, so that

$$k_y^2 = k^2 - k_x^2 - k_z^2 \tag{2.23}$$

holds. With all the foregoing and by denoting the arbitrary weighting constant by $\tilde{P}(k_x,k_z,\omega)$, the general solution of the 3D Helmholtz equation reads as

$$P(\mathbf{x},\omega) = \frac{1}{(2\pi)^2}\iint_{-\infty}^{\infty}\tilde{P}(k_x,k_z,\omega)\mathrm{e}^{-\mathrm{j}(k_xx+k_yy+k_zz)}\mathrm{d}k_x\mathrm{d}k_z. \tag{2.24}$$

Constant $\frac{1}{(2\pi)^2}$ is introduced as a Fourier transform normalization term. The general solution—describing the inverse Fourier transform of $\tilde{P}(k_x,k_z,\omega)\mathrm{e}^{-\mathrm{j}k_yy}$—therefore

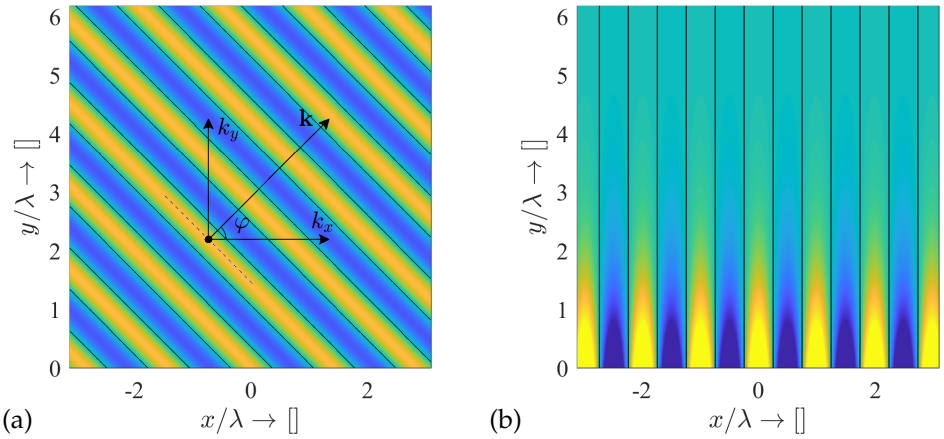

Figure 2.2. Illustration of a traveling plane wave (a) and an evanescent wave (b) with $\lambda = \frac{2\pi}{k}$ being the acoustic wavelength of the plane wave. In the present case the plane wave travels along the xy-plane, with $k_z = 0$. Variables $k_x = k\cos\varphi,\ \ k_y = k\sin\varphi$ give the wavenumber components along the x and y directions. For the case of the evanescent wave $k_x > \frac{\omega}{c}$, resulting in exponential decay into the y-direction. In a source-free region propagating and evanescent waves form a complete, orthonormal basis for the solution of the Helmholtz equation.

is obtained in the form of a spectral integral, similarly to the case of the temporal solution. Obviously, the spectral coefficients are obtained via a suitable forward Fourier transform, as explained in the next section.

One separated solution from integral (2.24) is in the form of

$$P(\mathbf{x},\omega) = \tilde{P}(\omega)\mathrm{e}^{-\mathrm{j}(k_x x + k_y y + k_z z)} = \tilde{P}(\omega)\mathrm{e}^{-\mathrm{j}\langle \mathbf{k}\cdot\mathbf{x}\rangle}, \tag{2.25}$$

where $\mathbf{k} = [k_x,\ k_y,\ k_z]^{\mathrm{T}}$ is the *wavenumber vector*, with its length equaling the acoustic wavenumber $k = |\mathbf{k}|$ and pointing into the direction of the maximum phase advance, given by the gradient of the phase function. The separated solution represents a *plane wave* component with the *acoustic wavelength* $\lambda = \frac{2\pi}{k}$, traveling in the direction

$$\mathbf{k} = -\nabla\phi^P(\mathbf{x},\omega), \tag{2.26}$$

where ϕ^P denotes the phase of function P. The terminology indicates that the surface of constant phase points are lying along an infinite plane, perpendicular to $\mathbf{k}$. Refer to Figure 2.2 (a) for the illustration of a traveling plane wave.

Since there is no constraint on the values of k_x and k_z, the dispersion relation is satisfied also when $k_x^2 + k_z^2 > k^2$ in which case k_y becomes complex. In order to ignore the non-physical exponentially increasing solution, k_y may be defined as

$$k_y = \begin{cases} \sqrt{\left(\frac{\omega}{c}\right)^2 - k_x^2 - k_z^2} & \text{if} \quad k_x^2 + k_z^2 \leq \left(\frac{\omega}{c}\right)^2 \\ -\mathrm{j}\sqrt{k_x^2 + k_z^2 - \left(\frac{\omega}{c}\right)^2} = -\mathrm{j}k_y' & \text{if} \quad k_x^2 + k_z^2 > \left(\frac{\omega}{c}\right)^2 . \end{cases} \tag{2.27}$$

Solutions with k_y' given as

$$P(\mathbf{x},\omega) = \hat{P}(\omega)\mathrm{e}^{-k_y' y}\mathrm{e}^{-\mathrm{j}(k_x x + k_z z)} \tag{2.28}$$

describe plane waves propagating perpendicular to the y-axis and exhibiting an exponentially decaying amplitude along the y-direction (see Figure 2.2 (b)): in those cases when one wavelength component is shorter than the acoustic wavelength, the wave can not propagate from the $y = 0$ surface, but an exponentially decaying radiation phenomena occurs. These type of waves are termed *evanescent waves*, opposed to *propagating waves* for which all wavenumber components are real valued.

Strong evanescent contribution is often the result of difference between the speed of sound in different materials: in solids the propagation speed of flexural bending waves is proportional to the square root of their temporal frequency. As a consequence, in the exemplary case of a vibrating plate higher-order modes will not be radiated into the free space, since the bending wave's wavelength on the surface may become shorter than the acoustic wavelength would be in air. In these cases air above the surface acts as a hydrodynamic short-circuit.

The evanescent contribution is of central importance in the field of *Nearfield Acoustic Holography*, when one needs a high-resolution image from the velocity distribution of the vibrating object's surface, however their contribution is often neglected in the field of sound field synthesis, when the listener is relatively far from the secondary loudspeaker array, and loudspeaker spacing is significantly higher than the evanescent wavelengths.

2.2.2 The angular spectrum representation

Based on the foregoing any source-free sound field may be expressed in terms of a double inverse Fourier transform, given by (2.24). This formulation is termed the *angular spectrum representation* [Wil99; Goo05; NV06; Ahr10; Ahr12] or the *plane wave expansion* [Spo05] of the sound field. By expressing the pressure by (2.24) at the infinite plane $y = 0$ it is revealed that the *angular spectrum* $\tilde{P}(k_x, k_z, \omega)$ is given as the corresponding forward Fourier transform of the pressure distribution at $y = 0$. In the following, the domain characterized by k_x, k_z is termed the *wavenumber domain*.

As a consequence, equation (2.24) relates the pressure distribution of an arbitrary sound field measured on the plane $y = 0$ to its pressure distribution on an arbitrary parallel plane. In the wavenumber domain the relation reads as

$$\mathcal{F}_x \mathcal{F}_z \left\{ P(\mathbf{x}, \omega) \right\} = \tilde{P}(k_x, y, k_z, \omega) = \tilde{P}(k_x, 0, k_z, \omega) \mathrm{e}^{-\mathrm{j} k_y y}, \tag{2.29}$$

with k_y given by (2.27). Since the propagation of a single plane wave component is determined merely by the phase change between the planes of investigation, therefore generally speaking the following equation holds:

$$\tilde{P}(k_x, y, k_z, \omega) = \tilde{P}(k_x, y_0, k_z, \omega) \mathrm{e}^{-\mathrm{j} k_y (y - y_0)}. \tag{2.30}$$

Furthermore, the y-derivative of the angular spectrum can be expressed by differentiating both sides of (2.30) with respect to the y-coordinate

$$\frac{\partial}{\partial y} \tilde{P}(k_x, y, k_z, \omega) = \frac{\partial}{\partial y} \left(\tilde{P}(k_x, y_0, k_z, \omega) \mathrm{e}^{-\mathrm{j} k_y (y - y_0)} \right) = -\mathrm{j} k_y \tilde{P}(k_x, y, k_z, \omega), \tag{2.31}$$

which is the Fourier transform differentiation theorem for wavefield extrapolation.

These statements lead to two important formulations: equation (2.30) written in the spatial domain by means of a double inverse Fourier transform yields

$$P(\mathbf{x},\omega) = \frac{1}{4\pi^2}\iint_{-\infty}^{\infty} \tilde{P}(k_x, y_0, k_z, \omega)\mathrm{e}^{-\mathrm{j}k_y(y-y_0)}\mathrm{e}^{-\mathrm{j}(k_x x + k_z z)}\mathrm{d}k_x\mathrm{d}k_z. \tag{2.32}$$

Wavefield extrapolation 1.

By expressing $\tilde{P}(k_x, y_0, k_z, \omega)$ in terms of the normal velocity $\tilde{V}_\mathrm{n}(k_x, y_0, k_z, \omega)$ using the Euler's equation (2.8), with the normal (y-) derivative at $y = y_0$ calculated by applying the differentiation theorem one obtains

$$P(\mathbf{x},\omega) = \frac{1}{4\pi^2}\iint_{-\infty}^{\infty} \underbrace{\mathrm{j}\omega\rho_0\tilde{V}_\mathrm{n}(k_x, y_0, k_z, \omega)}_{-\frac{\partial}{\partial y}\tilde{P}(k_x, y_0, k_z, \omega)} \frac{\mathrm{e}^{-\mathrm{j}k_y(y-y_0)}}{\mathrm{j}k_y}\mathrm{e}^{-\mathrm{j}(k_x x + k_z z)}\mathrm{d}k_x\mathrm{d}k_z. \tag{2.33}$$

Wavefield extrapolation 2.

These equations are of central importance in the field of Fourier acoustics. They state that an arbitrary sound field is completely determined by either the pressure, or by the normal velocity component measured along an infinite plane. Wave propagation is calculated by multiplying the measured spectra with an exponential term, referred to as the *pressure propagator* $\tilde{G}_p$ in (2.32) and the *velocity propagator* $\tilde{G}_v$ in (2.33):

$$\tilde{G}_p(k_x, y-y_0, k_z, \omega) = \mathrm{e}^{-\mathrm{j}k_y(y-y_0)}, \qquad \tilde{G}_v(k_x, y-y_0, k_z, \omega) = \omega\rho_0\frac{\mathrm{e}^{-\mathrm{j}k_y(y-y_0)}}{k_y} \tag{2.34}$$

$$\tilde{P}(k_x, y, k_z, \omega) = \tilde{P}(k_x, y_0, k_z, \omega)\,\tilde{G}_p(k_x, y-y_0, k_z, \omega) \tag{2.35}$$

$$= \tilde{V}_\mathrm{n}(k_x, y_0, k_z, \omega)\,\tilde{G}_v(k_x, y-y_0, k_z, \omega). \tag{2.36}$$

Wave propagation in source-free volumes thus can be modeled by 2D linear filtering of the sound field measured along a plane, where the filter transfer characteristics are given by the corresponding propagator. Formulation of the equations in the spatial domain results in 2D spatial convolutions, termed the Rayleigh I and II integrals, as it will be further discussed in later sections.

2.2.3 Solution in other geometries

Similarly to the presented Cartesian solution, the general solution of the free field homogeneous Helmholtz equation can be found for spherical and cylindrical coordinate systems. The required representations are given in the form of an infinite series of spherical and cylindrical harmonics respectively, relating the radiated sound at an arbitrary point to the sound field measured on a spherical or an infinite cylindrical surface. These solutions are of great importance when spherical or circular secondary source distributions are applied for sound field reconstruction. Since the present thesis does not include the explicit solution for synthesis in these geometries, the presentation of the spherical and cylindrical solutions are omitted. For a detailed investigation refer to [Wil99; Zot09; Faz10; Ahr12; Koy14].

2.3 Solution of the inhomogeneous wave equation

2.3.1 The Green's function

A common way to obtain the solution for the inhomogeneous wave equation is using the *Green's function*. The n-dimensional *Green's function* is defined as the solution for the following equation [Wil99; GD04]

$$\nabla^2_{\mathbf{x}} g(\mathbf{x}|\mathbf{x}_0, t) - \frac{1}{c^2}\frac{\partial^2}{\partial t^2} g(\mathbf{x}|\mathbf{x}_0, t) = -\delta(\mathbf{x} - \mathbf{x}_0)\,\delta(t)\,, \tag{2.37}$$

with $\mathbf{x}, \mathbf{x}_0 \in \mathbb{R}^n$ and $\delta()$ being the Dirac-delta distribution. The Green's function describes the sound field at $\mathbf{x}$ due to an impulsive disturbance located at $\mathbf{x}_0$ at the time instant $t = 0$. The Green's function is often referred to as the *spatio-temporal impulse response* of the domain of interest and its temporal Fourier transform $G(\mathbf{x}|\mathbf{x}_0, \omega)$ as the *spatio-temporal transfer function* of a point source at $\mathbf{x}_0$. In the following free field conditions are assumed by invoking the Sommerfeld radiation condition. Under these assumptions the *free field Green's function* is translation invariant, denoted by $g(\mathbf{x} - \mathbf{x}_0, t)$. Furthermore, in a stationary isotropic medium the *reciprocity principle* for the Green's function holds due to its symmetry [SH11]

$$g(\mathbf{x}_0|\mathbf{x}, t) = g(\mathbf{x}|\mathbf{x}_0, t) = g(\mathbf{x} - \mathbf{x}_0, t), \tag{2.38}$$

$$\nabla_{\mathbf{x}} g(\mathbf{x}_0|\mathbf{x}, t) = \nabla_{\mathbf{x}} g(\mathbf{x}|\mathbf{x}_0, t), \tag{2.39}$$

stating that a response at $\mathbf{x}$ caused by a unit source at $\mathbf{x}_0$ is the same as the response at $\mathbf{x}_0$ due to a unit source at $\mathbf{x}$.

The motivation behind the use of the Green's function is that assuming an arbitrary linear differential operator $\mathcal{L}_{\mathbf{x}}\{\}$ acting on a distribution $p(\mathbf{x})$ with an arbitrary excitation $-s(\mathbf{x})$, the solution of the inhomogeneous differential equation $\mathcal{L}_{\mathbf{x}}\{p(\mathbf{x})\} = -s(\mathbf{x})$ may be expressed by the convolution of the Green's function and the load term: [2]

$$\mathcal{L}_{\mathbf{x}}\{g(\mathbf{x} - \mathbf{x}_0)\} = -\delta(\mathbf{x} - \mathbf{x}_0) \quad \rightarrow \quad p(\mathbf{x}) = \int_\Omega g(\mathbf{x} - \mathbf{x}_0) s(\mathbf{x}_0) \mathrm{d}\Omega(\mathbf{x}_0). \tag{2.40}$$

The Green's function is usually obtained by the eigenfunction expansion of the operator in a given geometry with specified boundary conditions. Under free space assumptions, where harmonic functions give a full orthogonal basis a straightforward method is to perform a Fourier transform to equation (2.37) with $\mathbf{x}_0 = 0$ with respect to space and time, yielding in $\mathbf{x} \in \mathbb{R}^3$

$$\left(-(k_x^2 + k_y^2 + k_z^2) + \left(\frac{\omega}{c}\right)^2\right) \tilde{G}(\mathbf{k}, \omega) = -1, \tag{2.41}$$

[2] Multiplying both sides of the left equation of (2.40) by $-s(\mathbf{x}_0)$ and integrating along all dimensions according to $\mathbf{x}_0$ results in $-\int_\Omega s(\mathbf{x}_0)\mathcal{L}_{\mathbf{x}}\{g(\mathbf{x} - \mathbf{x}_0)\}\,\mathrm{d}\Omega(\mathbf{x}_0) = s(\mathbf{x})$. Since $\mathcal{L}_{\mathbf{x}}$ acts only on $\mathbf{x}$, the operator may be taken outside of the integration. Expressing the load term by $-\mathcal{L}_{\mathbf{x}}\{p(\mathbf{x})\}$ leads to $\mathcal{L}_{\mathbf{x}}\left\{\int_\Omega s(\mathbf{x}_0) g(\mathbf{x} - \mathbf{x}_0)\mathrm{d}\Omega(\mathbf{x}_0)\right\} = \mathcal{L}_{\mathbf{x}}\{p(\mathbf{x})\}$.

with $\mathbf{k} = [k_x,\ k_y,\ k_z]^{\mathrm{T}}$. The Green's function in the wavenumber domain is therefore given as [Dev12; Wat15]

$$\tilde{G}(\mathbf{k},\omega) = -\frac{1}{\left(\frac{\omega}{c}\right)^2 - k_x^2 - k_y^2 - k_z^2}. \tag{2.42}$$

Applying the Fourier convolution theorem to (2.40) the solution of (2.10) in the wavenumber domain reads as

$$\tilde{P}(\mathbf{k},\omega) = \tilde{S}(\mathbf{k},\omega)\tilde{G}(\mathbf{k},\omega) = -\frac{\tilde{S}(\mathbf{k},\omega)}{\left(\frac{\omega}{c}\right)^2 - k_x^2 - k_y^2 - k_z^2}, \tag{2.43}$$

and the solution in the spatio-temporal domain is yielded by the inverse Fourier transform

$$p(\mathbf{x},t) = \frac{1}{(2\pi)^4} \iiiint_{-\infty}^{\infty} -\frac{\tilde{S}(\mathbf{k},\omega)}{\left(\frac{\omega}{c}\right)^2 - k_x^2 - k_y^2 - k_z^2} \mathrm{e}^{-\mathrm{j}(\langle \mathbf{k}\cdot\mathbf{x}\rangle - \omega t)} \mathrm{d}k_x \mathrm{d}k_y \mathrm{d}k_z \mathrm{d}\omega. \tag{2.44}$$

The different representations of the free field Green's function may be obtained by the corresponding inverse Fourier transform of (2.42). The resulting formulas are collected in Table 2.1 by taking only the causal solutions into consideration, with two representations of the 3D Green's function are depicted in Figure 2.3.

Table 2.1. Free field acoustic Green's function representations ($\mathbf{x}_0 = 0$) [DeS92; Duf01; Gib08; AS10c; Dev12; Ahr12]. $\theta\,()$ denotes the Heaviside step function, $H_0^{(2)}\,()$ is the zeroth order Hankel function of the second kind and $K_0\,()$ is the modified Bessel function of the second kind [Olv+10]. The conditional expressions ensure that evanescent waves are attenuated with increasing distance from the source. For the sake of brevity in the following Greens function is expressed only in the propagating region, however it should be kept in mind that evanescent wavenumber components are given as (2.27), resulting in the presented conditional expressions.

	3-dimensional	2-dimensional
$\tilde{G}(k_x,k_y,k_z,\omega)$	$-\frac{1}{\left(\frac{\omega}{c}\right)^2 - k_x^2 - k_y^2 - k_z^2}$	$-\frac{1}{\left(\frac{\omega}{c}\right)^2 - k_x^2 - k_y^2}\delta(k_z)$
$\tilde{G}(k_x,k_y,z,\omega)$	$-\frac{\mathrm{j}}{2}\frac{\mathrm{e}^{-\mathrm{j}\sqrt{(\frac{\omega}{c})^2 - k_x^2 - k_y^2}\lvert z\rvert}}{\sqrt{(\frac{\omega}{c})^2 - k_x^2 - k_y^2}}$, $\sqrt{k_x^2+k_y^2} \le \left\lvert\frac{\omega}{c}\right\rvert$ $\frac{1}{2}\frac{\mathrm{e}^{-\sqrt{k_x^2+k_y^2-(\frac{\omega}{c})^2}\lvert y\rvert}}{\sqrt{k_x^2+k_y^2-(\frac{\omega}{c})^2}}$, $\sqrt{k_x^2+k_y^2} > \left\lvert\frac{\omega}{c}\right\rvert$	$-\frac{1}{\left(\frac{\omega}{c}\right)^2 - k_x^2 - k_y^2}$
$\tilde{G}(k_x,y,z,\omega)$	$-\frac{\mathrm{j}}{4}H_0^{(2)}\left(\sqrt{(\frac{\omega}{c})^2 - k_x^2}\sqrt{y^2+z^2}\right)$, $\lvert k_x\rvert < \left\lvert\frac{\omega}{c}\right\rvert$ $\frac{1}{2\pi}K_0\left(\sqrt{k_x^2 - (\frac{\omega}{c})^2}\sqrt{y^2+z^2}\right)$, $\lvert k_x\rvert > \left\lvert\frac{\omega}{c}\right\rvert$	$-\frac{\mathrm{j}}{2}\frac{\mathrm{e}^{-\mathrm{j}\sqrt{(\frac{\omega}{c})^2 - k_x^2}\lvert y\rvert}}{\sqrt{(\frac{\omega}{c})^2 - k_x^2}}$, $\lvert k_x\rvert \le \left\lvert\frac{\omega}{c}\right\rvert$ $\frac{1}{2}\frac{\mathrm{e}^{-\sqrt{k_x^2 - (\frac{\omega}{c})^2}\lvert y\rvert}}{\sqrt{k_x^2 - (\frac{\omega}{c})^2}}$, $\lvert k_x\rvert > \left\lvert\frac{\omega}{c}\right\rvert$
$G(x,y,z,\omega)$	$\frac{1}{4\pi}\frac{\mathrm{e}^{-\mathrm{j}\frac{\omega}{c}\sqrt{x^2+y^2+z^2}}}{\sqrt{x^2+y^2+z^2}}$	$-\frac{\mathrm{j}}{4}H_0^{(2)}\left(\frac{\omega}{c}\sqrt{x^2+y^2}\right)$
$g(x,y,z,t)$	$\frac{1}{4\pi}\frac{\delta\left(t - \sqrt{x^2+y^2+z^2}/c\right)}{\sqrt{x^2+y^2+z^2}}$	$\frac{1}{2\pi}\frac{\theta(t - \sqrt{x^2+y^2}/c)}{\sqrt{t^2 - \left(\frac{\sqrt{x^2+y^2}}{c}\right)^2}}$

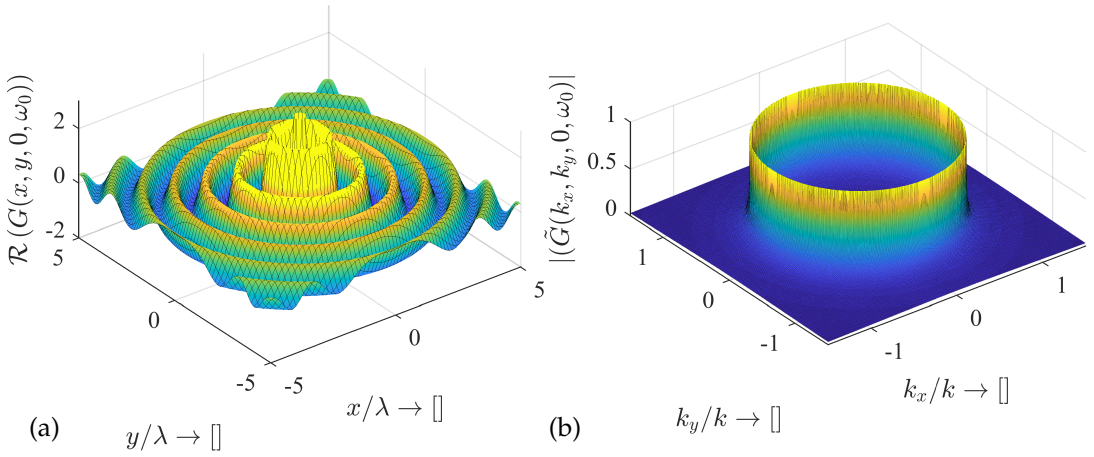

Figure 2.3. Different representations of the 3D free field Green's function in the angular frequency domain $G(x,y,z,\omega)$, with $\lambda = \frac{2\pi c}{\omega} = \frac{2\pi}{k}$ (a) and in the semi-wavenumber domain (i.e. the angular spectrum) $\tilde{G}(k_x,k_y,z,\omega)$ with $k = \frac{\omega}{c}$ (b), measured at $z = 0$.

In 3-dimensions the 2-dimensional Green's function represents the field of an infinite line source along the z-axis, that can be described as a continuous linear distribution of 3D point sources—explaining the infinite tail of the 2D impulse response—, thus the relation between the 3D and 2D Green's functions is given as

$$G_{2\mathrm{D}}(x,y,\omega) = \int_{-\infty}^{\infty} G_{3D}(x,y,z,\omega)\mathrm{d}z = \mathcal{F}_z\left\{G_{3D}(x,y,z,\omega)\right\}|_{k_z=0}\,, \tag{2.45}$$

obviously holding for any other representation, as it is reflected by the table above.

2.3.2 Solution of the general inhomogeneous wave equation

Now the solution of the general inhomogeneous wave equation, given by (2.13) is presented. From (2.40) the solution in the spatial domain is obtained by the convolution of the source term with the Green's function [3]:

$$P(\mathbf{x},t) = -\int_{\Omega} \mathrm{j}\omega\rho_0 Q(\mathbf{x}_0,\omega)G(\mathbf{x}-\mathbf{x}_0,\omega) + \langle \mathbf{F}(\mathbf{x}_0,\omega)\cdot\nabla_{\mathbf{x}}\,G(\mathbf{x}-\mathbf{x}_0,\omega)\rangle\,\mathrm{d}\Omega(\mathbf{x}_0), \tag{2.46}$$

where $\Omega(\mathbf{x})$ is the domain of interest, containing the source distribution. From the general solution the case of point-like disturbances are of special interest, with the distribution function described by a Dirac distribution:

- supposing that $Q(\mathbf{x},\omega) = Q(\omega)\delta(\mathbf{x})$ one obtains the field response to a point-like volume injection

$$P_{\mathrm{m}}(\mathbf{x},\omega) = -\frac{\mathrm{j}\omega\rho_0 Q(\omega)}{4\pi}\frac{\mathrm{e}^{-\mathrm{j}\frac{\omega}{c}|\mathbf{x}-\mathbf{x}_0|}}{|\mathbf{x}-\mathbf{x}_0|}. \tag{2.47}$$

  This is the field of an *acoustic monopole*, which is defined as a pulsating sphere, with its radius decreased to infinitesimal while the total volume velocity held constant [How07]. $Q(\omega)$ is often referred to as *monopole strength*. Monopoles

[3] The second term can be obtained by integration by parts: $\int \nabla\cdot\mathbf{F}(\mathbf{x}_0)G(\mathbf{x}-\mathbf{x}_0)\mathrm{d}\mathbf{x}_0 = \int \nabla\cdot(\mathbf{F}(\mathbf{x}_0)G(\mathbf{x}-\mathbf{x}_0))\,\mathrm{d}\mathbf{x}_0 - \int\langle\nabla G(\mathbf{x}-\mathbf{x}_0)\cdot\mathbf{F}(\mathbf{x}_0)\rangle\,\mathrm{d}\mathbf{x}_0$. Applying the Gauss theorem and invoking the Sommerfeld radiation condition reveals that the first term of the right handside vanishes.

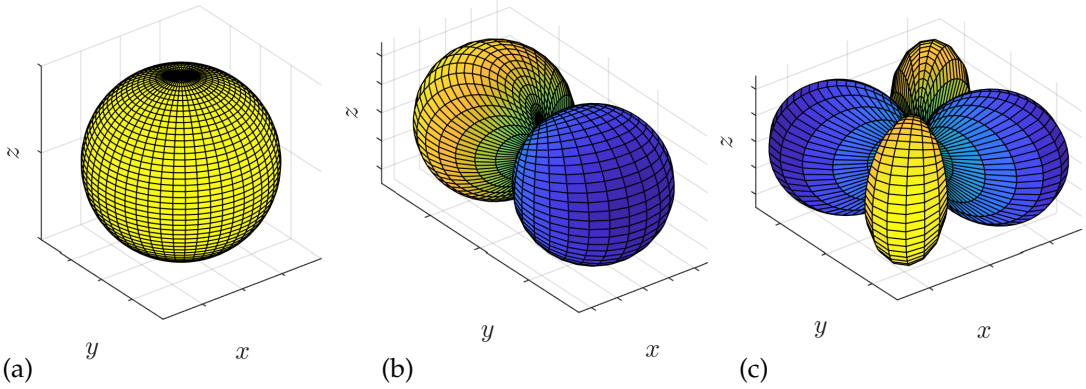

Figure 2.4. Qualitative illustration of the directivity characteristics of a monopole (a), a dipole with the dipole axis being the y axis (b) and a horizontal quadrupole constructed from two opposing dipoles in the horizontal plane (c). In the figures the distance from the origin denotes the absolute value of the directivity into the given direction, with the sign indicated by the color of the surface.

constitute a good farfield approximation of sources in the velocity field, e.g. a dynamical loudspeaker acting on a closed cabinet.

- assuming a point-like force excitation, described by $\mathbf{F}(\mathbf{x},\omega) = \mathbf{f}F(\omega)\delta(\mathbf{x})$, where the unit vector $\mathbf{f}$ denotes the direction of the force the solution for the inhomogeneous wave equation is given by

$$P_\mathrm{d}(\mathbf{x},\omega) = -F(\omega)\left\langle \mathbf{f}\cdot\nabla_\mathbf{x} G(\mathbf{x},\omega)\right\rangle . \tag{2.48}$$

The expression describes the field generated by an *acoustic dipole*, with vector $F(\omega)\mathbf{f}$ denoting the *dipole moment*. The terminology reflects that an acoustic dipole can be constructed by two antiphase point sources positioned infinitesimally close to each other [4]. By expressing the gradient of the Green's function the full form of a dipole field is given as

$$P_\mathrm{d}(\mathbf{x},\omega) = \hat{F}(\omega)\cos\theta\cdot\left(\frac{1}{|\mathbf{x}-\mathbf{x}_0|}+\mathrm{j}\frac{\omega}{c}\right)\frac{1}{4\pi}\frac{\mathrm{e}^{-\mathrm{j}\frac{\omega}{c}|\mathbf{x}-\mathbf{x}_0|}}{|\mathbf{x}-\mathbf{x}_0|}. \tag{2.49}$$

with $\cos\theta = \frac{\langle\mathbf{f}\cdot(\mathbf{x}-\mathbf{x}_0)\rangle}{|\mathbf{x}-\mathbf{x}_0|}$. Unlike monopoles, dipoles are directive sources, with the directivity characteristics described by $\cos\theta$. Dipoles give a good model for e.g. unbaffled loudspeakers, moving freely in the fluid, radiating maximally into the direction of motion $\mathbf{f}$ often termed the *dipole axis*, and without any lateral radiation.

The importance of monopoles and dipoles along with higher order *multipoles* lies in the farfield approximation of the field of extended sources, where a complex radiation pattern may be expanded into series of weighted multipole fields, termed *multipole expansion*. Figure 2.4 presents the directivity pattern of multipoles up to the third order. All multipoles are solutions to the wave equation due to its linearity.

[4] Such a distribution can be described by the directional gradient of a Dirac distribution $s(\mathbf{x},\omega) = \langle\mathbf{f}\cdot\nabla\delta(\mathbf{x})\rangle$.

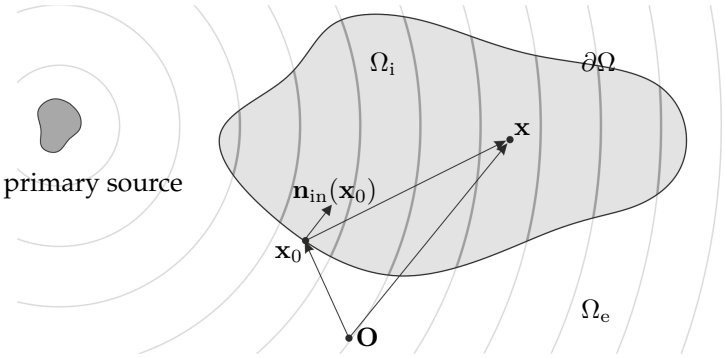

Figure 2.5. Geometry for the interior Kirchhoff-Helmholtz integral, representing the sound field inside an enclosure Ω_i generated by an exterior sound source in the form of a surface integral along $\partial\Omega$. For 2D problems the boundary degenerates to a closed contour, enclosing the area Ω_i.

Comparison of $\tilde{G}(k_x, y, k_z, \omega)$ in Table 2.1 with the pressure and velocity propagators (2.34) and by applying the Fourier differentiation theorem (2.31) reveals that

$$\tilde{G}_p(k_x, y, k_z, \omega) = 2\mathrm{j}k_y\tilde{G}(k_x, y, k_z, \omega) \;\; \rightarrow \;\; G_p(\mathbf{x}, \omega) = -2\frac{\partial}{\partial y}G(\mathbf{x}, \omega) = 2P_\mathrm{d}(\mathbf{x}, \omega), \tag{2.50}$$

$$\tilde{G}_v(k_x, y, k_z, \omega) = 2\mathrm{j}\omega\rho_0\tilde{G}(k_x, y, k_z, \omega) \;\; \rightarrow \;\; G_v(\mathbf{x}, \omega) = 2\mathrm{j}\omega\rho_0 G(\mathbf{x}, \omega) = -2P_\mathrm{m}(\mathbf{x}, \omega), \tag{2.51}$$

holds, i.e. the pressure and velocity propagators are given by the fields of dipoles and monopoles respectively. This finding will be further discussed in the section dealing with the Rayleigh integral formulation.

2.4 Boundary integral representation of sound fields

2.4.1 The Kirchhoff-Helmholtz integral equation

Any sound field obeying the homogeneous Helmholtz equation may be written in the form of a surface integral above an enclosing surface, termed the *Kirchhoff-Helmholtz integral equation*. This integral formulation, solving the homogeneous wave equation with inhomogeneous boundary conditions is of central importance in the field of acoustics, e.g. forming the backbone of the Boundary Element Method [Kir07; MN08], SVD-based Conformal Nearfield Acoustic Holography [Bai92; Wil99; Wu10], and sound field synthesis.

In this section the integral formulation of interior problems in source-free volumes is introduced, describing the sound field, generated by a *primary source* outside the volume of investigation. The effect of sources inside the enclosure may be straightforwardly included in the following results by the appropriate addition of the solution of the inhomogeneous Helmholtz equation [Spo05].

Let Ω_i be an n-dimensional enclosure, bounded by the surface $\partial\Omega$ with arbitrary position vectors $\mathbf{x}_0, \mathbf{x} \in \mathbb{R}^\mathrm{n}$. Refer to Figure 2.5 for the geometry. For two continuous, differentiable scalar valued functions $\Phi(\mathbf{x}_0)$, $\Psi(\mathbf{x}_0)$ the Green's theorem reads

$$\int_{\Omega_\mathrm{i}} \left(\Phi(\mathbf{x}_0)\nabla^2_{\mathbf{x}_0}\Psi(\mathbf{x}_0) - \Psi(\mathbf{x}_0)\nabla^2_{\mathbf{x}_0}\Phi(\mathbf{x}_0)\right) \mathrm{d}\Omega_\mathrm{i}(\mathbf{x}_0) = \\ = \oint_{\partial\Omega} \left(\Psi(\mathbf{x}_0)\frac{\partial\Phi(\mathbf{x}_0)}{\partial\mathbf{n}_\mathrm{in}} - \Phi(\mathbf{x}_0)\frac{\partial\Psi(\mathbf{x}_0)}{\partial\mathbf{n}_\mathrm{in}}\right) \mathrm{d}\partial\Omega(\mathbf{x}_0), \quad (2.52)$$

with $\frac{\partial}{\partial\mathbf{n}_\mathrm{in}}$ denoting the inward normal derivative $\langle\mathbf{n}_\mathrm{in}(\mathbf{x}_0)\cdot\nabla_{\mathbf{x}_0}\Phi(\mathbf{x}_0)\rangle$. Let $\Phi : P$ be the pressure field inside the enclosure and $\Psi : G$ be the Green's function located at $\mathbf{x}$, satisfying[5]

$$(\nabla^2_{\mathbf{x}_0} + k^2)P(\mathbf{x}_0,\omega) = 0, \qquad (\nabla^2_{\mathbf{x}_0} + k^2)G(\mathbf{x}_0|\mathbf{x},\omega) = -\delta(\mathbf{x}_0 - \mathbf{x}). \quad (2.53)$$

Substituting into the Green's theorem leads to

$$-\int_{\Omega_\mathrm{i}} P(\mathbf{x}_0,\omega)\delta(\mathbf{x}_0-\mathbf{x})\mathrm{d}\Omega_\mathrm{i}(\mathbf{x}_0) = \oint_{\partial\Omega}\left(G(\mathbf{x}_0|\mathbf{x},\omega)\frac{\partial P(\mathbf{x}_0,\omega)}{\partial\mathbf{n}_\mathrm{in}} - P(\mathbf{x}_0,\omega)\frac{\partial G(\mathbf{x}_0|\mathbf{x},\omega)}{\partial\mathbf{n}_\mathrm{in}}\right)\mathrm{d}\partial\Omega(\mathbf{x}_0). \quad (2.54)$$

The sifting property of the Dirac-delta may be exploited by taking into account that the singularity is located in the enclosure: if $\mathbf{x}$ lies outside the volume the integral is identically zero, while if it is on the surface it is assumed that "only half of the Dirac-impulse is in the volume". For a rigorous derivation refer to [Wil99]. Finally, by exploiting the symmetry and translation invariancy of the free field Green's function (2.38) the *Kirchhoff-Helmholtz integral equation* (KHIE) is obtained:

Kirchhoff-Helmholtz integral

$$\alpha P(\mathbf{x},\omega) = \oint_{\partial\Omega} -\left(\frac{\partial P(\mathbf{x}_0,\omega)}{\partial\mathbf{n}_\mathrm{in}}G(\mathbf{x}-\mathbf{x}_0,\omega) - P(\mathbf{x}_0,\omega)\frac{\partial G(\mathbf{x}-\mathbf{x}_0,\omega)}{\partial\mathbf{n}_\mathrm{in}}\right)\mathrm{d}\partial\Omega(\mathbf{x}_0), \quad (2.55)$$

with

$$\alpha = \begin{cases} 1 & \forall \quad \mathbf{x}\in\Omega_\mathrm{i} \\ \frac{1}{2} & \forall \quad \mathbf{x}\in\partial\Omega \\ 0 & \forall \quad \mathbf{x}\in\Omega_\mathrm{e}. \end{cases}$$

The equation states that the pressure field inside an enclosure is completely determined by the boundary conditions for the pressure and normal velocity on the boundary surface. The interior KHIE describes the pressure field only inside the volume of investigation, outside the volume the left-hand side is identically zero. For exterior radiation problems the exterior KHIE can be derived in a similar manner, describing the pressure field outside the volume and ensuring zero left-hand side inside [Wil99]. In both cases the approach is capable of dealing only with *forward propagation problems* i.e. capable to describe the effects of a source distribution based on the radiated field measured on a surface, but unable to describe the source properties from these data.

[5] Although the continuity requirement is not fulfilled for the Green's function, with proper mathematical workaround the singularity at $\mathbf{x}$ may be excluded from the enclosure [Wil99].

This latter scenario is called an acoustic *inverse problem*, forming the basis of Acoustic Holography and sound field synthesis [6].

A frequently used form of the KHIE—obtained by utilizing the Euler's equation (2.8) to express the normal derivative of the pressure in terms of the normal velocity on the surface—, is given as

$$\alpha P(\mathbf{x},\omega) = \oint_{\partial\Omega} \Big(V_\mathrm{n}(\mathbf{x}_0,\omega) \underbrace{\mathrm{j}\omega\rho_0 G(\mathbf{x}-\mathbf{x}_0,\omega)}_{-P_\mathrm{m}(\mathbf{x}-\mathbf{x}_0,\omega)} + P(\mathbf{x}_0,\omega) \underbrace{\frac{\partial G(\mathbf{x}-\mathbf{x}_0,\omega)}{\partial \mathbf{n}_\mathrm{in}}}_{-P_\mathrm{d}(\mathbf{x}-\mathbf{x}_0,\omega)} \Big) \mathrm{d}\partial\Omega(\mathbf{x}_0), \tag{2.56}$$

where the weighting factors containing the Green's function can be recognized as the fields of monopoles and dipoles, acting as velocity and pressure propagators similarly to the angular spectrum approach. KHIE therefore consists of two integral components, termed the *single layer potential* and the *double layer potential*: single layer potential describes the field of the weighted sum of a single layer of point sources, characterized by $G(\mathbf{x}|\mathbf{x}_0)$, while the double layer potential describes the field of an ensemble of dipole point sources, described by $\frac{\partial G(\mathbf{x}|\mathbf{x}_0,\omega)}{\partial \mathbf{n}_\mathrm{in}}$, realized by two anti-phase point sources: by a double layer.

The interior KHIE represents the sound field inside the domain of interest and ensures zero pressure outside, by utilizing both a single and a double layer potential[7]. In the aspect of sound field synthesis the presence of both layers is infeasible. By letting the sound field to be non-zero outside the enclosure it is possible to completely describe the sound field in the region of interest in terms of only single or double layer potentials. This is achieved by either modifying the Green's function in order to satisfy Dirichlet or Neumann boundary conditions, or imposing these boundary conditions on the sound field $P(\mathbf{x},\omega)$ itself in an equivalent scattering problem. In the following these approaches are introduced for the simplification of the KHIE.

2.4.2 The simple source formulation

The simple source formulation is derived from the KHIE by the construction of a separate exterior and interior radiation problem with prescribing the same inhomogeneous Dirichlet boundary condition for both fields on the boundary surface $\partial\Omega$ [Cop68].

Consider an exterior sound field $P_\mathrm{e}(\mathbf{x},\omega)$ in the geometry depicted in Figure 2.5, satisfying the homogeneous Helmholtz equation at $\mathbf{x} \in \Omega_\mathrm{e}$, meaning that all sources are located within the enclosure. The exterior wavefield is the combination of radiating, or diverging waves. On the other hand consider an interior sound field $P_\mathrm{i}(\mathbf{x},\omega)$ inside the enclosure $\mathbf{x} \in \Omega_i$, induced by a sound source located outside the volume of investigation. The interior field, constructed by a set of incoming or converging waves, also satisfies the homogeneous Helmholtz equation in the interior domain. The two

[6] Actually, the KHIE can be made able to solve inverse problems, by replacing the forward propagating Green's function by the backward propagating Green's function [WB89].

[7] Loosely speaking the anti-phase side of the double layer cancels the field of the single layer outside the region of interest.

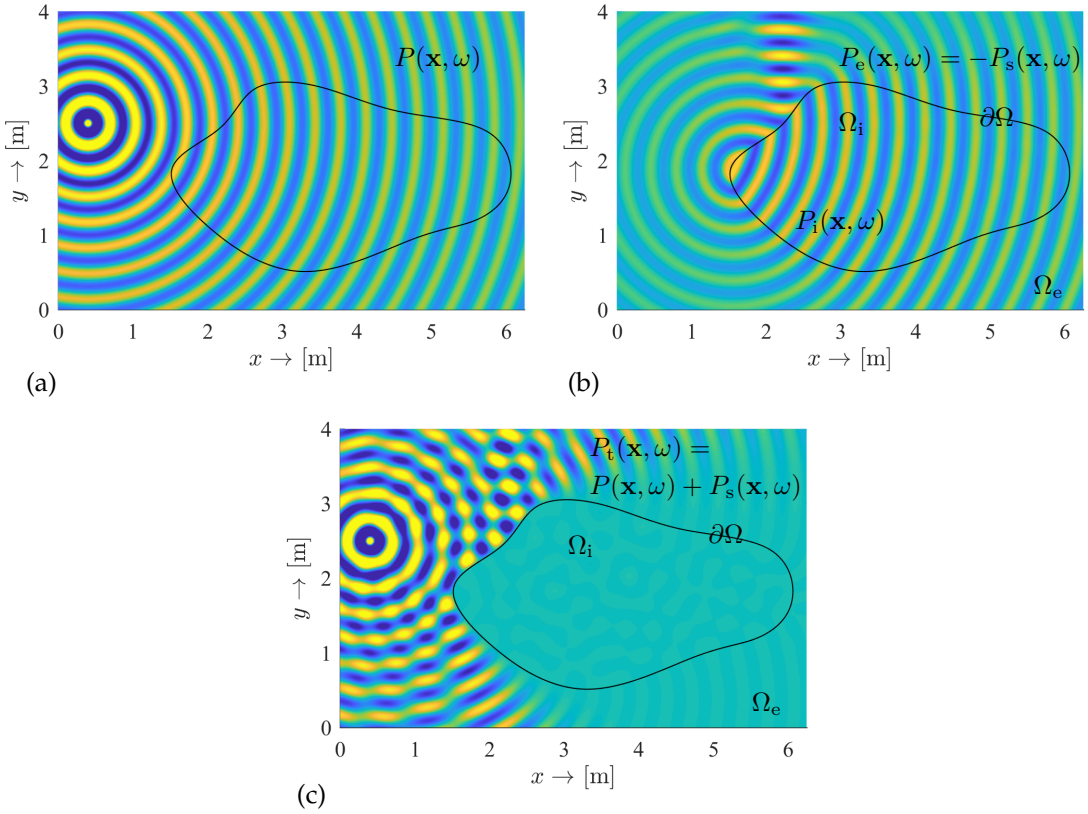

Figure 2.6. Illustration of the simple source formulation in a 2D interior problem ($\Omega \subset \mathbb{R}^2$). Figures show the incident/primary sound field (a), the field given by the simple source formulation (b) and the scattering of the incident field from a sound soft boundary (c). The incident field is the field of a 2D point source (i.e. a line source) located at $\mathbf{x}_\mathrm{s} = [-0.4,\ 2.5]^\mathrm{T}$ oscillating at $f_0 = 1$ kHz, with $f = \frac{\omega}{2\pi}$. Equation (2.58) was evaluated numerically using an open source C++ Boundary Element software [FR14]. The figures demonstrate, how simple source formulation expresses the incident field inside Ω_i, and the (-1) times the scattered field at Ω_e in an equivalent sound soft scattering problem. Figure (c) showing the difference between the incident field and the simple source field ((a)-(b)) therefore illustrates the total scattering in the exterior domain.

spatially disjunct problems are connected through the following boundary condition written onto the boundary surface

$$P_\mathrm{e}(\mathbf{x}_0,\omega) = P_\mathrm{i}(\mathbf{x}_0,\omega), \qquad \mathbf{x}_0 \in \partial\Omega. \tag{2.57}$$

Both fields may be expressed in terms of an exterior and an interior KHIE respectively. For the exterior KHIE expressed in terms of the inward normals refer to [Wil99, eq. 8.30]. By adding the exterior and interior KHIEs terms, weighted by the pressure on the boundary, will vanish due to the coupled boundary condition and the following integral expression is obtained [CH62; Kel67; Wil99]

$$\oint_{\partial\Omega} \left(\frac{\partial P_\mathrm{e}(\mathbf{x}_0,\omega)}{\partial \mathbf{n}_\mathrm{in}} - \frac{\partial P_\mathrm{i}(\mathbf{x}_0,\omega)}{\partial \mathbf{n}_\mathrm{in}} \right) G(\mathbf{x}-\mathbf{x}_0,\omega)\mathrm{d}\partial\Omega(\mathbf{x}_0) = \begin{cases} P_\mathrm{e}(\mathbf{x},\omega) & \forall \quad \mathbf{x} \in \Omega_e \\ P_\mathrm{e} = P_\mathrm{i} & \forall \quad \mathbf{x} \in \partial\Omega \\ P_\mathrm{i}(\mathbf{x},\omega) & \forall \quad \mathbf{x} \in \Omega_\mathrm{i}. \end{cases} \tag{2.58}$$

Simple source formulation

The equation states that either the interior or the exterior sound field, satisfying the homogeneous Helmholtz equation may be represented as a single layer potential, with the *single layer strength function* given in the integral (2.58) implicitly. The expression of this strength function, obtained as the amount of discontinuity in the pressure gradient is often termed the *jump relation*, indicating the fact that the sound field generated by the single layer potential is continuous in pressure on the boundary, while the gradient changes sign i.e. *jumps*.

As pointed out in [SS14; Faz10; FN13; ZS13] the following physical interpretation can be assigned to the simple source formulation: Suppose that the surface $\partial\Omega$ represents the boundary of a sound soft scattering object. In acoustic scattering problems it is assumed that an the *incident sound field* $P(\mathbf{x},\omega)$ that is reflected by the scattering object, generating the *scattered field* $P_\mathrm{s}(\mathbf{x},\omega)$ is known a priori. The field measured in the presence of the obstacle is termed the *total field* $P_\mathrm{t}(\mathbf{x},\omega)$, given by the sum of the incident and scattered fields, so that the total field obeys homogeneous boundary conditions on the sound soft scatterer surface, i.e. $P_\mathrm{s}(\mathbf{x}_0,\omega) = -P(\mathbf{x}_0,\omega),\ \ \mathbf{x}_0 \in \partial\Omega$. In this interpretation the incident field corresponds to the interior solution $P(\mathbf{x},\omega) \sim P_\mathrm{i}(\mathbf{x},\omega)$, while the scattered field corresponds to the exterior solution with reversed sign $P_\mathrm{s}(\mathbf{x},\omega) \sim -P_\mathrm{e}(\mathbf{x},\omega)$.

Comparing this result with the simple source formulation it is clear that the single layer strength function is the derivative of (-1) times the total field on the boundary. See Figure 2.6 for an illustration of the simple source formulation and for its interpretation as an equivalent scattering problem. In the presented general 2D scenario the single layer weighting factors were calculated numerically for an arbitrary enclosing reflecting surface.

2.4.3 The Rayleigh integrals

The Rayleigh integrals formulate a sound field based on the pressure field or the normal velocity measured along an infinite plane utilizing the Neumann or Dirichlet Green's functions.

In order to derive the Rayleigh integrals an interior problem is described by the KHIE written on a simply joint boundary, consisting of a disc $\partial\Omega_P$ and hemisphere $\partial\Omega_S$, as shown in Figure 2.7. With the radius of the hemisphere increased to infinity ($r \to \infty$) the Sommerfeld radiation condition is invoked and the contribution of the hemisphere vanishes: the radiated field is described by a surface integral written on an infinite plane, termed here the *Rayleigh plane*. The plane is located at $y = 0$ with its normal given by $\mathbf{n}_\mathrm{in} = [0,\ 1,\ 0]^\mathrm{T}$ and all the primary sources of sound are located at $y < 0$. In this geometry the KHIE (2.55) describing the field at $\mathbf{x} = [x,\ y > 0,\ z]^\mathrm{T}$ degenerates to

$$P(\mathbf{x},\omega) = \lim_{r\to\infty}\left(\int_{\partial\Omega_P} \mathrm{d}\partial\Omega_P + \int_{\partial\Omega_S} \mathrm{d}\partial\Omega_S\right) = \int_{\partial\Omega_P}\left(P(\mathbf{x}_0,\omega)\left.\frac{\partial G(\mathbf{x}_0|\mathbf{x},\omega)}{\partial y_0}\right|_{y_0=0} - \left.\frac{\partial P(\mathbf{x}_0,\omega)}{\partial y_0}\right|_{y_0=0} G(\mathbf{x}_0|\mathbf{x},\omega)\right)\mathrm{d}\partial\Omega_P(\mathbf{x}_0). \quad (2.59)$$

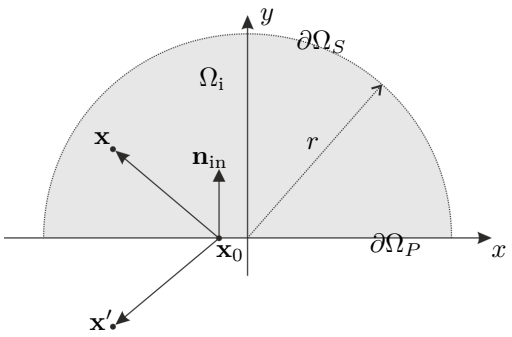

Figure 2.7. Geometry for deriving the Rayleigh integrals. The radius of the hemisphere $\partial\Omega_S$ is increased to infinity, therefore only the Rayleigh plane $\partial\Omega_P$ contributes to the radiated field at $y > y_0$. For this special geometry the required Neumann and Dirichlet Green's functions are given by the sum of a point source at the evaluation point $\mathbf{x}$ and a point source, positioned at $\mathbf{x}'$, obtained by mirroring $\mathbf{x}$ to the Rayleigh plane.

Obviously, any homogeneous solution of the Helmholtz equation may be added to the Green's function, the inhomogeneous wave equation and the Kirchhoff-Helmholtz integral still holds [8]. In the following this fact is exploited in order to eliminate either the single or the double layer potential in (2.59) by finding a proper additive term to the Green's function:

- The *Neumann Green's function* eliminates the double layer potential by describing Neumann boundary conditions for the Green's function along the infinite plane:

$$G_N(\mathbf{x}_0, \omega) = G(\mathbf{x}_0|\mathbf{x}, \omega) + G'_N(\mathbf{x}_0, \omega), \tag{2.60}$$

$$\frac{\partial G_N(\mathbf{x}_0, \omega)}{\partial \mathbf{n}_\mathrm{in}} = \frac{\partial G_N(\mathbf{x}_0, \omega)}{\partial y_0} = 0, \quad \forall \quad \mathbf{x}_0 \in \partial\Omega_P. \tag{2.61}$$

- The *Dirichlet Green's function* eliminates the single layer potential by describing Dirichlet boundary conditions for the Green's function, given by

$$G_D(\mathbf{x}_0, \omega) = G(\mathbf{x}_0|\mathbf{x}, \omega) + G'_D(\mathbf{x}_0, \omega) = 0, \quad \forall \quad \mathbf{x}_0 \in \partial\Omega_P. \tag{2.62}$$

In the general case of an arbitrary shaped enclosing surface the Neumann and Dirichlet Green's functions are given by the scattered field of a point source positioned at $\mathbf{x}$, reflected from a rigid or a sound soft boundary respectively. Their actual form therefore would depend on the evaluation point $\mathbf{x}$. In the present geometry the scattered field of a point source from a rigid or sound soft infinite plane can be easily obtained by mirroring the in-phase or anti-phase source to the scatterer plane, and the required Green's functions are given as

$$G_N(\mathbf{x}_0, \omega) = G(\mathbf{x}_0|\mathbf{x}, \omega) + G(\mathbf{x}_0|\mathbf{x}', \omega) \tag{2.63}$$

$$G_D(\mathbf{x}_0, \omega) = G(\mathbf{x}_0|\mathbf{x}, \omega) - G(\mathbf{x}_0|\mathbf{x}', \omega) \tag{2.64}$$

with $\mathbf{x}' = [x,\ 2y_0 - y,\ z]^\mathrm{T}$ as illustrated in Figure 2.7.

[8] This property can be exploited in order to solve the inhomogeneous wave equation in the presence of boundaries, by taking the reflected field into consideration.

Substituting them into the integral (2.59) with exploiting the symmetry and the translation invariance of the Green's function yields the Rayleigh I and II (or Neumann and Dirichlet) integrals respectively [Ber84]:

Rayleigh I and Rayleigh II integrals

$$P(\mathbf{x},\omega) = \int_{\partial\Omega_P} -2\,\frac{\partial P(\mathbf{x},\omega)}{\partial y_0}\bigg|_{y_0=0} G(\mathbf{x}-\mathbf{x}_0,\omega)\mathrm{d}\partial\Omega_P(\mathbf{x}_0) \tag{2.65}$$

$$P(\mathbf{x},\omega) = \int_{\partial\Omega_P} 2P(\mathbf{x}_0,\omega)\,\frac{\partial G(\mathbf{x}-\mathbf{x}_0,\omega)}{\partial y_0}\bigg|_{y_0=0} \mathrm{d}\partial\Omega_P(\mathbf{x}_0). \tag{2.66}$$

Obviously, the Rayleigh integrals do not ensure a zero sound field behind the Rayleigh plane at $y < 0$. In this region the Rayleigh I integral expresses the field of the primary source distribution, reflected from an infinite rigid plane, while the Rayleigh II integral gives that from a sound soft planar boundary according to the equivalent scattering interpretation.

In the present thesis the Rayleigh I integral is of special importance, being a single layer potential. As well as forming the basis of traditional Wave Field Synthesis it is used extensively for the calculation of radiated field from finite radiators, mounted in infinite walls, e.g. the field of loudspeaker pistons as given in Appendix E.1. The integral states that the radiated field from a rigid vibrating plane can be calculated by summing the field of point sources on the surface, driven by the normal velocity distribution, or mathematically speaking by convolving the Green's function with the velocity distribution over the infinite surface.

Besides the presented methodology, involving the Neumann and Dirichlet Greeen's function, the Rayleigh integral can be deduced directly using the equivalent scattering interpretation of the simple source approach: for a planar reflecting surface the reflected field can be obtained by mirroring the incident field to the scatterer, resulting in the same formulation. Another straightforward way to obtain the Rayleigh integrals stems from the direct inverse Fourier transform of the angular spectrum representations (2.32) and (2.33) by applying the Fourier transform convolution theorem and applying that the pressure and velocity propagators are given by the field of dipoles and monopoles, as it was stated in Section 2.3.2. The fact that all the presented three approaches lead to the same solution stems from the uniqueness of the single layer problem for a planar boundary. However this can not be generalized towards arbitrary boundary shapes: the coincidence of the Dirichlet/Neumann and the free space Green's function holds only for the present, simple geometry.

3 High frequency approximation of wavefields and radiation problems

The boundary integral representations introduced in the previous section give the possibility for controlling the sound field inside enclosures. However their direct application for sound field synthesis is of great computational complexity for arbitrary geometries. In order to derive integral representations more suitable for general sound field reproduction, the application of approximate solutions are inevitable. This chapter presents several high frequency asymptotic approximations of sound fields and their integral representations. These approximations will be of crucial interest for finding the driving function for general loudspeaker contours in the latter sections.

The presented local/asymptotic description of wavefields is not unknown in the fields of acoustics: with minor modifications it is a massively used concept in ray tracing and geometrical optics/acoustics. However, its application for sound field synthesis problems has been unprecedented so far.

3.1 Local attributes of sound fields

3.1.1 The local wavenumber vector

Consider an arbitrary steady-state harmonic sound field in $\mathbf{x} \in \mathbb{R}^3$ written in a general polar form with $A^P(\mathbf{x},\omega)$, $\phi^P(\mathbf{x},\omega) \in \mathbb{R}$

$$P(\mathbf{x},\omega) = A^P(\mathbf{x},\omega)\mathrm{e}^{\mathrm{j}\phi^P(\mathbf{x},\omega)}. \tag{3.1}$$

The dynamics of wave propagation is described by the phase of the sound field. From ray-tracing/geometrical optics theory the following quantity is introduced [BG04; Roe05]:

$$\mathbf{k}^P(\mathbf{x}) = -\nabla_{\mathbf{x}}\,\phi^P(\mathbf{x},\omega), \tag{3.2}$$

Local wavenumber vector

termed the *local wavenumber vector* of sound field P, being obviously the generalization of the plane wave wavenumber vector introduced by equation (2.26)[1]. Note that the local wavenumber vector is frequency dependent, which dependency is suppressed for the sake of brevity. In Cartesian coordinates the components of the local

[1] The negative sign ensures that the phase of the sound field decreases into the propagation direction, similarly to the case of a plane wave

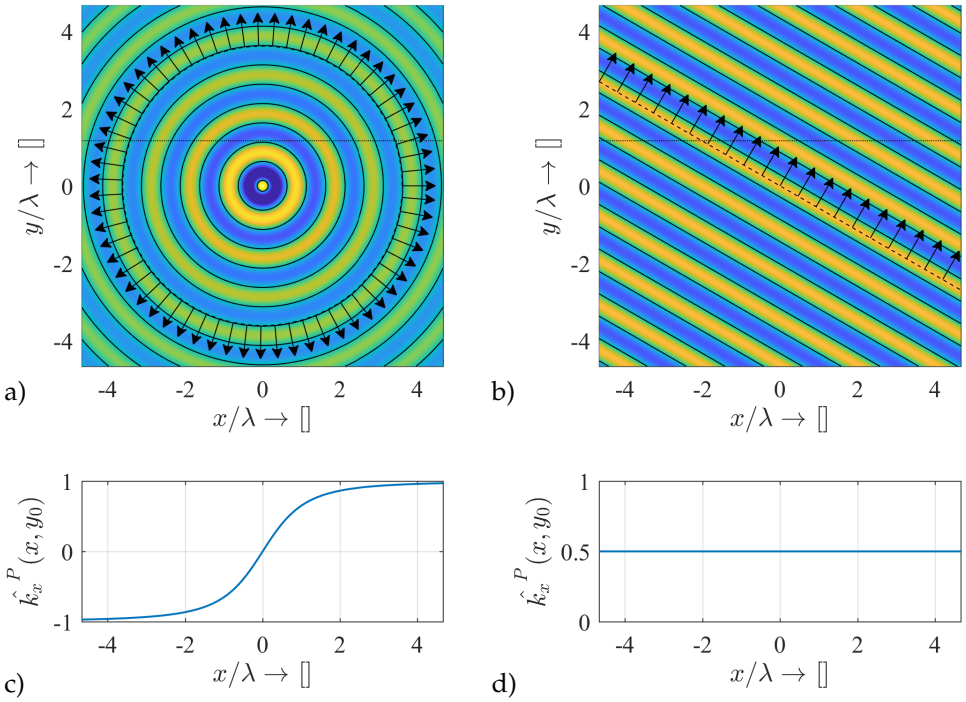

Figure 3.1. Illustration of the local wavenumber vector for a 2D acoustic point source (a,c) and a 2D plane wave (b,d). (a-b) show an arbitrarily chosen contour of constant phase (isochronous contour), along with the wavenumber vector on this contour. (c-d) show the x-component of the normalized local wavenumber vector ($\hat{k}_x(x, y_0)$), measured along the horizontal dashed black lines.

wavenumber vector are denoted as $\mathbf{k}^P(\mathbf{x}) = [k_x^P(\mathbf{x}),\ k_y^P(\mathbf{x}),\ k_z^P(\mathbf{x})]^{\mathrm{T}}$. In the following the existence of the superscript distinguishes local properties from the global ones, i.e. local wavenumber components of spectral decomposition. The wavenumber vector, defined as the negative gradient of the phase function points into the direction of maximal phase advance, i.e. it is perpendicular to the wavefront in any position. For an isotropic medium, where the propagation speed is constant the wavenumber vector points in the direction of the wave's energy flow, thus towards the local wave propagation direction [2].

Introducing the general formulation (3.1) into the Helmholtz equation (2.9), expressing the Laplace operator by its definition $\nabla_{\mathbf{x}}^2 = \nabla_{\mathbf{x}} \cdot \nabla_{\mathbf{x}}$ and expressing the derivative of the polar form yields (for the sake of transparency with suppressed function arguments)

$$\left(\frac{\nabla_{\mathbf{x}}^2 A^P}{A^P} - |\nabla_{\mathbf{x}} \phi^P|^2 + \mathrm{j} \left(\nabla_{\mathbf{x}}^2 \phi^P + 2 \frac{\left\langle \nabla_{\mathbf{x}} \phi^P \cdot \nabla_{\mathbf{x}} A^P \right\rangle}{A^P} \right) + \left(\frac{\omega}{c} \right)^2 \right) P = 0, \tag{3.3}$$

valid in an arbitrary coordinate system.

[2] This statement holds exclusively for isotropic media. Although the wavenumber vector is always perpendicular to the wavefront, in anisotropic media the energy of a wave not necessarily travels along the path as the wavefront normals [Pol77].

In order to have the equality satisfied for an arbitrary sound field both real and imaginary parts of the bracketed term have to vanish, resulting in the following equations:

$$\frac{\nabla_{\mathbf{x}}^2 A^P}{A^P} - |\nabla_{\mathbf{x}} \phi^P|^2 + \left(\frac{\omega}{c}\right)^2 = 0, \tag{3.4}$$

$$\nabla_{\mathbf{x}}^2 \phi^P + 2\frac{\left\langle \nabla_{\mathbf{x}} \phi^P \cdot \nabla_{\mathbf{x}} A^P \right\rangle}{A^P} = 0. \tag{3.5}$$

Assuming high frequency conditions, the phase changes rapidly compared to the amplitude, i.e. $\frac{\nabla_{\mathbf{x}}^2 A^P}{A^P} \ll |\nabla_{\mathbf{x}} \phi^P|^2$ holds, and by utilizing the definition of the local wavenumber vector equation (3.4) leads to the *local dispersion relation*

Local dispersion relation

$$|\mathbf{k}^P(\mathbf{x})|^2 = k_x^P(\mathbf{x})^2 + k_y^P(\mathbf{x})^2 + k_z^P(\mathbf{x})^2 = \left(\frac{\omega}{c}\right)^2 = k^2, \tag{3.6}$$

being again a generalization of the dispersion relation, given for plane waves by (2.22). Note that for the sake of brevity The equation holds trivially for simple sound fields: for plane waves, point sources and line sources excluding the singular point [3], however fails in the presence of strong interference phenomena, due to which the amplitude distribution varies rapidly over the space. Furthermore, the present form of the local dispersion relation is valid only for stationary sound fields in isotropic media. In Chapter 5 the theory will be extended to include non-stationary fields through the example of the sound field generated by a moving harmonic source.

Applying the local dispersion relation the *normalized local wavenumber vector* can be defined for a stationary sound field as

$$\hat{\mathbf{k}}^P(\mathbf{x}) = \frac{\mathbf{k}^P(\mathbf{x})}{|\mathbf{k}^P(\mathbf{x})|} = \frac{\mathbf{k}^P(\mathbf{x})}{\omega/c}, \tag{3.7}$$

being a vector of unit length (independent from frequency), pointing in the local propagation direction of the sound field. The normalized wavenumber vector, i.e. the normalized phase change of wavefields is a basic concept in ray tracing, massively used for solving wave propagation problems in anisotropic media. In the field of ray tracing expression $\Gamma(\mathbf{x}) = -\frac{\phi^P(\mathbf{x},\omega)}{k}$ is termed the *eikonal*, that's gradient defines the local propagation direction of the wavefield: $\nabla\Gamma(\mathbf{x}) = \hat{\mathbf{k}}(\mathbf{x})$. In that context, the local dispersion relation in the form of (3.4) is termed the *eikonal equation* [Pie91; Kin+00], having to be solved for the eikonal often at space-variant sound speeds, yielding the phase change of the sound rays over the ray path. The second basic ray tracing equation termed the *transport equation* is given by (3.5), with its solution providing the intensity change of sound rays.

[3] Since for isotropic media the Green's function's amplitude factor serves as the Green's function for the Laplace equation, satisfying $\nabla_{\mathbf{x}}^2 A^P = \nabla_{\mathbf{x}}^2 \frac{1}{4\pi} \frac{1}{|\mathbf{x}-\mathbf{x}_0|} = -\delta(\mathbf{x}-\mathbf{x}_0)$.

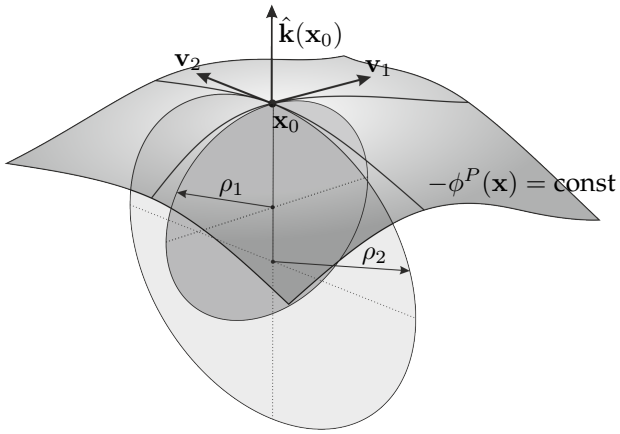

Figure 3.2. Illustration of the principal radii and principal curvatures at $\mathbf{x}_0$ of an arbitrary smooth wavefront, satisfying the local dispersion relation. The principal radii are denoted by ρ_1 and ρ_2, with the corresponding tangent vectors $\mathbf{v}_1$ and $\mathbf{v}_2$ respectively, showing into the direction of the largest and smallest curvature being two eigenvectors of the phase function's Hessian. The principal curvatures are given by the reciprocal of the principal radii. In the present treatise non-converging wavefields are discussed with both principal curvatures being non-negative.

3.1.2 The local wavefront curvature

Applying the local wavenumber vector concept the *local wavefront curvature* of arbitrary sound fields can be introduced. The wavefront curvature and the radius of curvature give an expressive physical interpretation and coordinate system independent description for the results of the asymptotic approximations developed in the following sections, and serves as a mathematical basis in order to distinguish *divergent* and *convergent* wavefronts. A wavefield is termed *divergent* with a convex wavefront propagating away from a source distribution and *convergent* or *focused*, if a concave wavefront propagates towards a focal point. Mathematically the local vergence of the wavefield may be described by the *principal curvatures* of the wavefront, or in a looser sense by the *mean curvature* of the wavefront.

The *principal curvature* components $\kappa_1^P(\mathbf{x}), \kappa_2^P(\mathbf{x})$ are defined geometrically as the reciprocal of the principal radii $\rho_1^P(\mathbf{x}), \rho_2^P(\mathbf{x})$, being the maximal and minimal radii of osculating circles at a point on the wavefront, as illustrated in Figure 3.2. Mathematically as long as the local dispersion relation holds, the principal curvatures are given by the two non-zero eigenvalues of the phase function's negative Hessian, normalized by ω/c, as discussed in details in the Appendix B.1 [Har99; Har01]. A wavefield is then divergent when both principal curvatures are positive [Ble84; Arn86; PT92].

The *mean curvature* of the wavefront—generally defined as the divergence of the surface normal [Gol05]—is given by the divergence of the normalized local wavenumber vector, or the negative trace of the Hessian:

Mean wavefront curvature

$$\overline{\kappa}^P(\mathbf{x}) = \frac{\nabla_{\mathbf{x}} \cdot \hat{\mathbf{k}}^P(\mathbf{x})}{2} = -\frac{\nabla_{\mathbf{x}}^2 \phi^P(\mathbf{x},\omega)}{2k} = -\frac{\left(\frac{\partial^2}{\partial x^2} + \frac{\partial^2}{\partial y^2} + \frac{\partial^2}{\partial z^2}\right)\phi^P(\mathbf{x},\omega)}{2k}, \tag{3.8}$$

with $k = \frac{\omega}{c}$ being the acoustic wavenumber. Employing the transport equation (3.5) the divergence of the local wavenumber vector can be expressed as

$$\overline{\kappa}^P(\mathbf{x}) = -\left\langle \hat{\mathbf{k}}^P(\mathbf{x}) \cdot \frac{\nabla_{\mathbf{x}} A^P(\mathbf{x},\omega)}{A^P(\mathbf{x},\omega)} \right\rangle = -\frac{1}{A^P(\mathbf{x},\omega)} \frac{\partial A^P(\mathbf{x},\omega)}{\partial \hat{\mathbf{k}}^P}, \tag{3.9}$$

hence the transport equation states that at an arbitrary point the relative amplitude change towards the wavefront's propagation direction is given by the mean curvature. This fact results in a formal definition for the vergence of the sound field in a mean sense: a field is divergent if its amplitude decreases in the local propagation direction and convergent if the intensity is focused towards the propagation direction.

As a strict definition—since the mean and the principal curvatures are related as $\overline{\kappa}^P(\mathbf{x}) = \frac{1}{2}\left(\kappa_1^P(\mathbf{x}) + \kappa_2^P(\mathbf{x})\right)$—wavefields may be classified as

$$\kappa_1^P(\mathbf{x}), \kappa_2^P(\mathbf{x}), \overline{\kappa}^P(\mathbf{x}) \begin{cases} > 0 & \text{for a locally diverging/non-focused wavefield} \\ = 0 & \text{for a plane-wave} \\ < 0 & \text{for a locally converging/focused wavefield.} \end{cases} \tag{3.10}$$

Within this thesis only non-converging wavefields will be discussed. Finally, one can define the *Gaussian curvature* of the wavefront, given by $\kappa_1^P \cdot \kappa_2^P$, being only negative, if the wavefront has a saddle point in the point of investigation.

As a summary of the foregoing the local wavenumber vector, the local wavefront curvatures and principal radii are given for frequently used sound field models in Table 3.1, with the Hessian for the Green's function, required for intermediate calculations given by (B.4).

Table 3.1. Local wavenumber vector $\mathbf{k}^P$, local wavefront curvatures κ and radii ρ of a 3D point source, an infinite vertical line source (i.e. a 2D point source) and a 3D plane wave. The phase of the line source is obtained from its high frequency approximation, given by (3.54)

	3D point source $\mathbf{x} = [x,\ y,\ z]^\mathrm{T}$	2D point source $\mathbf{x} = [x,\ y]^\mathrm{T}$	plane wave
$P(\mathbf{x}, \omega)$	$\frac{1}{4\pi}\frac{\mathrm{e}^{-\mathrm{j}k\lvert\mathbf{x}\rvert}}{\mathbf{x}}$	$-\frac{\mathrm{j}}{4}H_0^{(2)}(k\lvert\mathbf{x}\rvert)$	$\mathrm{e}^{-\langle\mathbf{k}\cdot\mathbf{x}\rangle}$
$\mathbf{k}^P(\mathbf{x})$	$\frac{k}{\lvert\mathbf{x}\rvert}\cdot[x,\ y,\ z]^\mathrm{T}$	$\frac{k}{\lvert\mathbf{x}\rvert}\cdot[x,\ y,\ 0]^\mathrm{T}$	$\mathbf{k}$
$\rho_{1,2}^P(\mathbf{x})$	$\lvert\mathbf{x}\rvert$	$\lvert\mathbf{x}\rvert$, ∞	∞
$\kappa_{1,2}^P(\mathbf{x})$	$\frac{1}{\lvert\mathbf{x}\rvert}$	$\frac{1}{\lvert\mathbf{x}\rvert}$, 0	0
$\overline{\kappa}^P(\mathbf{x})$	$\frac{1}{\lvert\mathbf{x}\rvert}$	$\frac{1}{2\lvert\mathbf{x}\rvert}$	0

3.1.3 High frequency gradient approximation

As a further approximation in the high frequency domain, the gradient of an arbitrary sound field may be expressed in a simplified form in terms of the local

wavenumber vector. By applying the product rule of differentiation, the gradient of an arbitrary polar form sound field, described by (3.1) reads as

$$\nabla_{\mathbf{x}} P(\mathbf{x},\omega) = \left(\frac{\nabla_{\mathbf{x}} A^P(\mathbf{x},\omega)}{A^P(\mathbf{x},\omega)} + \mathrm{j}\nabla_{\mathbf{x}} \phi^P(\mathbf{x},\omega)\right) P(\mathbf{x},\omega) = \left(\frac{\nabla_{\mathbf{x}} A^P(\mathbf{x},\omega)}{A^P(\mathbf{x},\omega)} - \mathrm{j}\mathbf{k}^P(\mathbf{x})\right) P(\mathbf{x},\omega). \quad (3.11)$$

In the high frequency region $|\mathbf{k}^P(\mathbf{x})| \approx (\frac{\omega}{c}) \gg \left|\frac{\nabla_{\mathbf{x}} A^P(\mathbf{x},\omega)}{A^P(\mathbf{x},\omega)}\right|$ holds, and the gradient can be approximated as

High freq. gradient appr.

$$\nabla_{\mathbf{x}} P(\mathbf{x},\omega) \approx -\mathrm{j}\mathbf{k}^P(\mathbf{x}) P(\mathbf{x},\omega). \quad (3.12)$$

For an interpretation of the local wavenumber concept and the high frequency gradient approximation the first order Taylor expansion of the phase function may be expressed around an arbitrary point $\mathbf{x}_0$ as

$$\phi^P(\mathbf{x},\omega) \approx \phi^P(\mathbf{x}_0,\omega) + \left\langle (\mathbf{x}-\mathbf{x}_0) \cdot \nabla_{\mathbf{x}} \phi^P(\mathbf{x}_0,\omega) \right\rangle. \quad (3.13)$$

By substitution into (3.1), with a slowly varying amplitude function—i.e. $A^P(\mathbf{x})$ is approximated by the first order Taylor expansion coefficient—in the proximity of $\mathbf{x}_0$ the sound field is approximated as

$$P(\mathbf{x},\omega) \approx P(\mathbf{x}_0,\omega) \mathrm{e}^{-\mathrm{j}\left\langle \mathbf{k}^P(\mathbf{x}_0)\cdot(\mathbf{x}-\mathbf{x}_0)\right\rangle}. \quad (3.14)$$

Therefore each point of a sound field is approximated as a local elementary plane wave, with the wavenumber and angular frequency given by $\mathbf{k}^P(\mathbf{x})$ and ω, respectively. Furthermore expressing the gradient of the local plane wave representation (3.14) leads to the high frequency gradient approximation (3.12) which is therefore obviously the gradient of locally plane wavefields.

Application example: Stereophony

As an application example for the local wavenumber vector concept the resultant sound field of two 3D point sources is investigated, modeling a stereo loudspeaker setup.

The point sources are positioned at a $\mathbf{x}_1 = [x_1,\ y_1,\ z_1 = 0]^{\mathrm{T}}$, $\mathbf{x}_2 = [-x_1,\ y_1,\ z_1 = 0]^{\mathrm{T}}$ in a standard stereo ensemble with the stereo axis being the y-axis, illustrated in Figure 3.3 [Hav+08]. In the case of *amplitude panning* the sources are driven in-phase, with only their frequency independent amplitude factor A_1, A_2 differing. The resultant sound field reads as

$$P(\mathbf{x},\omega) = \frac{A_1}{4\pi} \frac{\mathrm{e}^{-\mathrm{j}\frac{\omega}{c}|\mathbf{x}-\mathbf{x}_1|}}{|\mathbf{x}-\mathbf{x}_1|} + \frac{A_2}{4\pi} \frac{\mathrm{e}^{-\mathrm{j}\frac{\omega}{c}|\mathbf{x}-\mathbf{x}_2|}}{|\mathbf{x}-\mathbf{x}_2|}. \quad (3.15)$$

Generally the phase of the resultant field and the local wavenumber vector is described by a complex formula, derived in C.1. From the aspect of stereophonic applications only the investigation of the local propagation direction on the stereo axis

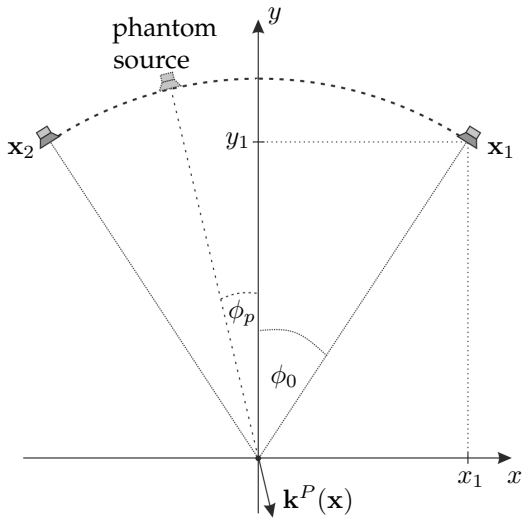

Figure 3.3. General two-channel stereophonic geometry consisting of two point sources positioned symmetrically to the y-axis, termed the *stereo axis*. The *aperture angle* is usually set to $2\phi_0 = 60°$ and the listener's position is at the origin [Rum01]. Simple amplitude panning techniques apply intensity difference between the loudspeaker pair, so that the listener perceives the illusion of a single sound source termed the *phantom source*, placed on the *active arc* between the two loudspeakers.

is of importance, since the listener's position is assumed to be at the origin. On the stereo axis, i.e. the y-axis, the local wavenumber vector simplifies to

$$\mathbf{k}^P(0,y,0) = -\nabla_{\mathbf{x}}\,\phi^P(\mathbf{x},\omega)\Big|_{x=0,z=0} = k\begin{bmatrix} \frac{A_1-A_2}{A_1+A_2}\,\frac{x-x_1}{|\mathbf{x}-\mathbf{x}_1|} \\ \frac{y-y_1}{|\mathbf{x}-\mathbf{x}_1|} \\ \frac{z-z_1}{|\mathbf{x}-\mathbf{x}_1|} = 0 \end{bmatrix}. \tag{3.16}$$

Hence, the local wavenumber vector and the position of the phantom source can be steered in the listener's position over the stereo axis by applying appropriate frequency independent gains to the point source pair in order to control the k_x^P component. The local wavenumber vector for a general stereophonic scenario is illustrated in Figure 3.4.

From (3.16) the gain factors may be expressed assuming that the position of the phantom source or the target propagation direction angle measured from the stereo axis is known, denoted by ϕ_p in Figure (3.3). The local propagation angle of the resultant field at the origin $\mathbf{0}$ can be written from the local wavenumber components as

$$\tan\phi_p = \frac{k_x^P(\mathbf{0})}{k_y^P(\mathbf{0})} = \frac{A_1 - A_2}{A_1 + A_2}\frac{x_1}{y_1}. \tag{3.17}$$

Exploiting that $\tan\phi_0 = \frac{x_1}{y_1}$ leads to the formula

$$\frac{A_1 - A_2}{A_1 + A_2} = \frac{\tan\phi_p}{\tan\phi_0}, \tag{3.18}$$

which is identical to the well-known *tangent law* of stereophony [Pul97; Pul01a; Pul01c; Ben+08], originally derived by applying different considerations [Ben+85]. The tangent law therefore ensures the matching of the local propagation directions of the target field and the reproduced wavefronts in the proximity of the listener's position, i.e. over the sweet spot.

Obviously the tangent law expresses merely the relationship between A_1 and A_2, the exact value of the gain factors can be calculated by applying some type of normalizing strategy [Moo90]. A frequently used strategy is keeping the power at a

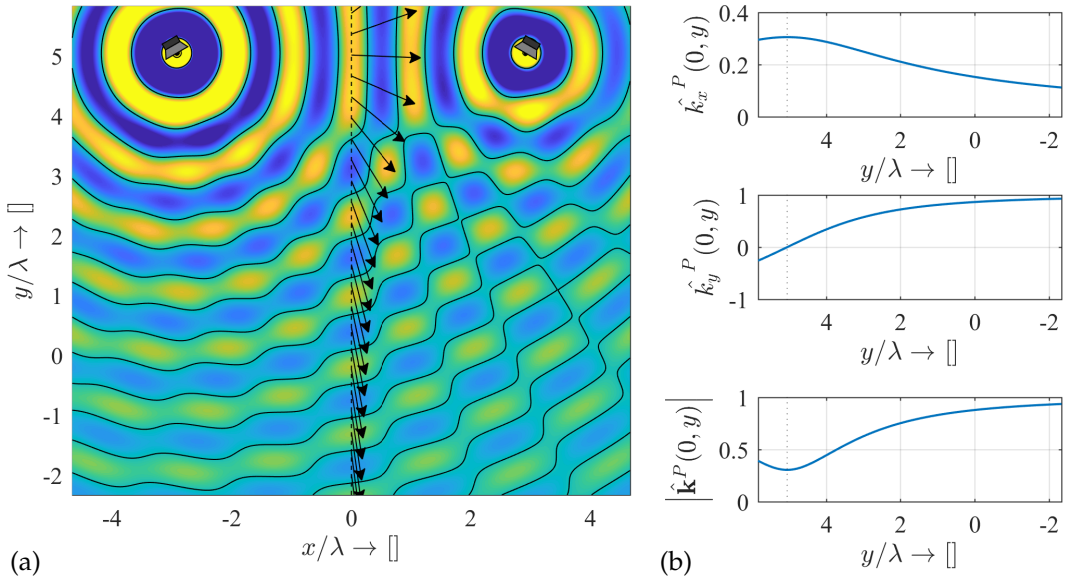

Figure 3.4. Sound field generated in a typical stereo setup. The point sources are positioned with a base angle of $\phi_0 = 30°$ with their distance from the origin being $R_0 = 2.5$ m. The gain factors A_1, A_2 were selected so that the angle of the local wavenumber vector at the origin would equal to $\phi_p = 10°$. In Figure (a) contour lines indicate isochronous surfaces with the normalized local wavenumber vector displayed along the stereo axis. Figure (b) shows the normalized wavenumber components along $x = 0$. Due to enhanced interference phenomena the amplitude changes rapidly, and the local dispersion relation (3.6) does not hold in the nearfield. The length of the wavenumber vector decreases between the sources, where standing waves may occur, and increases to infinity on the parts where the amplitude vanishes and the phase changes rapidly due to destructive interference.

constant value by requiring that $A_1^2 + A_2^2 =$ constant. Alternatively it may be exploited that the amplitude of the resultant field on the stereo axis equals to $\frac{1}{4\pi}\frac{A_1+A_2}{|\mathbf{x}-\mathbf{x}_1|}$ (as given by (C.10)) in order to match the amplitude to that of a phantom point source.

3.2 The Kirchhoff approximation

The Kirchhoff approximation is an important high frequency asymptotic approximation of the Kirchhoff-Helmholtz integral. Based on the equivalent scattering interpretation, the simple source formulation may be simplified in the high frequency region using the *Kirchhoff/Physical optics approximation*, applied frequently to estimate scattering from random surfaces [Vor99; Tsa+00]. In order to estimate the scattered field—and its normal derivative on the scatterer surface—two approximations are applied:

- According to *geometrical optics* or *ray acoustics* the scatterer surface can be divided into an *illuminated* and a *shadow region*: only those parts of the scatterer surface contribute to the scattered field that are directly illuminated by the primary source, i.e. where the local propagation directions of the incident and the scattered field—determined locally by the scatterer surface normal—coincide [LF47]. In the field of high frequency boundary element method this is termed

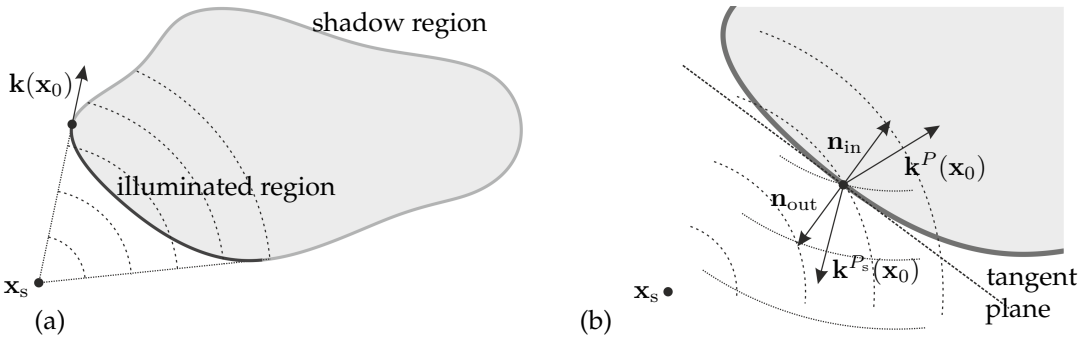

Figure 3.5. Illustration of the geometrical optics approximation (a) and the tangent plane approximation (b)

as *determining the visible elements* on the boundary [Her+03]. Mathematically this requirement is formulated as weighting the integral, describing the scattered field by the windowing function

$$w(\mathbf{x}_0) = \begin{cases} 1, & \forall \quad \langle \mathbf{k}^P(\mathbf{x}_0) \cdot \mathbf{n}_\mathrm{in}(\mathbf{x}_0) \rangle > 0 \\ 0 & \text{elsewhere,} \end{cases} \tag{3.19}$$

where $\mathbf{k}^P(\mathbf{x}_0)$ denotes the local wavenumber vector of the incident sound field at $\mathbf{x}_0$ and $\mathbf{n}_\mathrm{in}(\mathbf{x}_0)$ is the inward normal of the surface element. For an illustration see Figure 3.5 (a). This windowing means the neglection of both diffracting waves around the scattering object (as well as so-called *creeeping rays* [Ble84]) and reflections from one part of the scatterer to an other [Pig+15]. Due to this latter restriction the Kirchhoff approximation may be applied only to convex surfaces, free of secondary reflections.

- As a second simplification, the *tangent plane approximation* is applied on the illuminated region. It is supposed that there exists a local relation between the incident and the scattered field at each point on the surface. By assuming that the incident wave is reflected locally obeying the Snell's law [Vor07]—its amplitude changes proportionally to the local *reflection index*, with the angle of incidence equaling the angle of reflection measured from the local normal—the following relations are yielded for a sound soft scatterer [Ble84; Ble+00; PS02]

$$P_\mathrm{s}(\mathbf{x}_0, \omega) = -P(\mathbf{x}_0, \omega), \qquad \frac{\partial}{\partial \mathbf{n}_\mathrm{in}} P_\mathrm{s}(\mathbf{x}_0, \omega) = -\frac{\partial}{\partial \mathbf{n}_\mathrm{out}} P(\mathbf{x}_0, \omega), \qquad \mathbf{x}_0 \in \partial\Omega, \tag{3.20}$$

where $P(\mathbf{x}, \omega)$ is the incident field and $P_\mathrm{s}(\mathbf{x}, \omega)$ is the scattered field. The approximation therefore calculates the reflected wavefield by modeling each point on the scatterer with a tangential infinite plane. Obviously, the method also neglects the secondary reflections due to locally reacting assumptions. Furthermore, for low-frequencies and non-smooth boundaries the surface can not be considered locally planar, introducing further artifacts. In order to overcome these limitations several curvature correctional and iterative approaches exist [EG04].

Writing (3.20) in terms of the inward normal vector, with exploiting that the exterior sound field in the single source formulation is related to the scattered sound

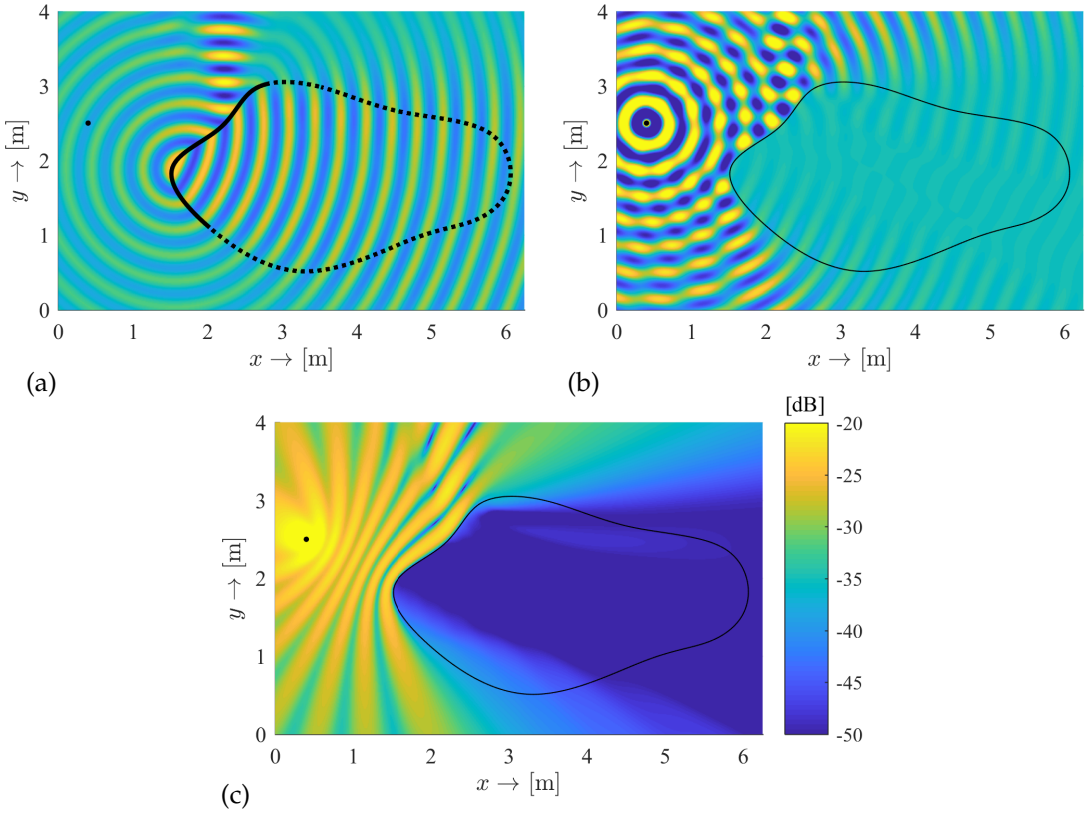

Figure 3.6. Illustration of the Kirchhoff approximation in a 2D problem ($\Omega \subset \mathbb{R}^2$) applied for the calculation of the scattering of a 2D point source, positioned at $\mathbf{x}_\mathrm{s} = [0.4,\ 2.5]^\mathrm{T}$, oscillating at $f_0 = 1$ kHz. Figure (a) depicts the numerical evaluation of the Kirchhoff approximation (3.21). Figure (b) describes the total field of the point source in the presence of a sound soft scattering object. Figure (c) shows the absolute value of the total field in field in a logarithmic scale. Inside the enclosure the sound field should be identically zero if no approximations were applied, hence in these region the non-zero field indicates the error of the Kirchhoff approximation. In Figure (a) the illuminated/active part of the scatterer contour is denoted by solid black line, whilst the shadow region is denoted by dotted line.

field according to $P_\mathrm{e}(\mathbf{x}) = -P_\mathrm{s}(\mathbf{x})$ in the equivalent scattering interpretation and introducing the windowing function into the simple source formulation, one obtains the Kirchhoff approximation of the simple source formulation

Kirchhoff approximation

$$\oint_{\partial\Omega} -2w(\mathbf{x}_0)\frac{\partial P(\mathbf{x}_0,\omega)}{\partial \mathbf{n}_\mathrm{in}} G(\mathbf{x}-\mathbf{x}_0,\omega)\mathrm{d}\partial\Omega(\mathbf{x}_0) \approx \begin{cases} P(\mathbf{x},\omega) & \forall \quad \mathbf{x}\in\Omega_\mathrm{i} \\ P=-P_\mathrm{s} & \forall \quad \mathbf{x}\in\partial\Omega \\ -P_\mathrm{s}(\mathbf{x},\omega) & \forall \quad \mathbf{x}\in\Omega_\mathrm{e}, \end{cases} \tag{3.21}$$

giving a fair approximation for smooth, convex surfaces in the high frequency and farfield region, where the wavelength and the wavefront curvature is significantly smaller, than the dimensions of the scattering object[4]. For the result of applying the approximation for the previous 2D example see Figure 3.6. The lack of diffracted waves around the enclosure gives rise to artifacts on parts of the space, where the local propagation direction of the incident field is nearly parallel with the contour.

[4] According to [BH75, Eq.(2.7.12)] the approximation holds when $k\rho_{1,2} \gg 1$, where $\rho_{1,2}$ are the local principal radii of the curved scatterer and k is the wavenumber.

3.3 The stationary phase approximation

This section introduces a basic tool of asymptotic analysis, the *stationary phase approximation (SPA)*, being of central importance in the present thesis. The method is applied to evaluate complex integrals by considering the greatest contribution stemming from critical points in the integral path. In the following chapters the SPA allows to extract asymptotic, local solutions from the global ones for radiation and reproduction problems written in terms of either boundary or spectral integrals.

For the sake of brevity the following notation convention is used hereinafter, as given also in the nomenclature: Given an n-dimensional function $f(\mathbf{x})$ with $\mathbf{x} = [x_1,\ x_2,\ ...,\ x_i]^{\mathrm{T}}$, $i = 1, 2, ..., n$, the first and second partial derivatives with respect to the i-th and j-th coordinates x_i, x_j evaluated at point $\mathbf{x}^*$ are denoted as

$$\frac{\partial}{\partial x_i} f(\mathbf{x})\bigg|_{\mathbf{x}=\mathbf{x}^*} = f'_{x_i}(\mathbf{x}^*), \qquad \frac{\partial^2}{\partial x_i \partial x_j} f(\mathbf{x})\bigg|_{\mathbf{x}=\mathbf{x}^*} = f''_{x_i x_j}(\mathbf{x}^*). \tag{3.22}$$

3.3.1 The integral approximation

Generally speaking the SPA yields approximate solutions of complex integrals in the general polar form with $\mathbf{x} \in \mathbb{R}^n$

$$I_{1\mathrm{D}} = \int_{-\infty}^{\infty} A(x)\, \mathrm{e}^{\mathrm{j}\phi(x)}\, \mathrm{d}x, \qquad I_{n\mathrm{D}} = \int_{-\infty}^{\infty} A(\mathbf{x})\, \mathrm{e}^{\mathrm{j}\phi(\mathbf{x})}\, \mathrm{d}\mathbf{x} \tag{3.23}$$

in one and n dimensions respectively, when $\mathrm{e}^{\mathrm{j}\phi(\mathbf{x})}$ is highly oscillating and $A(\mathbf{x})$ is comparably slowly varying.

For the 1D case a rigorous derivation of the SPA based on integration by parts is given in [BH75; Ble84; Wil99]. More informally the method relies on the second order truncated Taylor series of the exponent around the *stationary point* x^*, defined as the point in the integration path satisfying

$$\phi'_x(x^*) = 0, \qquad \text{and} \qquad \phi''_{xx}(x^*) \neq 0. \tag{3.24}$$

Around the stationary point the Taylor series reads as

$$\phi(x) \approx \phi(x^*) + \frac{1}{2}\phi''_{xx}(x^*)(x - x^*)^2. \tag{3.25}$$

Supposing that the amplitude $A(x)$ is a slowly varying smooth function compared to $\phi(x)$, it is assumed that where the phase varies (i.e. $\phi'_x(x) \neq 0$), the integral of rapid oscillation cancels out, thus the greatest contribution to the total integral comes from the immediate surroundings of the stationary point. Moreover in the proximity of the

stationary point $A(x)$ can be regarded as constant with the value $A(x^*)$. With these considerations the integral becomes

$$I_{1D} \approx A(x^*)\,\mathrm{e}^{+\mathrm{j}\phi(x^*)} \int_{-\infty}^{\infty} \mathrm{e}^{+\mathrm{j}\frac{1}{2}\phi''_{xx}(x^*)(x-x^*)^2}\,\mathrm{d}x. \tag{3.26}$$

The remaining integral can be evaluated analytically, and the SPA of (3.23) becomes [BH75, Ch. 2.8]

1D stationary phase approximation

$$I_{1D} \approx \sqrt{\frac{2\pi}{|\phi''_{xx}(x^*)|}} F(x^*)\,\mathrm{e}^{+\mathrm{j}\phi(x^*)+\mathrm{j}\frac{\pi}{4}\,\mathrm{sgn}(\phi''_{xx}(x^*))}. \tag{3.27}$$

Similarly, in higher dimensions a *simple stationary point* is defined as

$$\nabla_{\mathbf{x}}\,\phi(\mathbf{x})|_{\mathbf{x}=\mathbf{x}^*} = 0, \tag{3.28}$$

where

$$\det \mathbf{H}(\mathbf{x}^*) \neq 0, \qquad \mathbf{H}_{ij}(\mathbf{x}^*) = \left[\frac{\partial^2 \phi(\mathbf{x})}{\partial x_i \partial x_j}\right]\Bigg|_{\mathbf{x}=\mathbf{x}^*}, \qquad i,j = 1,2,...,n \tag{3.29}$$

holds, with $\mathbf{H}$ being the Hessian matrix of the phase function. The multidimensional formula for the integral value reads as

Multidimensional SPA

$$I_{nD} \approx \sqrt{\frac{(2\pi)^n}{|\det \mathbf{H}(\mathbf{x}^*)|}} F(\mathbf{x}^*) \mathrm{e}^{\mathrm{j}\phi(\mathbf{x}^*)+\mathrm{j}\frac{\pi}{4}\,\mathrm{sgn}(\mathbf{H}(\mathbf{x}^*))}, \tag{3.30}$$

where $\mathrm{sgn}\,(\mathbf{H}(\mathbf{x}^*))$ is the signature of the Hessian: the number of positive eigenvalues minus the number of negative eigenvalues [Ble+00].

In the following the physical interpretation of the SPA is discussed when applied to boundary and spectral integrals of sound fields and simple examples are given for its application. The conclusions of the presented examples will be further utilized in the following chapters.

3.3.2 Asymptotic approximation of boundary integrals

First the physical interpretation of the stationary position is discussed for the case when the SPA is applied to boundary integrals, for the sake of simplicity through the example of the Rayleigh I integral.

Assume that the Rayleigh integral describes an arbitrary sound field at $y > y_0$ in terms of a boundary integral along the plane $\mathbf{x}_0 = [x_0,\ y = y_0,\ z_0]^{\mathrm{T}}$ according to (2.65). It is supposed that all sources of sound are located behind the Rayleigh plane in the half space $y < y_0$, generating a non-converging wavefront. Since for the application of the SPA high frequency conditions are standard prerequisites, therefore

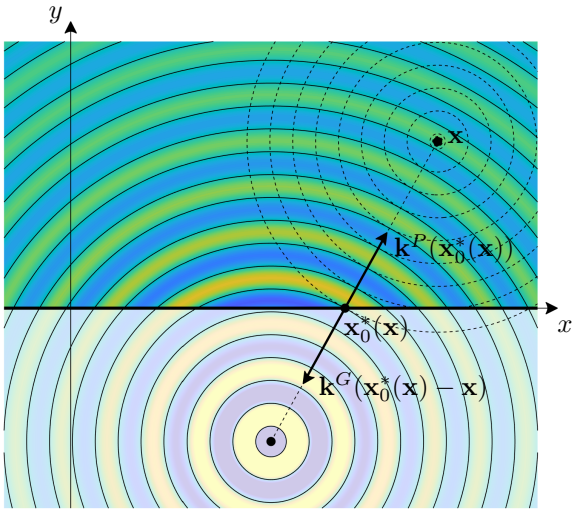

Figure 3.7. 2D Geometry for the physical interpretation of the stationary position for the Rayleigh integral. The stationary position is found along the integral surface/contour where the local propagation direction—and the local wavenumber vector—of the described wavefield and the spherical field of a point source positioned at $\mathbf{x}$ coincide. Equivalently, it means that the local propagation direction of the described field at $\mathbf{x}_0^*(\mathbf{x})$ equals with that of the Green's function positioned at $\mathbf{x}_0^*(\mathbf{x})$, measured at the receiver position $\mathbf{x}$.

the high frequency gradient approximation (3.12) may be applied, resulting in the high frequency Rayleigh integral

$$P(\mathbf{x},\omega) = 2\iint_{-\infty}^{\infty} \mathrm{j}k_y^P(\mathbf{x}_0)P(\mathbf{x}_0,\omega)G(\mathbf{x}-\mathbf{x}_0,\omega)\mathrm{d}x_0\mathrm{d}z_0. \tag{3.31}$$

The Rayleigh integral is to be evaluated applying the SPA at a given receiver position $\mathbf{x}$. The involved functions written in polar form read

$$P(\mathbf{x},\omega) = 2\iint_{-\infty}^{\infty} k_y^P(\mathbf{x}_0)A^P(\mathbf{x}_0,\omega)A^G(\mathbf{x}-\mathbf{x}_0,\omega)\mathrm{e}^{\mathrm{j}\left(\phi^P(\mathbf{x}_0,\omega)+\phi^G(\mathbf{x}-\mathbf{x}_0,\omega)+\frac{\pi}{2}\right)}\mathrm{d}x_0\mathrm{d}z_0. \tag{3.32}$$

According to (3.28) the stationary position for the integral is found where the phase gradient vanishes. Exploiting that the constant phase shift $+\frac{\pi}{2}$ vanishes due to differentiation, the stationary position $\mathbf{x}_0^*(\mathbf{x})$ for a given receiver position $\mathbf{x}$ is found, where

$$\begin{bmatrix}\frac{\partial}{\partial x_0}\\ \frac{\partial}{\partial z_0}\end{bmatrix}\phi^P(\mathbf{x}_0,\omega)\Big|_{\mathbf{x}_0=\mathbf{x}_0^*(\mathbf{x})} = -\begin{bmatrix}\frac{\partial}{\partial x_0}\\ \frac{\partial}{\partial z_0}\end{bmatrix}\phi^G(\mathbf{x}-\mathbf{x}_0,\omega)\Big|_{\mathbf{x}_0=\mathbf{x}_0^*(\mathbf{x})} \tag{3.33}$$

is satisfied. By the definition (3.2) the derivatives describe the corresponding components of the local wavenumber vector. Since two components completely determine the local wavenumber vector, therefore in the stationary position

Stationary position of boundary integrals

$$\begin{aligned} k_x^P(\mathbf{x}_0^*(\mathbf{x})) &= k_x^G(\mathbf{x}-\mathbf{x}_0^*(\mathbf{x}))\\ k_z^P(\mathbf{x}_0^*(\mathbf{x})) &= k_z^G(\mathbf{x}-\mathbf{x}_0^*(\mathbf{x}))\\ \mathbf{k}^P(\mathbf{x}_0^*(\mathbf{x})) &= \mathbf{k}^G(\mathbf{x}-\mathbf{x}_0^*(\mathbf{x})) = -\mathbf{k}^G(\mathbf{x}_0^*(\mathbf{x})-\mathbf{x}) \end{aligned} \tag{3.34}$$

holds. In the right hand side the chain rule and the reciprocity of the Green's function was exploited.

Hence, the SPA 'compares' the propagation direction/wavefronts of the described field and the Green's function along the integral path. The stationary position for a given receiver position is given by that point $\mathbf{x}_0^*(\mathbf{x})$, where the local propagation direction of the described wavefield is opposite to that of a monopole field centered at

the receiver position $\mathbf{x}$. Obviously, by translating back the 3D Green's function into $\mathbf{x}_0^*(\mathbf{x})$, its wavenumber vector at $\mathbf{x}$ will coincide with the described field's wavenumber vector. In other words, since the Rayleigh integral describes a sound field as the resultant field of a planar distribution of point sources, for a given receiver point that point source will have the greatest contribution, that's sound field propagates into the same direction as the primary sound field.

This interpretation is illustrated in Figure 3.7 with the example of a 2D point source described by the 2D Rayleigh integral. For the case of a point source at $\mathbf{x}_\mathrm{s}$ the stationary position is found at the intersection of vector $\mathbf{x} - \mathbf{x}_\mathrm{s}$ and the integration path. In a 3D example, if the primary field is a spherical one, the stationary point is found at the intersection of the Rayleigh plane and the vector pointing from the source into the evaluation position.

Application example #1: Asymptotic evaluation of the Rayleigh integral

As an application example for the SPA the evaluation of the Rayleigh integral around the stationary point is investigated in further details. As a result it is described, how the properties of wavefronts change over propagation.

The stationary point was found on the Rayleigh plane, where the local propagation direction of the primary sound field coincides (with a negative sign) with the spherical wavefront of the Green's function positioned at the receiver point. In order to evaluate integral (3.31) around its stationary position according to (3.30) (with $n = 2$), the signature and the determinant of the Hessian in the stationary point is required. In the present geometry the Hessian is given by the expression

$$\mathbf{H}^{P+G}(\mathbf{x}_0) = \begin{bmatrix} \frac{\partial^2}{\partial x_0^2} & \frac{\partial^2}{\partial x_0 \partial z_0} \\ \frac{\partial^2}{\partial x_0 \partial z_0} & \frac{\partial^2}{\partial z_0^2} \end{bmatrix} \left(\phi^P(\mathbf{x}_0, \omega) + \phi^G(\mathbf{x} - \mathbf{x}_0, \omega) \right). \tag{3.35}$$

In the stationary position the primary wavefront and the Green's function wavefront are tangential. Due to the spherical nature of the latter one, in the stationary point the eigenvectors of their Hessians can be chosen to coincide, and their principal curvatures (eigenvalues) are additive. Thus, the resultant Hessian (3.35) can be expressed in terms of the principal curvatures of the primary sound field κ_1^P, κ_2^P and the Green's function κ_1^G, κ_2^G as

$$\mathbf{H}^{P+G}(\mathbf{x}_0^*(\mathbf{x})) = -k\mathbf{V} \begin{bmatrix} \kappa_1^P(\mathbf{x}_0^*(\mathbf{x})) + \kappa_1^G(\mathbf{x} - \mathbf{x}_0^*(\mathbf{x})) & 0 \\ 0 & \kappa_2^P(\mathbf{x}_0^*(\mathbf{x})) + \kappa_2^G(\mathbf{x} - \mathbf{x}_0^*(\mathbf{x})) \end{bmatrix} \mathbf{V}^\mathrm{T}, \tag{3.36}$$

with $\mathbf{v}=\begin{bmatrix} v_{1x} & v_{2x} \\ v_{1z} & v_{2z} \end{bmatrix}$ being the x,z-components of the principal directions corresponding to κ_1^P and κ_2^P as shown in Figure 3.2. For a more detailed investigation see Appendix B.1. The determinant of the Hessian reads as

$$\det\mathbf{H}^{P+G}(\mathbf{x}_0^*(\mathbf{x})) = \left(\kappa_1^P(\mathbf{x}_0^*(\mathbf{x})) + \kappa_1^G(\mathbf{x}-\mathbf{x}_0^*(\mathbf{x}))\right)\left(\kappa_2^P(\mathbf{x}_0^*(\mathbf{x})) + \kappa_2^G(\mathbf{x}-\mathbf{x}_0^*(\mathbf{x}))\right)\cdot \\ \cdot k^2 \underbrace{\left(v_{1x}v_{2z} - v_{2x}v_{1z}\right)^2}_{\hat{k}_y^P(\mathbf{x}_0^*(\mathbf{x}))^2}, \quad (3.37)$$

where the underbraced part is the y-coordinate of a vector being perpendicular to $\mathbf{v}_1$ and $\mathbf{v}_2$, i.e. of the normalized local wavenumber vector. By taking into consideration that for a divergent field both curvatures of the wavefront are positive and the signature of the Hessian equals (-2), substitution into (3.30) yields the asymptotic Rayleigh integral, reading

$$P(\mathbf{x},\omega) = 4\pi \frac{P(\mathbf{x}_0^*(\mathbf{x}),\omega)G(\mathbf{x}-\mathbf{x}_0^*(\mathbf{x}),\omega)}{\sqrt{\left(\kappa_1^P(\mathbf{x}_0^*(\mathbf{x})) + \kappa_1^G(\mathbf{x}-\mathbf{x}_0^*(\mathbf{x}))\right)}\sqrt{\left(\kappa_2^P(\mathbf{x}_0^*(\mathbf{x})) + \kappa_2^G(\mathbf{x}-\mathbf{x}_0^*(\mathbf{x}))\right)}}, \quad (3.38)$$

$$P(\mathbf{x},\omega) = 4\pi\sqrt{\frac{\rho_1^P(\mathbf{x}_0^*(\mathbf{x}))\cdot\rho_1^G(\mathbf{x}-\mathbf{x}_0^*(\mathbf{x}))}{\rho_1^P(\mathbf{x}_0^*(\mathbf{x}))+\rho_1^G(\mathbf{x}-\mathbf{x}_0^*(\mathbf{x}))}}\sqrt{\frac{\rho_2^P(\mathbf{x}_0^*(\mathbf{x}))\cdot\rho_2^G(\mathbf{x}-\mathbf{x}_0^*(\mathbf{x}))}{\rho_2^P(\mathbf{x}_0^*(\mathbf{x}))+\rho_2^G(\mathbf{x}-\mathbf{x}_0^*(\mathbf{x}))}}P(\mathbf{x}_0^*(\mathbf{x}),\omega)G(\mathbf{x}-\mathbf{x}_0^*(\mathbf{x}),\omega),$$

written both in terms of the principal curvatures and radii.

Substituting the exact formulation of the 3D Green's function and by exploiting that according to (B.25) the principal radii increase proportional with the Euclidean distance along the local propagation direction, i.e. $\rho_i^P(\mathbf{x}) = \rho_i^P(\mathbf{x}_0^*(\mathbf{x})) + \rho_i^G(\mathbf{x}-\mathbf{x}_0^*(\mathbf{x}))$ holds, the asymptotic formula takes the form

$$P(\mathbf{x},\omega) = \underbrace{\sqrt{\frac{\rho_1^P(\mathbf{x}_0^*(\mathbf{x}))\cdot\rho_2^P(\mathbf{x}_0^*(\mathbf{x}))}{\rho_1^P(\mathbf{x})\cdot\rho_2^P(\mathbf{x})}}}_{\substack{\text{amplitude change}\\ \text{over propagation}}} \underbrace{\mathrm{e}^{-\mathrm{j}\omega\frac{|\mathbf{x}-\mathbf{x}_0^*(\mathbf{x})|}{c}}}_{\substack{\text{phase change}\\ \text{over propagation}}} P(\mathbf{x}_0^*(\mathbf{x}),\omega), \quad (3.39)$$

Asymptotic Rayleigh integral

where $\rho_1^P\cdot\rho_2^P$ is the reciprocal of the Gaussian curvature of the wavefront. Thus, in a ray-tracing manner the wavefield is approximated locally by its value at the stationary position: the numerator of the amplitude factor approximates the pressure field amplitude in the source position, attenuated by the denominator–describing the attenuation factor for the source-to-receiver distance—, while a simple phase shift term corresponds to the propagation time delay. The equation reflects the fact, that *the intensity of a 3D wavefield is proportional to the Gaussian curvature of the wavefront*, being a well-known fact in the field of optics [BW70, Sec. 3.1], [Bou+97, Sec. 1.3]. Similarly, a 2D wavefront's amplitude attenuates proportionally to the only non-zero curvature, given by $\sim\sqrt{\rho^P}$, which fact can be deduced from the SPA of the 2D Rayleigh integral.

Note that since points $\mathbf{x}$ and $\mathbf{x}_0^*(\mathbf{x})$ are related by the local wavenumber vector, therefore equation (3.39) generally describes the relation of field variables along the direction of the local wavenumber vector, providing the amplitude and phase change along the path of propagation. Departing from the Rayleigh plane concept, as a more

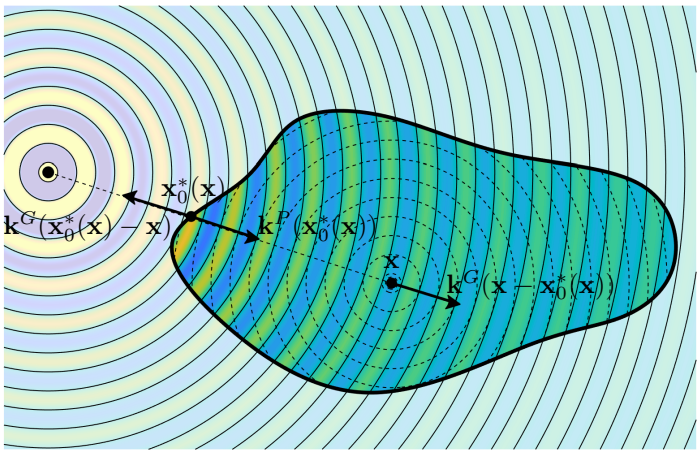

Figure 3.8. 2D geometry for the illustration of the stationary position for the Kirchhoff-Helmholtz integral.

general statement, any propagating pressure field may be approximated along the propagation path as

$$P(\mathbf{x} + \mathrm{d}x \cdot \hat{\mathbf{k}}^P(\mathbf{x}), \omega) = \sqrt{\frac{\rho_1^P(\mathbf{x})\rho_2^P(\mathbf{x})}{(\rho_1^P(\mathbf{x}) + \mathrm{d}x)\,(\rho_2^P(\mathbf{x}) + \mathrm{d}x)}}\,\mathrm{e}^{-\mathrm{j}\omega\frac{\mathrm{d}x}{c}}\,P(\mathbf{x}, \omega) \tag{3.40}$$

as long as high frequency/farfield assumptions hold[5].

Application example #2: The Kirchhoff approximation

As a second application example for the SPA of boundary integrals an alternative derivation of the Kirchhoff approximation is presented directly from the Kirchhoff-Helmholtz integral. Suppose that an interior radiation problem is described by the KHIE inside an enclosure Ω, bounded by $\partial\Omega$. The field is given by

$$P(\mathbf{x}, \omega) = \oint_{\partial\Omega} -\left(\frac{\partial P(\mathbf{x}_0, \omega)}{\partial \mathbf{n}_{\mathrm{in}}} G(\mathbf{x} - \mathbf{x}_0, \omega) - P(\mathbf{x}_0, \omega)\frac{\partial G(\mathbf{x} - \mathbf{x}_0, \omega)}{\partial \mathbf{n}_{\mathrm{in}}}\right) \mathrm{d}\partial\Omega(\mathbf{x}_0). \tag{3.41}$$

Assuming high frequency conditions both the sound field and the Green's function normal derivatives may be approximated using the high frequency gradient approximation, resulting in

$$P(\mathbf{x}, \omega) = \oint_{\partial\Omega} \left(\mathrm{j}k_{\mathrm{n}}^P(\mathbf{x}_0) + \mathrm{j}k_{\mathrm{n}}^G(\mathbf{x} - \mathbf{x}_0)\right) P(\mathbf{x}_0, \omega) G(\mathbf{x} - \mathbf{x}_0, \omega) \mathrm{d}\partial\Omega(\mathbf{x}_0). \tag{3.42}$$

Again, it can be assumed that for a given receiver position $\mathbf{x}$ most part of the integral cancels out, and the field is dominated by one particular stationary point on the surface. Obviously, the stationary point is found on $\partial\Omega$ where the phase gradient vanishes, i.e. where the local wavenumber vector/local propagation direction of the described sound field and the Green's function positioned at $\mathbf{x}$ coincide, satisfying

[5] From the above equation the relative amplitude change can be expressed by applying the L'Hospital's rule, reading as $\frac{\langle \mathbf{k}^P(\mathbf{x}) \cdot \nabla_{\mathbf{x}} A^P(\mathbf{x},\omega)\rangle}{A^P(\mathbf{x},\omega)} = \lim_{\mathrm{d}x \to 0} \frac{\sqrt{\frac{\rho_1^P(\mathbf{x})\rho_2^P(\mathbf{x})}{(\rho_1^P(\mathbf{x})+\mathrm{d}x)(\rho_2^P(\mathbf{x})+\mathrm{d}x)}} - 1}{\mathrm{d}x} = -\frac{1}{2}\frac{\rho_1^P(\mathbf{x}) + \rho_2^P(\mathbf{x})}{\rho_1^P(\mathbf{x})\rho_2^P(\mathbf{x})} = -\overline{\kappa}^P(\mathbf{x})$, which result is in agreement with the definition of the mean curvature using the transport equation (3.8).

$\mathbf{k}^P(\mathbf{x}_0^*(\mathbf{x})) = \mathbf{k}^G(\mathbf{x} - \mathbf{x}_0^*(\mathbf{x})) = -\mathbf{k}^G(\mathbf{x}_0^*(\mathbf{x}) - \mathbf{x})$. This interpretation is illustrated in Figure 3.8 in case of a primary point source.

As an approximation the amplitude factor of the integral can be substituted by its value at the stationary point, i.e. with $k_\mathrm{n}^G(\mathbf{x}-\mathbf{x}_0) = k_\mathrm{n}^P(\mathbf{x}_0)$. Furthermore, only that part of the integral path contributes to the total sound field that serves as a stationary point for any receiver position inside the enclosure, resulting in the windowing function (3.19) and the KHIE may be further simplified towards

$$P(\mathbf{x},\omega) = \oint_{\partial\Omega} 2w(\mathbf{x}_0)\mathrm{j}k_\mathrm{n}^P(\mathbf{x}_0)P(\mathbf{x}_0,\omega)G(\mathbf{x}-\mathbf{x}_0,\omega)\mathrm{d}\partial\Omega(\mathbf{x}_0). \tag{3.43}$$

Kirchhoff approximation

This is obviously equivalent to the Kirchhoff approximation (3.21), derived by physically motivated considerations from the equivalent scattering interpretation of the simple source formulation.

3.3.3 Asymptotic approximation of spectral integrals

There is a strong relationship between the local wavenumber vector concept and the plane wave decomposition/angular spectrum of sound fields. The relation is established by the SPA.

Consider the forward and inverse Fourier transform of a general polar form sound field $P(\mathbf{x},\omega)$ given by (3.1)

$$\tilde{P}(k_x, y, k_z, \omega) = \iint_{-\infty}^{\infty} A^P(\mathbf{x},\omega)\mathrm{e}^{\mathrm{j}\phi^P(\mathbf{x},\omega)}\mathrm{e}^{\mathrm{j}k_x x}\mathrm{e}^{\mathrm{j}k_z z}\mathrm{d}x\mathrm{d}z, \tag{3.44}$$

$$P(\mathbf{x},\omega) = \frac{1}{(2\pi)^2}\iint_{-\infty}^{\infty} A^{\tilde{P}}(k_x, y, k_z, \omega)\mathrm{e}^{\mathrm{j}\Phi^{\tilde{P}}(k_x,y,k_z,\omega)}\mathrm{e}^{-\mathrm{j}k_x x}\mathrm{e}^{-\mathrm{j}k_z z}\mathrm{d}k_x\mathrm{d}k_z, \tag{3.45}$$

with $\tilde{P}(k_x, y, k_z, \omega) = A^{\tilde{P}}(k_x, y, k_z, \omega)\mathrm{e}^{\mathrm{j}\Phi^{\tilde{P}}(k_x,y,k_z,\omega)}$ with $A^{\tilde{P}}, \Phi^{\tilde{P}} \in \mathbb{R}$. The forward and inverse transforms describe projection and composition of the sound field P to and from *spectral plane waves*, whose specific propagation direction (i.e. the wavenumber vector) is completely determined by k_x and k_z along with the acoustic wavenumber k via the dispersion relation.

Supposing that the sound field fulfills the SPA requirements—i.e. under high frequency assumptions—the forward transform (3.44) may be evaluated asymptotically applying the stationary phase method [Arn95; TM05]. The stationary point $\mathbf{x}^*(k_x, k_z)$ is found for a given k_x and k_z, where the gradient of the exponent is zero. Assuming that the local dispersion relation holds, two local wavenumber components completely define the local wavenumber vector and the stationary position for the spectral integral is found where

Stationary position of spectral integrals

$$\frac{\partial}{\partial x}\phi^P(\mathbf{x},\omega)\Big|_{\mathbf{x}=\mathbf{x}^*(k_x,k_z)} + k_x = 0 \quad\rightarrow\quad k_x^P(\mathbf{x}^*(k_x,k_z)) = k_x, \tag{3.46}$$

$$\frac{\partial}{\partial z}\phi^P(\mathbf{x},\omega)\Big|_{\mathbf{x}=\mathbf{x}^*(k_x,k_z)} + k_z = 0 \quad\rightarrow\quad k_z^P(\mathbf{x}^*(k_x,k_z)) = k_z, \tag{3.47}$$

$$\nabla_\mathbf{x}\,\phi^P(\mathbf{x},\omega)\Big|_{\mathbf{x}=\mathbf{x}^*(\mathbf{k})} + \mathbf{k} = 0 \quad\rightarrow\quad \mathbf{k}^P(\mathbf{x}^*(\mathbf{k})) = \mathbf{k}. \tag{3.48}$$

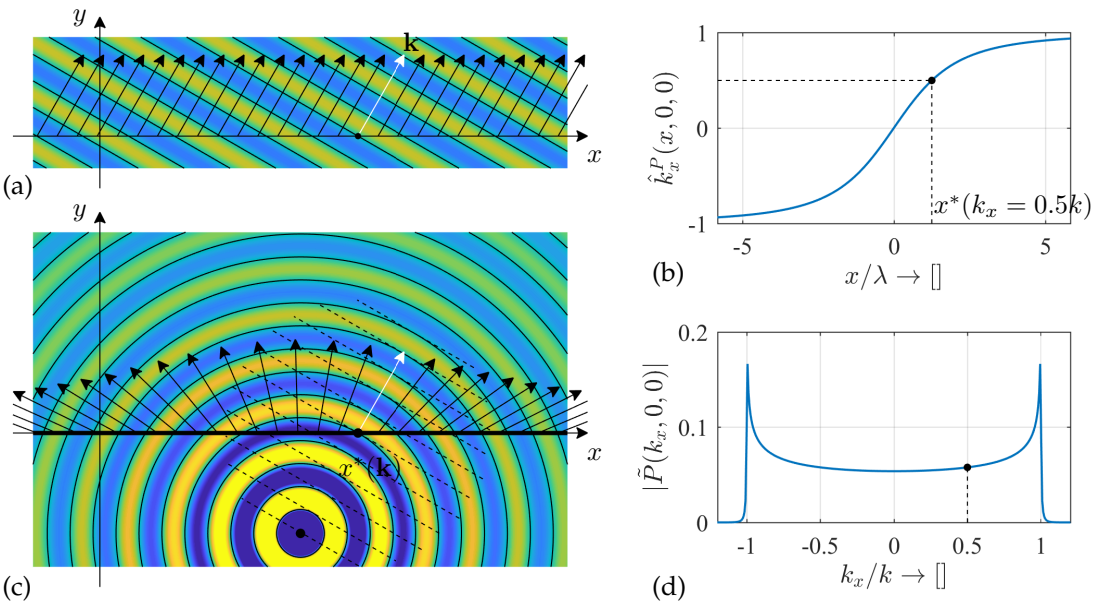

Figure 3.9. Illustration of the stationary position for the SPA of the Fourier transform in case of a 3D point source with its one-dimensional Fourier transform evaluated along the x-axis. Figure (a) presents a spectral basis function (i.e. a horizontal plane wave) which is at this example chosen as $k_x = 0.5k$. For this spectral component the stationary phase point in the field of the point source, shown in Figure (c) is found, where the local propagation direction of the point source coincides with that of the plane wave, indicated by white arrow. Coincidence of local propagation directions is ensured by the assumption that in the plane of investigation $k_z^G(x, y, 0) \equiv 0$, and the spectral plane wave is assumed to propagate with $k_z = 0$. The spectrum, shown in Figure (d) (as given analytically in Table (2.1)) will be dominated around $k_x = 0.5k$ by this stationary position, denoted by $x^*(k_x)$ in Figure (b).

is satisfied, with $\mathbf{k}$ being the wavenumber vector of the spectral plane wave.

This finding states that each point in the angular spectrum of a sound field is dominated by the parts of the space, where the local propagation direction coincides with the corresponding spectral plane wave's global propagation direction. The local wavenumber components therefore may be also defined alternatively as the stationary points of the spatial Fourier transform (3.44) as a function of space [6]. The interpretation of the stationary position for the Fourier transform SPA is illustrated in Figure 3.9 through the exemplary transformation of a point source.

The counterpart of this statement is that the greatest contribution to the inverse transform (3.45) is associated to those plane waves—the stationary phase of the inverse integral for given $\mathbf{x}$—, whose wave number vector coincide with the local wavenumber components of the sound field at $\mathbf{x}$.

So far it was assumed that in the region of investigation (along an infinite plane or line, depending on the transform dimensionality) the stationary phase position and thus each propagation direction is unique. This trivially does not hold for the case of e.g. a plane wave, or complex acoustic fields produced by multiple sources of sound. The SPA however can be extended for multiple stationary positions and the result of the approximation is obtained by summing the SPA contributions over the stationary positions [Ble+00, p. 129]. In the present treatise this limitation is not investigated

[6] This definition if often termed *Lagrange submanifolds*, playing a central role in phase space representation of sound fields [SM93; Arn95; TM05].

further, since the results involving the SPA of the Fourier transform hold without any modification for a virtual plane wave as a limiting case.

Application example #1: 1D spectrum of the Green's function

As an example the 1D spatial Fourier transform of the 3D Green's function is investigated, with the transform taken along the x-dimension. As a result a frequently used high frequency asymptotic approximation of the Hankel function is obtained. For the sake of simplicity the point source is located in the origin.

The exact solution for the problem is available analytically in Table (2.1), given by the second order Hankel function in the propagation region:

$$\tilde{G}(k_x, y, z, \omega) = \frac{1}{4\pi}\int_{-\infty}^{\infty} \frac{\mathrm{e}^{-\mathrm{j}k\sqrt{x^2+y^2+z^2}}}{\sqrt{x^2+y^2+z^2}} \mathrm{e}^{\mathrm{j}k_x x}\mathrm{d}x = -\frac{\mathrm{j}}{4}H_0^{(2)}\left(\sqrt{k^2-k_x^2}\sqrt{y^2+z^2}\right) \tag{3.49}$$

In this simple case, the stationary positions can be found explicitly for a given wavenumber and the SPA of the Fourier transform can be evaluated analytically. By definition the stationary position for an arbitrary spectral wavenumber k_x is found, where the x-derivative of the phase function vanishes and $x^*(k_x)$ satisfies

$$k_x^G(x^*(k_x)) = k\frac{x^*(k_x)}{\sqrt{x^*(k_x)^2+y^2+z^2}} = k_x \qquad \rightarrow \qquad x^*(k_x) = \rho\frac{k_x}{k_\rho}, \tag{3.50}$$

with $\rho = \sqrt{y^2+z^2}$ being the radial distance from the x-axis and $k_\rho = \sqrt{k^2-k_x^2}$ being the corresponding radial wavenumber. For the geometric interpretation of the stationary point refer to Figure 3.9. At the stationary point the phase of the integrand and its second derivative reads

$$\phi^G(x^*(k_x)) = -\rho k_\rho, \qquad \phi''^G_{xx}(x^*(k_x)) = -k\frac{y^2+z^2}{\sqrt{x^*(k_x)^2+y^2+z^{2^3}}} = -\frac{k_\rho^3}{k^2\rho}. \tag{3.51}$$

Substitution into the SPA (3.27) with $\sqrt{x^*(k_x)^2+y^2+z^2} = \rho\frac{k}{k_\rho}$ and accounting for the negative sign of the second derivative yields the asymptotic form of the 3D point source spectrum

$$\tilde{G}(k_x, y, z, \omega) = -\frac{\mathrm{j}}{4}H_0^{(2)}(k_\rho\rho) \approx \frac{1}{\sqrt{8\pi\mathrm{j}}}\frac{\mathrm{e}^{-\mathrm{j}\rho k_\rho}}{\sqrt{\rho k_\rho}}. \tag{3.52}$$

Field of a linear radiator

This result is the Hankel function's well-known asymptotic expansion for large arguments [Olv+10, p. 10.17.6]

$$H_0^{(2)}(z) \approx \sqrt{\frac{2\mathrm{j}}{\pi z}}\mathrm{e}^{-\mathrm{j}z}. \tag{3.53}$$

In the current case, when the function to be transformed is the Green's function, (3.49) can be interpreted as the sound field of an infinite line source with a harmonic spatial distribution, evaluated at $x = 0$. Such a line source radiates attenuating conical wavefronts propagating radially away from the x-axis with the local wavenumber vector given by $\mathbf{k}^P(\mathbf{x}) = [k_x,\ k_\rho]^\mathrm{T}$, as illustrated in Figure 3.10 (a). The amplitude of

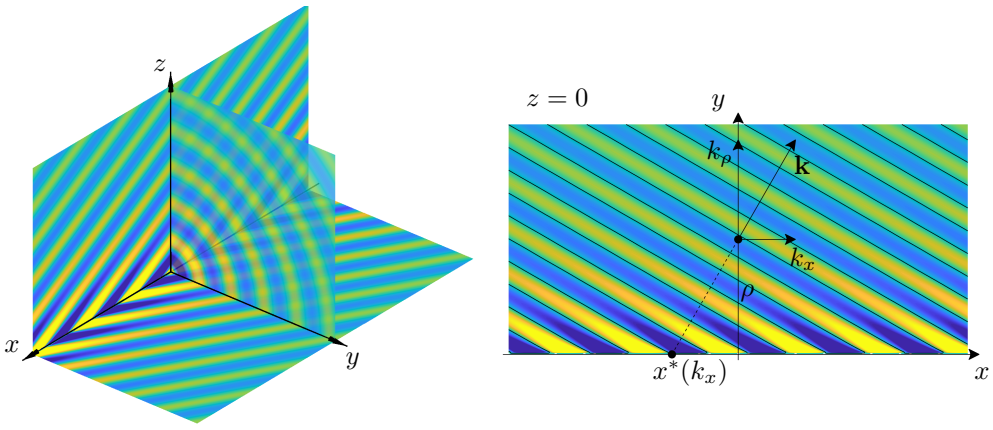

(a) (b)

Figure 3.10. Interpretation of the Green's function's spectrum as the field of a line source with harmonic spatial distribution described by wavenumber k_x, evaluated at $x = 0$. Such a source, shown in Figure (a), radiates a cylindrical symmetric sound field with the radial wavenumber k_ρ and the longitudinal wavenumber k_x, so that $k = \sqrt{k_x^2 + k_\rho^2}$ satisfies. In case $k_x = 0$ this corresponds to the field of the 2D Green's function. From geometrical considerations, and applying the interpretation of the SPA for boundary integrals the stationary position for integral (3.49) is found at $x^*(k_x) = \rho \frac{k_x}{k_\rho}$, as shown in Figure (b).

the waves depends on the propagation direction: lateral waves (with small k_ρ) are extremely enhanced.

The DC ($k_x = 0$) component of the spectrum of the 3D Green's function describes the sound field generated by an infinite line source along the x-axis, i.e. a 2D point source. The high frequency approximation of the 2D Green's function—which therefore stems from the asymptotic approximation of (2.45) by the SPA [Wil99, p. 118]—is thus given by

Approximate 2D Green's function

$$G_{2\mathrm{D}}(\mathbf{x}, \omega) \approx \frac{1}{\sqrt{8\pi \mathrm{j}}} \frac{\mathrm{e}^{-\mathrm{j}k|\mathbf{x}|}}{\sqrt{k|\mathbf{x}|}} = \sqrt{\frac{2\pi|\mathbf{x}|}{\mathrm{j}k}} G_{3\mathrm{D}}(\mathbf{x}, \omega), \tag{3.54}$$

with $\mathbf{x} = [y,\ z]^{\mathrm{T}}$. This result indicates that the 2D Green's function and the 3D Green's function's phase—and therefore their local wavenumber vector—are equal in the high frequency region, with the 3D distances substituted with the 2D ones. Opposed to a 3D source's flat frequency response, a 2D one exhibits a frequency response of $\sim 1/\sqrt{\mathrm{j}\omega}$, corresponding with the infinite tail of a 2D field's impulse response.

Application example #2: 2D spectrum of the Green's function

As a second example the 2D spatial Fourier transform of the Green's function, positioned at the origin is discussed. The Fourier transform reads as

$$\tilde{G}(k_y, y, k_z, \omega) = \iint_{-\infty}^{\infty} G(x, y, z, \omega) \mathrm{e}^{\mathrm{j}k_x x} \mathrm{e}^{\mathrm{j}k_z z} \mathrm{d}x \mathrm{d}z. \tag{3.55}$$

On a fixed $y = \text{const}$ plane the stationary point for the integral is found, where

$$k_x^G(x^*(k_x), y, z^*(k_z)) = k_x, \quad \rightarrow \quad k\frac{x^*(k_x)}{|\mathbf{x}^*(k_x, k_z)|} = k_x \tag{3.56}$$

$$k_z^G(x^*(k_x), y, z^*(k_z)) = k_z, \quad \rightarrow \quad k\frac{z^*(k_z)}{|\mathbf{x}^*(k_x, k_z)|} = k_z \tag{3.57}$$

$$|\mathbf{k}^G(\mathbf{x}^*(k_x, k_z))| = |\mathbf{k}|, \quad \rightarrow \quad k\frac{y}{|\mathbf{x}^*(k_x, k_z)|} = k_y \tag{3.58}$$

holds, i.e where the local propagation direction of the spherical wavefront coincides with that of the spectral plane wave, described by k_x, k_z.

From the same consideration as used in 3.3.2 the determinant of the phase function's Hessian is given in terms of the principal curvatures, known analytically for the Green's function. By definition, around the stationary position $k_y^G(\mathbf{x}^*(k_x, k_z)) = k_y$ holds, and the determinant reads as

$$\det H(\mathbf{x}^*(k_x, k_z)) = k^2\kappa_1^G(\mathbf{x}^*(k_x, k_z))\kappa_2^G(\mathbf{x}^*(k_x, k_z))\hat{k}_y^G(\mathbf{x}^*(k_x, k_z))^2 = \frac{k_y^2}{|\mathbf{x}^*(k_x, k_z)|^2}. \tag{3.59}$$

Accounting for the positive curvatures (the signature of the Hessian equals (-2)) the 2D Fourier transform can be approximated by the 2D SPA of (3.55) as

$$\tilde{G}(k_y, y, k_z) = \frac{2\pi}{\sqrt{|\det H(\mathbf{x}^*(k_x, k_z))|}}\frac{1}{4\pi}\frac{\mathrm{e}^{-\mathrm{j}k|\mathbf{x}^*(k_x,k_z)|}}{|\mathbf{x}^*(k_x, k_z)|}\mathrm{e}^{-\mathrm{j}\frac{\pi}{2}}, \tag{3.60}$$

Substituting the determinant and expressing the stationary positions by (3.56) leads finally to

$$\tilde{G}(k_y, y, k_z) = \frac{1}{2}\frac{\mathrm{e}^{-\mathrm{j}k_y y}}{\mathrm{j}k_y} = \frac{1}{2}\frac{\mathrm{e}^{-\mathrm{j}\sqrt{\left(\frac{\omega}{c}\right)^2 - k_x^2 - k_z^2}\,y}}{\mathrm{j}\sqrt{\left(\frac{\omega}{c}\right)^2 - k_x^2 - k_z^2}}. \tag{3.61}$$

Field of a planar radiator

Comparison with Table (2.1) reveals that in this special case the 2D SPA yields the exact spectrum of the Green's function in the propagation region.

Similarly to the previous example, the above equation describes the field of an infinite planar set of point sources with a harmonic spatial distribution, generating plane waves into the direction $\mathbf{k} = [k_x,\ k_y,\ k_z]^{\mathrm{T}}$, measured at $\mathbf{x} = [0,\ y,\ 0]^{\mathrm{T}}$. Furthermore at $k_x = k_z = 0$ the spectrum yields the 1D Green's function

$$G_{1\mathrm{D}}(y, \omega) = \frac{1}{2}\frac{\mathrm{e}^{-\mathrm{j}ky}}{\mathrm{j}k}, \tag{3.62}$$

1D Green's function

describing the field of a vibrating infinite planar surface, with the frequency response given by $\sim \frac{1}{\mathrm{j}\omega}$ and the impulse response being a Heaviside step function. The 1D Green's function therefore realizes the full integration of the source time history, while the 2D Green's function's impulse response can be interpreted as the half-integration of the source signal [DB83; WR09; Sch+13; Wan16].

4 Theory of sound field synthesis

In the following the general sound field synthesis (SFS) problem is formulated. Consider a source-free volume $\Omega \subset \mathbb{R}^3$, bounded by a continuous set of acoustic sources forming the boundary surface $\partial\Omega$. The enclosing source ensemble is termed the *secondary source distribution (SSD)*. The general geometry is depicted in Figure 4.1. For the sake of simplicity it is assumed that the boundary is acoustically transparent and the secondary sources are acoustic point sources described by the free field Green's function. Since closed-box, dynamic loudspeakers can be modeled as 3D monopoles in the low-frequency region, this choice of secondary sources is reasonable.

With these assumptions the synthesized pressure at any receiver position $\mathbf{x} \in \Omega$ is given by the superposition of the fields of individual secondary sources, written as a single layer potential [Ahr10; Ahr12; Wie14; SS14]

$$P(\mathbf{x}, \omega) = \oint_{\partial\Omega} D(\mathbf{x}_0, \omega)\, G(\mathbf{x} - \mathbf{x}_0, \omega) \mathrm{d}\partial\Omega(\mathbf{x}_0), \tag{4.1}$$

with $G(\mathbf{x}, \omega)$ denoting the 3D free field Green's function. The weighting factor $D(\mathbf{x}_0, \omega)$, i.e. the loudspeaker driving signal is termed the *driving function* for the given SSD. The sound field synthesis problem can be formulated as the following: Given a *target sound field* or the sound field of a *virtual source* $P(\mathbf{x}, \omega)$, the aim is to solve the above integral equation for $D(\mathbf{x}_0, \omega)$, so that the superposition of the SSD's sound field—the *synthesized field*—equals to the target sound field. The problem is therefore an inverse problem with unique solution for general enclosures [Faz10].

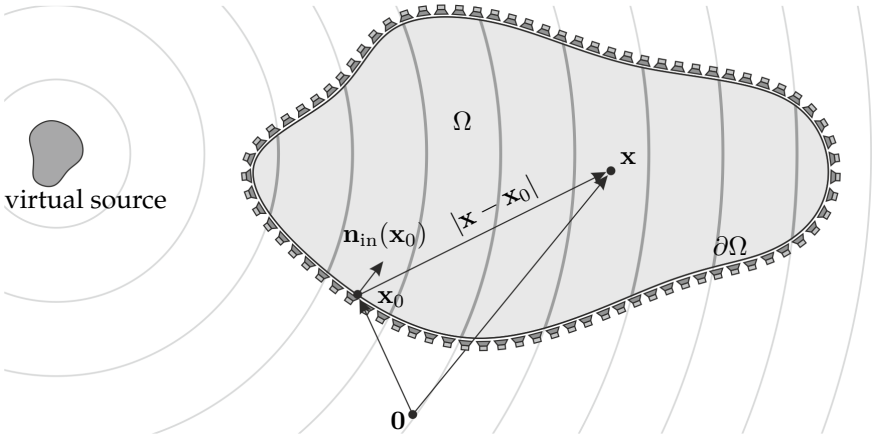

Figure 4.1. Geometry for the general sound field synthesis problem

Comparing the general SFS formulation (4.1) with the Kirchhoff-Helmholtz integral (2.55) it becomes obvious that SFS with a single layer SSD is not able to ensure identically zero sound field outside the enclosure. Practically, the dipole sources that would cancel the field of the monopoles outside the volume are excluded from the superposition. In the present thesis free field conditions are assumed: the exterior sound field satisfies the Sommerfeld radiation condition, thus the effects of the listening environment in practical applications (i.e. wall reflections) are not considered. For the inclusion of room effects to the SFS problem refer to [Spo05; Cec+18].

The above discussed general 3D SFS setup requires an enclosing surface of 3D point sources, making practical implementations hardly realizable. In practice it is often sufficient to restrict the reproduction to the $z = 0$ plane, containing a 2D contour of secondary sources. This reproduction scenario is termed *2.5D synthesis*, referring to the fact that although the problem dimensionality is reduced to $n = 2$, still the 2D SSD contour consists of 3D point source elements. In this geometry the general 2.5D synthesis problem is formulated as

$$P(\mathbf{x}, \omega) = \oint_C D(x_0, y_0, 0, \omega) G(x - x_0, y - y_0, 0, \omega) \, \mathrm{d}s(x_0, y_0), \tag{4.2}$$

where $C(x_0, y_0)$ is the SSD contour and $\mathrm{d}s$ is the infinitesimal arc length. Obviously, neither 2D nor 3D sound fields can be perfectly synthesized in this geometry due to dimensionality inconsistency between the target field and the SSD. Overcoming the artifacts of this *dimensionality mismatch* is the central question of practical sound field synthesis and is the main topic of the present chapter.

In the followings this chapter presents the approaches to solve the 3D and 2.5D SFS problems including physically based implicit and particularly mathematical explicit solutions.

4.1 Implicit solution: Wave Field Synthesis

The implicit solution for the SFS problem aims at the derivation of a single layer potential representation of the target sound field, containing the required SSD driving function implicitly. In the following section it is discussed, how this appropriate surface, or more practically contour integral representation of an arbitrary 3D sound field may be expressed in the form of (4.1) and (4.2), from which the driving function can be extracted.

4.1.1 3D Wave Field Synthesis

In case of a 3D SFS problem obtaining the implicit solution is straightforward, based on the boundary integral representations discussed in the previous chapters. Assume a general enclosing 3D SSD surface consisting of 3D point sources. Comparing the Kirchhoff approximation of the Kirchhoff-Helmholtz integral (3.21) or (3.43) with

the general SFS equation (4.1) reveals that the Kirchhoff approximation implicitly contains the driving function $D(\mathbf{x}_0, \omega)$ for a general enclosing SSD:

$$D(\mathbf{x}_0, \omega) = -2w(\mathbf{x}_0) \frac{\partial P(\mathbf{x}_0, \omega)}{\partial \mathbf{n}_{\text{in}}}, \tag{4.3}$$

or, making use of the high frequency gradient approximation, as

3D WFS driving function

$$D(\mathbf{x}_0, \omega) = 2w(\mathbf{x}_0) \mathrm{j} k_{\text{n}}^{P}(\mathbf{x}_0) P(\mathbf{x}_0, \omega) \tag{4.4}$$

with $k_{\text{n}}^{P}(\mathbf{x}_0)$ being the normal component of the target field's local wavenumber vector taken on the SSD and $w(\mathbf{x}_0)$ being the window function, as introduced in the previous chapter:

$$w(\mathbf{x}_0) = \begin{cases} 1, & \forall \quad \langle \mathbf{k}^{P}(\mathbf{x}_0) \cdot \mathbf{n}_{\text{in}}(\mathbf{x}_0) \rangle > 0 \\ 0 & \text{elsewhere.} \end{cases} \tag{4.5}$$

In the context of WFS the windowing is termed *secondary source selection* [NE99; Spo07a; Spo07b], selecting the *active secondary sources* contributing to the synthesized field.

The driving function (4.4) is a common generalization of the 3D WFS driving function given by [ZS13, (20)] specifically for a virtual point source. Both formulations are valid in the high frequency region within the validity of the Kirchhoff approximation: in the farfield of the virtual source distribution, i.e. where the local plane wave approximation of the virtual field holds.

In the special case of an infinite planar boundary surface, located along the plane $y = y_0$, the Kirchhoff-Helmholtz integral degenerates to the Rayleigh I (Neumann) integral representing the field of any source distribution located at $y < y_0$ in terms of a single layer potential, as discussed in Section 2.4.3. Therefore, in this geometry with a planar SSD the driving function (4.3) is capable of the perfect synthesis of an arbitrary virtual sound field in the listening half-space $y > y_0$ without any approximations involved. In this case no windowing is required, i.e. $w(\mathbf{x}_0) \equiv 1$ and the normal derivative is simply given by the y-derivative of the target/virtual sound field.

The following physical interpretation can be assigned to the 3D WFS driving function: As it was discussed in Section 3.3.3, the frequency response of the 1D Green's function, given by (3.62)—representing an infinite planar distribution of 3D point sources—is proportional to $\sim \frac{1}{\mathrm{j}k} = \frac{c}{\mathrm{j}\omega}$ expressing an infinite impulse response of a step function, performing the integration of the source time history. In case of a non-homogeneous distribution a directivity factor is also present, given by $\frac{1}{\mathrm{j}k_y}$ for a harmonic distribution as given by (3.61) and approximated locally by (3.37). This directivity factor of $\frac{1}{\mathrm{j}k_y^{P}(\mathbf{x}_0)}$ indicates that a surface of point sources generates larger pressure field into lateral directions than into the normal direction. Within the validity of the Kirchhoff approximation this statement can be extended towards arbitrary SSD surfaces, radiating with an enhanced amplitude into locally lateral directions.

The factor $\mathrm{j}k_{\text{n}}^{P}(\mathbf{x}_0)$ in (4.4) and in the Rayleigh/Kirchhoff-Helmholtz integral may be therefore interpreted as a correction term, ensuring flat frequency response for the SSD surface by inverse filtering (taking the time derivative) of the excitation signal, and compensating for the SSD directive radiation characteristics locally.

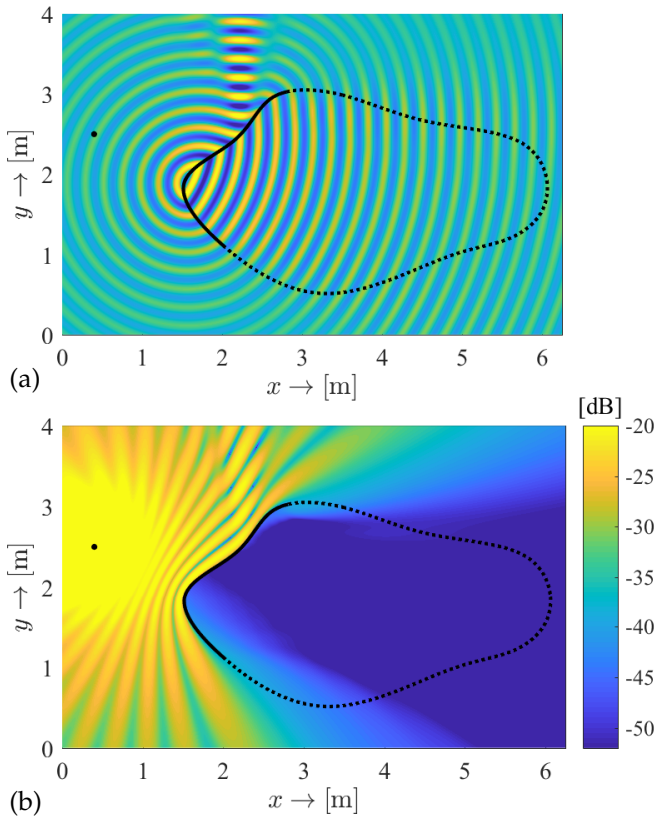

Figure 4.2. 3D synthesis of a 3D point source located at $\mathbf{x}_\mathrm{s} = [0.4,\ 2.5,\ 0]^\mathrm{T}$, radiating at $f_0 = 1.5$ kHz. The SSD surface is chosen to be independent of the z-coordinate as illustrated in Figure 4.3. For the numerical calculation the SSD was truncated along the vertical dimension by choosing parameters, so that diffraction effects due to the truncation are negligible in the simulation results. Figure (a) depicts the real part of the synthesized field and part (b) presents the absolute error of synthesis (the discrepancy between the synthesized and the target sound field) in a logarithmic scale measured in the horizontal plane, containing the virtual point source. The active arc of the SSD is denoted by solid black line, and the inactive part with dotted by black line.

Application example: 3D synthesis of a virtual point source

As a simple example the 3D WFS of a virtual point source is discussed. Assume a 3D point source located behind the SSD at $\mathbf{x}_\mathrm{s} = [x_s,\ y_s,\ z_s]^\mathrm{T}$ with $y_s < y_0$. Substituting the Green's function into (4.4) yields the point source specific high frequency 3D WFS driving function

$$D(\mathbf{x}_0, \omega) = w(\mathbf{x}_0) \frac{\mathrm{j}k}{2\pi} \frac{\langle \mathbf{x}_0 - \mathbf{x}_\mathrm{s} \cdot \mathbf{n}_\mathrm{in}(\mathbf{x}_0) \rangle}{|\mathbf{x}_0 - \mathbf{x}_\mathrm{s}|} \frac{\mathrm{e}^{-\mathrm{j}k|\mathbf{x}_0 - \mathbf{x}_\mathrm{s}|}}{|\mathbf{x}_0 - \mathbf{x}_\mathrm{s}|}, \tag{4.6}$$

being equivalent to [ZS13, Eq. 20.] and [Spo+08, Eq. 19.].

The result of synthesis is depicted in Figure 4.2 for the special case of an SSD surface, being invariant to translation along the z-axis, as illustrated by Figure 4.3 in the following section. The driving function ensures amplitude correct synthesis within the validity of the Kirchhoff approximation: amplitude errors arise

- in the proximity of secondary sources with large local curvature of the SSD surface, due to the local failure of the tangent plane approximation
- in the proximity of secondary sources where the normal component of the local wavenumber vector is small—i.e. at parts of the SSD that are nearly parallel to the local virtual field propagation direction— since at these positions the high frequency gradient approximation fails, with also the lack of diffracted waves causing amplitude errors.
- at space regimes for which the above described secondary sources serve as stationary positions as discussed in Section 3.3.2.

The driving function (4.6) expresses the loudspeaker driving signal for a virtual point source radiating at a single frequency component. Assuming a wideband source excitation with the time history given by $s(t)$ and its frequency content being $S(\omega)$ the time domain WFS driving function is given by the inverse temporal Fourier transform of (4.6) weighted by the excitation spectrum:

$$d(\mathbf{x}_0, t) = \frac{w(\mathbf{x}_0)}{2\pi} \int_{-\infty}^{\infty} \frac{\langle \mathbf{x}_0 - \mathbf{x}_\mathrm{s} \cdot \mathbf{n}_\mathrm{in}(\mathbf{x}_0) \rangle}{|\mathbf{x}_0 - \mathbf{x}_\mathrm{s}|} \frac{\mathrm{j}\omega}{2\pi c} S(\omega) \frac{\mathrm{e}^{\mathrm{j}\omega(t - \frac{|\mathbf{x}_0 - \mathbf{x}_\mathrm{s}|}{c})}}{|\mathbf{x}_0 - \mathbf{x}_\mathrm{s}|} \mathrm{d}\omega. \tag{4.7}$$

By realizing that $\mathrm{j}\omega\, S(\omega)$ describes the temporal derivative of the source time history (being equivalent with filtering the source signal with a 6 dB/octave highpass filter) and exploiting the Fourier transform shift theorem, the time domain 3D WFS driving function for a virtual point source is obtained as

$$d(\mathbf{x}_0, t) = \frac{w(\mathbf{x}_0)}{2\pi c} \frac{\langle \mathbf{x}_0 - \mathbf{x}_\mathrm{s} \cdot \mathbf{n}_\mathrm{in}(\mathbf{x}_0) \rangle}{|\mathbf{x}_0 - \mathbf{x}_\mathrm{s}|} \frac{s_t'(t - \frac{|\mathbf{x}_0 - \mathbf{x}_\mathrm{s}|}{c})}{|\mathbf{x}_0 - \mathbf{x}_\mathrm{s}|}, \tag{4.8}$$

where differentiation with respect to time compensates for the SSD frequency response, as discussed above.

4.1.2 The 2.5D Kirchhoff approximation

Before getting involved with the questions of 2.5D Wave Field Synthesis a further simplification of the Kirchhoff approximation is introduced. This simplification reduces the 3D Kirchhoff integral into a 2D contour integral representing a 3D sound field as the superposition of 3D Green's functions. The approximation is therefore referred to as the *2.5D Kirchhoff integral*, frequently occurring in the field of seismic migration and inversion problems. The dimensionality reduction is performed by applying the stationary phase approximation to the Kirchhoff integral along the vertical dimension.

Assume a 3D interior radiation problem, with the sound field under consideration described by the Kirchhoff integral (3.43) written on a surface, being translation invariant along the z-axis. The problem geometry is depicted in Figure 4.3. In the following the receiver position is assumed to be at $z = 0$ inside the enclosure at $\mathbf{x} = [x,\ y,\ 0]^\mathrm{T} \in \Omega$. In this special geometry the integral variables are separable and the Kirchhoff integral can be written as

$$P(\mathbf{x}, \omega) = \oint_C \int_{-\infty}^{\infty} 2w(\mathbf{x}_0)\mathrm{j}k_\mathrm{n}^P(\mathbf{x}_0) P(\mathbf{x}_0, \omega) G(\mathbf{x} - \mathbf{x}_0, \omega)\, \mathrm{d}z_0\, \mathrm{d}s(x_0, y_0), \tag{4.9}$$

with the integral variable $\mathrm{d}s$ being the infinitesimal arc length along the contour $C(x_0, y_0) = \partial\Omega(x_0, y_0, 0)$.

The integral along z_0 is approximated applying the stationary phase approximation. Application of the 1D SPA formulation (3.27) requires the definition of the stationary position and the sign of the integrand's phase function's second vertical derivative (i.e. the signature of the 1D Hessian) at the stationary position.

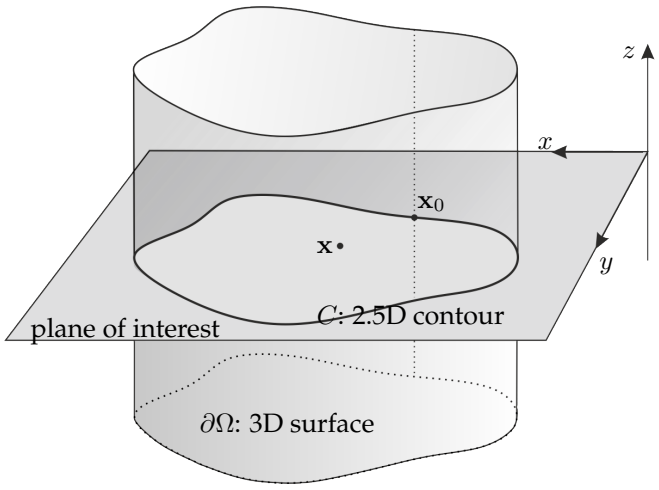

Figure 4.3. Geometry for the derivation of 2.5D Kirchhoff integral. The enclosing surface $\partial\Omega(x_0, y_0)$ is chosen to be independent of the z-coordinate in order to be able to evaluate the Kirchhoff integral with respect to z_0 using the SPA. If the sound field to be described is a 2D one propagating in the direction parallel to the listening plane, then the surface can be interpreted as a continuous set of infinite vertical line sources along C, capable of the perfect description of a 2D field inside the enclosure by a 2D countour integral.

Definition of the vertical stationary position: The vertical stationary position in the geometry under investigation is straightforward: Since the contour of integration is chosen to lie at the $z = 0$ plane, therefore the vertical stationary position has to be found at $z_0^* = 0$. Based on the foregoing this requirement can be formulated as

$$k_z^P(x_0, y_0, 0) = k_z^G(x - x_0, y - y_0, 0) = 0, \tag{4.10}$$

stating the trivial fact that a sound field can be described by a 2.5 dimensional contour integral only in the plane, where all the sound sources are located, and which plane the emerging waves propagate parallel with. In the plane of investigation $k_z^P(x, y, 0) \equiv 0$ holds for the field of 3D sources located at the plane of investigation and of 2D sources being invariant along the vertical dimension. Throughout the present thesis when dealing with 2.5D synthesis problems these types of virtual fields are considered exclusively.

Definition of the Hessian's signature: An important property of wavefields under consideration is that their vertical curvature—given by $\phi_{zz}^{P''}(x_0, y_0, 0, \omega)$—is one of their principal curvatures itself, denoted by κ_{v}^P. Hence, as it is discussed in Appendix B.1 in the stationary position ($z_0 = 0$) the principal curvatures are additive, and the second phase derivative is the negative sum of the principal curvatures of the target sound field and the Green's function:

$$\begin{aligned}\phi_{zz}^{P+G''}(x_0, y_0, 0, \omega) = \phi_{zz}^{P''}(x_0, y_0, 0, \omega) + \phi_{zz}^{G''}(x - x_0, y - y_0, 0, \omega) = \\ = -k\left(\kappa_{\mathrm{v}}^P(x_0, y_0, 0) + \kappa_{\mathrm{v}}^G(x - x_0, y - y_0, 0)\right).\end{aligned} \tag{4.11}$$

Note that here it was exploited that $\phi_{zz}^{P''} = \phi_{z_0 z_0}^{P''}$ and $\phi_{zz}^{G''} = \phi_{z_0 z_0}^{G''}$ holds. By definition, for an arbitrary diverging sound field (including the Green's function) the principal curvatures are positive and $\operatorname{sgn}\left(\phi_{zz}^{P+G''}(x_0, y_0, 0, \omega)\right) = -1$ trivially holds. For a converging wavefront the signature of the resultant curvature depends on the receiver position: in regions of the receiver plane where sound field P locally converges the resultant curvature is positive, while in regions where the sound field diverges, e.g.

after passing a focal point the resultant curvature is negative. In the present thesis only locally diverging wavefields are discussed.

With these considerations application of the SPA to (4.9) results in the *2.5D Kirchhoff integral* for diverging sound fields, reading as

2.5D Kirchhoff integral

$$P(\mathbf{x},\omega) = \oint_C 2w(\mathbf{x}_0)\sqrt{\frac{2\pi}{\mathrm{j}|\phi_{zz}^{P\prime\prime}(\mathbf{x}_0,\omega)+\phi_{zz}^{G\prime\prime}(\mathbf{x}-\mathbf{x}_0,\omega)|}}\cdot \cdot \underbrace{\mathrm{j}k_{\mathrm{n}}^{P}(\mathbf{x}_0)P(\mathbf{x}_0,\omega)}_{\approx -\frac{\partial P(\mathbf{x}_0,\omega)}{\partial \mathbf{n}_{\mathrm{in}}}} G(\mathbf{x}-\mathbf{x}_0,\omega)\mathrm{d}s(x_0,y_0), \quad (4.12)$$

with both $\mathbf{x} = [x,\ y,\ 0]^{\mathrm{T}}$ and $\mathbf{x}_0 = [x_0,\ y_0,\ 0]^{\mathrm{T}}$ denoting in-plane positions in the following when 2.5D scenarios are considered. Again, in this formulation the coincidence of the second derivatives with respect to z and z_0 of both P and G is exploited.

4.1.3 2.5D Wave Field Synthesis

The 2.5D Kirchhoff integral implicitly contains the 2.5D WFS driving function for a continuous contour of 3D point sources at the $z = 0$ plane. The resulting driving function is, however, still dependent on the listener position through the argument of $\phi_{zz}^{G\prime\prime}(\mathbf{x}-\mathbf{x}_0,\omega)$, which dependency may be avoided by fixing the listener position. This strategy would only allow the synthesis of the virtual field, optimized to a single, fixed receiver position termed the *reference point*, while in other points in the listening plane amplitude errors would be present. In the following it is presented how the driving function can be further manipulated in order to ensure correct synthesis along an arbitrary receiver curve termed the *reference curve* within the validity of the stationary phase approximation resulting in what was termed *unified 2.5D WFS theory* [Fir+17].

As it was stated in Section 3.3.2 for any receiver position $\mathbf{x}$ the Kirchhoff integral is dominated by that stationary contour element $\mathbf{x}_0^*(\mathbf{x})$, from which the emerging spherical wavefronts locally coincide with the target field wavefront, i.e. where $\mathbf{k}^P(\mathbf{x}_0^*(\mathbf{x})) = \mathbf{k}^G(\mathbf{x}-\mathbf{x}_0^*(\mathbf{x}))$ is satisfied. As a consequence, the 2.5D Kirchhoff integral may be further approximated by expressing the amplitude factor with its value at the stationary position as

$$P(\mathbf{x},\omega) = \oint_C 2w(\mathbf{x}_0)\sqrt{\frac{2\pi}{\mathrm{j}|\phi_{zz}^{P\prime\prime}(\mathbf{x}_0^*(\mathbf{x}))+\phi_{zz}^{G\prime\prime}(\mathbf{x}-\mathbf{x}_0^*(\mathbf{x}))|}}\cdot \cdot \mathrm{j}k_{\mathrm{n}}^{P}(\mathbf{x}_0)P(\mathbf{x}_0,\omega)G(\mathbf{x}-\mathbf{x}_0,\omega)\mathrm{d}s(x_0,y_0), \quad (4.13)$$

where $\mathbf{x}_0^*(\mathbf{x})$ is defined by the implicit relation above.

The statement can be expressed by reversing causality, forming the main idea of 2.5D WFS theory: every point $\mathbf{x}_0$ on the secondary distribution contributes to the total sound field at the set of positions $\mathbf{x}(\mathbf{x}_0)$ where the local propagation direction of a point source positioned at $\mathbf{x}_0$ coincides with that of the target field, i.e. where their local wavenumber vectors coincide. Hence $\mathbf{x}$ and $\mathbf{x}_0$ are *stationary point pairs*, mutually determining each other. By reversing the causality choosing $\mathbf{x}_0$ as an independent

parameter the driving function can be extracted from (4.13) resulting in the *unified 2.5D WFS driving function*

2.5D WFS driving function

$$D(\mathbf{x}_0,\omega) = w(\mathbf{x}_0)\sqrt{\frac{8\pi}{\mathrm{j}k}}\sqrt{d_{\mathrm{ref}}(\mathbf{x}_0)}\mathrm{j}k_{\mathrm{n}}^{P}(\mathbf{x}_0)P(\mathbf{x}_0,\omega), \tag{4.14}$$

with the term $d_{\mathrm{ref}}(\mathbf{x}_0)$ denoting the *referencing function*, defined as

$$d_{\mathrm{ref}}(\mathbf{x}_0) = \frac{k}{|\phi_{zz}^{P''}(\mathbf{x}_0) + \phi_{zz}^{G''}(\mathbf{x}_{\mathrm{ref}}(\mathbf{x}_0) - \mathbf{x}_0)|} = \tag{4.15}$$

$$= \frac{1}{\kappa_{\mathrm{v}}^{P}(\mathbf{x}_0) + \kappa_{\mathrm{v}}^{G}(\mathbf{x}_{\mathrm{ref}}(\mathbf{x}) - \mathbf{x}_0)} = \tag{4.16}$$

$$= \frac{\rho_{\mathrm{v}}^{P}(\mathbf{x}_0)\cdot\rho_{\mathrm{v}}^{G}(\mathbf{x}_{\mathrm{ref}}(\mathbf{x}) - \mathbf{x}_0)}{\rho_{\mathrm{v}}^{P}(\mathbf{x}_0) + \rho_{\mathrm{v}}^{G}(\mathbf{x}_{\mathrm{ref}}(\mathbf{x}) - \mathbf{x}_0)}, \tag{4.17}$$

where κ_{v}^{P}, κ_{v}^{G} and ρ_{v}^{P},ρ_{v}^{G} are the vertical principal curvatures and radii of the involved sound fields, respectively. Position $\mathbf{x}_{\mathrm{ref}}(\mathbf{x}_0)$ is the *reference position* for the SSD element at $\mathbf{x}_0$, for which receiver position $\mathbf{x}_0$ serves as a stationary phase point on the SSD, defined by

2.5D WFS reference position

$$\mathbf{k}^{P}(\mathbf{x}_0) = \mathbf{k}^{G}(\mathbf{x}_{\mathrm{ref}}(\mathbf{x}_0) - \mathbf{x}_0). \tag{4.18}$$

By substituting the explicit expression for the Green's function's wavenumber ($\mathbf{k}^{G}(\mathbf{x}) = k\frac{\mathbf{x}}{|\mathbf{x}|}$) into (4.18) the set of positions for which a given $\mathbf{x}_0$ serves as stationary point reads as

$$\mathbf{x}_{\mathrm{ref}}(\mathbf{x}_0) = \mathbf{x}_0 + \hat{\mathbf{k}}^{P}(\mathbf{x}_0)|\mathbf{x}_{\mathrm{ref}}(\mathbf{x}_0) - \mathbf{x}_0|, \tag{4.19}$$

with $\hat{\mathbf{k}}^{P}(\mathbf{x}_0)$ denoting the normalized local wavenumber vector, being the unit vector into the target field's local propagation direction. The equation describes straight lines passing through $\mathbf{x}_0$ into the direction of the local wavenumber vector of the target sound field $\mathbf{k}^{P}(\mathbf{x}_0)$. Along this straight line inside the listening region the virtual field wavefront matches the actual SSD element's wavefront. Each SSD element therefore dominates the synthesized field towards the direction of the virtual field's local propagation direction measured at the SSD position, and a unique reference position can be defined for each SSD element along this path, where the target field's and the secondary source's wavefronts match in amplitude as well.

In practical applications the set of the reference positions for all secondary sources form a prescribed continuous *reference curve* C_{ref}, so that the reference position for an SSD element is found at the intersection of the straight line, described by (4.19) and the reference curve. The reference curve must be a smooth convex curve inside the listening region, ensuring that each reference point has a unique stationary point pair. Once the reference position $\mathbf{x}_{\mathrm{ref}}(\mathbf{x}_0) \in C_{\mathrm{ref}}$ is known for each SSD element the WFS driving function (4.14) can be evaluated. Referencing the WFS driving function is therefore done by prescribing a unique reference point for each SSD element with the aid of the SPA, so that the set of these reference points form the continuous reference curve. The resulting driving function will result in amplitude correct synthesis over the reference curve within the validity of the integral formulation (4.13).

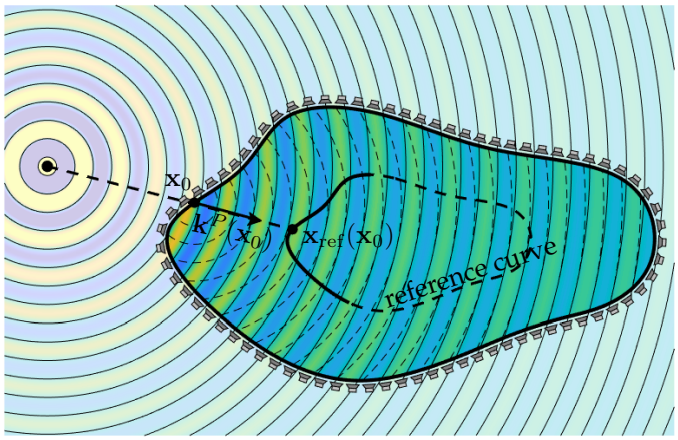

Figure 4.4. Location of the reference position for an SSD element positioned at $\mathbf{x}_0$. Due to the phase characteristics of the Green's function the reference position $\mathbf{x}_{\mathrm{ref}}(\mathbf{x}_0)$ for an arbitrary SSD element can be found at the intersection of the reference curve and the line emerging from $\mathbf{x}_0$ pointing into the local wavenumber vector of the virtual field $\mathbf{k}^P(\mathbf{x}_0)$. The location of the arbitrarily chosen reference curve is denoted by dashed black line with solid line indicating the positions, for which a stationary SSD position can be found. Amplitude correct synthesis may be only achieved along this part of the reference curve.

The location of the reference position for a given SSD element is illustrated in Figure 4.4 for the case of a virtual point source. Once the reference position is expressed for each SSD element, the driving function can be evaluated.

In order to gain a physical interpretation of the structure of the resulting driving function, the referencing function can be expressed in terms of the vertical principal radii of the virtual field and the Green's function, yielding

Detailed 2.5D WFS driving function

$$D(\mathbf{x}_0,\omega) = \underbrace{\sqrt{\frac{2\pi\rho_{\mathrm{v}}^G(\mathbf{x}_{\mathrm{ref}}(\mathbf{x}_0)-\mathbf{x}_0)}{\mathrm{j}k}}}_{\substack{\text{SSD}\\ \text{compensation}}} \underbrace{\sqrt{\frac{\rho_{\mathrm{v}}^P(\mathbf{x}_0)}{\rho_{\mathrm{v}}^P(\mathbf{x}_0)+\rho_{\mathrm{v}}^G(\mathbf{x}_{\mathrm{ref}}(\mathbf{x}_0)-\mathbf{x}_0)}}}_{\substack{\text{virtual source}\\ \text{compensation}\\ = \sqrt{\frac{\rho_{\mathrm{v}}^P(\mathbf{x}_0)}{\rho_{\mathrm{v}}^P(\mathbf{x}_{\mathrm{ref}}(\mathbf{x}_0))}}}} \underbrace{2w(\mathbf{x}_0)\mathrm{j}k_{\mathrm{n}}^P(\mathbf{x}_0)P(\mathbf{x}_0,\omega)}_{\substack{\text{2D high freq.}\\ \text{driving function}}}. \tag{4.20}$$

Again, ρ_v^P and ρ_v^G denote the principal radii of the virtual field and the Green's function along the vertical direction, with the absolute value operation in (4.15) omitted due to their positive sign for diverging virtual fields. The Green's function's principal radius is given simply as $\rho_{\mathrm{v}}^G(\mathbf{x}_{\mathrm{ref}}(\mathbf{x}_0)-\mathbf{x}_0) = |\mathbf{x}_{\mathrm{ref}}(\mathbf{x}_0)-\mathbf{x}_0|$ and the virtual field's principal radius $\rho_{\mathrm{v}}^P(\mathbf{x}_{\mathrm{ref}}(\mathbf{x}_0))$ is expressed by applying (B.25).

The terms in the driving function can be identified as compensation factors for the *dimensionality mismatch*, emerging in the 2.5D Kirchhoff integral. Expressing the Kirchhoff approximation (3.21) for an entirely 2D problem, an arbitrary 2D sound field may be described in the area of investigation by a contour integral. The enclosing boundary can be interpreted as the continuous distribution of two dimensional secondary point sources described by the 2D Green's function, representing infinite vertical line sources in three dimensions. The 2D Green's function is weighted by the normal derivative of the sound field, taken on the SSD contour. Application of the 2.5D WFS driving function aims to describe a 3D sound field in terms of a 2D contour integral with the kernel being the 3D Green's function, weighted by the normal derivative of the 3D

sound field. This results in a dimensionality mismatch for both the virtual field and the secondary source elements. The interpretation of the compensation factors in the driving function is then the following:

- Term $\sqrt{\frac{2\pi|\mathbf{x}_{\mathrm{ref}}(\mathbf{x}_0)-\mathbf{x}_0|}{\mathrm{j}k}}$ is the compensation factor for the *secondary source dimensionality mismatch*. Comparison with (3.54) indicates that the compensation factor approximates the frequency response and attenuation factor of the 2D Green's function in terms of the 3D Green's function. Obviously, the attenuation factors can be matched only at a particular distance from a given SSD element $\mathbf{x}_0$, chosen to be at the reference position $\mathbf{x}_{\mathrm{ref}}(\mathbf{x}_0)$. On the other hand, the frequency response compensation term ensures the flat frequency response of the SSD: a 2D contour of point sources exhibits the frequency response of $\sim \frac{1}{\sqrt{\mathrm{j}k}}$, which along with the normal derivative term would result in a transfer function of $\sim \sqrt{\mathrm{j}k}$, that has to be compensated for.
- The virtual source compensation factor resolves the *virtual source dimensionality mismatch*, correcting the virtual source attenuation factor from a 2D to a 3D one. It is assumed that the general relationship between a 2D and a 3D sound field, generated by the same planar source distribution at $z = 0$ reads as

$$P_{\mathrm{3D}}(\mathbf{x},\omega) = \sqrt{\frac{\mathrm{j}k}{2\pi}}\frac{P_{\mathrm{2D}}(\mathbf{x},\omega)}{\sqrt{\rho_{\mathrm{v}}^{P}(\mathbf{x})}}, \tag{4.21}$$

  at $x = [x,\ y,\ 0]^{\mathrm{T}}$. This is a straightforward generalization of (3.54) towards general sound fields. Expressing a 2D sound field at $\mathbf{x}_{\mathrm{ref}}(\mathbf{x}_0)$ in terms of the 2D Kirchhoff integral and rewriting in terms of the corresponding 3D sound fields by applying (4.21) leads to the virtual source correction factor under discussion. A detailed explanation for the virtual source dimensionality compensation is given for the special case of a virtual point source in [VF12].

Referencing the synthesis therefore can be interpreted physically as adjusting both attenuation correction factors for each SSD element to be amplitude correct on the reference curve, performed by prescribing a frequency independent curvature correction factor.

The introduced driving function is capable of the synthesis of arbitrary sound fields applying arbitrary shaped convex SSDs, referencing the synthesis to an arbitrary reference curve. The result of such a general 2.5D WFS scenario is presented in Figure 4.5. As the image depicting the synthesis error indicates: on those part of the reference curve for which a stationary point pair can be found on the SSD amplitude correct synthesis is ensured, as the error exhibits a minimum.

If a parametrization of the SSD contour and the reference curve along with an analytical virtual source model is known, the referencing function can be expressed analytically, resulting in closed form driving function specific to the SSD and the referencing contour. The following two examples are presented in order to demonstrate the analytical application of the presented driving function.

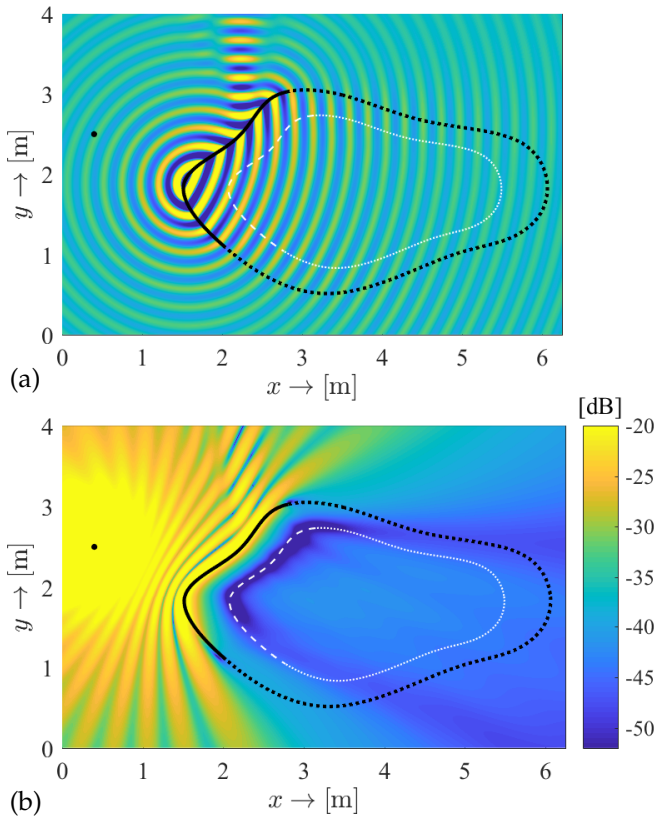

Figure 4.5. 2.5D synthesis of a 3D point source located at $\mathbf{x}_\mathrm{s} = [0.4,\ 2.5,\ 0]^\mathrm{T}$, radiating at $f_0 = 1.5$ kHz. Figure (a) depicts the real part of the synthesized field, (b) presents the absolute error of synthesis in a logarithmic scale. The reference curve was defined by simple rescaling of the SSD contour, however, an arbitrary convex reference contour could be chosen. The active arc of the SSD is denoted by solid black line, and the inactive part with dotted by black line. The reference position on the reference curve for each active SSD element is evaluated numerically. Obviously in the present geometry there exist secondary sources, for which no unique reference position can be found. In order to ensure smooth driving function and avoid truncation artifacts for these SSD positions the referencing function is extrapolated.

Application example #1: Synthesis of a 3D point source applying a linear SSD

As a first example assume an infinite linear SSD located at $\mathbf{x}_0 = [x_0,\ 0,\ 0]^\mathrm{T}$. The reference contour is set to be an infinite line parallel to the SSD, located at $\mathbf{x}_\mathrm{ref} = [x_0,\ y_\mathrm{ref},\ 0]^\mathrm{T}$. This geometry has a distinctive role in the field of sound field synthesis, being the arrangement for which traditional WFS was first formulated [Ber88; Ber+93; Sta97; Ver97]. In this arrangement the driving function may be derived from the vertical SPA of the Neumann Rayleigh integral, which describes a sound field precisely in terms of a planar single layer potential. Therefore application of a linear SSD involves the least approximations, avoiding errors present in the Kirchhoff approximation. Furthermore, choosing a reference line parallel to the SSD ensures the existence of a unique reference position for each SSD element, therefore amplitude correct synthesis may be ensured over the entire reference line. Finally, explicit solution can be found directly for this special geometry as described in the following section.

Generally speaking, the evaluation of the referencing function (4.15) requires the definition of the Green's function's principal radius, centered at $\mathbf{x}_0$ and measured at the reference position. For the special case of the Green's function this is given by the simple Euclidean distance of the two points. Hence, the determination of the distance between the reference position and the corresponding secondary sources is required by solving equation (4.18) for $|\mathbf{x}_\mathrm{ref}(\mathbf{x}_0) - \mathbf{x}_0|$, termed the *reference distance*. The terminology indicates that it denotes the distance measured from the individual secondary sources at which the synthesis is optimized.

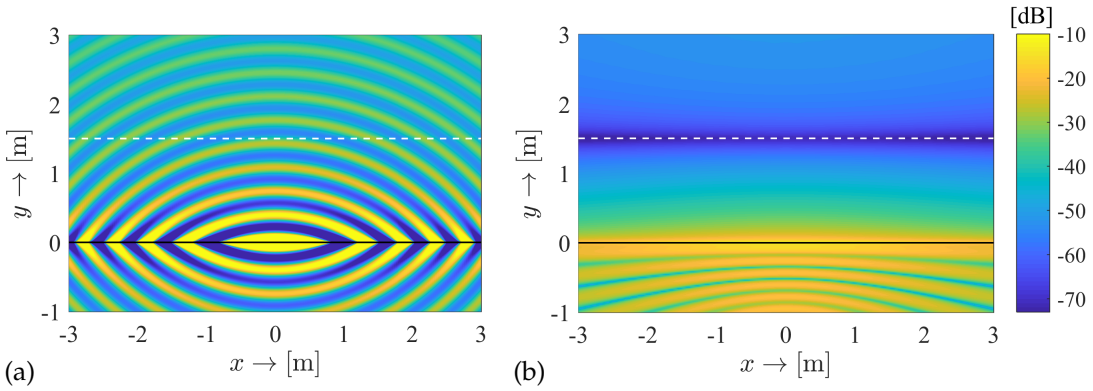

Figure 4.6. 2.5D synthesis of a 3D point source located at $\mathbf{x}_\mathrm{s} = [0,\ -2,\ 0]^\mathrm{T}$, radiating at $f_0 =$ kHz with the reference line set at $y_\mathrm{ref} = 1.5$ m. Figure (a) depicts the real part of the synthesized field, (b) shows the error of synthesis. Based on the equivalent scattering interpretation of the synthesis the discrepancy between the synthesized field and the virtual field at $y < 0$ can be interpreted as the field of a point source reflected from a planar scatterer surface. Due to the problem symmetry the scattered field is given amplitude correctly along $y = -y_\mathrm{ref}$.

In the arrangement under discussion both $\mathbf{x}_0$ and $\mathbf{x}_\mathrm{ref}$ are lying along infinite parallel lines, with the y-coordinates of both curves fixed to constant, thus for the second coordinates of equation (4.18)

$$y_\mathrm{ref} = y_0 + \hat{k}_y^P(\mathbf{x}_0)|\mathbf{x}_\mathrm{ref}(\mathbf{x}_0) - \mathbf{x}_0| \tag{4.22}$$

must hold. With $y_0 = 0$ the above equation yields the reference distance for the present geometry

$$|\mathbf{x}_\mathrm{ref}(\mathbf{x}_0) - \mathbf{x}_0| = \frac{y_\mathrm{ref}}{\hat{k}_y^P(\mathbf{x}_0)} = \rho_\mathrm{v}^G(\mathbf{x}_\mathrm{ref}(\mathbf{x}) - \mathbf{x}_0). \tag{4.23}$$

Substitution into (4.20) yields the linear 2.5D WFS driving function, ensuring amplitude correct synthesis of an arbitrary sound field on a reference line, reading as

$$D(\mathbf{x}_0, \omega) = \sqrt{\frac{8\pi}{\mathrm{j}k}}\sqrt{\rho_\mathrm{v}^P(\mathbf{x}_0)}\sqrt{\frac{y_\mathrm{ref}}{y_\mathrm{ref} + \rho_\mathrm{v}^P(\mathbf{x}_0)\hat{k}_y^P(\mathbf{x}_0)}}\mathrm{j}k_y^P(\mathbf{x}_0)P(\mathbf{x}_0, \omega). \tag{4.24}$$

Finally, expressing the pressure field and the normalized local wavenumber vector of the virtual point source results in the virtual source-SSD shape-receiver shape specific driving function

Linear WFS point source driv. fun.

$$D(\mathbf{x}_0, \omega) = -\frac{1}{4\pi}\sqrt{\frac{8\pi}{\mathrm{j}k}}\sqrt{\frac{y_\mathrm{ref}}{y_\mathrm{ref} - y_s}}\mathrm{j}ky_s\frac{\mathrm{e}^{-\mathrm{j}k|\mathbf{x}_0 - \mathbf{x}_\mathrm{s}|}}{|\mathbf{x}_0 - \mathbf{x}_\mathrm{s}|^{\frac{3}{2}}}. \tag{4.25}$$

This result is equivalent with the traditional WFS driving function of a point source [Ver97, (2.27)], [Sta97, (3.16)&(3.17)], and furthermore identical to the farfield/high frequency approximated explicit solution presented in the next section [SA10, (25)], [F.S16, Ch. 2.3]. The result of synthesis is depicted in Figure 4.6 confirming that by applying the derived driving function amplitude correct synthesis is ensured along the reference line.

Taking the temporal inverse Fourier transform of the driving function weighted by $S(\omega)$ yields the temporal driving function for a virtual point source with the source time history of $s(t)$. Exploiting the shift theorem and the associativity of convolution yields the temporal driving function

Linear time domain point source driv. fun.

$$d(\mathbf{x}_0, t) = -\sqrt{\frac{1}{2\pi c}}\sqrt{\frac{y_{\text{ref}}}{y_{\text{ref}} - y_s}}\, y_s \frac{s_t'(t - \frac{|\mathbf{x}_0 - \mathbf{x}_\text{s}|}{c})}{|\mathbf{x}_0 - \mathbf{x}_\text{s}|^{\frac{3}{2}}}, \tag{4.26}$$

where $s_t'(t) = h(t) *_t s(t)$, with $*_t$ denoting convolution in the time domain. The source time history is pre-equalized with a filter, exhibiting the frequency response of $H(\omega) = \sqrt{\text{j}\omega}$ being a half-differentiator. The filter compensates the frequency response of a 2D SSD contour as the part of the secondary source compensation factor, as discussed above, and is therefore always the part of the 2.5D diving function for an arbitrary target sound field and for an arbitrary SSD shape. The impulse response of the SSD compensation filter can be expressed by differentiating the half-integrator's impulse response as given in [DB83]

$$h(t) = \frac{\delta(t)}{\sqrt{\pi t}} - \frac{1}{2}\frac{\theta(t)}{t^{3/2}}, \tag{4.27}$$

where $\theta(t)$ is the Heaviside step function. Practical implementation of this prefilter is discussed in details in [Sch+13] applying IIR filters, while in [F.S16, Sec. 2.5] the ideal FIR filter coefficients are given analytically.

Application example #2: Synthesis of a plane wave applying a circular SSD

As a second example the synthesis of a plane wave applying a circular SSD, centered at the origin with the radius of R_SSD is presented. The synthesis is referenced to a concentric circle inside the SSD with the radius of R_ref. For this geometry the explicit driving function is also available [AS08a; AS09b; AS09a], which are however not discussed in details in the present thesis.

Again, the system of equations describing the reference distance for each SSD element is given by

$$\mathbf{x}_\text{ref}(\mathbf{x}_0) = \mathbf{x}_0 + \hat{\mathbf{k}}^P(\mathbf{x}_0)|\mathbf{x}_\text{ref}(\mathbf{x}_0) - \mathbf{x}_0|, \tag{4.28}$$

$$|\mathbf{x}_\text{ref}(\mathbf{x}_0)| = R_\text{ref}. \tag{4.29}$$

Expressing the reference distance leads to a second order equation. By exploiting that $|\mathbf{x}_0| = R_\text{SSD}$, $|\hat{\mathbf{k}}^P(\mathbf{x}_0)| = 1$ and taking only the smaller root into consideration—corresponding to the closer arc of the reference circle to the actual SSD position—yields the reference distance

$$|\mathbf{x}_\text{ref}(\mathbf{x}_0) - \mathbf{x}_0| = R_\text{SSD}\left(\hat{k}_r^P(\mathbf{x}_0) + \sqrt{\hat{k}_r^P(\mathbf{x}_0)^2 + \left(\frac{R_\text{ref}}{R_\text{SSD}}\right)^2 - 1}\right), \tag{4.30}$$

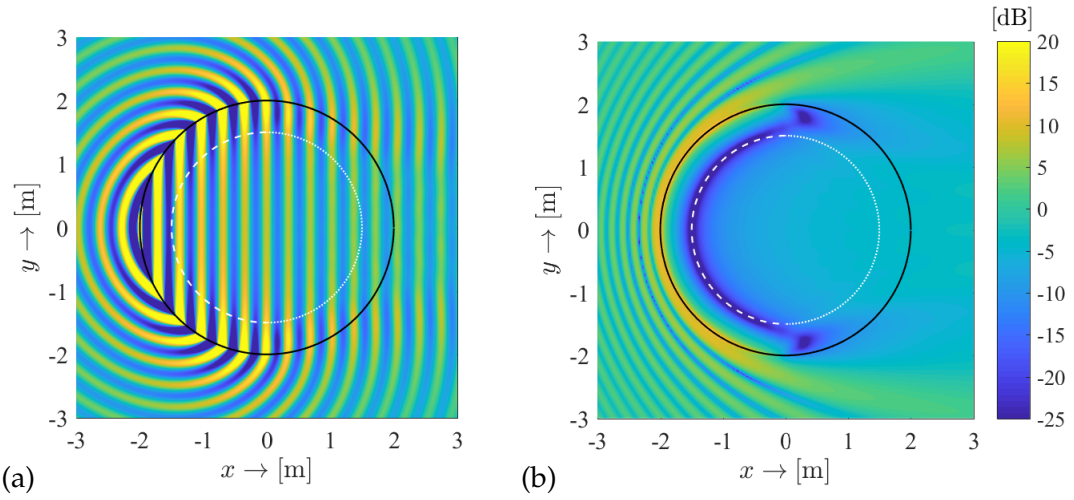

Figure 4.7. 2.5D synthesis of a 2D plane wave with the angular frequency $f_0 = 1$ kHz propagating into the direction $\mathbf{k}^{\mathrm{PW}} = [k_x^{\mathrm{PW}},\ 0,\ 0]^{\mathrm{T}}$. The SSD is a circular one, with the radius of $R_{\mathrm{SSD}} = 2$ m. The reference curve is a circle with the radius of $R_{\mathrm{ref}} = 1.5$ m. Figure (a) depicts the real part of the synthesized field, (b) shows the error of synthesis.

with $\hat{k}_r^P(\mathbf{x}_0)$ denoting the radial component of the normalized wavenumber vector. Applying this reference distance in the general 2.5D WFS driving function (4.14) allows the synthesis of an arbitrary sound field referenced on a reference circle inside the SSD.

Assume the special case of a virtual 2D plane wave, propagating parallel to the synthesis plane described by the wavenumber vector $\mathbf{k}^{\mathrm{PW}} = [k_x^{\mathrm{PW}},\ k_y^{\mathrm{PW}},\ 0]^{\mathrm{T}}$. For a 2D sound field invariant along the vertical dimension the vertical wavefront curvature is zero ($\phi''^P_{zz}(\mathbf{x}_0) = 0$) and the referencing function is the reference distance itself. The driving function synthesizing a 2D plane wave is then given as

$$D(\mathbf{x}_0, \omega) = -w(\mathbf{x}_0)\sqrt{\frac{8\pi}{\mathrm{j}k}}\sqrt{|\mathbf{x}_{\mathrm{ref}}(\mathbf{x}_0) - \mathbf{x}_0|}\mathrm{j}k_r^{\mathrm{PW}}(\mathbf{x}_0)\mathrm{e}^{-\mathrm{j}\langle \mathbf{k}^{\mathrm{PW}} \cdot \mathbf{x}_0 \rangle}, \tag{4.31}$$

with the reference distance given by (4.30). As an application of this driving function a simple example is depicted in Figure 4.7 for the synthesis of a harmonic plane wave.

In order to find the driving signal for the synthesis of a plane wave carrying a broadband excitation time history $s(t)$, (4.31) is inverse Fourier transformed weighted by the excitation spectrum, resulting in

$$d(\mathbf{x}_0, t) = -w(\mathbf{x}_0)\sqrt{\frac{8\pi}{c}|\mathbf{x}_{\mathrm{ref}}(\mathbf{x}_0) - \mathbf{x}_0|}\,\hat{k}_r^{\mathrm{PW}}(\mathbf{x}_0)h(t) *_t s(t - \frac{1}{c}\left\langle \hat{\mathbf{k}}^{\mathrm{PW}} \cdot \mathbf{x}_0 \right\rangle), \tag{4.32}$$

where $h(t) = \mathcal{F}_\omega^{-1}\{\sqrt{\mathrm{j}\omega}\}$ is the SSD compensation filter, performing half-derivation on the time history and $\hat{\mathbf{k}}^{\mathrm{PW}} = [\hat{k}_x^{\mathrm{PW}},\ \hat{k}_y^{\mathrm{PW}},\ 0]^{\mathrm{T}}$ is a unit vector pointing into the plane wave propagation direction.

4.2 Explicit solution: Spectral Division Method

The explicit solution for the general sound field synthesis problem aims at the direct solution of the inverse problems, described by integral equations (4.1) and (4.2).

Generally speaking the explicit methodology utilizes compact operator theory by exploiting that integral (4.1) constitutes a compact Fredholm operator with the kernel being the Green's function [MF53; Ahr12]. Such an operator and the involved acoustic fields can by expanded into the series of orthogonal eigenfunctions of the wave equation on a control surface, that form a complete basis of the required solution. The inverse problem can be straightforwardly solved for the driving function expansion coefficients by a comparison of the corresponding eigenvalues, as long as none of the expansion coefficients of the operator kernel is zero (otherwise the problem is termed *ill-conditioned*). Finally the explicit analytical solution is found for the driving function as an infinite sum of the weighted basis functions. The method is often referred to as *mode-matching* solutions, since the eigenfunctions of a given geometry are termed the *modes*. This solution is unique for general enclosures and also for the (strictly speaking) non-enclosing planar case as shown in [ZS13] and [Faz10], respectively. In the latter case the compact operator degenerates to the continuous eigenvalue domain instead of countable eigenvalues as presented in the followings.

The determination of the appropriate eigenfunctions for a general geometry is a tough challenge. For spherical and circular geometries spherical and circular harmonics form the demanded basis functions. For a rigorous treatment for mode-matching SFS using spherical and circular SSDs see [AS08a; AS09b; AS09a; Zot09; Ahr10; Ahr12; SS14] and [Koy+14; Koy14] for the cylindrical solution. In the present thesis only the planar and linear geometries are investigated in details. This

4.2.1 3D Spectral Division Method

Assume an infinite planar SSD located at $\mathbf{x}_0 = [x_0,\ 0,\ z_0]^{\mathrm{T}}$, degenerated from the geometry introduced for the Rayleigh integrals in the previous chapter, shown in Figure 2.7. The half-space of synthesis is chosen to be at $y > 0$, therefore all the virtual sources are assumed to be located at $y < 0$. The synthesized field in this geometry is given by a Fredholm integral of the first kind

$$P(\mathbf{x},\omega) = \iint_{-\infty}^{\infty} D(x_0, z_0, \omega) G(x - x_0, y, z - z_0, \omega) \mathrm{d}x_0 \mathrm{d}z_0 = D(x, z, \omega) *_{x,z} G(x, y, z, \omega), \tag{4.33}$$

describing a continuous convolution along the SSD plane. Here $G(x, y, z, \omega)$ denotes the sound field of a secondary source element placed at the origin and $*_{x,z}$ denotes convolution along the x and z dimensions.

For this geometry the orthogonal basis is given by the continuous set of exponentials, and the decomposition of the involved quantities is given by a double Fourier transform [AW05; Ahr12; SS14], with the physical interpretation of a plane wave decomposition as discussed in Section 2.2.2. Applying the convolution theorem to

the angular spectrum representation, the convolution transforms into a multiplication [Gir+01]:

$$\tilde{P}(k_x, y, k_z, \omega) = \tilde{D}(k_x, k_z, \omega) \cdot \tilde{G}(k_x, y, k_z, \omega). \tag{4.34}$$

The expansion coefficients are therefore obtained by a comparison of the spectral coefficients and the driving function in the wavenumber and the spatial domain takes the form:

$$\tilde{D}(k_x, k_z, \omega) = \frac{\tilde{P}(k_x, y, k_z, \omega)}{\tilde{G}(k_x, y, k_z, \omega)} = \frac{\mathcal{F}\{P(\mathbf{x}, \omega)\}}{\mathcal{F}\{G(\mathbf{x}, \omega)\}}, \tag{4.35}$$

3D SDM driving fun.

$$D(x_0, z_0, \omega) = \frac{1}{4\pi^2} \iint_{-\infty}^{\infty} \frac{\tilde{P}(k_x, y, k_z, \omega)}{\tilde{G}(k_x, y, k_z, \omega)} \mathrm{e}^{-\mathrm{j}(k_x x_0 + k_z z_0)} \mathrm{d}k_x \mathrm{d}k_z, \tag{4.36}$$

respectively. Since the driving function spectrum is yielded by a division in the spectral domain the approach is termed the *Spectral Division Method* [AS10c; AS11a; AS10a; AS12].

Substituting the $k_x - k_z$ representation of the 3D Green's function given by (3.61) the driving function (4.36) reads as

$$D(x_0, z_0, \omega) = \frac{1}{4\pi^2} \iint_{-\infty}^{\infty} 2\mathrm{j}k_y \frac{\tilde{P}(k_x, y, k_z, \omega)}{\mathrm{e}^{-\mathrm{j}k_y y}} \mathrm{e}^{-\mathrm{j}(k_x x_0 + k_z z_0)} \mathrm{d}k_x \mathrm{d}k_z. \tag{4.37}$$

with k_y defined by (2.27). Expressing the target field spectrum by extrapolating from the plane $y = 0$ according to (2.29)—i.e. as $\tilde{P}(k_x, y, k_z, \omega) = \tilde{P}(k_x, 0, k_z, \omega)\mathrm{e}^{-\mathrm{j}k_y y}$—the exponential pressure propagators cancel out and the driving function becomes independent from the y-coordinate. The driving function in the wavenumber domain therefore reads as

$$\tilde{D}(k_x, k_z, \omega) = 2\mathrm{j}k_y \tilde{P}(k_x, 0, k_z, \omega) = -2 \left. \frac{\partial}{\partial y} \tilde{P}(k_x, y, k_z, \omega) \right|_{y=0}, \tag{4.38}$$

for which it was exploited that according to (2.31) multiplication by $\mathrm{j}k_y$ represents differentiation along the y-dimension. Straightforwardly, the explicit expression of the driving function in the spatial domain is obtained by the corresponding inverse Fourier transform according to (4.36):

$$D(x_0, z_0, \omega) = -2 \left. \frac{\partial}{\partial y} P(\mathbf{x}, \omega) \right|_{y=0}. \tag{4.39}$$

The planar explicit driving function is thus equivalent to the implicit solution, in a planar geometry provided by the Rayleigh integral. The coincidence of the explicit and implicit driving functions is a consequence of the uniqueness of the problem in the present geometry. It is also indirectly proven that the wavefield extrapolation equations are the spectral domain representations of the Rayleigh integrals.

However, an important difference between the implicit and explicit solution exists: until (4.36) the present method does not pose any constraints on the actual form of the Green's function. Theoretically an arbitrary transfer function may be assigned for the secondary sources. As long the spectrum of the transfer function does not exhibit zeros unique driving function may be derived applying the explicit methodology.

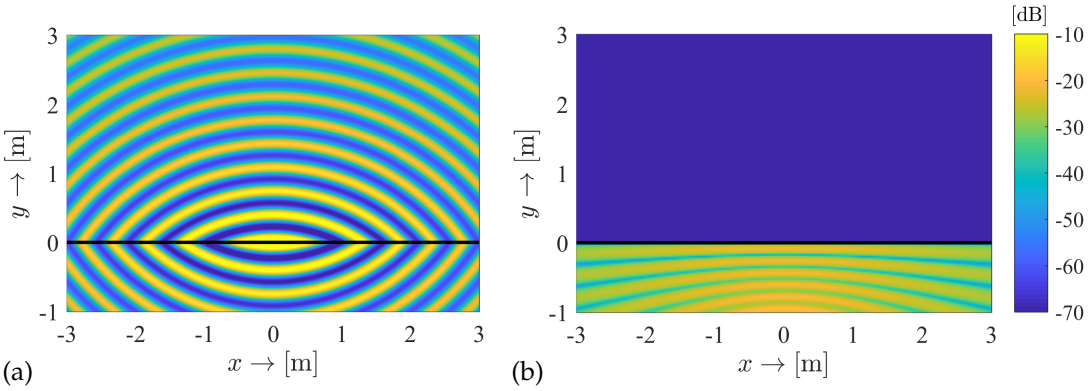

Figure 4.8. Synthesis of a virtual point source using a planar SSD applying the SDM driving function. The SSD is located at $\mathbf{x}_0 = [x_0,\ 0,\ z_0]^{\mathrm{T}}$ denoted by solid black line. The virtual source is located at $\mathbf{x}_\mathrm{s} = [0,\ -2,\ 0]^{\mathrm{T}}$ oscillating at $f_0 = 1$ kHz. The figures depict the real part of the synthesized field (a) and the deviation from the target sound field (b) measured at $z = 0$.

If the secondary sources are 3D point sources the following physical interpretation can be assigned to the explicit solution: as it was stated in Section 3.3.3 a planar distribution of point sources with a harmonic spatial distribution described by k_x, k_z radiate plane waves with the same wavenumber components and a wavenumber/direction dependent amplitude factor $\frac{1}{2\mathrm{j}k_y}$ (c.f. (3.61), degenerating at $k_x = k_z = 0$ to the 1D Green's function). The driving function (4.38) thus compensates the planar SSD's response for the synthesis of a single plane wave component. Finally, the explicit driving function for an arbitrary virtual field is found as the sum of the individual plane wave driving function weighted by the virtual field' plane wave expansion coefficients.

Application example: Synthesis of a 3D point source using a planar SSD

The application of the planar explicit solution is presented via the synthesis of a 3D virtual point source positioned at $\mathbf{x}_\mathrm{s} = [x_s,\ y_s,\ z_s]^{\mathrm{T}}$ behind the SSD plane, located at $\mathbf{x}_0 = [x_0,\ 0,\ z_0]^{\mathrm{T}}$. The wavenumber domain representation of the driving function is obtained by substituting the angular spectrum of a 3D point source into (4.35) with applying the Fourier transform shift theorem[1]

$$\tilde{D}(k_x, k_z, \omega) = \frac{-\frac{\mathrm{j}}{2}\frac{\mathrm{e}^{-\mathrm{j}k_y(y-y_s)}}{k_y}\mathrm{e}^{\mathrm{j}(k_x x_s + k_z z_s)}}{-\frac{\mathrm{j}}{2}\mathrm{e}^{-\mathrm{j}k_y y}/k_y} = \mathrm{e}^{-\mathrm{j}k_y y_s}\mathrm{e}^{\mathrm{j}(k_x x_s + k_z z_s)}. \tag{4.40}$$

The double inverse Fourier transform can be carried out analytically by taking the y-derivative of the Weyl's integral representation of the Green's function (See [Lal68] or [Wil99, (2.65)]):

$$\frac{\partial}{\partial y}G(\mathbf{x}_0 - \mathbf{x}_\mathrm{s}, \omega) = \frac{1}{4\pi^2}\iint_{-\infty}^{\infty} -\frac{1}{2}\mathrm{e}^{-\mathrm{j}k_y(y-y_s)}\mathrm{e}^{\mathrm{j}(k_x x_s + k_z z_s)}\mathrm{e}^{-\mathrm{j}(k_x x_0 + k_z z_0)}\mathrm{d}k_x\mathrm{d}k_z. \tag{4.41}$$

[1] This is the corrected version of [SS14, eq. (A11)].

Comparing (4.40) and (4.41) it is revealed that the driving function in the spatial domain is given by

$$D(x_0, z_0, \omega) = -2\frac{\partial}{\partial y} G(\mathbf{x}_0 - \mathbf{x}_\mathrm{s}, \omega)|_{y=0} = -\frac{y_s}{2\pi}\left(\frac{1}{|\mathbf{x}_0 - \mathbf{x}_\mathrm{s}|} + \mathrm{j}k\right)\frac{\mathrm{e}^{-\mathrm{j}k|\mathbf{x}_0 - \mathbf{x}_\mathrm{s}|}}{|\mathbf{x}_0 - \mathbf{x}_\mathrm{s}|^2}, \quad (4.42)$$

which is in agreement with equation (4.39).

The result of synthesizing the steady-state field of a point source is illustrated in Figure 4.8. In the target half space $y > 0$ perfect synthesis is achieved, as it is indicated in Figure 4.8 (b), depicting the discrepancy between the synthesized and the target sound field. Obviously, the figure also presents the result of 3D planar WFS of a spherical wave without applying the high frequency gradient approximation.

4.2.2 2.5D Spectral Division Method

As the geometry for the derivation of the 2.5D explicit driving function assume an infinite linear distribution of secondary point sources, located at $\mathbf{x}_0 = [x_0,\ 0,\ 0]^\mathrm{T}$. The synthesized field in this arrangement reads as

$$P(x, y, z, \omega) = \int_{-\infty}^{\infty} D(x_0, \omega) G(x - x_0, y, z, \omega) \mathrm{d}x_0. \quad (4.43)$$

Similarly to the planar case the basis functions for a linear SSD are given by exponentials: by realizing that the above equation is a convolution along the x-axis, the convolution can be transformed into a multiplication by means of a spatial forward Fourier transform

$$\tilde{P}(k_x, y, z, \omega) = \tilde{D}(k_x, \omega) \cdot \tilde{G}(k_x, y, z, \omega). \quad (4.44)$$

The driving function spectrum is then obtained as a spectral ratio

$$\tilde{D}(k_x, \omega) = \frac{\tilde{P}(k_x, y, z, \omega)}{\tilde{G}(k_x, y, z, \omega)} = \frac{\mathcal{F}_x\{P(\mathbf{x}, \omega)\}}{\mathcal{F}_x\{G(\mathbf{x}, \omega)\}}, \quad (4.45)$$

and the frequency domain driving function is obtained as the spatial inverse Fourier transform with respect to k_x

$$D(x_0, \omega) = \frac{1}{2\pi}\int_{-\infty}^{\infty} \frac{\tilde{P}(k_x, y, z, \omega)}{\tilde{G}(k_x, y, z, \omega)} \mathrm{e}^{-\mathrm{j}k_x x_0} \mathrm{d}k_x. \quad (4.46)$$

Again, theoretically the transfer function may describe the field of an arbitrary sound source, as long as it does not exhibit zeros in order to keep the problem well-conditioned.

Unlike the planar case the present driving function depends on the listener position: Equation (4.46) may be solved only for positions on the surface of a cylinder with fixed radius $d = \sqrt{y^2 + z^2}$ [Ahr10, p. 60.]. This is a direct consequence of the fact that the pressure of an arbitrary 3D sound field measured on the SSD does not determine completely the pressure on the reference line—and vice versa—. Furthermore,

an infinite line source—i.e. the SSD—can only radiate wavefronts with cylindrical symmetry as it was discussed in details in 3.3.3. Phase correct synthesis therefore can be achieved only in a plane containing the SSD in which the radial wavenumber of the synthesized field and the target field coincide. Amplitude correct synthesis is ensured in this plane at a distance $d_{\mathrm{ref}} = \sqrt{y^2 + z^2}$, for which the driving function is calculated.

For practical applications the plane of synthesis is chosen to be the horizontal plane $z = 0$, requiring that for the virtual field $k_z(x, y, 0) = 0$ holds. The driving function thus reads as

2.5D SDM driving function

$$D(x_0, \omega) = \frac{1}{2\pi} \int_{-\infty}^{\infty} \frac{\tilde{P}(k_x, y_{\mathrm{ref}}, 0, \omega)}{\tilde{G}(k_x, y_{\mathrm{ref}}, 0, \omega)} \mathrm{e}^{-\mathrm{j}k_x x_0} \mathrm{d}k_x. \tag{4.47}$$

In this geometry amplitude correct synthesis is restricted to the *reference line* by setting $y = y_{\mathrm{ref}}$.

Similarly to the 3D case the following physical interpretation can be assigned to the 2.5D explicit solution: Given an infinite distribution of point sources along the x-axis with a harmonic spatial distribution described by k_x, the radiated sound field is given by

$$\begin{aligned} \int_{-\infty}^{\infty} G(x - x_0, y, z) \mathrm{e}^{\mathrm{j}k_x x_0} \mathrm{d}x_0 = \hat{G}(k_x, y, z, \omega) \mathrm{e}^{-\mathrm{j}k_x x} = \\ = -\frac{\mathrm{j}}{4} H_0^{(2)} \left(\sqrt{\left(\frac{\omega}{c}\right)^2 - k_x^2} \sqrt{y^2 + z^2} \right) \mathrm{e}^{-\mathrm{j}k_x x}, \end{aligned} \tag{4.48}$$

at $x = 0$ resulting in the 2D Green's function as discussed in Section 3.3.3. Such a source radiates cylindrical symmetric sound fields with conical wavefronts as depicted in Figure (3.10) (a). Along a fixed reference line at $z = 0$ the SSD reproduces a harmonic spatial distribution $\mathrm{e}^{-\mathrm{j}k_x x}$ attenuated approximately by $\frac{1}{\sqrt{k_y |y_{\mathrm{ref}}|}}$, corresponding to attenuating plane waves with $k_z = 0$. Therefore, the wavenumber domain driving function ensures the compensation of the linear SSD response for the synthesis of a single plane wave component propagating in the plane of synthesis. Obviously, for sound fields that can be expanded into the series of plane waves with $k_z = 0$ the driving function is the weighted sum of the plane wave driving function, resulting in (4.47).

It is worth noting that the analytic Fourier transform coefficients of the target sound field are available only for limited simple virtual source models. Even in these cases the inverse transform of the driving function can rarely be evaluated analytically, therefore numerical transforms are needed. For a practical and optimized implementation of the SDM for an arbitrary target sound field refer to [Ahr+13].

Application example: Synthesis of a 3D point source using a linear SSD

As an example for the 2.5D SDM the reproduction of a 3D point source is presented. The virtual source is located at $\mathbf{x}_{\mathrm{s}} = [x_s,\ y_s,\ 0]^{\mathrm{T}}$, with $y_s < 0$. The SSD is a linear

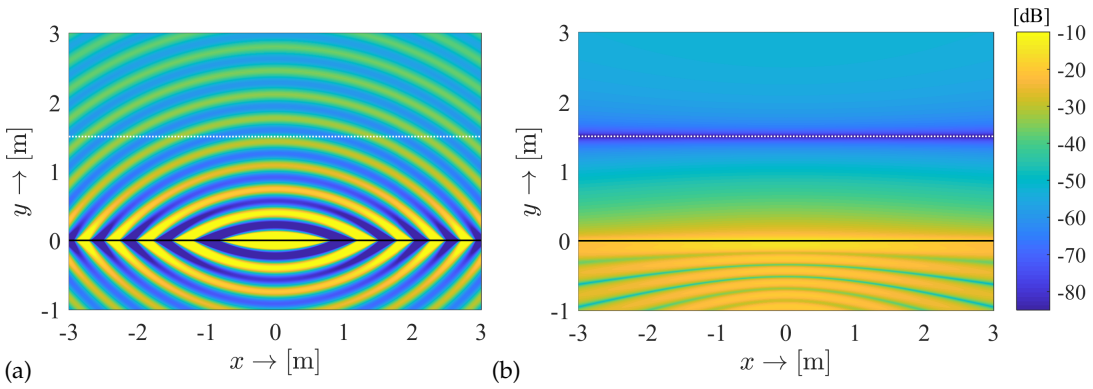

Figure 4.9. Synthesis of a virtual point source employing a linear SSD applying the 2.5D SDM driving function. The SSD is located at $\mathbf{x}_0 = [x_0,\ 0,\ 0]^{\mathrm{T}}$, denoted by a solid black line. The virtual source is located at $\mathbf{x}_\mathrm{s} = [0,\ -2,\ 0]^{\mathrm{T}}$ oscillating at $f_0 = 1$ kHz. The reference line is at $y_\mathrm{ref} = 1.5$ m. The figure depicts the synthesized field at the synthesis plane ($z = 0$) with (a) depicting the real part of the synthesized field, (b) depicting the error of synthesis.

set of 3D point sources, located along $\mathbf{x}_0 = [x_0,\ 0,\ 0]^{\mathrm{T}}$. The explicit driving function for a linear SSD is given by (4.47). Substituting the 1D spectra of the virtual and the secondary point sources along with applying the Fourier shift theorem the driving function is given in the propagation region as

$$\hat{D}(k_x,\omega) = \frac{-\frac{\mathrm{j}}{4}H_0^{(2)}\left(\sqrt{\left(\frac{\omega}{c}\right)^2 - k_x^2}\,|y_\mathrm{ref} - y_s|\right)\mathrm{e}^{\mathrm{j}k_x x_s}}{-\frac{\mathrm{j}}{4}H_0^{(2)}\left(\sqrt{\left(\frac{\omega}{c}\right)^2 - k_x^2}\,|y_\mathrm{ref}|\right)}, \tag{4.49}$$

and the spatial inverse Fourier transform yields the spatial domain driving function, reading as

Linear SDM point source driv. fun.

$$D(x_0,\omega) = \frac{1}{2\pi}\int_{-\infty}^{\infty} \frac{H_0^{(2)}\left(\sqrt{\left(\frac{\omega}{c}\right)^2 - k_x^2}\,|y_\mathrm{ref} - y_s|\right)}{H_0^{(2)}\left(\sqrt{\left(\frac{\omega}{c}\right)^2 - k_x^2}\,|y_\mathrm{ref}|\right)}\mathrm{e}^{-\mathrm{j}k_x(x_0 - x_s)}\mathrm{d}k_x. \tag{4.50}$$

The synthesized field using this driving function is depicted in 4.9 (a). As it can be seen from Figure (b) displaying the discrepancy between the synthesized field and the target field, application of the explicit driving function ensures perfect synthesis on the reference line. In other points amplitude errors are present.

As discussed in [**Spors10ahrens:analysis**] the derived driving function spectrum can be simplified by applying the large-argument/asymptotic approximation of the Hankel function, given by (3.53). The asymptotic form gives a fair approximation for (4.50) if $k_y|y_\mathrm{ref}| \gg 1$ holds, valid in the farfield of the SSD in front of the virtual source, where $k_y \gg k_x$ dominates the inverse transform. Applying the Hankel function's approximation the inverse transform can be carried out analytically, resulting in

$$D(x_0,\omega) \approx \frac{1}{2}\sqrt{\frac{y_\mathrm{ref}}{y_\mathrm{ref} - y_s}}\mathrm{j}\frac{\omega}{c}\frac{y_s}{|\mathbf{x}_0 - \mathbf{x}_\mathrm{s}|}H_1^{(2)}\left(\frac{\omega}{c}|\mathbf{x}_0 - \mathbf{x}_\mathrm{s}|\right). \tag{4.51}$$

A further large-argument approximation of the first order Hankel function returns the 2.5D WFS driving function for a 3D point source referencing the synthesis on a

reference line, given by (4.25). This indicates that the implicit solution constitutes a high frequency approximation for the explicit solution in case of a virtual point source. The equivalence of the SDM and 2.5D WFS referencing the synthesis of a virtual plane wave on a reference line was further discussed in [Fir+17; SS16; F.S16]. In the following the general relation of the explicit solution and 2.5D WFS is investigated.

4.2.3 Explicit solution in the spatial domain

The determination of a single spectral coefficient for the explicit solution requires the knowledge of the entire target field over the boundary surface in order to perform the spectral decomposition. The explicit solution is therefore often termed a *global solution*. In contrary, the implicit solution requires the value of the local field variables only at the actual SSD position at which the driving function is to be expressed. The implicit solution is thus referred to as a *local solution*. In the followings it is presented how the global solution can be approximated asymptotically by the application of the stationary phase method, resulting in an alternative local solution.

As it was discussed in Section 3.3.3 the stationary phase approximation allows the evaluation of forward and inverse Fourier integrals around stationary positions in the spatial and spectral domain. The SPA therefore may be employed in order to give an approximate formulation for the 2.5D explicit driving function solely in the spatial domain.

The complete derivation is presented in details in Appendix D.1, here only the result of the approximation is discussed. The derivation consists of two main steps:

1. First the spectral driving function is expressed in an asymptotic form, resulting in (D.7). The calculus can be done by assuming that the involved spectra are obtained via the SPA of the corresponding forward Fourier transforms. This step links the spectral coefficients to stationary positions on the reference line (see (D.4)).
2. It is followed by the inverse Fourier transform of the asymptotic spectral driving function. The evaluation of the inverse transform with the SPA relates the forward transform stationary positions to positions along the SSD.

As the result of the derivation for a linear SSD located along $\mathbf{x}_0 = [x_0,\ 0,\ 0]^\mathrm{T}$ the asymptotic SDM driving function, expressed entirely in the spatial domain reads as

$$D(x_0,\omega) \approx \sqrt{\frac{\left|\phi_{xx}^{G''}(\mathbf{x}_\mathrm{ref}(\mathbf{x}_0)-\mathbf{x}_0,\omega)\right|^2}{\left|\phi_{xx}^{P''}(\mathbf{x}_\mathrm{ref}(\mathbf{x}_0),\omega)-\phi_{xx}^{G''}(\mathbf{x}_\mathrm{ref}(\mathbf{x}_0)-\mathbf{x}_0,\omega)\right|}}\sqrt{\frac{\mathrm{j}}{2\pi}}\frac{P(\mathbf{x}_\mathrm{ref}(\mathbf{x}_0),\omega)}{G(\mathbf{x}_\mathrm{ref}(\mathbf{x}_0)-\mathbf{x}_0,\omega)}. \tag{4.52}$$

2.5D explicit driv. fun.

In the driving function $\mathbf{x}_\mathrm{ref}(\mathbf{x}_0) = [x_\mathrm{ref}(x_0),\ y,\ 0]^\mathrm{T}$ is the reference position for the SSD element at x_0, measured along a reference line, satisfying the relation

$$\mathbf{k}^P(\mathbf{x}_\mathrm{ref}(\mathbf{x}_0)) = \mathbf{k}^G(\mathbf{x}_\mathrm{ref}(\mathbf{x}_0)-\mathbf{x}_0). \tag{4.53}$$

2.5D SDM reference position

Hence, in the explicit driving function for a given SSD coordinate x_0 the reference point $\mathbf{x}_\mathrm{ref}$ is found on the reference line, where the local propagation direction of the

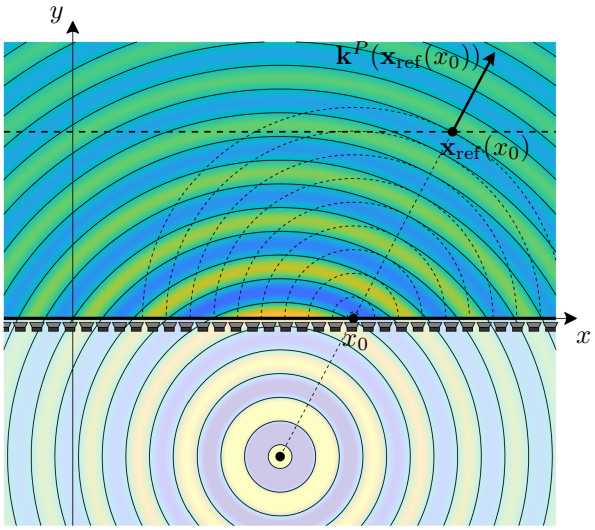

Figure 4.10. Illustration of the stationary position $\mathbf{x}_{\mathrm{ref}}(x_0)$ for the evaluation of the spatial explicit driving function. For a given SSD position x_0 the reference (stationary) position is found on a given reference line, where the virtual field propagation direction coincides with that of the SSD element under discussion. Under the validity of the Kirchhoff approximation this principle may be extended towards arbitrary SSD and reference contours.

target field P coincides with that of a point source positioned at $[x_0,\ 0,\ 0]^{\mathrm{T}}$. For an illustration refer to Figure 4.10.

The driving function (4.52) states that an arbitrary sound field may be synthesized by finding the positions along the reference line, where the propagation direction/wavefront of the target field matches the field of the actual secondary sources. In this stationary position the driving function is obtained by the ratio of the target field and the actual SSD element, corrected by the factor, containing the wavefront radii/curvatures at the same position. Therefore the explicit, global solution can be approximated by local wavefront matching.

One important fact is pointed out here: although having derived the above driving function in terms of a forward and an inverse spatial Fourier transform along a straight line, there is no restriction on the y-coordinate of the stationary point in (4.52) due to the local approximations involved: the y-coordinate might be x_0-dependent. This means that an arbitrary referencing curve may be defined as $\mathbf{x}_{\mathrm{ref}}(x_0)$, and the driving function can be calculated by finding the stationary positions satisfying $k_x^P(\mathbf{x}_{\mathrm{ref}}(x_0)) = k_x^G(\mathbf{x}_{\mathrm{ref}}(x_0) - \mathbf{x}_0)$ along this curve. Evaluating the driving function in the stationary positions will result in amplitude correct synthesis along the reference curve. This means that the presented driving function is equivalent to the 2.5D WFS driving function with the important difference that here the target field needs to be evaluated on the reference curve. Furthermore, within the validity of the Kirchhoff approximation the SSD does not necessarily need to be linear: the spatial explicit driving function can be applied using an arbitrary shaped SSD contour. In that case (4.54) has to be evaluated with $\hat{k}_y^P(\mathbf{x}_{\mathrm{ref}}(x_0)) \rightarrow \hat{k}_{\mathrm{n}}^P(\mathbf{x}_{\mathrm{ref}}(\mathbf{x}_0))$, i.e. with the wavenumber component along the normal direction of the stationary SSD element.

With the considerations above and by expressing the second derivatives in terms of the principal radii according to (B.6) the explicit driving function can be cast into the final form

$$D(\mathbf{x}_0,\omega) = \underbrace{\sqrt{\frac{\mathrm{j}k}{2\pi\rho_{\mathrm{h}}^{G}(\mathbf{x}_{\mathrm{ref}}(\mathbf{x}_0)-\mathbf{x}_0)}}}_{\substack{\text{SSD}\\ \text{compensation}}} \underbrace{\sqrt{\frac{\rho_{\mathrm{h}}^{P}(\mathbf{x}_{\mathrm{ref}}(\mathbf{x}_0))}{\rho_{\mathrm{h}}^{P}(\mathbf{x}_{\mathrm{ref}}(\mathbf{x}_0))-\rho_{\mathrm{h}}^{G}(\mathbf{x}_{\mathrm{ref}}(\mathbf{x}_0)-\mathbf{x}_0)}}}_{\substack{\text{virtual source}\\ \text{compensation}}} \frac{\hat{k}_{\mathrm{n}}^{P}(\mathbf{x}_{\mathrm{ref}}(\mathbf{x}_0))P(\mathbf{x}_{\mathrm{ref}}(\mathbf{x}_0),\omega)}{G(\mathbf{x}_{\mathrm{ref}}(\mathbf{x}_0)-\mathbf{x}_0,\omega)}, \quad \underbrace{\sqrt{\frac{\rho_{\mathrm{h}}^{P}(\mathbf{x}_{\mathrm{ref}}(\mathbf{x}_0))}{\rho_{\mathrm{h}}^{P}(\mathbf{x}_0)}}}$$

Detailed 2.5D explicit driv. fun.

(4.54)

with $\mathbf{x}_0 = [x_0,\ y_0,\ 0]^{\mathrm{T}}$ and $\mathbf{x}_{\mathrm{ref}}(\mathbf{x}_0) = [x_{\mathrm{ref}}(\mathbf{x}_0),\ y_{\mathrm{ref}}(\mathbf{x}_0),\ 0]^{\mathrm{T}}$ now denoting arbitrary SSD and reference contours. The formulation implies the fact that similarly to the implicit solution, the explicit driving function also requires the derivative of the target field, measured on the reference position. The driving function explicitly contains a virtual source compensation factor, compensating for the relative amplitude change of the virtual sound field between the SSD and the reference curve in terms of its horizontal principal radius. Furthermore, the transfer function of the SSD contour—or more specifically the stationary SSD element— is compensated regarding both its frequency response being a half-integrator and its attenuation factor.

Application example: Synthesis of a 3D point source using a linear SSD

In the following a simple example is presented in order to demonstrate the validity of the spatial SDM driving function for the synthesis of a virtual 3D point source. For the synthesis a linear secondary source distribution is applied, located at $\mathbf{x}_0 = [x_0,\ 0,\ 0]^{\mathrm{T}}$. The virtual source is positioned at $\mathbf{x}_{\mathrm{s}} = [x_s,\ y_s,\ 0]^{\mathrm{T}}$ with $y_s < 0$, with the reference curve chosen to be a circle around the virtual point source with the radius of R_{ref}. Along with the equation describing the reference curve $\mathbf{x}_{\mathrm{ref}}(x_0) = [x_{\mathrm{ref}}(x_0),\ y_{\mathrm{ref}}(x_0),\ 0]^{\mathrm{T}}$ the stationary points satisfy the following equations

$$\mathbf{k}^{G}(\mathbf{x}_{\mathrm{ref}}(\mathbf{x}_0)-\mathbf{x}_{\mathrm{s}}) = \mathbf{k}^{G}(\mathbf{x}_{\mathrm{ref}}(\mathbf{x}_0)-\mathbf{x}_0), \tag{4.55}$$

$$|\mathbf{x}_{\mathrm{ref}}-\mathbf{x}_{\mathrm{s}}| = R_{\mathrm{ref}}. \tag{4.56}$$

The solution for the equations is given by

$$\mathbf{x}_{\mathrm{ref}}(\mathbf{x}_0) = \mathbf{x}_{\mathrm{s}} + R_{\mathrm{ref}}\frac{\mathbf{x}_0-\mathbf{x}_{\mathrm{s}}}{|\mathbf{x}_0-\mathbf{x}_{\mathrm{s}}|}. \tag{4.57}$$

Substituting the spherical virtual field into (4.54)—with the principal radii given by simple distances from the point sources—yields the explicit driving function in the spatial domain for a virtual point source

$$D(x_0) = \sqrt{\frac{|\mathbf{x}_{\mathrm{ref}}-\mathbf{x}_{\mathrm{s}}|}{|\mathbf{x}_{\mathrm{ref}}-\mathbf{x}_{\mathrm{s}}|-|\mathbf{x}_{\mathrm{ref}}-\mathbf{x}_0|}}\sqrt{\frac{\mathrm{j}k}{2\pi|\mathbf{x}_{\mathrm{ref}}-\mathbf{x}_0|}}\hat{k}_y^{G}(\mathbf{x}_{\mathrm{ref}}(\mathbf{x}_0)-\mathbf{x}_{\mathrm{s}})\frac{G(\mathbf{x}_{\mathrm{ref}}(\mathbf{x}_0)-\mathbf{x}_{\mathrm{s}})}{G(\mathbf{x}_{\mathrm{ref}}(\mathbf{x}_0)-\mathbf{x}_0)} \tag{4.58}$$

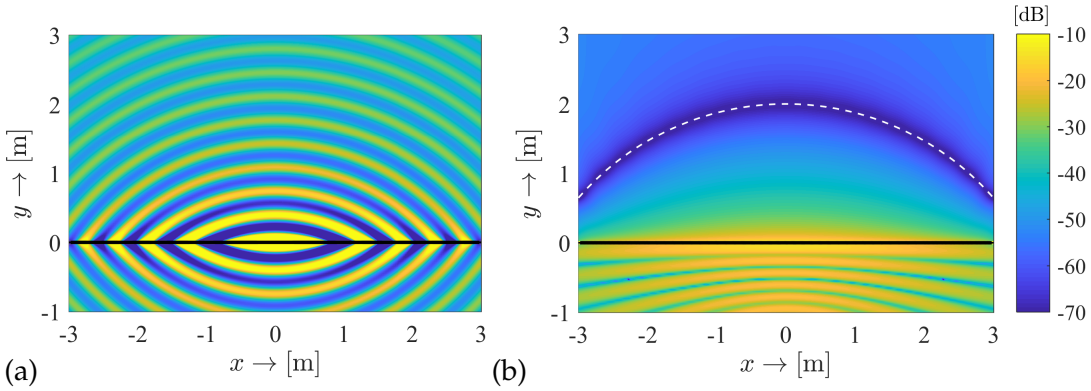

Figure 4.11. 2.5D synthesis of a 3D point source located at $\mathbf{x}_\mathrm{s} = [0,\ -2,\ 0]^\mathrm{T}$, radiating at $f_0 = 1$ kHz. The synthesis is referenced on a circle around the virtual source, with a radius of $R_\mathrm{ref} = 4$ m. Figure (a) depicts the real part of the synthesized field, (b) shows the error of synthesis.

Finally, substituting the reference position coordinates along the reference circle (4.57) specifies the driving function, optimizing the synthesis on the reference circle

$$D(x_0) = -y_s \sqrt{\frac{R_\mathrm{ref} - |\mathbf{x}_0 - \mathbf{x}_\mathrm{s}|}{R_\mathrm{ref}}} \sqrt{\frac{\mathrm{j}k}{2\pi}} \frac{\mathrm{e}^{-\mathrm{j}k|\mathbf{x}_0 - \mathbf{x}_\mathrm{s}|}}{|\mathbf{x}_0 - \mathbf{x}_\mathrm{s}|^{\frac{3}{2}}}. \tag{4.59}$$

Investigating Figure 4.11 verifies that the synthesis is optimized on the prescribed reference curve.

Although having derived the above driving function from the pressure measured along the reference curve, (4.59) is already written merely in terms of the target field measured on the actual SSD element, equivalently to the WFS solution. In the followings this relation is generalized by expressing the explicit driving function for an arbitrary target sound field that is written in terms of pressure measured along the SSD, revealing the general connection between the implicit and explicit solutions.

4.3 Relation of implicit and explicit solutions

The explicit SFS driving function, given by (4.54) requires the knowledge of the virtual sound field, measured along the reference curve. By applying the findings presented in Section 3.3.2, for the special case of a linear SSD the required quantities can be expressed in terms of the the virtual field properties, measured on the SSD. The obtained formulation allows the comparison of the implicit and explicit solutions.

In order to express the driving function merely in terms of the involved quantities measured along the SSD, all the local wavenumber vector, the principal radii and the pressure of the target field has to be defined along the $y = 0$ line. For the local wavenumber vector this relationship can be simply established: Assuming isotropic medium, the propagation direction—and the local wavenumber vector—does not change along the propagation path, thus $\mathbf{k}^P(\mathbf{x}_\mathrm{ref}(\mathbf{x}_0)) = \mathbf{k}^P(\mathbf{x}_0)$ holds.

The change of the principal radii over the propagation path is given by (B.25), stating that the principal radii of an arbitrary field increase linearly along the path of

propagation. The relation between the target field, measured at an arbitrary reference position and measured along the SSD can be established by the asymptotic evaluation of the Rayleigh integral, given for a general wavefield by (3.38). However, both relations were only formulated for an independent receiver position $\mathbf{x}$ in terms of a dependent SSD position $\mathbf{x}_0^*(\mathbf{x})$, related through the implicit relation

$$\mathbf{k}^P(\mathbf{x}_0^*(\mathbf{x})) = \mathbf{k}^G(\mathbf{x} - \mathbf{x}_0^*(\mathbf{x})). \tag{4.60}$$

Comparing this definition of the stationary points for the Rayleigh integral (4.60) and the stationary SDM evaluation points (4.53), it is revealed that they describe stationary point pairs. Hence, without the loss of generality both the principal radii and the pressure field, measured on the reference curve can be formulated with choosing the SSD position $\mathbf{x}_0$ as an independent variable, resulting in

$$\rho_{\mathrm{h}}^P(\mathbf{x}_{\mathrm{ref}}(\mathbf{x}_0)) = \rho_{\mathrm{h}}^P(\mathbf{x}_0) + \rho_{\mathrm{h}}^G(\mathbf{x}_{\mathrm{ref}}(\mathbf{x}_0) - \mathbf{x}_0), \tag{4.61}$$

and

$$\begin{aligned} P(\mathbf{x}_{\mathrm{ref}}(\mathbf{x}_0), \omega) = 4\pi \sqrt{\frac{\rho_{\mathrm{h}}^P(\mathbf{x}_0) \cdot \rho_{\mathrm{h}}^G(\mathbf{x}_{\mathrm{ref}}(\mathbf{x}_0) - \mathbf{x}_0)}{\rho_{\mathrm{h}}^P(\mathbf{x}_0) + \rho_{\mathrm{h}}^G(\mathbf{x}_{\mathrm{ref}}(\mathbf{x}_0) - \mathbf{x}_0}}\cdot \\ \cdot \sqrt{\frac{\rho_{\mathrm{v}}^P(\mathbf{x}_0) \cdot \rho_{\mathrm{v}}^G(\mathbf{x}_{\mathrm{ref}}(\mathbf{x}_0) - \mathbf{x}_0)}{\rho_{\mathrm{v}}^P(\mathbf{x}_0) + \rho_{\mathrm{v}}^G(\mathbf{x}_{\mathrm{ref}}(\mathbf{x}_0) - \mathbf{x}_0)}} P(\mathbf{x}_0, \omega) G(\mathbf{x}_{\mathrm{ref}}(\mathbf{x}_0) - \mathbf{x}_0, \omega), \end{aligned} \tag{4.62}$$

where positions $\mathbf{x}_{\mathrm{ref}}$ and $\mathbf{x}_0$ are related through (4.53) and where it was exploited that the principal radii are given by the vertical and horizontal radii components in the present geometry.

With substituting all these expressions into the spatial explicit driving function (4.54) and after simplification the driving function takes the form

$$D(x_0, \omega) = 2\sqrt{\frac{2\pi \rho_{\mathrm{v}}^G(\mathbf{x}_{\mathrm{ref}}(\mathbf{x}_0) - \mathbf{x}_0)}{\mathrm{j}k}} \sqrt{\frac{\rho_{\mathrm{v}}^P(\mathbf{x}_0)}{\rho_{\mathrm{v}}^P(\mathbf{x}_0) + \rho_{\mathrm{v}}^G(\mathbf{x}_{\mathrm{ref}}(\mathbf{x}_0) - \mathbf{x}_0)}} \mathrm{j}k_y^P(\mathbf{x}_0) P(\mathbf{x}_0, \omega), \tag{4.63}$$

or expressed in terms of the second phase derivatives

$$D(x_0, \omega) = 2\sqrt{\frac{2\pi}{\mathrm{j}}} \frac{1}{\sqrt{|\phi_{zz}^{P\prime\prime}(\mathbf{x}_0) + \phi_{zz}^{G\prime\prime}(\mathbf{x}_{\mathrm{ref}}(\mathbf{x}_0) - \mathbf{x}_0)|}} \mathrm{j}k_y^P(\mathbf{x}_0) P(\mathbf{x}_0, \omega). \tag{4.64}$$

Comparison with (4.20) and (4.14) reveals that the asymptotic SDM driving function exactly coincidec the 2.5D WFS driving function when applied for a linear—and within the validity of the Kirchhoff approximation for an arbitrary shaped—SSD. It is therefore verified that under high frequency assumptions WFS is the asymptotic and local approximation of the global explicit solution.

An important difference is however that the WFS driving function was obtained from the 2.5D Neumann Rayleigh integral in an intuitive manner, by introducing the reference curve concept with interchanging the role of the receiver position and its stationary SSD position. On the other hand the explicit driving function (4.52) inherently contains the horizontal SPA and the reference curve concept.

4.4 Synthesis applying discrete secondary source distribution

Throughout this thesis synthesis applying the continuous distribution of secondary sources has been discussed so far. In practical applications the SSD is realized by a densely spaced loudspeaker ensemble with the source elements positioned at discrete locations. The violation of the continuous SSD assumption leads to severe artifacts in the synthesized field, commonly referred to as *spatial aliasing phenomena*.

An advantage of the explicit solution is that it allows the analytical description of aliasing artifacts, which can be directly applied to the results of WFS as well, due to the presented asymptotic equivalence of the two methods. As a complex application example for the equivalence of the explicit and implicit solutions, this section discusses the analysis and mitigation of spatial aliasing in a unified manner.

4.4.1 Description of spatial aliasing

Physically, spatial aliasing can be interpreted as follows: in case of steady-state analysis above a certain temporal frequency—termed as the *aliasing frequency*— the field of the individual secondary sources no longer form a continuous virtual wavefront but rather the fields of the individual secondary sources create a complex interference pattern. The actual value of the aliasing frequency highly depends on the local propagation direction of the virtual wavefront: waves propagating laterally to the SSD are more likely to cause aliasing due to the rapid change of phase between adjacent secondary sources.

In the foregoing only stead-state analysis of wavefields was discussed. However, spatial aliasing gains a simple physical interpretation when time domain analysis is considered. As discussed already, the 2.5D WFS driving function applies a half-differentiation to the input signal in order to compensate for the infinite tail (i.e. the half-integrator characteristics) of the secondary source response, emerging due to the geometry of the SSD. Compensation is therefore performed by each SSD element canceling out the fields of the adjacent secondary sources after the virtual wavefront is emitted. In case of a discrete SSD this cancellation can not be performed below the aliasing frequency, hence in the synthesized field the spherical wavefields of the individual secondary sources will be present. Spatial aliasing therefore manifests in a series of echoes—each produced by one individual secondary source element—, following the intended virtual wavefront carrying the driving function of the individual secondary sources, high-pass filtered above the aliasing frequency [SA09b].

Note that in a given receiver position due to the short time interval between the arrival of the high-pass filtered echo wavefronts, aliasing is perceived rather as the coloration of the virtual sound field, than actual echoes/reverberation, while due to the precedence effect the localization of the virtual field is not degraded [2]. A detailed

[2] This is true only for the synthesis of non-focused fields. In case of reproducing e.g. a focused point source spatial aliasing appears as pre-echoes, arriving before the intended virtual wavefront [SA09a].

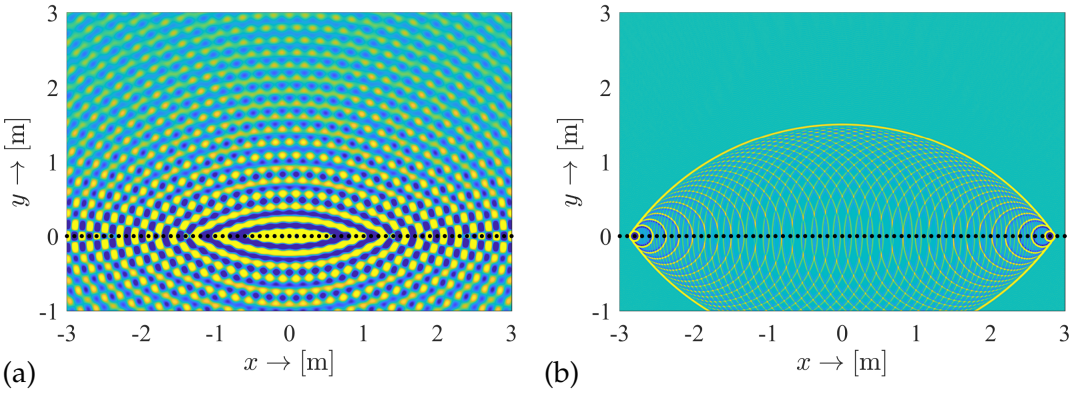

Figure 4.12. 2.5D synthesis of a 3D point source located at $\mathbf{x}_\mathrm{s} = [0,\ -2,\ 0]^\mathrm{T}$, radiating at $f_0 = 2\,\mathrm{kHz}$ (a), or emitting an impulse, bandlimited to 15 kHz measured at $t_0 = 10\,\mathrm{ms}$ (b). The synthesis is referenced on a reference line with $y_\mathrm{ref} = 1.5\,\mathrm{m}$. Synthesis is performed using a linear SSD with the secondary source spacing set to $\Delta x = 10\,\mathrm{cm}$.

investigation of the perception of spatial aliasing in WFS can be found in [Win+18b]. In the followings only an objective description of the above phenomena is presented.

In a recent publication it was shown that by applying the unified WFS framework introduced in the present thesis, spatial aliasing artifacts can be directly described in the spatial domain [Win+18a]. As an alternative, the following derivation approaches the problem by utilizing the spectral description of the synthesized field applying a discretized SSD, as introduced in [Ahr12].

Assume the synthesis of an arbitrary sound field by applying a linear SSD, located at $\mathbf{x}_0 = [x_0,\ 0,\ 0]^\mathrm{T}$. The synthesized field in the spatial and wavenumber domains is given by (4.43) and (4.44) respectively, in case of a continuous SSD. Discretization of the SSD can be mathematically modeled by the sampling of the driving function with a sampling distance being the actual loudspeaker spacing Δx:

$$D^\mathrm{S}(x,\omega) = \sum_{\eta=-\infty}^{\infty} D(x,\omega) \cdot \delta\left(x - \eta\Delta x\right). \tag{4.65}$$

Since each secondary source is represented by a Dirac delta, hence in this model the SSD consists of a discrete set of 3D point sources. Exploiting that the spectrum of a series of Dirac deltas is a pulse train itself [Gir+01], and applying the sifting property of the Dirac delta, the wavenumber content of the sampled driving function reads as

$$\tilde{D}^\mathrm{S}(k_x,\omega) = \frac{1}{\Delta x} \sum_{\eta=-\infty}^{\infty} \tilde{D}\left(k_x - \eta\frac{2\pi}{\Delta x}, \omega\right). \tag{4.66}$$

Thus, as the result of discretization the driving function spectrum is obtained as the infinite sum of the original spectrum, repeating on the multiples of the sampling wavenumber $k_{x,s} = \frac{2\pi}{\Delta x}$. Mathematically, spatial aliasing originates from the overlapping of the repetitive spectra.

The discretization process of the driving function is illustrated in the $k_x - \omega$ domain in Figure 4.13 via the example of discretizing the driving function for a virtual point source, given by (4.25). From simple geometrical considerations it can be deduced that below a given angular frequency—the spatial aliasing frequency, obtained

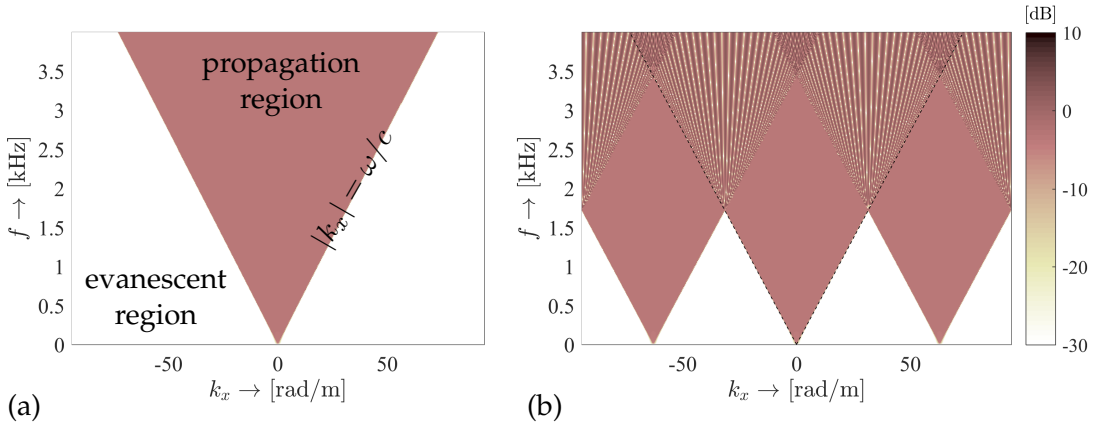

Figure 4.13. Illustration of the discretization process of the linear WFS driving function. Figure (a) shows the spectrum of the theoretically continuous driving function $\tilde{D}(k_x, \omega)$, Figure (b) shows the spectrum of the discretized driving function $\tilde{D}^{\mathrm{S}}(k_x, \omega)$ with the baseband spectrum repeating on the multiples of the sampling wavenumber. The secondary source distance is set to $\Delta x = 10$ cm, corresponding to the sampling wavenumber $k_{x,s} \approx 63$ rad/m and resulting in an aliasing frequency $\omega_a \approx 2\pi \cdot 1.7$ krad/s.

from $\frac{\omega_a}{c} = \frac{k_{x,s}}{2} = \frac{\pi}{\Delta x}$—no spectral overlapping occurs between the propagation regions. Since WFS theory assumes high frequency/farfield conditions, neglecting the evanescent components is feasible[3]. Above the aliasing frequency high wavenumber components ($|k_x| > k_{x,s}/2$) of translated spectra overlap into the propagation region of the baseband driving function spectrum.

The wavenumber content of the synthesized field, applying a discrete SSD can be written as

$$\tilde{P}(k_x, y, z, \omega) = \tilde{D}^{\mathrm{S}}(k_x, \omega) \cdot \tilde{G}(k_x, y, z, \omega) = \frac{1}{\Delta x} \sum_{\eta=-\infty}^{\infty} \tilde{D}\left(k_x - \eta \frac{2\pi}{\Delta x}, \omega\right) \cdot \tilde{G}(k_x, y, z, \omega). \tag{4.67}$$

The reproduction process is illustrated by Figure 4.14 with the involved quantities measured along an arbitrary reference line, $y \gg 0$. As it is demonstrated in 4.14 (b) the transfer function from the SSD to the reference line, i.e. the Green's function acts as a spatial low-pass filter (with analogy to signal processing acting as a reconstruction filter), restricting the reproduced field on a given angular frequency to $|k_x| < \omega/c$, i.e. to the propagation region. Note that again, nearfield investigation, where the spectrum of the Green's function would exhibit a high evanescent contribution is out of the scope of the present thesis.

Figure 4.14 (c) reflects the fact that aliasing components present in the synthesized field are described mathematically as additive, overlapping spectral components remaining in the propagation region of the baseband spectrum, described by (4.67) with $|\eta| > 0$. This additive error manifests in additive wavefronts superimposed on to the non-aliased ideal wavefront (described by the $\eta = 0$ component in (4.67)) in the time-domain.

[3] A more detailed analysis on the aliasing occurring in the reproduction of virtual point sources is found in [SA09b], where aliasing components are classified based on whether propagating/evanescent component overlaps into the propagating or evanescent region of the baseband

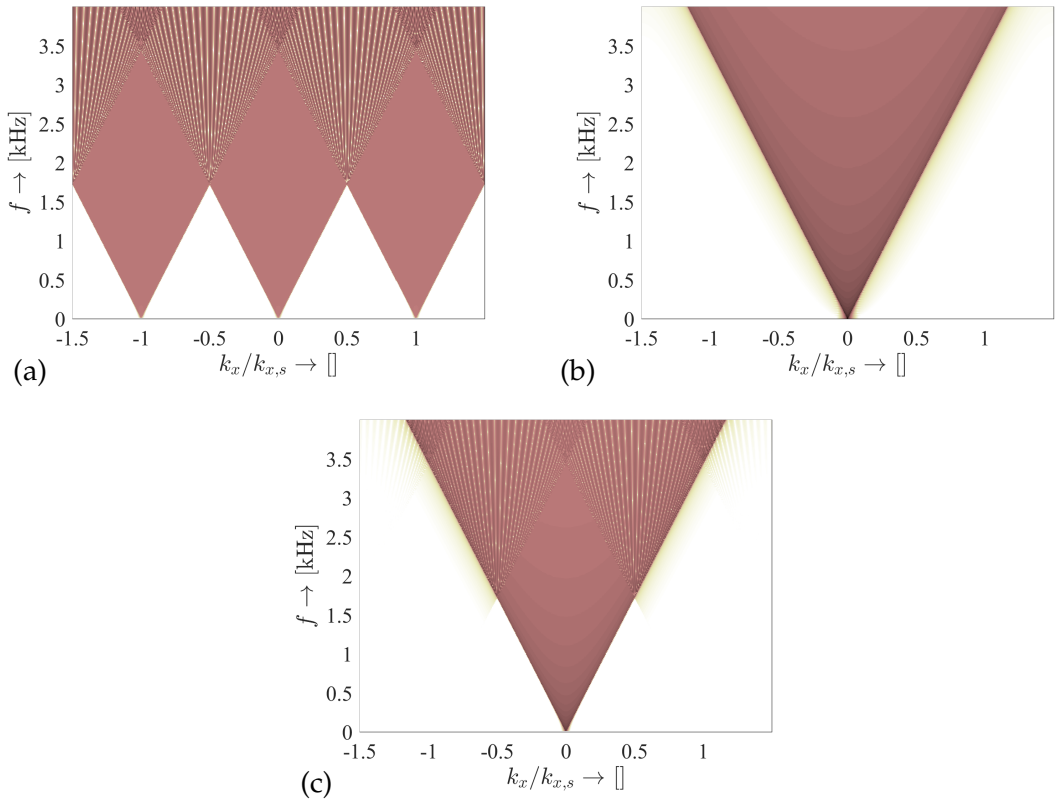

Figure 4.14. Illustration of aliased synthesis of a virtual point source in the setup, used for 4.13. Figure (a) shows the spectrum of the discretized driving function with overlapping spectral repetition. Figure (b) shows the spectrum of the 3D Green's function and Figure (c) shows the spectrum of the synthesized field, both measured along the reference line.

As discussed earlier, components in the spectrum of the synthesized field correspond to synthesized attenuating plane waves oscillating at the angular frequency ω and propagating into the direction described by k_x in the plane of synthesis. Hence Figure 4.14 (c) suggests that arbitrary directed plane waves with the angular frequency below the aliasing frequency can be synthesized with a discretized SSD. Above the aliasing frequency lateral waves cannot be synthesized without the presence of aliasing plane wave components, propagating into the opposite direction (with reversed k_x value). Finally, above twice the aliasing frequency even plane waves propagating perpendicular to the SSD can not be synthesized without aliasing.

4.4.2 Avoiding spectral overlapping

A straightforward way to avoid spectral overlapping is to spatially bandlimit the driving function to the Nyquist wavenumber $k_{x,\mathrm{Nyq}} = k_{x,s}/2$ before discretization, i.e. by eliminating plane wave components that would cause spatial aliasing. This requires the application of a spatial low-pass filter that's implementation is straightforward only for the present, linear SSD case. A detailed investigation on the direct spatial pre-filtering of the linear SFS driving function can be found in [FF12; Ahr12] [4]. However, applying the local wavenumber vector concept and exploiting the general asymptotic

[4] There it is discussed that pre-filtering the SFS driving function is equivalent with extending the virtual source distribution according the impulse response of the spatial filter impulse response.

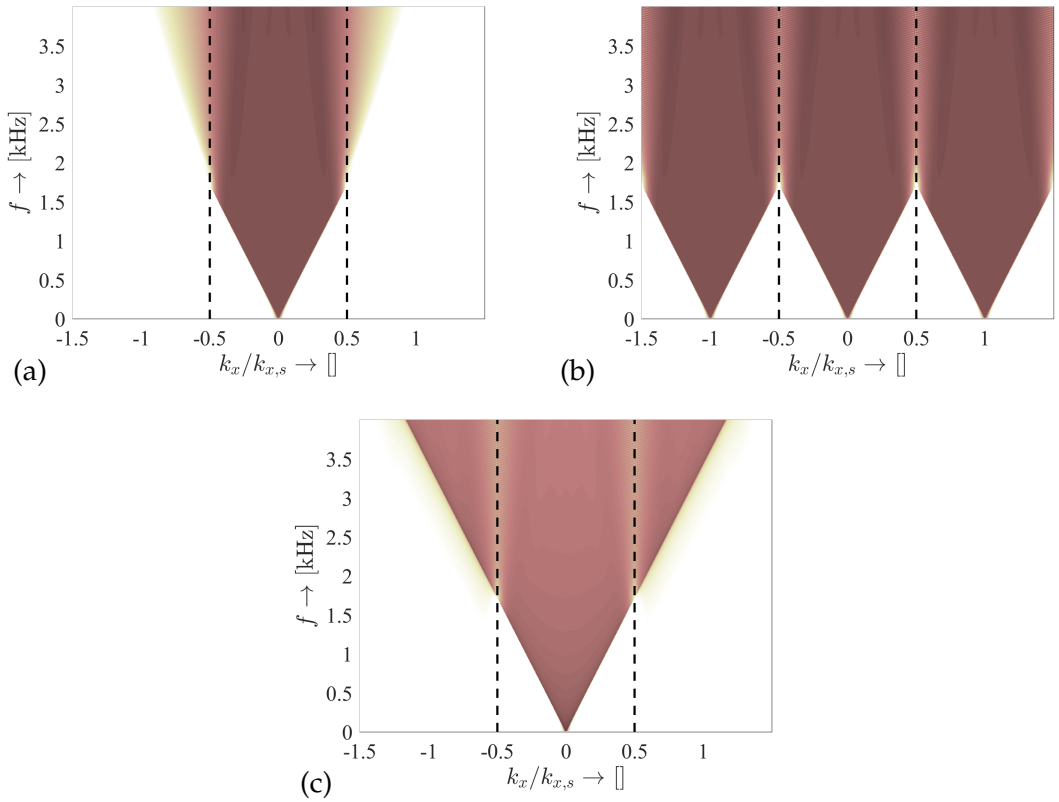

Figure 4.15. Illustration of the ideal anti-aliasing filtering of the WFS driving function for a virtual point source in the setup, used for Figure 4.13. Figure (a) shows the spatially band-limited driving function spectrum, low-pass filtered with the low-pass filtering performed in spatial domain used the introduced approach. Figure (b) shows the spectrum of the discretized driving function containing non-overlapping spectral repetition. Figure (c) shows spectrum of the synthesized field, measured along the reference line.

equivalence of the SDM and WFS, a more simple, general anti-aliasing strategy may be introduced, as given in the following.

According to (D.4) a given wavenumber component k_x in the SDM driving function is dominated by that particular position of the SSD, where the local propagation direction of the virtual wavefield coincides with that of the actual spectral plane wave, i.e. where $k_x^P(x_0) = k_x$ holds. Hence, on a given angular frequency only those parts of the SSD will cause spectral overlapping, where the x-component of the virtual field's local wavenumber vector is above the Nyquist wavenumber, i.e. where

$$|k_x^P(x_0)| = \frac{\omega}{c}|\hat{k}_x^P(x_0)| > k_{x,\mathrm{Nyq}} = \frac{\pi}{\Delta x} \tag{4.68}$$

is satisfied. Therefore, within the validity of the SPA spatial aliasing components can be assigned to particular positions along the SSD. This formulation allows the elimination of the overlapping spectral components by simple temporal low-pass filtering the driving function, with the angular cut-off frequency given as

$$D(x_0, \omega) = 0, \quad \text{where} \quad \omega \geq \frac{\pi}{\Delta x}\frac{c}{|\hat{k}_x^P(x_0)|}. \tag{4.69}$$

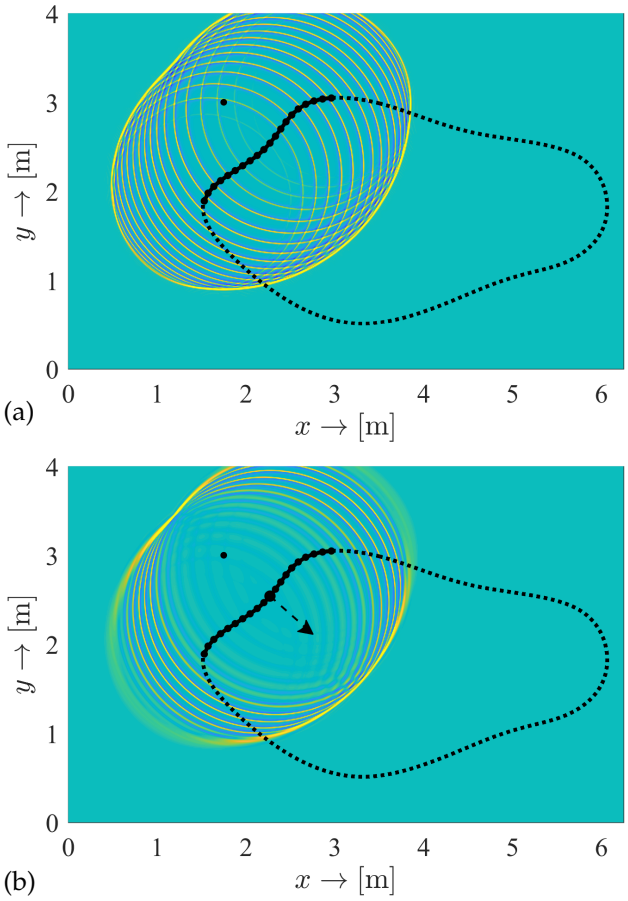

Figure 4.16. 2.5D synthesis of a 3D point source, located in $\mathbf{x}_\mathrm{s} = [1.5,\ 3,\ 0]^\mathrm{T}$ m, emitting a bandlimited impulse, applying an arbitrary shaped discrete SSD with the secondary source spacing being $\Delta x = 10$ cm, and with the snapshot taken at $t_0 \approx 6$ ms. Figure (a) shows the effect of the discrete SSD, resulting in aliasing echoes following the intended wavefront. Figure (b) shows the result of spatial anti-aliasing filtering. As a result anti-aliased synthesis may be achieved behind the virtual wavefront into the particular direction, denoted by dashed arrow. The arrow originates at the SSD element with no angular bandwidth limitation, i.e. performing full-band synthesis. This full-band SSD element is found, where the local propagation direction of the virtual field coincides with the SSD normal (i.e. the tangential local wavenumber component is zero).

This finding may be generalized towards the application of an arbitrary shaped SSD, within the validity of the Kirchhoff approximation. In this general scenario the SSD is assumed to be locally linear, and the role of k_x^P is taken over by the tangential component of the local wavenumber vector. Hence, the ideal anti-aliasing condition for a general SFS problem is formulated as

$$D(\mathbf{x}_0, \omega) = 0, \quad \text{where} \quad \omega \geq \frac{\pi}{\Delta x} \frac{c}{|\hat{k}_t^P(\mathbf{x}_0)|}, \tag{4.70}$$

Symmetric anti-aliasing condition

where $\hat{k}_t^P$ is the normalized local wavenumber vector component, tangential with the SSD.

The above formulation can be interpreted as a frequency dependent secondary source selection criterion: basically the window function in the general WFS driving function (4.5) became frequency dependent. The application of an ideal low-pass filter, given directly by (4.70) would result in truncation effects emerging from the muted and unmuted transition of the SSD, due to the discontinuity of the driving function [Sta97]. Hence, in practical applications anti-aliasing should be performed by an appropriately smooth low-pass filter design with the cut-off frequency given by (4.70).

In the following the locations of anti-aliased synthesis is investigated. Although spectral overlapping can be avoided by the presented strategy, due to the non-directive nature of the 3D secondary point sources, lateral aliasing waves are present in the

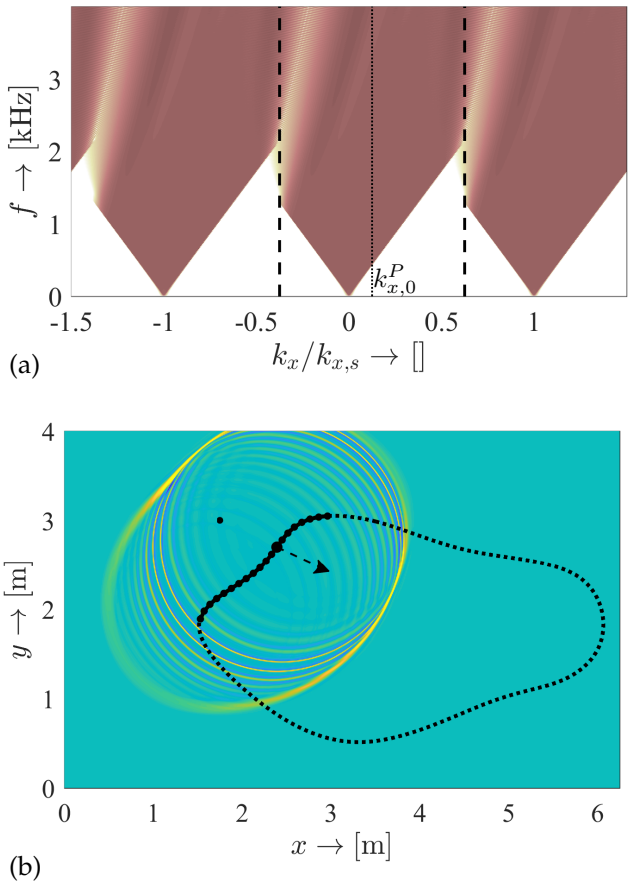

Figure 4.17. 2.5D synthesis of a 3D point source, located in $\mathbf{x}_\mathrm{s} = [1.5,\ 3,\ 0]^\mathrm{T}$ m, emitting a bandlimited impulse, applying an arbitrary shaped discrete SSD with the secondary source spacing being $\Delta x = 10$ cm, and with the snapshot taken at $t_0 \approx 6$ ms. Figure (a) shows the sampled driving function spectrum with asymmetric bandwidth limitation. Figure (b) presents the synthesized field. The synthesis is performed by optimizing spatial anti-aliasing into the direction, indicated by dashed arrow in Figure (b) by simple bandlimitation of the driving function in the angular frequency domain, according to (4.71). The corresponding center wavenumber is indicated by dotted line in Figure (a).

synthesized wavefield, emerging from the partial reproduction of the mirror spectra. Investigating Figure 4.15 (c) suggests that at a given angular frequency ω with a given SSD element at $\mathbf{x}_0$ anti-aliased synthesis can be performed into directions for which $|k_t^P(\mathbf{x}_0)| < k_{t,\mathrm{Nyq}}$ holds. Above the Nyquist wavenumber, components of the mirror spectra are reproduced as well, present as lateral waves in the synthesized field. It is restated here that one particular SSD element at $\mathbf{x}_0$ dominates the synthesized field along the local propagation direction of the synthesized field, hence along a straight line through the SSD element into the direction of the virtual field's local wavenumber vector. This means that anti-aliased synthesis can be achieved along a beam, centered around the normal vector of the SSD element, where $|k_t^P(\mathbf{x}_0)| = 0$ holds locally, and the opening angle of the beam decreases with frequency. At high frequencies therefore anti-aliased, full band synthesis can be only achieved with that SSD element, where $|k_t^P(\mathbf{x}_0)| = 0$ holds locally, and the positions of full band, anti-aliased synthesis in the reproduced field will be that, dominated by the full-band SSD element.

Figure 4.16 illustrates the effect of the presented anti-aliasing strategy. It is verified that into the direction dominated by the SSD element at $\mathbf{x}_0$, where $k_t^P(\mathbf{x}_0) = 0$ holds, aliasing components can be almost entirely eliminated behind the virtual wavefront, and still into this particular direction full-band synthesis can be achieved. Into other directions lateral aliasing components are present and the synthesized virtual wavefront is bandlimited.

So far only symmetrical anti-aliasing filtering was discussed. However, overlapping of the mirror spectra may be eliminated by bandlimiting the driving function

wavenumber content around an arbitrary chosen center wavenumber (below the Nyquist wavenumber) to the bandwidth of $\frac{2\pi}{\Delta x}$, as illustrated in Figure 4.17 (a). The center wavenumber $k_{t,0}^P$ defines the direction into which full-band, anti-aliased synthesis can be achieved: the SSD element, with $k_t^P(\mathbf{x}_0) = k_{t,0}^P$ performs full-band synthesis and dominates the synthesized field into the direction $\mathbf{k}^P(\mathbf{x}_0)$. Asymmetric anti-aliasing filtering can be performed by the angular low-pass filtering of the driving function according to

$$D(\mathbf{x}_0, \omega) = 0, \quad \text{where} \quad \omega \geq \frac{\pi}{\Delta x} \frac{c}{|\hat{k}_t^P(\mathbf{x}_0) - \hat{k}_{t,0}^P|}. \tag{4.71}$$

Asymmetric anti-aliasing condition

The result of asymmetric anti-aliasing filtering is presented in Figure 4.17 (b), illustrating how anti-aliased synthesis may be optimized into an arbitrary direction. This local increase of synthesis accuracy is referred to as *Local Wave Field Synthesis (LWFS)* in the related literature, being the subject of extensive study in the recent years. [AS10b; AS11b; Spo+11; WS15a; WS15b; Hah+17; Hah+16; Win+16] Local increase of accuracy is usually achieved by some spatial bandwidth limitation strategy applied to the driving function, performed in simple SSD geometries (e.g. linear, circular SSDs). The above derivation hence gives an asymptotic approximation of these spatial bandwidth limitation techniques, valid for an arbitrary SSD contour.

4.4.3 Avoiding the reproduction of mirror spectra

As presented in the foregoing, even besides ideal anti-aliasing filtering (spatial bandlimition) of the driving function, lateral aliasing components following the virtual wavefront will still be present. Mathematically, these aliasing artifacts originate from the reproduction of the adjacent mirror spectra components above the Nyquist wavenumber, as illustrated in Figure 4.15 (c). Obviously, the reproduction of mirror spectra can be avoided only by applying a secondary source distribution with spatially low-pass filtered transfer function—instead of the simple 3D Green's function—with high attenuation factor above the Nyquist wavenumber[5]. This requirement is fulfilled by directive secondary sources, radiating with low intensity into lateral directions, i.e. to large tangential wavenumbers. In a signal processing analogy, directive secondary sources therefore act as reproduction filters.

Physically, source directivity stems from the physical extension of radiating surfaces due to the constructive and destructive interference of waves, originating from different positions on the surface. At high frequencies and in the farfield (compared to the physical extension) baffled vibrating surfaces can be modeled as directive point sources. In fact, this can be proven by using the local wavenumber concept as presented in Appendix E.1. The optimal shape of extended secondary sources in the aspect of suppressing the mirror spectra has been studied in the related literature

[5] In fact, mirror spectrum reproduction may be avoided by applying more strict low-pass anti-aliasing, by also filtering out those components, which would be present as lateral mirror spectra after discretization. Hence the spectrum of the filtered driving function would be a romboid shape in Figure 4.15 (a), entirely bandlimited to $\omega = \frac{k_{x,s}}{c}$. This strategy is equivalent with the solution, given in [Win+18a].

[Ver97]. Here the optimal SSD directivity is discussed within the context of the unified WFS framework.

The farfield approximation of an extended radiator as a directive point source is given by (E.7). The field of a directive point source at the horizontal plane, containing the source (i.e. at $\theta = 0$) is given by

$$G_\Theta(\mathbf{x} - \mathbf{x}_0, \omega) = \Theta(\phi(\mathbf{x}, \mathbf{x}_0), \omega) \cdot G(\mathbf{x} - \mathbf{x}_0, \omega), \tag{4.72}$$

with the directivity function given by $\Theta(\cdot)$. Here ϕ denotes the polar angle, measured from the main direction of the source, in case of modeling baffled sources given by the source-surface normal: $\cos\phi = \frac{\langle \mathbf{x}-\mathbf{x}_0 \cdot \mathbf{n}(\mathbf{x}_0) \rangle}{|\mathbf{x}-\mathbf{x}_0|}$.

First the wavenumber domain representation of a theoretical directive point source is investigated. The transfer function of a directive point source at the origin, measured along a fixed y reads as

$$\tilde{G}_\Theta(k_x, y, \omega) = \int_{-\infty}^{\infty} \Theta(\phi(\mathbf{x}), \omega) \cdot G(\mathbf{x}, \omega)\, \mathrm{e}^{\mathrm{j}k_x x} \mathrm{d}x. \tag{4.73}$$

As an approximation, the amplitude factor of the integral is approximated around its stationary point. For the sake of simplicity it is assumed that the directivity function is real-valued. Since in case of baffled radiators the directivity function is the 2D Fourier transform of the surface normal velocity distribution, the directivity is real-valued, if the radiator is symmetrical both to the x- and z-axes (i.e. its is even function). This holds for simple geometries, e.g. for a circular piston, which model is applied frequently for modeling a dynamic loudspeaker.

Following (D.4), by assuming a real-valued directivity the stationary point of the integral is simply found where $k_x^G(\mathbf{x}^*(k_x), y) = k_x$ is satisfied. Around the stationary point the directivity function is approximated by its stationary value and the integral simplifies to

$$\tilde{G}_\Theta(k_x, y, \omega) = \Theta(\phi(\mathbf{x}^*(k_x)), \omega) \cdot \int_{-\infty}^{\infty} G(\mathbf{x}, \omega)\, \mathrm{e}^{\mathrm{j}k_x x} \mathrm{d}x = \Theta(\phi(\mathbf{x}^*(k_x)), \omega) \cdot \tilde{G}(k_x, y, \omega), \tag{4.74}$$

thus in the wavenumber domain the directivity function acts as a simple spatial filter transfer function. Since for the Green's function's local wavenumber vector $k_x^G(\mathbf{x}) = k \sin\phi(\mathbf{x}) = k_x$ holds (c.f. (E.6)), therefore as a final result the transfer function of a directive point source is given by

$$\tilde{G}_\Theta(k_x, y, \omega) = \Theta(\arcsin \frac{k_x}{k}, \omega) \cdot \tilde{G}(k_x, y, \omega), \tag{4.75}$$

while the spectrum of the synthesized field, applying a discrete secondary distribution of directive point sources becomes

$$\tilde{P}(k_x, y, \omega) = \tilde{D}^S(k_x, \omega) \cdot \Theta(\arcsin \frac{k_x}{k}, \omega) \cdot \tilde{G}(k_x, y, \omega). \tag{4.76}$$

This allows one to derive the directivity characteristics of an ideal spatial low-pass secondary source, which suppresses lateral waves above the Nyquist wavenumber,

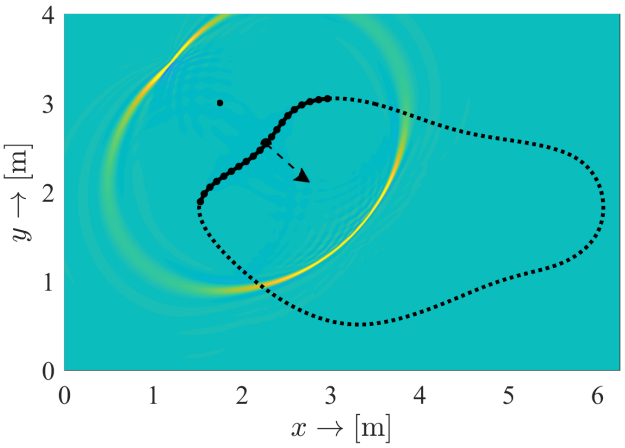

Figure 4.18. 2.5D synthesis of a 3D point source, located in $\mathbf{x}_\mathrm{s} = [1.5,\ 3,\ 0]^\mathrm{T}$ m, emitting a bandlimited impulse, applying an arbitrary shaped discrete SSD with the secondary source spacing being $\Delta x = 10$ cm. The synthesis is performed by ideal anti-aliasing filtering of the driving function and applying the distribution of ideally directive secondary sources.

hence avoiding the reproduction of mirror spectra. The transfer function of the ideal anti-aliasing SSD is given as

$$\Theta(\arcsin\frac{k_x}{k},\omega) = 0, \quad \text{if} \quad k_x \geq \frac{\pi}{\Delta x} \tag{4.77}$$

which can be formulated in the angular domain as

Ideal anti-aliasing SSD directivity

$$\Theta(\phi,\omega) = 0, \quad \text{if} \quad \sin\phi \geq \frac{\pi}{\Delta x}\frac{c}{\omega}. \tag{4.78}$$

The theoretical, ideal secondary sources therefore would only radiate within a beam with a unit amplitude, so that the width of the beam decreases at increasing frequency. By applying such ideal secondary sources, aliasing could be theoretically completely avoided, still ensuring full band, anti-aliased synthesis into one particular direction, as described above. Into other directions the synthesized wavefront is bandlimited (low-pass filtered). Obviously, unlike for the anti-aliasing filtering, the direction of perfect synthesis is fixed towards the main lobe of the applied secondary sources.

The result of synthesis applying secondary sources with ideal directivity can be seen in Figure 4.18, depicting the theoretical best case scenario when applying a discrete SSD.

Obviously, the above „ideally directed secondary sources" are not realizable, however the presented framework is useful for predicting the suppression factor in the wavenumber region, once the directivity of the applied secondary sources is known. As a simple example, the directivity of a circular piston is given by (E.10), reading

$$\Theta(\arcsin\frac{k_x}{k},\omega) = 2\frac{J_1\left(r_0 k_x\right)}{r_0 k_x}, \tag{4.79}$$

with $J_1(\cdot)$ being the first order Bessel function. The circular piston therefore acts as a spatial low-pass filter, with the -3 dB cut-off wavenumber being $k_{x,c} \approx \frac{2.22}{r_0}$, calculated numerically. Real-life dynamic loudspeakers with circular membranes are often modeled as circular pistons at frequencies, at which the modal behaviour of the diaphragm is not considerable. In a linear array the largest possible loudspeaker

radius is the half of the loudspeaker spacing ($r_0 = \Delta x/2$), hence, the lowest achievable cut-off wavenumber is $k_{x,c} = \frac{4.44}{\Delta x}$. This is still higher, than the Nyquist wavenumber ($k_{x,\mathrm{Nyq}} = \frac{\pi}{\Delta x}$), meaning that even with the closest physically possible loudspeaker spacing in case of an in-line loudspeaker array, spatial aliasing components will be slightly present in the reproduced field.

5 Synthesis of moving sound sources

In the previous chapters the description and reproduction of stationary sound fields were discussed. The presented sound field synthesis methods, however, were not restricted to the synthesis of stationary sound fields. In addition to the static case the synthesis of moving sources gained increasing interest. This chapter deals with the synthesis of the sound fields generated by moving sources of sound, constituting a complex application example for the foregoing.

For this dynamic case the primary challenge is the proper reconstruction of the *Doppler effect*, occurring due to the constant, finite wave propagation velocity in a homogeneous medium. Since wavefronts generated by a source under motion propagate away from the excitation position with a finite sound speed, therefore in front of the source—towards the direction of the source motion—the wavefronts are compressed, while behind the source a rarefaction of wavefronts occurs. This phenomenon leads to a modified, time dependent attenuation factor and a clearly audible altered perceived frequency in case of a harmonic source excitation, termed as the *Doppler shift*.

The proper reconstruction of the Doppler effect is, however, inherently solved when analytical source models are applied. Thus, first the analytical description of a sound field generated by a moving source is investigated.

5.1 Description of moving sources

This section extends the description and high frequency/asymptotic properties of stationary sound fields to the particular case of a moving 3D point source. The solution obtained in the followings can be applied in order to describe spatially extended moving sources, while an inclusion of source directivity can be found in [War76; AS11c].

5.1.1 Time domain description

As a general case for a moving sound source, the field excited by a 3D point source under arbitrary motion is examined in details [DW83; Hoo05]. Assume a point source moving along an arbitrary trajectory with an arbitrary velocity profile, with the source

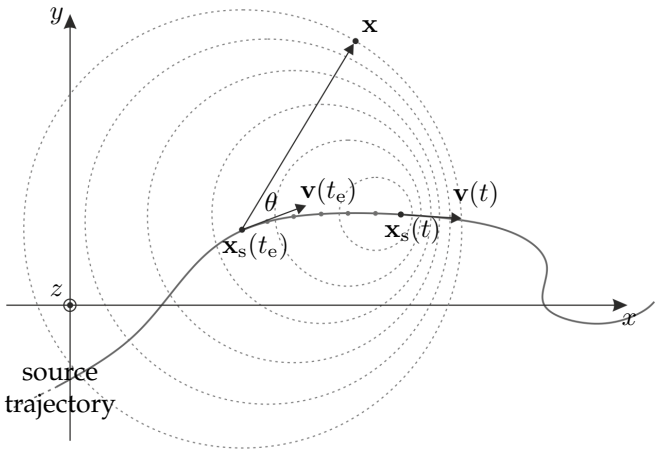

Figure 5.1. Geometry for the description of the sound field of a moving point source, moving at an arbitrary trajectory described by $\mathbf{x}_\mathrm{s}(t)$. The figure illustrates a moving source emitting impulses, with the position at the emission time instants denoted by grey dots on the trajectory. The first impulse, emitted at t_e is received in the receiver position $\mathbf{x}$ at the time instant t, when the „snapshot" is taken.

location time history given by $\mathbf{x}_\mathrm{s}(t) = [x(t),\ y(t),\ z(t)]^\mathrm{T}$. The spatio-temporal impulse response of such a moving source, satisfying the inhomogeneous wave equation

$$\left(\nabla_\mathbf{x}{}^2 - \frac{1}{c^2}\frac{\partial^2}{\partial t^2}\right) g_\mathrm{m}(\mathbf{x} - \mathbf{x}_\mathrm{s}(t_\mathrm{e}), t - t_\mathrm{e}) = -\delta\left(\mathbf{x} - \mathbf{x}_\mathrm{s}(t_\mathrm{e})\right) \cdot \delta\left(t - t_\mathrm{e}\right), \tag{5.1}$$

is given by the *retarded Green's function* [Jac99]

$$g_\mathrm{m}(\mathbf{x} - \mathbf{x}_\mathrm{s}(t_\mathrm{e}), t - t_\mathrm{e}) = \frac{1}{4\pi}\frac{\delta(t - t_\mathrm{e} - \frac{|\mathbf{x}-\mathbf{x}_\mathrm{s}(t_\mathrm{e})|}{c})}{|\mathbf{x} - \mathbf{x}_\mathrm{s}(t_\mathrm{e})|}. \tag{5.2}$$

Time instant t_e is referred to as the *emission time*: the time instant at which the impulse was emitted that arrives to the receiver position $\mathbf{x}$ at the time instant t. Formally, the field of a moving impulsive point source is obtained from the stationary Green's function, by letting the source position to be the function of time. A moving point source therefore radiates spherical wavefronts with the center being the source position at the emission time. This general case is illustrated in Figure 5.1.

The field generated by a moving source with a source excitation time history $s(t)$ is obtained by modeling the excitation signal as the sum of a continuous sequence of Dirac-pulses [Gir+01; Ahr12]. Each pulse is weighted by the retarded Green's function describing the wave propagation from the source position at the emission time to the receiver position. The radiated field therefore can be written as

$$p_\mathrm{m}(\mathbf{x}, t) = \int_{-\infty}^{\infty} s(t_\mathrm{e}) g_\mathrm{m}(\mathbf{x} - \mathbf{x}_\mathrm{s}(t_\mathrm{e}), t - t_\mathrm{e}) \mathrm{d}t_\mathrm{e} = \frac{1}{4\pi}\int_{-\infty}^{\infty} s(t_\mathrm{e}) \frac{\delta(t - t_\mathrm{e} - \frac{|\mathbf{x}-\mathbf{x}_\mathrm{s}(t_\mathrm{e})|}{c})}{|\mathbf{x} - \mathbf{x}_\mathrm{s}(t_\mathrm{e})|} \mathrm{d}t_\mathrm{e}, \tag{5.3}$$

describing a non-stationary convolution with the time-variant convolution kernel being the moving source impulse response [Mar98].

The convolution may be evaluated by the generalization of the Dirac delta's sifting property for arguments of general functions [DW83; Cri+92; Jac99], given as[1]

$$\int_{-\infty}^{\infty} f(t)\delta(g(t))\mathrm{d}t = \sum_i \frac{f(t_i)}{\left|\frac{\partial}{\partial t} g(t)\right|_{t=t_i}}, \quad \text{where} \quad g(t_i) = 0. \tag{5.4}$$

[1] Equivalently, the same result is obtained by introducing a new variable for $t'(t_\mathrm{e}) = t_\mathrm{e} + |\mathbf{x} - \mathbf{x}_\mathrm{s}(t_\mathrm{e})|/c$.

In the present case the derivative of the argument, i.e. the Jacobian is expressed by applying the chain rule, reading

$$\frac{\mathrm{d}}{\mathrm{d}t_\mathrm{e}} g(t_\mathrm{e}) = -1 + \frac{1}{c} \frac{\left\langle \frac{\partial}{\partial t_\mathrm{e}} \mathbf{x}_\mathrm{s}(t_\mathrm{e}) \cdot (\mathbf{x} - \mathbf{x}_\mathrm{s}(t_\mathrm{e})) \right\rangle}{|\mathbf{x} - \mathbf{x}_\mathrm{s}(t_\mathrm{e})|}. \tag{5.5}$$

The temporal derivative of the source trajectory $\mathbf{v}_\mathrm{s}(t_\mathrm{e}) = \frac{\partial}{\partial t_\mathrm{e}} \mathbf{x}_\mathrm{s}(t_\mathrm{e})$ can be recognized as the source velocity vector at the emission time. Convolution with the Dirac delta sifts out the zeros of its argument, given by the emission time for which

$$t_\mathrm{e}(t, \mathbf{x}) = t - \frac{|\mathbf{x} - \mathbf{x}_\mathrm{s}(t_\mathrm{e}(t, \mathbf{x}))|}{c} \tag{5.6}$$

holds. Note that for a given receiver position $\mathbf{x}$ and receiving time t, the emission time instant $t_\mathrm{e}(t, \mathbf{x})$ is a dependent variable. For subsonic velocities (i.e. $v < c$) only the positive real root for this quadratic equation is considered, while the Jacobian (5.5) is negative. With all these considerations the non-stationary convolution (5.3) can be evaluated, yielding the sound field of a moving point source

$$p_\mathrm{m}(\mathbf{x}, t) = \frac{1}{4\pi} \frac{s(t - \frac{|\mathbf{x} - \mathbf{x}_\mathrm{s}(t_\mathrm{e}(\mathbf{x}, t))|}{c})}{|\mathbf{x} - \mathbf{x}_\mathrm{s}(t_\mathrm{e}(\mathbf{x}, t))| - \frac{1}{c} \left\langle \mathbf{v}_\mathrm{s}(t_\mathrm{e}(\mathbf{x}, t)) \cdot (\mathbf{x} - \mathbf{x}_\mathrm{s}(t_\mathrm{e}(\mathbf{x}, t))) \right\rangle}, \tag{5.7}$$

with t_e satisfying equation (5.6).

Conventionally the radiated field is expressed in terms of the propagation time-delay $\tau(\mathbf{x}, t) = t - t_\mathrm{e}(\mathbf{x}, t)$ given by the non-linear quadratic equation

$$\tau(\mathbf{x}, t) = \frac{|\mathbf{x} - \mathbf{x}_\mathrm{s}(t - \tau(\mathbf{x}, t))|}{c}. \tag{5.8}$$

Propagation time delay

Again, for subsonic velocities only the positive root of the quadratic equation ($\tau(\mathbf{x}, t) > 0$) is taken into consideration [Hoo05]. In the present thesis exclusively subsonic velocities are discussed. For a detailed treatment on sources moving at supersonic velocities refer to [AS08d; Ahr12]. Introducing $\Delta(\mathbf{x}, t)$ for the attenuation factor the radiated field is given as

$$p_\mathrm{m}(\mathbf{x}, t) = \frac{1}{4\pi} \frac{s(t - \tau(\mathbf{x}, t))}{\Delta(\mathbf{x}, t - \tau(\mathbf{x}, t))}, \tag{5.9}$$

Field of a moving source

with

$$\Delta(\mathbf{x}, t) = |\mathbf{x} - \mathbf{x}_\mathrm{s}(t)| - \left\langle \frac{1}{c} \mathbf{v}_\mathrm{s}(t) \cdot (\mathbf{x} - \mathbf{x}_\mathrm{s}(t)) \right\rangle = |\mathbf{x} - \mathbf{x}_\mathrm{s}(t)| \left(1 - M(t) \cos \vartheta(\mathbf{x}, t)\right), \tag{5.10}$$

where $M(t) = |\mathbf{v}_\mathrm{s}(t)|/c$ is the *Mach number*, $\vartheta(\mathbf{x}, t)$ is the angle between the velocity vector and the source-receiver vector and the term $\left(1 - M(t) \cos \vartheta(\mathbf{x}, t)\right)^{-1}$ is referred to as the *Doppler factor*. The geometry along with the notation used, is illustrated in Figure 5.1. Equation (5.10) states that as a part of the Doppler effect, due to the compression of wavefronts towards the direction of the source motion the resulting spatial amplitude distribution of the wavefield increases compared to that of a stationary source. Similarly, behind the moving source due to the rarefaction of the wavefronts

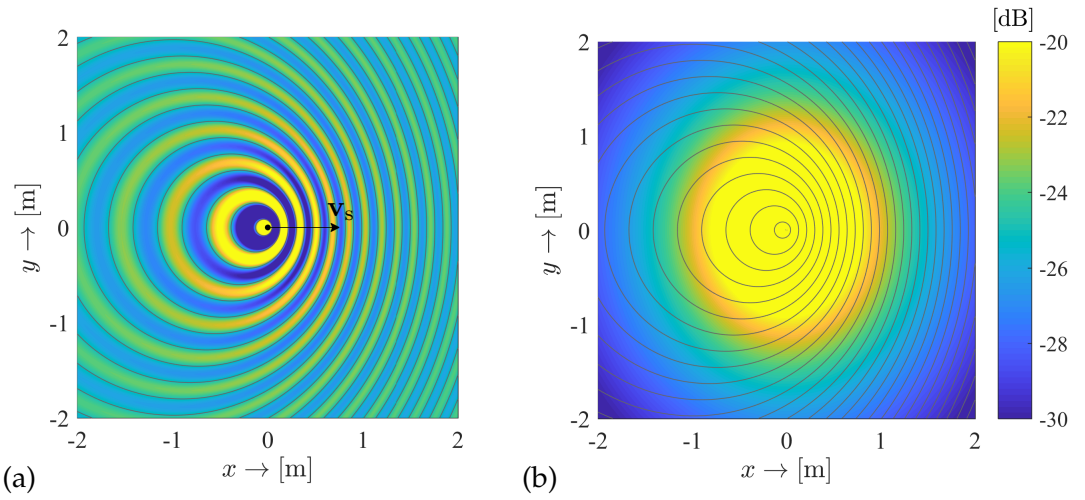

Figure 5.2. Sound field, generated by a moving point source, oscillating at a source angular frequency $f_0 = 1$ kHz traveling along a straight source trajectory, described by $\mathbf{x}_s(t) = [v \cdot t,\ 0,\ 0]^T$ with the velocity given by $v = \frac{c}{2} = 171.5$ m/s. Figure (a) shows the real part of the radiated field and (b) shows the amplitude distribution in a logarithmic scale, demonstrating the result of the Doppler effect. In this special case of uniform motion the amplitude distribution is axially symmetric with the axis being perpendicular to the source trajectory.

the amplitude of the source decreases. This relative change of the attenuation factor is described by the Doppler factor.

Obviously, the evaluation of the radiated field emitted by a moving source is not straightforward: it requires the determination of the emission time or the propagation time-delay by solving (5.6) or (5.8), respectively, for each receiver position and time. Analytical solutions for the general problem are barely available. For the special case of a sound source under uniform motion, i.e. moving along a straight trajectory with a constant velocity the quadratic equations can be solved. Assuming the source moving along the x-axis, i.e. the source position vector is given as $\mathbf{x}_s(t) = [v \cdot t,\ 0,\ 0]^T$ the required quantities read as

$$\tau(\mathbf{x}, t) = \frac{|\mathbf{x} - \mathbf{x}_s(t_e(\mathbf{x}, t))|}{c} = \frac{M(x - vt) + \Delta(\mathbf{x}, t)}{c(1 - M^2)}, \tag{5.11}$$

with $M = \frac{v}{c}$ being the time independent Mach number and

$$\Delta(\mathbf{x}, t) = \sqrt{(x - vt)^2 + (y^2 + z^2)(1 - M^2)}. \tag{5.12}$$

For sources moving inclined to the x-axis the corresponding quantities can be obtained by a rotation of the coordinate system as discussed in Appendix G.1 [FF15a; Ahr; FF16b].

5.1.2 Time-frequency domain description

In order to extend the asymptotic/local attributes—introduced for steady-state sound fields in Chapter 3—for the dynamic scenario, a mixed time-frequency representation of moving sources is investigated next. Assume a moving source with a

harmonic excitation time dependence given by $s(t) = \mathrm{e}^{\mathrm{j}\omega_0 t}$, oscillating at the angular frequency ω_0. The radiated field reads as

$$P_{\mathrm{m}}(\mathbf{x}, t, \omega_0) = \frac{1}{4\pi} \frac{\mathrm{e}^{\mathrm{j}\omega_0 (t - \tau(\mathbf{x},t))}}{\Delta(\mathbf{x}, t - \tau(\mathbf{x},t))}. \tag{5.13}$$

An arbitrary non-stationary sound field can be written in a general polar form $P_{\mathrm{m}}(\mathbf{x}, t, \omega_0) = A^P(\mathbf{x}, t, \omega_0)\mathrm{e}^{\mathrm{j}\phi^P(\mathbf{x},t,\omega_0)}$, with $A^P(\mathbf{x}, t, \omega_0), \phi^P(\mathbf{x}, t, \omega_0) \in \mathbb{R}$. For such a harmonic field the local wavenumber vector can be defined in the same manner as for a stationary sound field being the negative phase gradient

$$\mathbf{k}^P(\mathbf{x}, t) = [k_x^P(\mathbf{x}, t),\ k_y^P(\mathbf{x}, t),\ k_z^P(\mathbf{x}, t)]^{\mathrm{T}} = -\nabla_{\mathbf{x}}\, \phi^P(\mathbf{x}, t, \omega_0). \tag{5.14}$$

This vector is perpendicular to the isophase surfaces, i.e. to the wavefront at an arbitrary position and time instant. Since in the present thesis only isotropic medium is considered, the local wavenumber vector points into the local propagation direction of the wavefront. For the case of a moving point source the local wavenumber vector is given by the phase gradient of (5.13) reading

Moving source local wavenumber

$$\mathbf{k}^P(\mathbf{x}, t) = -\nabla_{\mathbf{x}}\, \phi^P(\mathbf{x}, t, \omega_0) = \frac{\omega_0}{c} \frac{\mathbf{x} - \mathbf{x}_{\mathrm{s}}(t - \tau(\mathbf{x},t))}{\Delta(\mathbf{x}, t - \tau(\mathbf{x},t))}. \tag{5.15}$$

The local dispersion relation (or the eikonal equation) and the attenuation over the propagation path (or the transport equation) for a non-stationary sound field can be obtained by substituting the general polar form into the time domain wave equation (2.5) and expanding the differential operators. Setting the real and imaginary parts to zero results in the equations

$$\frac{\nabla_{\mathbf{x}}^2 A^P}{A^P} - |\nabla_{\mathbf{x}}\, \phi^P|^2 - \frac{1}{c^2}\frac{A_{tt}^{P\prime\prime}}{A^P} + \frac{1}{c^2}|\phi_t^{P\prime}|^2 = 0, \tag{5.16}$$

$$\nabla_{\mathbf{x}}^2 \phi^P + 2\frac{\left\langle \nabla_{\mathbf{x}}\, \phi^P \cdot \nabla_{\mathbf{x}}\, A^P \right\rangle}{A^P} - \frac{1}{c^2}\phi_{tt}^{P\prime\prime} - \frac{1}{c^2} 2 \frac{A_t^{P\prime}\phi_t^{P\prime}}{A^P} = 0. \tag{5.17}$$

Obviously, for a moving point source the above equations have to be singular at the source position, following (2.37). Assuming high frequency conditions the local dispersion relation results in

$$|\nabla_{\mathbf{x}}\, \phi^P|^2 = k_x^P(\mathbf{x}, t)^2 + k_y^P(\mathbf{x}, t)^2 + k_z^P(\mathbf{x}, t)^2 \approx \frac{1}{c^2}|\phi_t^{P\prime}|^2, \tag{5.18}$$

holding with equality for a point source under motion excluding the moving singularity. Obviously, unlike for the stationary case, the length of the local wavenumber vector is not constant, but depends on both the receiver position and time. As a result the wavefront is not described by a normal form, as for the stationary case.

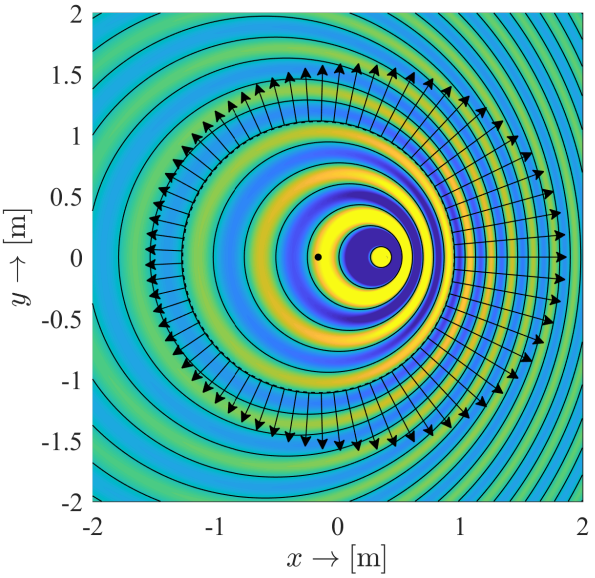

Figure 5.3. Illustration of the wavefronts and the local wavenumber vector of a moving sound source. The figure illustrates the local wavenumber vector on an isophase surface, with the source position at the corresponding emission time denoted by black dot. The generated wavefronts are spherical ones, with the local wavenumber vector being radial. The length of the local wavenumber vector is defined by the instantaneous perceived angular frequency, described by the Doppler factor.

The temporal derivative of the phase function can be recognized as the generalization of the perceived angular frequency at a fixed receiver position [MI68]. For the case of a moving virtual point source the perceived frequency can be expressed as

Perceived angular frequency

$$\frac{\partial}{\partial t}\phi^P(\mathbf{x},t) = \omega(\mathbf{x},t) = \omega_0 \frac{|\mathbf{x}-\mathbf{x}_\mathrm{s}(t-\tau(\mathbf{x},t))|}{\Delta(\mathbf{x},t-\tau(\mathbf{x},t))} = \frac{\omega_0}{1-M(t)\cos\vartheta(\mathbf{x},t)}. \tag{5.19}$$

This expression is the general Doppler formula, describing the relative frequency shift in case of a harmonic source signal [MI68]. Thus both the perceived frequency and amplitude of the source is altered, and the alteration is described by the Doppler factor.

The local dispersion relation (5.18) therefore states that the local wavenumber vector is perpendicular to the wavefront with the length being proportional to the local perceived angular frequency. Hence, the normalized local wavenumber vector, defined as being a unit vector pointing to the local propagation direction, can be generalized as

$$\hat{\mathbf{k}}^P(\mathbf{x},t) = -\frac{\nabla_\mathbf{x}\,\phi^P(\mathbf{x},t)}{\frac{1}{c}\frac{\partial}{\partial t}\phi^P(\mathbf{x},t)} = \frac{\mathbf{k}^P(\mathbf{x},t)}{\omega(\mathbf{x},t)/c}. \tag{5.20}$$

For the moving point source the normalized local wavenumber vector is given from (5.15) and (5.19) as

Normalized local wavenumber

$$\hat{\mathbf{k}}^P(\mathbf{x},t) = \frac{\mathbf{x}-\mathbf{x}_\mathrm{s}(t-\tau(\mathbf{x},t))}{|\mathbf{x}-\mathbf{x}_\mathrm{s}(t-\tau(\mathbf{x},t))|}, \tag{5.21}$$

reflecting the fact that a moving point source radiates spherical wavefronts with the center being the source position at the emission time instant.

Finally, in the non-stationary case, the transport equation (5.17) describes, how the amplitude of a wavefront element changes over its propagation path:

$$\frac{\left\langle \hat{\mathbf{k}}^P \cdot \nabla_\mathbf{x}\, A^P \right\rangle + \frac{1}{c}A_t^{P'}}{A^P} = \frac{1}{2}\frac{\nabla_\mathbf{x}^2\phi^P - \frac{1}{c^2}\phi_{tt}^{P''}}{\frac{1}{c}\phi_t^{P'}} \tag{5.22}$$

The left hand side of the equation can be interpreted as the relative amplitude change of the radiated wavefront over its propagation path. Mathematically, it is given by the rate of change of the amplitude factor with respect to a change $\mathrm{d}x$ in the receiver position into the direction of $\hat{\mathbf{k}}$ and a change $\frac{\mathrm{d}x}{c}$ in the receiving time. The right hand side of the equation can be recognized as the general local mean curvature of the wavefront [Gol05, p. 4.2][2], thus (5.22) can be rewritten as

$$\overline{\kappa}^P(\mathbf{x},t) = -\frac{1}{2}\nabla_{\mathbf{x}} \cdot \hat{\mathbf{k}}^P(\mathbf{x},t) = \\ -\frac{\left\langle \hat{\mathbf{k}}^P \cdot \nabla_{\mathbf{x}} A^P \right\rangle + \frac{1}{c} A_t^{P'}}{A^P} = -\frac{1}{2}\left(\frac{\nabla_{\mathbf{x}}^2 \phi^P}{\omega(\mathbf{x},t)/c} - \frac{\hat{\mathbf{k}}^P(\mathbf{x},t)^{\mathrm{T}} \mathbf{H}^P \hat{\mathbf{k}}^P(\mathbf{x},t)}{\omega(\mathbf{x},t)/c} \right). \quad (5.23)$$

As a result, similarly to the stationary case, the relative attenuation of the wavefront over the propagation is given by the local mean curvature of the wavefront. Obviously, for a moving point source the mean curvature is that of a spherical wavefront being also equal to the principal curvatures, given as

$$\overline{\kappa}^P(\mathbf{x},t) = \kappa_{1/2}^P(\mathbf{x},t) = \frac{1}{|\mathbf{x} - \mathbf{x}_{\mathrm{s}}(t - \tau(\mathbf{x},t))|}. \quad (5.24)$$

This result reflects that although the spatial distribution of the amplitude factor is altered according to the Doppler factor, the attenuation of the individual wavefronts over the propagation path is inversely proportional to the distance from the source position at the emission time instant. This fact trivially follows the definition of the retarded Green's function (5.2).

5.2 Wave Field Synthesis of moving sources

So far only boundary integral formulations of steady-state sound fields were discussed merely in the frequency domain. In order to synthesize the temporally varying sound field of a moving point source by using implicit SFS methodology, an appropriate time domain boundary integral representation of arbitrary sound fields is required.

Assume a source-free volume inside an enclosure Ω_{i}, bounded by the surface $\partial\Omega$. Any sound field obeying the homogeneous time domain wave equation inside the enclosure can be expressed by the *time domain Kirchhoff-Helmholtz integral equation*. The formulation is obtained by the direct inverse Fourier transform of the spectral KHIE (2.55) by exploiting the Fourier convolution theorem, reading

$$p(\mathbf{x},t) = \oint_{\partial\Omega} \int_{t_0} p(\mathbf{x}_0,t_0) \frac{\partial}{\partial \mathbf{n}_{\mathrm{in}}} g(\mathbf{x}-\mathbf{x}_0, t-t_0) - \frac{\partial}{\partial \mathbf{n}_{\mathrm{in}}} p(\mathbf{x}_0,t_0) g(\mathbf{x}-\mathbf{x}_0, t-t_0) \mathrm{d}t_0 \mathrm{d}\partial\Omega(\mathbf{x}_0), \quad (5.25)$$

Time domain KHIE

with $\mathbf{x} \in \Omega_{\mathrm{i}}$.

Assuming convex boundaries and high frequency conditions—i.e. source time histories with dominant high frequency content—the tangent plane approximation

[2] As given in [Gol05] the mean curvature of a general implicit surface F is given by $\overline{\kappa}^F(\mathbf{x}) = \frac{1}{2} \frac{\nabla_{\mathbf{x}} F^{\mathrm{T}} H^F \nabla_{\mathbf{x}} F - |\nabla_{\mathbf{x}} F|^2 \nabla_{\mathbf{x}}^2 F}{|\nabla_{\mathbf{x}} F|^3}$. In the present case also $\frac{1}{c^2}\phi_{tt}^{P''} = \frac{\nabla_{\mathbf{x}} \phi^{\mathrm{T}} \mathbf{H}^P \nabla_{\mathbf{x}} \phi}{|\nabla_{\mathbf{x}} \phi|^2}$ holds.

(3.20) holds and the above integral can be approximated by the *time domain Kirchhoff approximation*

Time domain Kirchhoff approx.

$$p(\mathbf{x},t) \approx -2 \oint_{\partial\Omega} \int_{t_0} w(\mathbf{x}_0,t_0) \frac{\partial}{\partial \mathbf{n}_{\text{in}}} p(\mathbf{x}_0,t_0) g(\mathbf{x}-\mathbf{x}_0,t-t_0) \mathrm{d}t_0 \mathrm{d}\partial\Omega(\mathbf{x}_0), \tag{5.26}$$

obtained by the direct inverse Fourier transform of equation (3.21). The time domain approximation describes an arbitrary sound field in terms of a spatio-temporal convolution over the boundary surface. The convolution kernel/wave propagator is the time domain Green's function, describing the spatio-temporal impulse response of a point source on the boundary, emitting an impulse at t_0. The time dependent windowing function can be defined by assuming a harmonic time dependency, for which the local wavenumber vector is defined as (5.14). The windowing function is then given as

$$w(\mathbf{x}_0,t_0) = \begin{cases} 1, & \forall \quad \langle \mathbf{k}^P(\mathbf{x}_0,t_0) \cdot \mathbf{n}_{\text{in}}(\mathbf{x}_0) \rangle > 0 \\ 0 & \text{elsewhere,} \end{cases} \tag{5.27}$$

as a straightforward generalization of the stationary case.

Similarly to the stationary case, for the special geometry of the boundary being an infinite plane the Kirchhoff approximation degenerates to the time domain Rayleigh integral, describing an arbitrary pressure field in front of the Rayleigh plane without any approximations involved.

5.2.1 3D Wave Field Synthesis of a moving point source

Assume the general sound field synthesis problem formulation in the time domain, taken as the inverse Fourier transform of the single layer potential (4.1)

$$p(\mathbf{x},t) = \oint_{\partial\Omega} \int_{t_0} d(\mathbf{x}_0,t_0) g(\mathbf{x}-\mathbf{x}_0,t-t_0) \mathrm{d}t_0 \, \mathrm{d}\partial\Omega(\mathbf{x}_0). \tag{5.28}$$

Comparison with (5.26) reveals that similarly to the stationary, harmonic case the time domain Kirchhoff approximation implicitly contains the required time domain driving signals, reading

$$d(\mathbf{x}_0,t_0) = -2w(\mathbf{x}_0,t_0) \frac{\partial}{\partial \mathbf{n}_{\text{in}}} p(\mathbf{x}_0,t_0). \tag{5.29}$$

By assuming a harmonic source time dependency the high frequency gradient approximation can be applied for a non-stationary sound field, reading

$$\nabla_{\mathbf{x}} P(\mathbf{x},t,\omega_0) \approx -\mathrm{j}\mathbf{k}^P(\mathbf{x},t) P(\mathbf{x},t,\omega_0), \tag{5.30}$$

which is again, a local plane wave approximation. The 3D WFS driving function can be approximated then by

$$D(\mathbf{x}_0,t_0,\omega_0) = 2w(\mathbf{x}_0,t_0)\mathrm{j}k_{\text{n}}^P(\mathbf{x}_0,t_0) P(\mathbf{x}_0,t_0,\omega_0), \tag{5.31}$$

with k_{n}^P being the normal component of the local wavenumber vector.

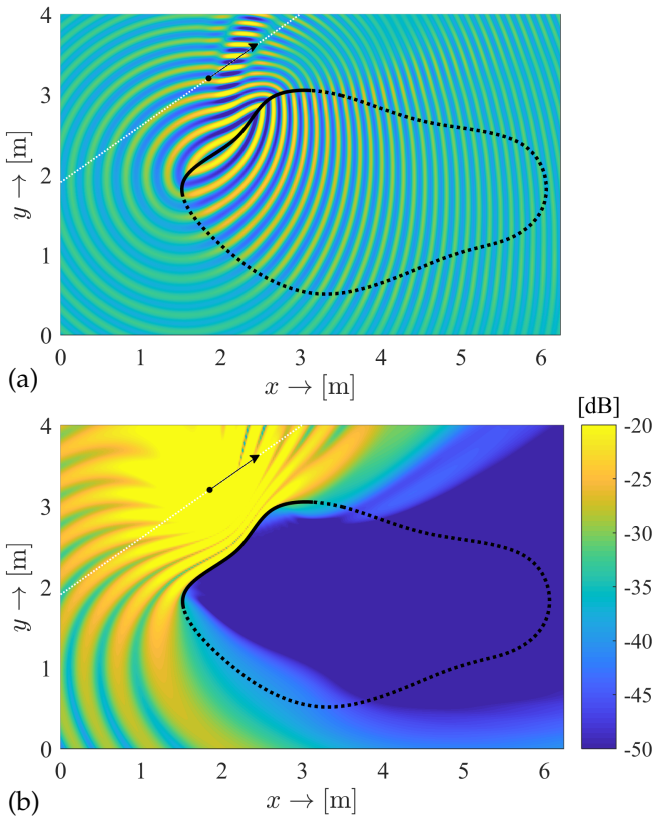

Figure 5.4. 3D synthesis of a moving 3D point source radiating at $f_0 = 1.5$ kHz. The source is under uniform motion with the source trajectory given by $\mathbf{x}_\mathrm{s} = [1.85 + v_x \cdot t,\ 3.2 + v_y \cdot t,\ 0]^\mathrm{T}$ with $|\mathbf{v}_\mathrm{s}| = 150$ m/s and $v_x = 140$ m/s, $v_y = 98$ m/s. The snapshot is taken at $t = 0$ s. The SSD surface is chosen to be independent of the z-coordinate as illustrated in Figure 4.3. Figure (a) depicts the real part of the synthesized field and part (b) presents the absolute error of synthesis (the discrepancy between the synthesized and the target sound field) in a logarithmic scale measured in the horizontal plane, containing the virtual point source. The active arc of the SSD *at the time instant* $t = 0$ s is denoted by solid black line, and the inactive part with dotted by black line.

Since the sound field generated by a moving point source satisfies the homogeneous wave equation inside the listening volume, therefore it can be described by the Kirchhoff integral, and its sound field can be reproduced by applying the driving function above. Suppose that a point source is moving along an arbitrary trajectory $\mathbf{x}_\mathrm{s}(t) = [x(t),\ y(t),\ z(t)]^\mathrm{T}$ outside the listening volume, bounded by a convex SSD. Assuming a harmonic source excitation with the angular frequency being ω_0 the driving function for the synthesis of the virtual source is obtained from (5.31) by substituting the pressure field and the local wavenumber vector of a moving point source, given by (5.13) and (5.15), respectively. The resulting driving function reads as

$$D(\mathbf{x}_0, t_0, \omega_0) = w(\mathbf{x}_0, t_0) \frac{\mathrm{j}k_0}{2\pi} \frac{\langle \mathbf{x}_0 - \mathbf{x}_\mathrm{s}(t_0 - \tau(\mathbf{x}_0, t_0)) \cdot \mathbf{n}_\mathrm{in}(\mathbf{x}_0) \rangle}{\Delta(\mathbf{x}_0, t_0 - \tau(\mathbf{x}_0, t_0))} \frac{\mathrm{e}^{\mathrm{j}\omega_0 (t_0 - \tau(\mathbf{x}_0, t_0))}}{\Delta(\mathbf{x}_0, t_0 - \tau(\mathbf{x}_0, t_0))}, \tag{5.32}$$

3D WFS driving function

with $k_0 = \frac{\omega_0}{c}$, the amplitude factor given as

$$\Delta(\mathbf{x}_0, t_0) = |\mathbf{x} - \mathbf{x}_\mathrm{s}(t_0)| - \left\langle \frac{1}{c} \mathbf{v}_\mathrm{s}(t_0) \cdot (\mathbf{x} - \mathbf{x}_\mathrm{s}(t_0)) \right\rangle \tag{5.33}$$

and the propagation time delay satisfiing $\tau(\mathbf{x}_0, t_0) = |\mathbf{x}_0 - \mathbf{x}_\mathrm{s}(t_0 - \tau(\mathbf{x}_0, t_0))|/c$. For moving sources with a wideband excitation signal with the frequency content $S(\omega) = \int_{-\infty}^{\infty} s(t) \mathrm{e}^{-\mathrm{j}\omega t} \mathrm{d}t$, the driving function is yielded by the weighted sum of the individual spectral components

$$d(\mathbf{x}_0, t_0) = w(\mathbf{x}_0, t_0) \frac{\langle \mathbf{x}_0 - \mathbf{x}_\mathrm{s}(t_0 - \tau(\mathbf{x}_0, t_0)) \cdot \mathbf{n}_\mathrm{in}(\mathbf{x}_0) \rangle}{\Delta(\mathbf{x}_0, t_0 - \tau(\mathbf{x}_0, t_0))^2} \int_{-\infty}^{\infty} \frac{\mathrm{j}\omega_0}{2\pi c} S(\omega_0) \mathrm{e}^{\mathrm{j}\omega_0 (t_0 - \tau(\mathbf{x}_0, t_0))} \mathrm{d}\omega_0, \tag{5.34}$$

describing a temporal inverse Fourier transform, taken at $t_0 - \tau(\mathbf{x}_0, t_0)$. By realizing that multiplication by $\mathrm{j}\omega_0$ performs the temporal differentiation of the input signal the time domain driving function takes the form

3D time domain driving function

$$d(\mathbf{x}_0, t_0) = \frac{\langle \mathbf{x}_0 - \mathbf{x}_\mathrm{s}(t_0 - \tau(\mathbf{x}_0, t_0)) \cdot \mathbf{n}_\mathrm{in}(\mathbf{x}_0) \rangle}{\Delta(t_0 - \tau(\mathbf{x}_0, t_0))} \frac{w(\mathbf{x}_0, t_0)}{2\pi c} \frac{s_t'(t_0 - \tau(\mathbf{x}, t_0))}{\Delta(t_0 - \tau(\mathbf{x}_0, t_0))}. \tag{5.35}$$

Comparison with (4.6) and (4.8) indicates that the moving source driving function coincides with that for a stationary point source with the static distances/attenuation factors replaced with the dynamic ones. The same result can be obtained by the direct substitution of a moving point source's pressure field into (5.29) with taking only the dominant part into consideration.

As a simple example Figure 5.4 shows the result of the synthesis of a point source under uniform motion. For the sake of computational simplicity the SSD is chosen to be invariant along the z-dimension as it was illustrated in Figure 4.3. As presented in the previous section for sources under uniform motion the propagation time delay and the amplitude distribution can be expressed analytically, given by (5.11) and (5.12), respectively. Similarly to the stationary case the above driving function ensures amplitude correct synthesis over most parts of the listening are within the validity of the Kirchhoff approximation. Apart from the errors discussed for the case of the synthesis of a stationary point source—illustrated in Figure 5.4—, amplitude errors and slight phase errors arise here as the source approaches the SSD surface and the high frequency/farfield gradient approximation does not hold.

5.2.2 The time domain 2.5D Kirchhoff approximation

In order to reproduce the sound field of a moving source by applying a contour of secondary sources an appropriate 2.5D integral representation is required. The dimensionality reduction is again done by the stationary phase approximation of the Kirchhoff integral, resulting in the *time domain 2.5D Kirchhoff approximation*.

Assume a 3D volume, bounded by a surface, for the sake of simplicity being invariant along the vertical dimension, as illustrated in Figure 5.5. An arbitrary non-stationary sound sound field inside the enclosure can be described by the time domain Kirchhoff integral (5.26), which in this special geometry, is written with separated integral variables. With a harmonic time dependency the radiated field inside the enclosure reads as

$$P(\mathbf{x}, t, \omega_0) = \oint_C \int_{z_0} \int_{t_0} 2w(\mathbf{x}_0, t_0)\mathrm{j}k_\mathrm{n}^P(\mathbf{x}_0, t_0)P(\mathbf{x}_0, t_0, \omega_0)g(\mathbf{x} - \mathbf{x}_0, t - t_0)\,\mathrm{d}t_0\,\mathrm{d}z_0\,\mathrm{d}s(x_0, y_0), \tag{5.36}$$

with the integral variable $\mathrm{d}s$ being the arc length along the contour.

Applying the explicit formula for the time domain 3D Green's function ($g(\mathbf{x} - \mathbf{x}_0, t - t_0) = \frac{1}{4\pi}\frac{\delta(t - t_0 - |\mathbf{x} - \mathbf{x}_0|/c)}{|\mathbf{x} - \mathbf{x}_0|}$) integration with respect to the emission time measured

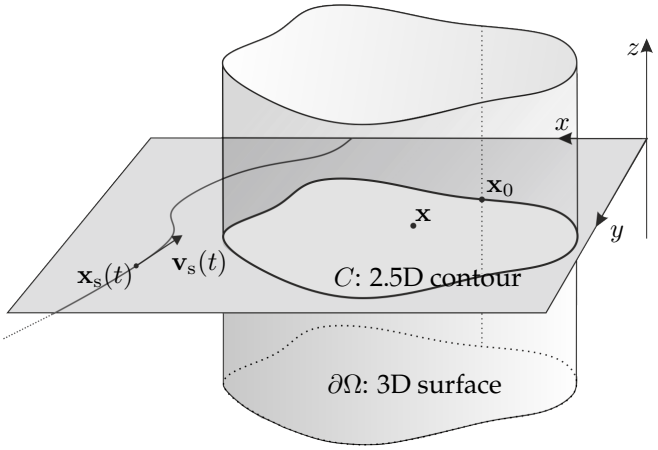

Figure 5.5. Geometry for the derivation of 2.5D Kirchhoff integral. The enclosing surface $\partial\Omega(x_0, y_0)$ is chosen to be independent of the z-coordinate in order to be able to evaluate the Kirchhoff integral with respect to z_0 using the SPA. If the sound field to be described is a 2D one propagating in the direction parallel to the listening plane, then the surface can be interpreted as a continuous set of infinite vertical line sources along C, capable of the perfect description of a 2D field inside the enclosure by a 2D countour integral.

on the boundary (i.e. with respect to t_0) can be evaluated by exploiting the Dirac delta sifting property, and the radiated field is given as

$$P(\mathbf{x}, t, \omega_0) = \frac{1}{2\pi} \oint_C \int_{z_0} w(\mathbf{x}_0, t - \tfrac{|\mathbf{x}-\mathbf{x}_0|}{c}) \mathrm{j} k_{\mathrm{n}}^P(\mathbf{x}_0, t - \tfrac{|\mathbf{x}-\mathbf{x}_0|}{c}) \frac{P(\mathbf{x}_0, t - \frac{|\mathbf{x}-\mathbf{x}_0|}{c}, \omega_0)}{|\mathbf{x} - \mathbf{x}_0|} \, \mathrm{d}z_0 \, \mathrm{d}s(x_0, y_0). \tag{5.37}$$

In order to recast to a contour integral formulation this integral is approximated by the stationary phase method along the vertical dimension.

Generally speaking, the stationary point of the integral is found, where the gradient of the integrand's phase function vanishes:

$$\nabla_{\mathbf{x}_0} \, \phi^P(\mathbf{x}_0, t - \tfrac{|\mathbf{x}-\mathbf{x}_0|}{c}, \omega_0)\Big|_{\mathbf{x}_0 = \mathbf{x}_0^*(\mathbf{x},t)} = 0. \tag{5.38}$$

The gradient can be evaluated by taking the total derivative of the phase function, which after rearrangement yields

$$-\frac{\nabla_{\mathbf{x}_0} \, \phi^P(\mathbf{x}_0^*(\mathbf{x}, t), t - \frac{|\mathbf{x}-\mathbf{x}_0^*(\mathbf{x},t)|}{c}, \omega_0)}{\frac{1}{c}\frac{\partial}{\partial t}\phi^P(\mathbf{x}_0^*(\mathbf{x}, t), t - \frac{|\mathbf{x}-\mathbf{x}_0^*(\mathbf{x},t)|}{c}, \omega_0)} = \frac{\mathbf{x} - \mathbf{x}_0^*(\mathbf{x}, t)}{|\mathbf{x} - \mathbf{x}_0^*(\mathbf{x}, t)|} \tag{5.39}$$

being satisfied in the stationary position. The left hand side describes the normalized local wavenumber vector of the general sound field P *taken at the time instant* $t - \frac{|\mathbf{x}-\mathbf{x}_0|}{c}$ (c.f. (5.20)), while the right term is recognized as the normalized local wavenumber of the Green's function. The stationary position for the Kirchhoff integral is thus found where

$$\hat{\mathbf{k}}^P(\mathbf{x}_0^*(\mathbf{x}, t), t - \tfrac{|\mathbf{x}-\mathbf{x}_0^*(\mathbf{x},t)|}{c}) = \hat{\mathbf{k}}^G(\mathbf{x} - \mathbf{x}_0^*(\mathbf{x}, t)) \tag{5.40}$$

is satisfied. As a generalization of the results presented in Section 3.3.2, the equation states the following: The Kirchhoff integral represents an arbitrary primary sound field at the receiver position $\mathbf{x}$ as the sum of the individual spherical waves of a continuous distribution of point sources along the boundary. For the integral the stationary/dominant secondary point source position $\mathbf{x}_0^*$ is found, where its spherical wavefront's propagation direction measured at $\mathbf{x}, t$, generated at $\mathbf{x}_0^*, t - \frac{|\mathbf{x}-\mathbf{x}_0^*(\mathbf{x},t)|}{c}$ coincides with that of the primary wavefront measured on the boundary at $\mathbf{x}_0^*, t -$

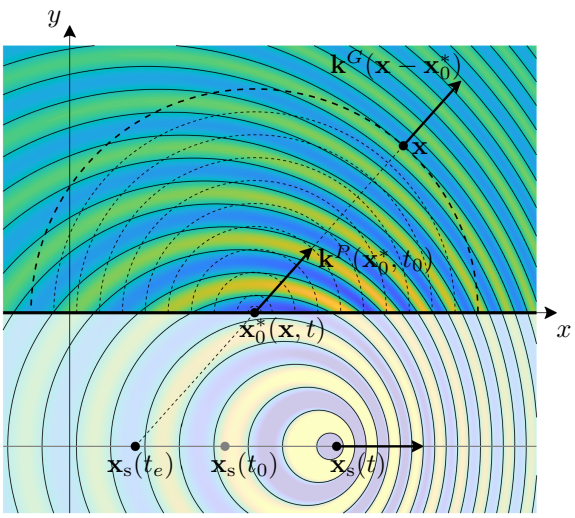

Figure 5.6. Illustration of the stationary position for the boundary integral representation of the field of a moving source. The snapshot is taken at time instant t. The source position is indicated at three time instants: at the receiver time t, the boundary emission time $t_0 = t - \frac{|\mathbf{x}-\mathbf{x}_0^*(\mathbf{x},t)|}{c}$ and the source emission time $t_e = t - \frac{|\mathbf{x}-\mathbf{x}_0^*(\mathbf{x},t)|}{c} - \tau(\mathbf{x}_0^*, t_0)$. The stationary position for $\mathbf{x}$ at time instant t is found, so that the spherical wavefront generated by the moving source at t_e coincides at $\mathbf{x}, t$ with the spherical wavefront of the stationary point source generated at t_0.

$\frac{|\mathbf{x}-\mathbf{x}_0^*(\mathbf{x},t)|}{c}$. Obviously—since after the time instant $t - \frac{|\mathbf{x}-\mathbf{x}_0^*(\mathbf{x},t)|}{c}$ the secondary and primary wavefronts „propagate together" along the common propagation direction—this requirement ensures, that the stationary boundary element's wavefront and the primary wavefront match at the receiver position $\mathbf{x}$ at the receiving time instant t, thus

$$\hat{\mathbf{k}}^P(\mathbf{x},t) = \hat{\mathbf{k}}^G(\mathbf{x}-\mathbf{x}_0^*(\mathbf{x},t)) \tag{5.41}$$

also holds.

This result is illustrated in Figure 5.6 via the example of the stationary point for the field of a moving point source. For this case the normalized local wavenumber vector is given by (5.21) and the stationary position $\mathbf{x}_0^*(\mathbf{x},t)$ is found by denoting $t_0 = t - \frac{|\mathbf{x}-\mathbf{x}_0|}{c}$ where

Time domain KI stat. point

$$\frac{\mathbf{x}_0^*(\mathbf{x},t) - \mathbf{x}_\mathrm{s}(t_0 - \tau(\mathbf{x}_0^*,t_0))}{|\mathbf{x}_0^*(\mathbf{x},t) - \mathbf{x}_\mathrm{s}(t_0 - \tau(\mathbf{x}_0^*,t_0))|} = \frac{\mathbf{x}-\mathbf{x}_0^*(\mathbf{x},t)}{|\mathbf{x}-\mathbf{x}_0^*(\mathbf{x},t)|} \tag{5.42}$$

is satisfied. This means that the stationary point is given, where the local propagation direction of the spherical wavefront generated by the moving source at $t_0 - \tau(\mathbf{x}_0^*, t_0)$, measured on the boundary at t_0 coincides with that of the spherical wavefront of the stationary point source, measured at position $\mathbf{x}$. Geometrically this point lies at the intersection of the boundary and the vector pointing from the moving point source at the emission time to the receiver position.

Having found the general stationary point for the Kirchhoff integral for a moving source the vertical integration can be approximated by the SPA. Similarly to the stationary case, choosing the plane of investigation to $\mathbf{x} = [x,\ y,\ 0]^\mathrm{T}$ implicitly fixes the vertical stationary position to lie independently from the receiver time at $z_0^*(\mathbf{x},t) \to z_0^* = 0$. Due to the definition of the stationary point for moving sources (5.42) this requirement is trivially satisfied by sound sources moving along trajectories fixed to the plane of investigation, therefore in the followings only in-plane source trajectories are considered, described by $\mathbf{x}_\mathrm{s}(t) = [x_s(t),\ y_s(t),\ 0]^\mathrm{T}$.

With the source trajectory fixed to $z_0 = 0$ and the receiver position fixed to the plane of investigation $z = 0$ the second phase derivative around the stationary point

simplifies to terms of the source-boundary and boundary-receiver point distances, reading

$$\frac{\partial^2}{\partial z_0^2}\phi^P(\mathbf{x}_0, t-\tfrac{|\mathbf{x}-\mathbf{x}_0|}{c}, \omega_0)\Big|_{z_0=z_0^*=0} = -\frac{\omega(\mathbf{x}_0,t_0)}{c}\left(\frac{1}{|\mathbf{x}_0-\mathbf{x}_\mathrm{s}(t_e)|}+\frac{1}{|\mathbf{x}-\mathbf{x}_0|}\right), \quad (5.43)$$

with $t_0 = t - \frac{|\mathbf{x}-\mathbf{x}_0|}{c}$ being the boundary emission time, $t_e = t - \frac{|\mathbf{x}-\mathbf{x}_0|}{c} - \tau(\mathbf{x}_0, t_0)$ the source emission time and $\omega(\mathbf{x}_0, t_0)$ the perceived angular frequency given by (5.19) along the boundary surface. Similarly to the stationary case (c.f. (4.11)), the second phase derivative is given by the sum of the vertical curvatures of the primary sound field and the Green's function measured on the boundary.

Finally—by taking the negative sign of (5.43) into consideration—the stationary phase approximation of integral (5.37) yields the *2.5D Kirchhoff integral for a moving source*:

Moving source 2.5D Kirchhoff approx.

$$P(\mathbf{x},t,\omega_0) = \oint_C 2w(\mathbf{x}_0,t_0)\sqrt{\frac{2\pi}{\mathrm{j}\frac{\omega(\mathbf{x}_0,t_0)}{c}}}\sqrt{\frac{|\mathbf{x}-\mathbf{x}_0|\cdot|\mathbf{x}_0-\mathbf{x}_\mathrm{s}(t_e)|}{|\mathbf{x}-\mathbf{x}_0|+|\mathbf{x}_0-\mathbf{x}_\mathrm{s}(t_e)|}}\cdot$$
$$\cdot\,\mathrm{j}k_\mathrm{n}^P(\mathbf{x}_0,t_0)\frac{1}{4\pi}\frac{P(\mathbf{x}_0,t_0,\omega_0)}{|\mathbf{x}-\mathbf{x}_0|}\,\mathrm{d}s(x_0,y_0), \quad (5.44)$$

now $\mathbf{x} = [x,\ y,\ 0]^\mathrm{T}$ and $\mathbf{x}_0 = [x_0,\ y_0,\ 0]^\mathrm{T}$ denoting in-plane positions.

5.2.3 2.5D Wave Field Synthesis of a moving point source

In order to extract the implicit driving function from the Kirchhoff integral it is exploited, that all the time variables in (5.44) are present with a constant temporal shift $t - \frac{|\mathbf{x}-\mathbf{x}_0|}{c}$. The integral therefore can be reformulated in terms of a temporal convolution with the 3D time domain Green's function as

$$P(\mathbf{x},t,\omega_0) = \oint_C \int_{t_0} 2w(\mathbf{x}_0,t_0)\sqrt{\frac{2\pi}{\mathrm{j}\frac{\omega(\mathbf{x}_0,t_0)}{c}}}\sqrt{\frac{|\mathbf{x}-\mathbf{x}_0|\cdot|\mathbf{x}_0-\mathbf{x}_\mathrm{s}(t_0-\tau(\mathbf{x}_0,t_0))|}{|\mathbf{x}-\mathbf{x}_0|+|\mathbf{x}_0-\mathbf{x}_\mathrm{s}(t_0-\tau(\mathbf{x}_0,t_0))|}}\cdot$$
$$\mathrm{j}k_\mathrm{n}^P(\mathbf{x}_0,t_0)P(\mathbf{x}_0,t_0,\omega_0)\underbrace{\frac{1}{4\pi}\frac{\delta(t-t_0-\frac{|\mathbf{x}-\mathbf{x}_0|}{c})}{|\mathbf{x}-\mathbf{x}_0|}}_{g(\mathbf{x}-\mathbf{x}_0,t-t_0)}\,\mathrm{d}t_0\,\mathrm{d}s(x_0,y_0). \quad (5.45)$$

Comparison with the time domain SFS problem (5.28) reveals that this formulation implicitly contains the time domain 2.5D WFS driving function for a harmonic moving source, being dependent on the receiver position. The dependency may be resolved by exploiting that the contour integral is dominated by its horizontal stationary point, defined by (5.42), therefore the amplitude correction factor can be substituted by its stationary value $\mathbf{x}_0 \to \mathbf{x}_0^*(\mathbf{x})$. Furthermore, the role of the stationary SSD position and the receiver position may be interchanged by letting the SSD position $\mathbf{x}_0$ to be the

independent variable. This results in SSD position dependent receiver points, termed as reference position $\mathbf{x}_0^*(\mathbf{x}) \leftrightarrow \mathbf{x}_{\mathrm{ref}}(\mathbf{x}_0)$. The extracted driving function then reads as

2.5D WFS moving source harmonic driv. fun.

$$D(\mathbf{x}_0, t_0, \omega_0) = \underbrace{\sqrt{\frac{2\pi|\mathbf{x}_{\mathrm{ref}}(\mathbf{x}_0, t_0) - \mathbf{x}_0|}{\mathrm{j}\frac{\omega(\mathbf{x}_0, t_0)}{c}}}}_{\substack{\text{SSD}\\ \text{compensation}}} \underbrace{\sqrt{\frac{|\mathbf{x}_0 - \mathbf{x}_{\mathrm{s}}(t_0 - \tau(\mathbf{x}_0, t_0))|}{|\mathbf{x}_{\mathrm{ref}}(\mathbf{x}_0, t_0) - \mathbf{x}_0| + |\mathbf{x}_0 - \mathbf{x}_{\mathrm{s}}(t_0 - \tau(\mathbf{x}_0, t_0))|}}}_{\substack{\text{virtual source}\\ \text{compensation}}} \cdot \underbrace{2w(\mathbf{x}_0, t_0)\mathrm{j}k_{\mathrm{n}}^P(\mathbf{x}_0, t_0)P(\mathbf{x}_0, t_0, \omega_0)}_{\substack{\text{2D}\\ \text{driving function}}}, \quad (5.46)$$

with $\tau(\mathbf{x}_0, t_0)$ being the propagation time delay from the moving source position at the emission time to the actual SSD position, having to be evaluated for each SSD position at each time instant. The reference position and the SSD position are connected by (5.40), reading as

$$\hat{\mathbf{k}}^P(\mathbf{x}_0, t_0) = \hat{\mathbf{k}}^G(\mathbf{x}_{\mathrm{ref}}(\mathbf{x}_0, t_0) - \mathbf{x}_0), \quad (5.47)$$

$$\frac{\mathbf{x}_0 - \mathbf{x}_{\mathrm{s}}(t_0 - \tau(\mathbf{x}_0, t_0))}{|\mathbf{x}_0 - \mathbf{x}_{\mathrm{s}}(t_0 - \tau(\mathbf{x}_0, t_0))|} = \frac{\mathbf{x}_{\mathrm{ref}}(\mathbf{x}_0, t_0) - \mathbf{x}_0}{|\mathbf{x}_{\mathrm{ref}}(\mathbf{x}_0, t_0) - \mathbf{x}_0|}. \quad (5.48)$$

The driving function above is a straightforward generalization of the 2.5D WFS driving function (4.20) towards non-stationary sound fields, consisting of the ideal 2D WFS driving function along with two dimensionality correction factors:

- The secondary source correction factor compensates for the attenuation factor and the frequency response of the 2D SSD contour. Again, the attenuation correction can be optimized to a predefined distance for each SSD element, allowing the referencing of the synthesis on a prescribed reference curve. The frequency correction term compensates for the half-integrator nature of 2D SSD, which, along with the differentiation in the driving function, would result in enhanced high-pass characteristics. As a local/asymptotic approximation the correction is performed by the instantaneous perceived angular frequency altered by the Doppler shift, as measured along the SSD.
- The virtual source correction factor corrects the synthesized field amplitude at the receiver position from a 2D to a 3D one. As it was expressed by (5.23) and (5.24)—regardless of the instantaneous spatial distribution—a 3D wavefront attenuates inversely proportional to its mean curvature along its propagation path. For the case of a moving point source the corresponding mean radius is obviously the distance from the source at the emission time and the point of investigation. Hence, the virtual source compensation factor matches the amplitude factor of the *synthesized wavefront* to the *target wavefront* (rather than the amplitude distribution) by taking the wavefront propagation dynamics into consideration.

Similarly to the stationary case, referencing the synthesis can be done by prescribing an arbitrary reference curve $\mathbf{x}_{\mathrm{ref}}$ being independent of time and expressing the SSD and virtual source compensation factors, so that the reference/stationary points for each SSD element $\mathbf{x}_{\mathrm{ref}}(\mathbf{x}_0, t_0)$ lie along the reference curve, and satisfy (5.47). Obviously, in

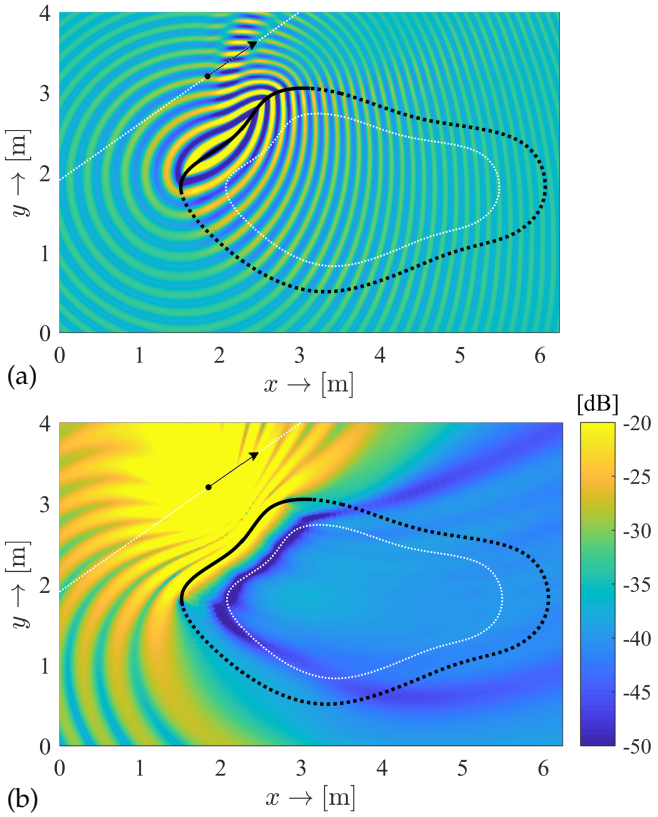

Figure 5.7. 2.5D synthesis of a moving 3D point source radiating at $f_0 = 1.5$ kHz applying an arbitrary shaped SSD. The source is under uniform motion with the source trajectory given by $\mathbf{x}_\mathrm{s} = [1.85 + v_x \cdot t,\ 3.2 + v_y \cdot t,\ 0]^\mathrm{T}$ with $|\mathbf{v}| = 150$ m/s and $v_x = 140$ m/s, $v_y = 98$ m/s. The synthesis is referenced on a concentric reference contour, denoted by white dots. The snapshot is taken at $t = 0$ s. Figure (a) depicts the real part of the synthesized field and part (b) presents the absolute error of synthesis in a logarithmic scale. The active arc of the SSD *at the time instant* $t = 0$ s is denoted by solid black line, and the inactive part with dotted by black line. In order to ensure a smooth driving function, the referencing function is extrapolated.

a general case due to the source motion the reference position for an arbitrary SSD element varies with time, thus $\mathbf{x}_\mathrm{ref}(\mathbf{x}_0, t_0)$ has to be found for each SSD element at each time instant. This requires the a-priori calculation of the moving source position at the emission time. In a Section 5.4.1 it is discussed, how these computational expensive problems can be solved numerically.

Once the source position and reference position has been found for each SSD element at each time instant, the driving function on a single source frequency component (5.46) can be evaluated. For a wideband excitation with the frequency content $S(\omega) = \int_{-\infty}^{\infty} s(t)\mathrm{e}^{-\mathrm{j}\omega t}\mathrm{d}t$, the driving function is obtained by summing the individual spectral components. The perceived frequency is expressed in terms of the source's angular frequency according to (5.19), resulting in the inverse Fourier integral

$$d(\mathbf{x}_0, t_0, \omega_0) = 2w(\mathbf{x}_0, t_0)\sqrt{\frac{\Delta(\mathbf{x}_0, t_0 - \tau(\mathbf{x}_0, t_0))}{|\mathbf{x}_\mathrm{ref}(\mathbf{x}_0, t_0) - \mathbf{x}_0| + |\mathbf{x}_0 - \mathbf{x}_\mathrm{s}(t_0 - \tau(\mathbf{x}_0, t_0))|}} \cdot \int_{-\infty}^{\infty} S(\omega_0)\sqrt{\frac{2\pi|\mathbf{x}_\mathrm{ref}(\mathbf{x}_0, t_0) - \mathbf{x}_0|}{\mathrm{j}\frac{\omega_0}{c}}}\mathrm{j}k_\mathrm{n}^P(\mathbf{x}_0, t_0)P(\mathbf{x}_0, t_0, \omega_0)\mathrm{d}\omega_0. \quad (5.49)$$

Expressing both the moving source's pressure field and its local wavenumber vector explicitly results in the expression

$$d(\mathbf{x}_0, t_0, \omega_0) = w(\mathbf{x}_0, t_0)\sqrt{\frac{|\mathbf{x}_\mathrm{ref}(\mathbf{x}_0, t_0) - \mathbf{x}_0|}{|\mathbf{x}_\mathrm{ref}(\mathbf{x}_0, t_0) - \mathbf{x}_0| + |\mathbf{x}_0 - \mathbf{x}_\mathrm{s}(t_0 - \tau(\mathbf{x}_0, t_0))|}} \cdot \langle \mathbf{x}_0 - \mathbf{x}_\mathrm{s}(t_0 - \tau(\mathbf{x}_0, t_0)) \cdot \mathbf{n}_\mathrm{in} \rangle \int_{-\infty}^{\infty} S(\omega_0)\sqrt{\frac{\mathrm{j}\frac{\omega_0}{c}}{2\pi}}\frac{\mathrm{e}^{\mathrm{j}\omega_0(t_0 - \tau(\mathbf{x}_0, t_0))}}{\Delta(\mathbf{x}_0, t_0 - \tau(\mathbf{x}_0, t_0))^{\frac{3}{2}}}\mathrm{d}\omega_0 \quad (5.50)$$

The integral can be recognized as the inverse Fourier transform of the pre-filtered source time history, taken at $t_0 - \tau(\mathbf{x}_0, t_0)$. Similarly to the stationary case the source signal is pre-equalized with a half-differentiator filter with the transfer function described by $H(\omega) = \sqrt{\mathrm{j}\omega}$, compensating for the 2D SSD contour frequency response. The time domain driving function for the synthesis of a moving point source with a wideband excitation signal reads as

2.5D WFS moving source driv. fun.

$$d(\mathbf{x}_0, t_0, \omega_0) = w(\mathbf{x}_0, t_0) \sqrt{\frac{|\mathbf{x}_{\mathrm{ref}}(\mathbf{x}_0, t_0) - \mathbf{x}_0|}{|\mathbf{x}_{\mathrm{ref}}(\mathbf{x}_0, t_0) - \mathbf{x}_0| + |\mathbf{x}_0 - \mathbf{x}_{\mathrm{s}}(t_0 - \tau(\mathbf{x}_0, t_0))|}} \cdot \langle \mathbf{x}_0 - \mathbf{x}_{\mathrm{s}}(t_0 - \tau(\mathbf{x}_0, t_0)) \cdot \mathbf{n}_{\mathrm{in}} \rangle \sqrt{\frac{1}{2\pi c}} \frac{s_t'(t_0 - \tau(\mathbf{x}_0, t_0))}{\Delta(\mathbf{x}_0, t_0 - \tau(\mathbf{x}_0, t_0))^{\frac{3}{2}}}, \quad (5.51)$$

where the prefiltered input signal is given by $s_t'(t) = h(t) *_t s(t)$, with the pre-equalization filter's impulse response given by $h(t) = \mathcal{F}_\omega^{-1}\{\sqrt{\mathrm{j}\omega}\}$. Note that unlike for the stationary case, here the order of pre-filtering and delaying of the excitation signal is not interchangeable due to the time-dependent propagation time delay.

The driving function is capable of the synthesis of a source under motion, with an arbitrary source trajectory and velocity profile applying an arbitrary SSD contour, with ensuring optimized synthesis on an arbitrary shaped reference contour. The synthesis in such a general scenario is depicted in Figure 5.7, illustrating the reproduction of a source, moving along a straight trajectory. In this case the parametrization of the SSD contour and the reference contour is available, along with an analytically known source trajectory, closed form analytical driving function may be expressed, as discussed in the following example.

Application example: Synthesis of a uniformly moving source applying a linear SSD

As a simple example the reproduction of a point source under uniform motion is investigated, applying a linear SSD and optimizing the synthesis on a reference line. The importance of the example lies in the fact that for this geometry the analytical explicit solution is also known—presented in the following section—allowing the direct comparison of the implicit and explicit methodologies for this non-stationary scenario.

For the sake of simplicity the source is chosen to move uniformly along the x-axis with a trajectory given by $\mathbf{x}_{\mathrm{s}} = [x_s + v \cdot t,\ y_s,\ 0]^{\mathrm{T}}$, oscillating at the angular frequency ω_0. The infinite linear SSD is located at $\mathbf{x}_0 = [x_0,\ 0,\ 0]^{\mathrm{T}}$ and the reference line is set to $\mathbf{x}_{\mathrm{ref}} = [x,\ y_{\mathrm{ref}},\ 0]^{\mathrm{T}}$. For this geometry the windowing function is identically $w(\mathbf{x}, t_0) \equiv 1$ and the driving function from (5.46) reads as

$$D(\mathbf{x}_0, t_0, \omega_0) = \sqrt{\frac{8\pi}{\mathrm{j}\frac{\omega_0}{c}}} \cdot \sqrt{\frac{|\mathbf{x}_{\mathrm{ref}}(\mathbf{x}_0, t_0) - \mathbf{x}_0| \cdot \Delta(t_0 - \tau(\mathbf{x}_0, t_0))}{|\mathbf{x}_{\mathrm{ref}}(\mathbf{x}_0, t_0) - \mathbf{x}_0| + |\mathbf{x}_0 - \mathbf{x}_{\mathrm{s}}(t_0 - \tau(\mathbf{x}_0, t_0))|}} \mathrm{j} k_y^P(\mathbf{x}_0, t_0) P(\mathbf{x}_0, t_0, \omega_0). \quad (5.52)$$

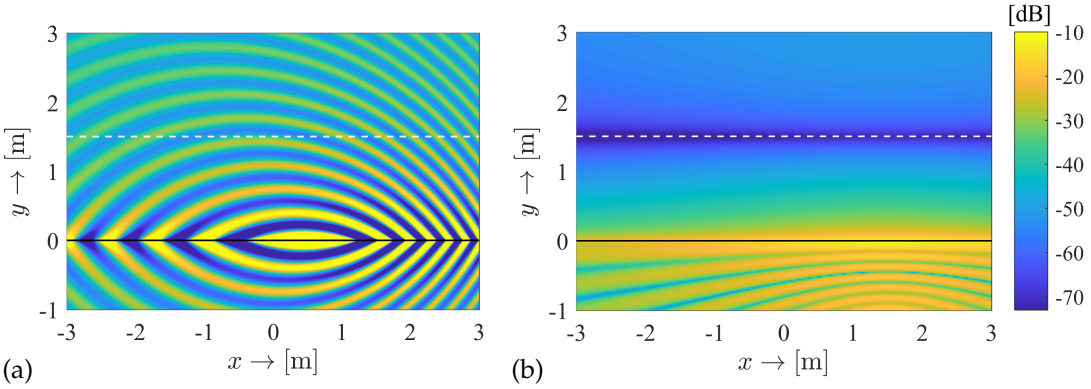

Figure 5.8. 2.5D synthesis of a moving 3D point source located at $\mathbf{x}_\mathrm{s}(t) = [1.5 + v \cdot t,\ -2,\ 0]^\mathrm{T}$ with $v = \frac{3}{4}c$, radiating at $f_0 = 1$ kHz with the reference line set at $y_\mathrm{ref} = 1.5$ m. Figure (a) depicts the real part of the synthesized field, (b) shows the error of synthesis.

The reference distance $|\mathbf{x}_\mathrm{ref}(\mathbf{x}_0, t_0) - \mathbf{x}_0|$ can be expressed by the definition of the stationary position (5.47) written merely for the y-coordinates

$$|\mathbf{x}_\mathrm{ref}(\mathbf{x}_0, t_0) - \mathbf{x}_0| = -\frac{y_\mathrm{ref}}{y_s(t_0 - \tau(\mathbf{x}_0, t_0))} |\mathbf{x}_0 - \mathbf{x}_\mathrm{s}(t_0 - \tau(\mathbf{x}_0, t_0))|. \tag{5.53}$$

Finally expressing the radiated field and its local wavenumber vector explicitly and exploiting that y_s is constant yields the driving function

$$D(\mathbf{x}_0, t_0, \omega_0) = -\sqrt{\frac{\mathrm{j}k_0}{2\pi}} \sqrt{\frac{y_\mathrm{ref}}{y_\mathrm{ref} - y_s}} y_s \frac{\mathrm{e}^{\mathrm{j}\omega_0(t_0 - \tau(\mathbf{x}_0, t_0))}}{\Delta(\mathbf{x}_0, t_0)^{\frac{3}{2}}}, \tag{5.54}$$

with the propagation time delay and the attenuation factor given by (5.11) and (5.12) respectively. The time domain driving function for a source excitation time history $s(t)$ is given by the inverse Fourier transform of (5.54) with respect to ω_0, reading

$$d(\mathbf{x}_0, t_0) = -\sqrt{\frac{1}{2\pi c}} \sqrt{\frac{y_\mathrm{ref}}{y_\mathrm{ref} - y_s}} y_s \frac{s_t'(t_0 - \tau(\mathbf{x}_0, t_0))}{\Delta(\mathbf{x}_0, t_0)^{\frac{3}{2}}}, \tag{5.55}$$

where $s_t'(t) = h(t) *_t s(t)$, with $h(t) = \mathcal{F}_\omega^{-1}\{\sqrt{\mathrm{j}\omega}\}$.

The result of synthesis is illustrated in Figure 5.8, verifying that the presented driving function optimizes the synthesis along the reference line. Comparison with (4.25) reveals that the moving source driving function formally coincides with the traditional WFS driving function given for a stationary point source [Ver97, (2.27)], [Sta97, (3.16)&(3.17)] with the stationary distances, delays and amplitude factor changed for the corresponding dynamic variables.

The above driving function can be easily extended for sources moving inclined to the SSD the driving function with the substitution of a space-time dependent source position $y_s \rightarrow y_s(t_0 - \tau(\mathbf{x}_0, t_0))$ as discussed in details in [FF16b]. In this case, however, the moving source crosses the theoretically infinite SSD resulting in singular driving function at the time instant of the crossing, and converging virtual wavefronts afterwards. The synthesis of this type of focused moving sources is not investigated in the present thesis.

5.3 Explicit solution for the synthesis of moving sources

So far only the time domain and a mixed time-frequency domain representations of moving sources were discussed, applied directly for WFS of sources under motion. For the special case of sources under uniform motion the frequency domain and wavenumber domain representations of the radiated sound field can be expressed analytically, by applying the Fourier theorem for a non-stationary convolution.

5.3.1 Spectral representation of moving sources

Assume a harmonic source moving along a straight trajectory parallel with the x-axis (i.e. the source position time history is given by $\mathbf{x}_\mathrm{s}(t) = [x_s + v \cdot t,\ 0,\ 0]^\mathrm{T}$), radiating with a wide-band excitation time history $s(t)$. According to (5.3) the radiated field can be written in the form of a convolution with the kernel being the moving source Green's function

$$p_\mathrm{m}(\mathbf{x}, t) = \int_{t_\mathrm{e}} g_\mathrm{m}(x - x_s - v \cdot t_\mathrm{e}, y, z, t - t_\mathrm{e}) s(t_\mathrm{e}) \mathrm{d}t_\mathrm{e}, \tag{5.56}$$

with t_e being the emission time and g_m representing the retarded Green's function. Comparison with (F.1) reveals that the radiated field is written in terms of a non-stationary convolution, for which the spectral representation is known, given by (F.10). By applying the Fourier shift theorem (by a factor of $x - x_s$) and the scaling theorem (by v) to (F.10) the spectrum of the radiated field is given by

$$P_\mathrm{m}(\mathbf{x}, \omega) = \frac{1}{v} \int_{-\infty}^{\infty} S(\omega_0) \tilde{G}(\frac{\omega - \omega_0}{v}, y, z, \omega) \mathrm{e}^{-\mathrm{j}\frac{\omega-\omega_0}{v}(x-x_s)} \mathrm{d}\omega_0. \tag{5.57}$$

Hence, the radiated field in the spectral domain is obtained by a non-stationary

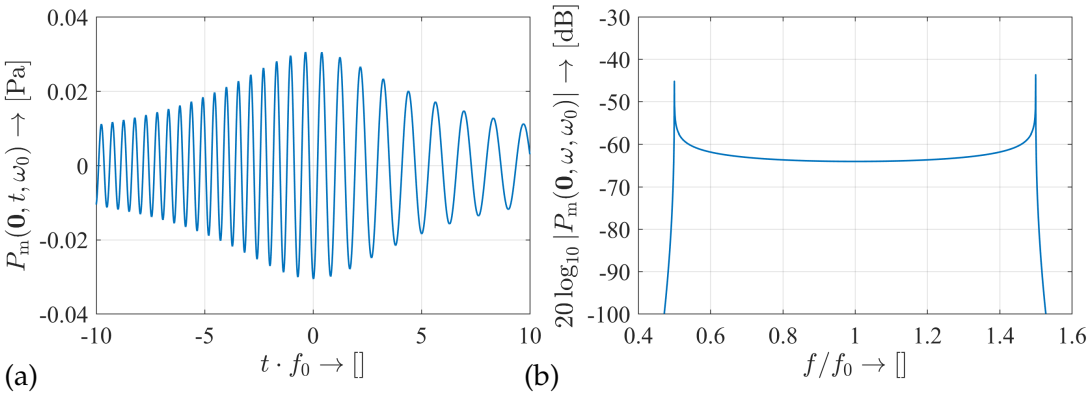

Figure 5.9. The time history and spectrum of a moving source pass-by, moving on a trajectory $\mathbf{x}_\mathrm{s}(t) = [v \cdot t,\ -2,\ 0]^\mathrm{T}$ with $v = \frac{c}{2}$, measured at the origin. Both, the time history and spectrum are normalized by the source frequency. The spectrum is described by the Hankel function as given by (5.58). The poles/singularities of the spectrum are the *dominant frequencies* of the approaching ($t \rightarrow -\infty$) and the diverging ($t \rightarrow \infty$), given by (5.19) as $\omega_d = \omega_0 \frac{1}{1 \pm M}$, with $M = \frac{v}{c}$ being the Mach number.

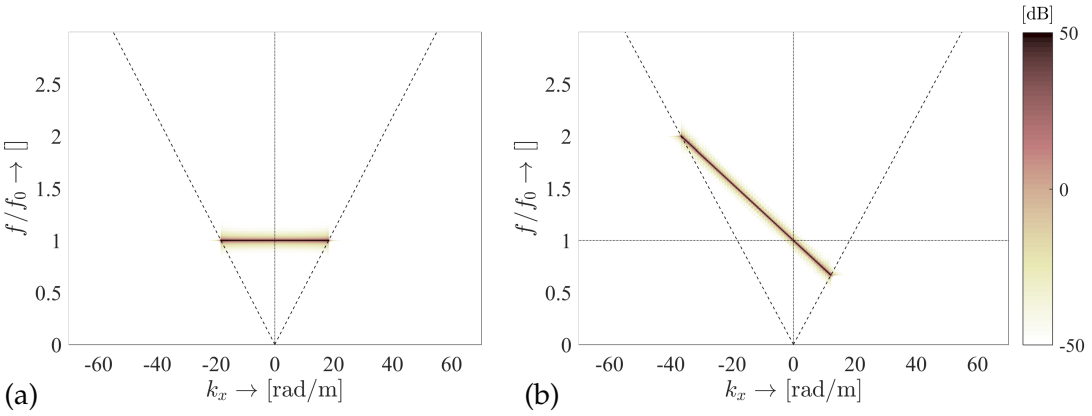

Figure 5.10. Spectrum of a stationary (a) and moving (b) harmonic source in the $k_x - \omega$ domain. In the dynamic case the source is moving with a constant velocity, $v = \frac{c}{2}$.

convolution as well. Since integration is performed over the frequency content of the source input signal $S(\omega_0)$, the weighting kernel can be recognized as the frequency content of a moving source pass-by, radiating at a single frequency component ω_0. The field of a harmonic moving source is therefore given by

$$P_{\mathrm{m}}(\mathbf{x}, \omega, \omega_0) = \frac{1}{v} \tilde{G}(\frac{\omega - \omega_0}{v}, y, z, \omega) \mathrm{e}^{-\mathrm{j}\frac{\omega-\omega_0}{v}(x-x_s)}, \tag{5.58}$$

Moving source in $\mathbf{x} - \omega$ domain

with the Green's function's wavenumber content given in Table 2.1 as

$$\tilde{G}(\frac{\omega - \omega_0}{v}, y, z, \omega) = -\frac{\mathrm{j}}{4} H_0^{(2)} \left(\sqrt{\left(\frac{\omega}{c}\right)^2 - \left(\frac{\omega - \omega_0}{v}\right)^2} y \right). \tag{5.59}$$

The equation states that the frequency domain representation of a moving point source pass-by at a given receiver point is completely described by its 1D spatio temporal spectrum $\tilde{G}(k_x, y, z, \omega)$ with the substitution $k_x \rightarrow \frac{\omega-\omega_0}{v}$. This is the immediate consequence of the fact that in the present geometry the time history of the measured pass-by is invariant along the x-axis up to a constant time delay. The time history of a uniformly moving source pass-by and the corresponding angular spectrum is illustrated in Figure 5.9.

Due to the spatio-temporal invariance of the spectrum (5.58) along the x-dimension, the spatial Fourier transform is straightforward, yielding

$$\tilde{P}_{\mathrm{m}}(k_x, y, z, \omega, \omega_0) = \frac{2\pi}{v} \tilde{G}(\frac{\omega - \omega_0}{v}, y, z, \omega) \mathrm{e}^{\mathrm{j}\frac{\omega-\omega_0}{v}x_s} \delta(k_x - \frac{\omega - \omega_0}{v}). \tag{5.60}$$

Moving source in $k_x - z$ domain

The angular spectrum representation (i.e. $k_x - y - k_z$ representation) is given as

$$\tilde{P}_{\mathrm{m}}(k_x, y, k_z, \omega, \omega_0) = \frac{2\pi}{v} \tilde{G}(\frac{\omega - \omega_0}{v}, y, k_z, \omega) \mathrm{e}^{\mathrm{j}\frac{\omega-\omega_0}{v}x_s} \delta(k_x - \frac{\omega - \omega_0}{v}). \tag{5.61}$$

Moving source in $k_x - k_z$ domain

Note that the representation does not pose any constraint on the actual form of the Green's function, the above equations theoretically describe the field of an arbitrary source under uniform motion.

The spectral $k_x - \omega$ domain representation of a moving source field is depicted in Figure 5.10 (b), allowing the comparison with a stationary source. In both cases the amplitude distribution of the spectra are described by the wavenumber content of the Green's function, $\tilde{G}(k_x, y, z, \omega)$. It is illustrated that bringing a sound source into uniform motion will result in the rotation of its spectrum around $k_x = 0$ and rescaling in order to fill the propagation region. The amount of rotation is given directly by the source velocity (the angle of rotation is $\frac{\pi}{2} \cdot \frac{v}{c}$).

The above spectral formulations can be extended for sources moving inclined to the x-axis, as given in Appendix G.1. These formulations may be applied for deriving implicit and explicit driving functions for virtual sources moving uniformly along arbitrary directed straight trajectories, as it is discussed in details in [FF15a]. Since, however, the previous section presented a more general methodology for the reproduction of sources under arbitrary motion, it is sufficient to restrict the investigation of the explicit SFS methodology for sources moving parallel with the x-axis, resulting in closed form analytic formulations.

5.3.2 3D Spectral Division Method for moving sources

The spectral representations given in the foregoing allows the derivation of explicit SFS driving function for the synthesis of moving sources. The following driving functions are specialized to the case of sources under uniform motion, reproduced by planar and linear SSDs in contrary to WFS, allowing the reproduction of moving sources in a general geometry. Still, the importance of the explicit solution is that it constitutes a reference solution for the synthesis problem, and allows the investigation of aliasing artifacts in the followings.

Assuming an infinite planar distribution of secondary sources along the plane $\mathbf{x}_0 = [x_0,\ 0,\ z_0]^{\mathrm{T}}$, the explicit driving function in the $k_x - k_z$ domain is given by the angular spectrum representation of the field generated by a moving source (5.61) substituted into the general 3D explicit driving function (4.38)

$$D(k_x, k_z, \omega) = \frac{2\pi}{v} \frac{\tilde{G}(\frac{\omega-\omega_0}{v}, y - y_s, k_z, \omega)}{\tilde{G}(k_x, y, k_z, \omega)} \mathrm{e}^{\mathrm{j}\frac{\omega-\omega_0}{v}x_s} \delta(k_x - \frac{\omega - \omega_0}{v}), \tag{5.62}$$

with $k_y = \sqrt{(\frac{\omega}{c})^2 - k_x^2 - k_z^2}$. The spatial driving function is obtained from the double inverse Fourier transform of the wavenumber domain driving function. Integration along k_x can be evaluated analytically, with the Dirac delta sifting out $k_x = \frac{\omega-\omega_0}{v}$. Hence, in the spatial domain the driving function takes the form

$$D(x_0, z_0, \omega) = \frac{1}{2\pi} \int_{-\infty}^{\infty} \frac{1}{v} \frac{\tilde{G}(\frac{\omega-\omega_0}{v}, y - y_s, k_z, \omega)}{\tilde{G}(\frac{\omega-\omega_0}{v}, y, k_z, \omega)} \mathrm{e}^{-\mathrm{j}\frac{\omega-\omega_0}{v}(x_0 - x_s)} \mathrm{e}^{-\mathrm{j}k_z z_0} \mathrm{d}k_z. \tag{5.63}$$

Substituting the explicit formula for the 3D Green's function's angular spectrum representation, as given in Table 2.1 allows simplification by $\sqrt{(\frac{\omega}{c})^2 - (\frac{\omega-\omega_0}{v})^2 - k_z^2}$

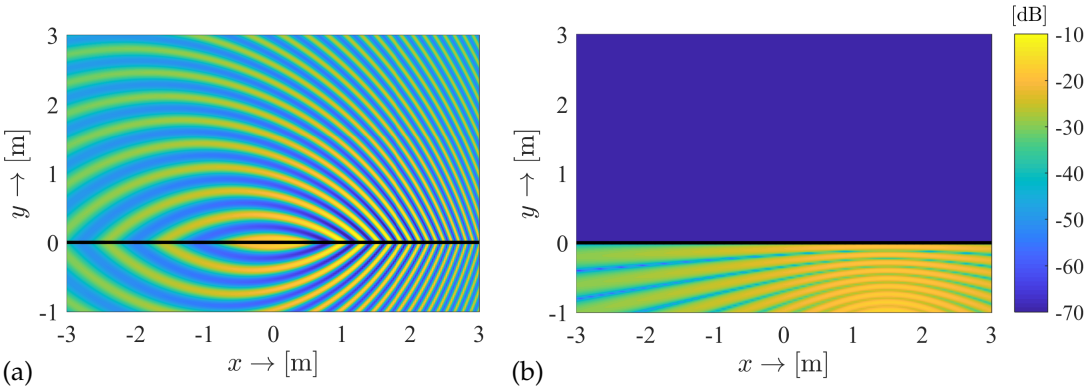

Figure 5.11. Synthesis of a moving virtual point source using a planar SSD applying the SDM driving function. The SSD is located at $\mathbf{x}_0 = [x_0,\ 0,\ z_0]^{\mathrm{T}}$ denoted by solid black line. The virtual source is located at $\mathbf{x}_{\mathrm{s}}(t) = [1.5 + v \cdot t,\ -2,\ 0]^{\mathrm{T}}$ with $v = \frac{3}{4}c$, oscillating at $f_0 = 1$ khz. The figures depict the real part of the synthesized field (a) and the deviation from the target sound field (b) measured at $z = 0$.

and division of the exponentials, making the driving function independent from the y-coordinate.

$$D(x_0, z_0, \omega) = \frac{1}{2\pi} \int_{-\infty}^{\infty} \frac{1}{v} \frac{\underbrace{\mathrm{e}^{-\mathrm{j}\sqrt{\left(\frac{\omega}{c}\right)^2 - \left(\frac{\omega-\omega_0}{v}\right)^2 - k_z^2}\,|y_s|}}}{-2\frac{\partial}{\partial y}\frac{\mathrm{e}^{-\mathrm{j}\sqrt{\left(\frac{\omega}{c}\right)^2 - \left(\frac{\omega-\omega_0}{v}\right)^2 - k_z^2}\,|y-y_s|}}{-\mathrm{j}\sqrt{\left(\frac{\omega}{c}\right)^2 - \left(\frac{\omega-\omega_0}{v}\right)^2 - k_z^2}}\Bigg|_{y=0}} \mathrm{e}^{-\mathrm{j}k_z z_0}\,\mathrm{d}k_z \mathrm{e}^{-\mathrm{j}\frac{\omega-\omega_0}{v}(x_0 - x_s)}. \tag{5.64}$$

The integrand can be recognized as a multiple of the y-derivative of the Green's function, taken on the SSD (cf. Table 2.1).

Hence, evaluating the integration with respect to k_z results in the frequency domain explicit driving function

$$D(x_0, z_0, \omega, \omega_0) = -\frac{2}{v}\frac{\partial}{\partial y}\tilde{G}\left(\frac{\omega - \omega_0}{v}, y - y_s, z_0, \omega\right)\Big|_{y=0} \mathrm{e}^{-\mathrm{j}\frac{\omega-\omega_0}{v}(x_0 - x_s)}. \tag{5.65}$$

This formulation describes the y-derivative of the field of a moving point source. From the mixed time-frequency formulation this can be expressed as

$$D(x_0, z_0, t, \omega_0) = -\frac{1}{2\pi}\frac{y_s}{\Delta(\mathbf{x}_0, t_0)}\left(\frac{1 - M^2}{\Delta(\mathbf{x}_0, t_0)} + \mathrm{j}k_0\right)\frac{\mathrm{e}^{\mathrm{j}\omega_0(t_0 - \tau(\mathbf{x}_0, t_0))}}{\Delta(\mathbf{x}_0, t_0)}, \tag{5.66}$$

3D SDM driv. fun.

with $\tau(\mathbf{x}_0, t_0)$ and $\Delta(\mathbf{x}_0, t_0)$ given by (5.11) and (5.12), respectively.

The result of synthesis applying the above driving function is depicted in Figure 5.11, verifying that applying an infinite planar SSD perfect synthesis can be achieved in front of the SSD. Obviously, the explicit driving function coincides with the implicit solution for the same SSD geometry, without applying the high frequency gradient approximation.

5.3.3 2.5D Spectral Division Method for moving sources

Applying the wavenumber domain formulation of the field generated by a uniformly moving source the explicit driving function for an infinite linear SSD may be obtained. As discussed in the foregoing, the application of a linear SSD allows the synthesis of a source distribution located at the plane of the SSD and the reference line, hence in the following the investigation is fixed to the plane of synthesis at $z = 0$.

As the simplest case the virtual source moves parallel to the SSD, with the source position given as $\mathbf{x}_\mathrm{s}(t) = [v \cdot t,\ y_s,\ 0]^\mathrm{T}$, with $y_s < 0$, oscillating at ω_0. The SSD is a linear set of 3D point sources, located along $\mathbf{x}_0 = [x_0,\ 0,\ 0]^\mathrm{T}$. The general 2.5D explicit driving function for a linear SSD is given by (4.45), with in the present case the required wavenumber content of the virtual field is given by (5.60). By applying this formulation the wavenumber domain driving function, optimizing the synthesis on a line, parallel with the SSD is expressed as

$$\tilde{D}(k_x, \omega, \omega_0) = \frac{2\pi}{v} \frac{\tilde{G}(\frac{\omega-\omega_0}{v}, y_\mathrm{ref} - y_s, 0, \omega)}{\tilde{G}(k_x, y_\mathrm{ref}, 0, \omega)} \delta(k_x - \frac{\omega - \omega_0}{v})\, \mathrm{e}^{\mathrm{j}\frac{\omega-\omega_0}{v}x_s}, \tag{5.67}$$

with y_ref being the y-position of the reference line. The spatial representation of the driving function is obtained by a spatial inverse Fourier transform of the above expression. Unlike in the stationary case, due to the spatial invariancy of the virtual source field (up to a phase shift) the inverse transform may be evaluated analytically by exploiting the Dirac delta sifting property, resulting in

$$D(x_0, \omega, \omega_0) = \frac{1}{v} \frac{\tilde{G}(\frac{\omega-\omega_0}{v}, y_\mathrm{ref} - y_s, 0, \omega)}{\tilde{G}(\frac{\omega-\omega_0}{v}, y_\mathrm{ref}, 0, \omega)} \mathrm{e}^{-\mathrm{j}\frac{\omega-\omega_0}{v}(x_0 - x_s)}. \tag{5.68}$$

Expressing $\tilde{G}(k_x, y, z = 0, \omega)$ explicitly yields the final 2.5D SDM driving function

2.5D SDM driving function

$$D(x_0, \omega, \omega_0) = \frac{1}{v} \frac{H_0^{(2)}\left(\sqrt{\left(\frac{\omega}{c}\right)^2 - \left(\frac{\omega-\omega_0}{v}\right)^2}\,|y_\mathrm{ref} - y_s|\right)}{H_0^{(2)}\left(\sqrt{\left(\frac{\omega}{c}\right)^2 - \left(\frac{\omega-\omega_0}{v}\right)^2}\,|y_\mathrm{ref}|\right)} \mathrm{e}^{-\mathrm{j}\frac{\omega-\omega_0}{v}(x_0 - x_s)}. \tag{5.69}$$

For a moving source with wide-band excitation signal $s(t)$ the explicit driving function reads as

$$D(x_0, \omega) = \frac{1}{2\pi v} \int_\infty^\infty S(\omega_0) \frac{H_0^{(2)}\left(\sqrt{\left(\frac{\omega}{c}\right)^2 - \left(\frac{\omega-\omega_0}{v}\right)^2}\,|y_\mathrm{ref} - y_s|\right)}{H_0^{(2)}\left(\sqrt{\left(\frac{\omega}{c}\right)^2 - \left(\frac{\omega-\omega_0}{v}\right)^2}\,|y_\mathrm{ref}|\right)} \mathrm{e}^{-\mathrm{j}\frac{\omega-\omega_0}{v}(x_0 - x_s)} \mathrm{d}\omega_0, \tag{5.70}$$

where $S(\omega) = \int_{-\infty}^{\infty} s(t)\mathrm{e}^{-\mathrm{j}\omega t}\mathrm{d}t$ is the temporal spectrum of the source excitation.

The result of synthesis applying the explicit driving function in case of a harmonic moving source is depicted in (5.12). It is verified that the explicit method theoretically ensures perfect synthesis along the reference line, therefore it may serve as a reference solution.

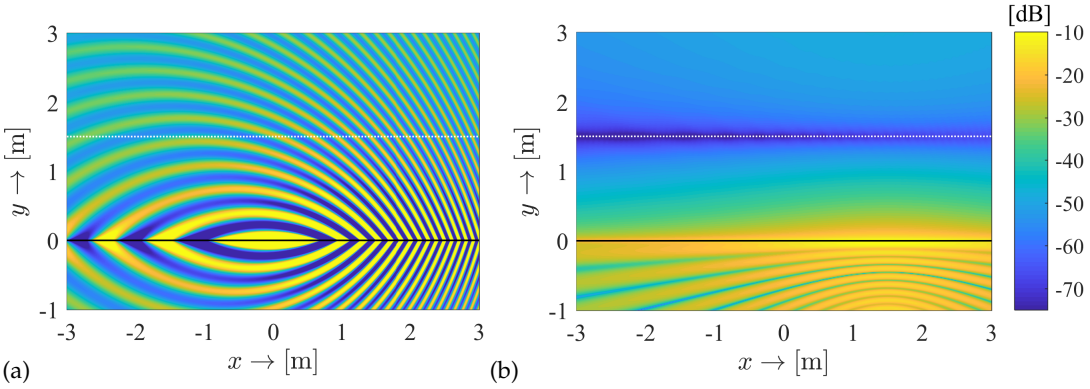

Figure 5.12. Synthesis of a uniformly moving virtual point source employing a linear SSD applying the 2.5D SDM driving function. The SSD is located at $\mathbf{x}_0 = [x_0,\ 0,\ 0]^{\mathrm{T}}$, denoted by a solid black line. The virtual source is located at $\mathbf{x}_{\mathrm{s}}(t) = [v \cdot t + 1.5,\ -2,\ 0]^{\mathrm{T}}$ with $v = \frac{3}{4}c$ oscillating at $f_0 = 1$ kHz. The reference line was set to $y_{\mathrm{ref}} = 1.5$ m. The figure depicts the synthesized field at the synthesis plane ($z = 0$) with (a) depicting the real part of the synthesized field, (b) depicting the error of synthesis.

Assuming high frequency conditions the Hankel function can be approximated by its asymptotic expansion as given by (3.53). Applying the formulation the spectral division can be carried out analytically, resulting in the approximate driving function

$$D(x_0, \omega, \omega_0) = \frac{1}{v}\sqrt{\frac{y_{\mathrm{ref}}}{y_{\mathrm{ref}} - y_s}}\,\mathrm{e}^{-\mathrm{j}\sqrt{\left(\frac{\omega}{c}\right)^2 - \left(\frac{\omega-\omega_0}{v}\right)^2}\,|y_s|}\,\mathrm{e}^{-\mathrm{j}\frac{\omega-\omega_0}{v}(x_0 - x_s)}. \tag{5.71}$$

Approximate 2.5D SDM driv. fun.

This formulation coincides with the implicit Wave Field Synthesis driving function for a moving source, derived entirely in the spectral domain: the frequency domain representation of a moving source (5.58) allows an alternative derivation of the 2.5D WFS driving function by applying the stationary phase approximation entirely in the frequency domain. The approach—described in details in [FF15a]—is not discussed here further, since it is superseded by the time domain WFS formulation introduced in the foregoing in Section 5.2. The coincidence of the driving functions, however indicates that Wave Field Synthesis is a high frequency/wavefront matching approximation of the explicit solution, proven for a general stationary sound field in the previous chapter.

5.4 Practical aspects of the synthesis of moving sources

So far the theoretical foundations of physically correct synthesis of source movements were discussed. The practical implementation of the foregoing raises numerous questions. The definition of several quantities, present in the driving function and assumed to be a-priori known is not straightforward. Furthermore, the choice of the SSD shape, the applied referencing scheme and the applied anti-aliasing strategy is crucial in the aspect of synthesizing dynamic sound scenes. The following final

subsection presents several practical considerations and solutions for the challenges, arising for the special case of synthesizing a moving point source, following [FF18b].

5.4.1 Calculation of source trajectory

Direct implementation of the moving source driving function (5.46) assumes that the time dependence of the source position $\mathbf{x}_\mathrm{s}(t)$ is known a-priori. This is an optimistic assumption in the aspect of practical applicability. Instead, more often a parametric curve $\mathbf{y}(u)$ is given, which the virtual source follows with a pre-defined velocity profile. This requirement can be formulated as finding a reparameterization, so that

$$\mathbf{y}(u(t)) = \mathbf{x}_\mathrm{s}(t), \qquad \left|\frac{\mathrm{d}\mathbf{x}_\mathrm{s}(t)}{\mathrm{d}t}\right| = |\mathbf{v}_\mathrm{s}(t)| \tag{5.72}$$

holds. The goal is to find the explicit parametrization $u(t)$ so that substitution into (5.72) yields the desired source position vector.

Differentiation of (5.72) with respect to time and application of the chain rule, for $\mathrm{d}u/\mathrm{d}t$ results in

$$\frac{\mathrm{d}u(t)}{\mathrm{d}t} = \frac{|\mathbf{v}_\mathrm{s}(t)|}{|\mathrm{d}\mathbf{y}(u(t))/\mathrm{d}u|}. \tag{5.73}$$

In order to express $u(t)$ both sides are multiplied by $\mathrm{d}t$, and according the first fundamental theorem of calculus taking the definite integral leads to

$$u(t) = \int_{t_0}^{t} \frac{|\mathbf{v}_\mathrm{s}(s)|}{|\mathrm{d}\mathbf{y}(u(s))/\mathrm{d}u|}\mathrm{d}s, \tag{5.74}$$

with t_0 being a user-defined initial time. Note that for sources moving with constant velocity ($|\mathbf{v}_\mathrm{s}(s)| = v$) the parametrization is referred to as reparametrization to arc-length.

For an arbitrary trajectory and velocity profile the parametrization (5.74) can be evaluated only numerically. A detailed discussion on the frequently used numerical methods can be found in [Par12]. As a simplest approach, the integral may be approximated numerically with the forward-Euler method, approximating the integral with the iteration scheme

Approximate source trajectory

$$u_{i+1} = u_i + \mathrm{d}t\frac{|\mathbf{v}_\mathrm{s}(u_i)|}{|\mathrm{d}\mathbf{y}(u_i)/\mathrm{d}u|}, \qquad i \geq 0, \tag{5.75}$$

where $\mathrm{d}t = \frac{1}{fs}$ is the sampling period of the source trajectory. Once the parametrization u_i is found, the required source trajectory vector at the time instant t_i can be obtained from $\mathbf{x}_\mathrm{s}(t_i) = \mathbf{y}(u_i)$.

5.4.2 Calculation of propagation time delay

Having found the source trajectory the implementation of the driving function would still require the knowledge of the propagation time delay, i.e. the time it takes for the wavefront to travel from the source position at the emission time to the receiver

position at the receiving time. This requires the solution of the quadratic equation (5.8) for each SSD element at each time instant, which makes real-time implementation infeasible.

The computational complexity may be considerably decreased by implementing a further Euler iteration scheme, i.e. by approximating $\tau(\mathbf{x}, t)$ by its first order Taylor series

$$\tau(\mathbf{x}, t + \mathrm{d}t) \approx \tau(\mathbf{x}, t) + \mathrm{d}t \frac{\mathrm{d}\tau(\mathbf{x}, t)}{\mathrm{d}t}. \tag{5.76}$$

The temporal derivative of τ can be obtained from the implicit derivation of its definition (5.8), reading as

$$\frac{\mathrm{d}\tau(\mathbf{x}, t)}{\mathrm{d}t} = \tau'(\mathbf{x}, t) = \frac{-\frac{1}{c}\left\langle \mathbf{v}_\mathrm{s}(t-\tau) \cdot (\mathbf{x} - \mathbf{x}_\mathrm{s}(t-\tau)) \right\rangle}{|\mathbf{x} - \mathbf{x}_\mathrm{s}(t)|}. \tag{5.77}$$

τ derivative

Hence the iteration scheme at the time instant t_i becomes

$$\tau(\mathbf{x}, t_i) = \tau(\mathbf{x}, t_{i-1}) + \mathrm{d}t \cdot \tau'(\mathbf{x}, t_{i-1}), \tag{5.78}$$

τ iteration scheme

with $\mathrm{d}t = \frac{1}{f_s}$ being the sampling period of the driving function [FF17b]. Obviously, when only numerically available, $\mathbf{x}_\mathrm{s}(t-\tau)$ may be interpolated from the trajectory vector, from which the source velocity $\mathbf{v}_\mathrm{s}(t-\tau)$ may be calculated by differentiating it numerically with respect to time.

It is important to note that the sampling frequency for the calculation of the source trajectory and propagation time delay may be chosen significantly lower than the actual source driving signal's sampling frequency. As a result computational cost can be decreased, besides still ensuring numerical stability.

5.4.3 Effects of the SSD discretization

Description of spatial aliasing

In the followings the effects of the SSD discretization is discussed in case of synthesizing a moving source, extending the anti-aliasing strategy presented in Section 4.4 to non-stationary sound fields.

The effects of the SSD discretization is illustrated in Figure 5.13 in case of a moving source with a harmonic (a) and wideband (b) excitation signal. Similarly to the stationary case, above a certain frequency the resultant field of the secondary sources does not form a smooth wavefront, but the individual wavefronts of the secondary sources will be present in the synthesized field creating an interference pattern. In the time domain spatial aliasing manifests in spherical wavefronts of the individual secondary sources, following the intended virtual wavefront. These secondary waveefronts are high-pass filtered to the spatial aliasing frequency.

In case of a moving point source the local perceived frequency is altered by the Doppler effect, having a strong influence on spatial aliasing artifacts. Those SSD positions, where the perceived frequency is locally increased (i.e. in front of the moving source) contribute dominantly to aliasing, while behind the virtual source

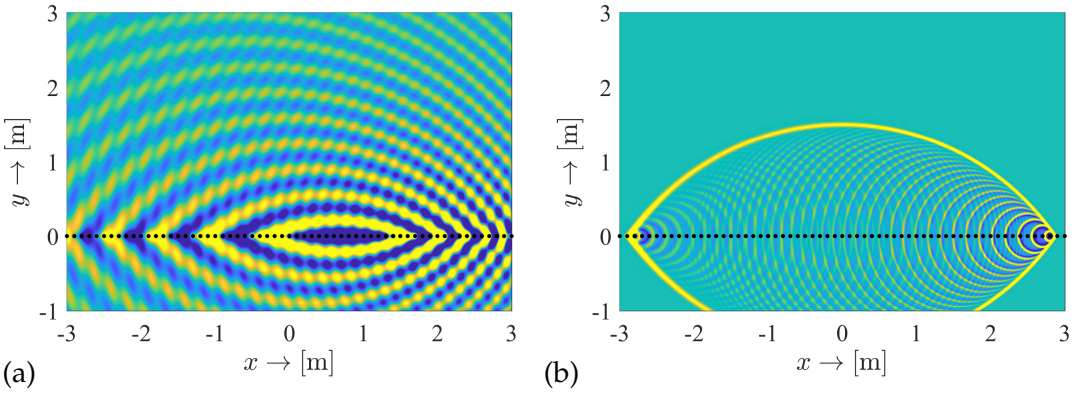

Figure 5.13. 2.5D synthesis of a moving 3D point source located at $\mathbf{x}_\mathrm{s} = [v \cdot t + 1.5,\ -2,\ 0]^\mathrm{T}$ with $v = \frac{c}{2}$, radiating at $f_0 = 1$ kHz (a), or emitting an impulse, bandlimited to 15 kHz (b). The screenshot is taken at $t = 0$. The synthesis is referenced on a reference line with $y_\mathrm{ref} = 1.5$ m. Synthesis is performed using a linear SSD with the secondary source spacing set to $\Delta x = 10$ cm.

aliasing waves are less emphasized. This can be examined in Figure 5.13 (a), where in case of a moving harmonic source aliasing waves originate from in front of the moving source, radiating laterally backwards at the angular frequency of the local perceived frequency measured at the aliasing SSD element. This, however, means that aliasing waves arrive to a given receiver point with a frequency, differing from the virtual source's local perceived frequency. In the time domain this means that aliasing wavefronts arriving to a given receiver position following the virtual wavefront suffer a different Doppler shift than the intended wavefront. This is illustrated in Figure 5.13 (b). As a result spatial aliasing artifacts are extremely enhanced, compared to the stationary case: while for the stationary case aliasing results only in the coloration of the synthesized field, for the dynamic case undesired frequency components will be also present in the synthesized sound, that can be clearly audible in case of high virtual source velocities.

The following section discusses the analysis and mitigation of spatial aliasing artifacts are discussed. Again, it is exploited that WFS constitutes a high frequency approximation for the explicit solution, the latter allowing the analytical description of spatial aliasing. Hence, the effects of discretization is introduced via the example of synthesis applying a linear SSD with a known explicit solution, which is generalized towards arbitrary SSDs in the following.

Assume the synthesis of a moving source applying a discrete, linear SSD, located at $\mathbf{x}_0 = [x_0,\ 0,\ 0]^\mathrm{T}$ with the loudspeaker spacing being Δx. The source moves uniformly along a straight trajectory, parallel to the SSD. Again, the effect of the SSD discretization can be described as the sampling of the ideal, continuous driving function, resulting in the repetition of the driving function spectra on the multiples of the sampling wavenumber. According to (4.67) the synthesized field reads as

$$\tilde{P}(k_x, y, z, \omega) = \frac{1}{\Delta x} \sum_{\eta=-\infty}^{\infty} \tilde{D}\left(k_x - \eta \frac{2\pi}{\Delta x}, \omega\right) \cdot \tilde{G}(k_x, y, z, \omega), \tag{5.79}$$

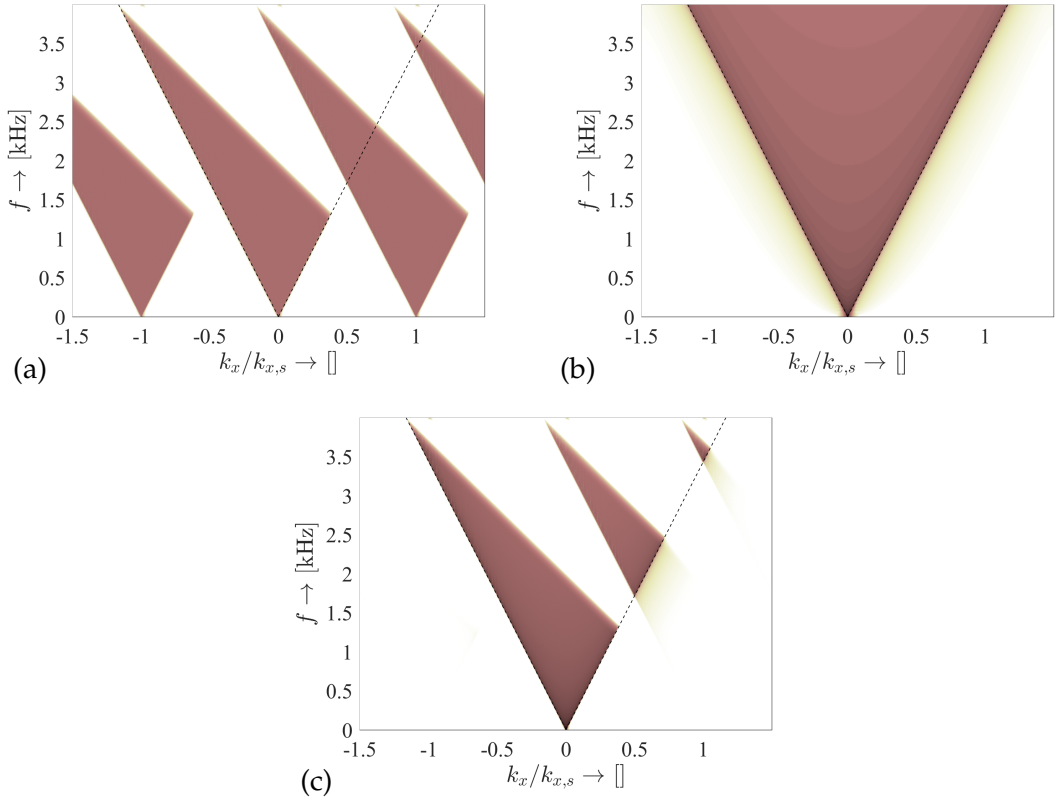

Figure 5.14. Illustration of the aliased synthesis of a moving virtual point source, located at $\mathbf{x}_\mathrm{s}(t) = [v \cdot t + 1.5,\ -2,\ 0]^\mathrm{T}$, emitting an impulse, bandlimited to 2 kHz. Figure (a) shows the spectrum of the discretized moving source driving function with overlapping spectral repetition. Figure (b) shows the spectrum of the 3D Green's function and Figure (c) shows the spectrum of the synthesized field, both measured along the reference line.

where the driving function spectrum is given by (5.67) for the special case of a harmonic source signal. For a wideband excitation the driving function is obtained as the spectral integral of the harmonic driving function, weighted by the source excitation frequency content. The process of the synthesis of a moving source with wide-band excitation applying a discrete SSD is illustrated in the wavenumber domain in Figure 5.14.

Again, the spectrum of the driving function is obtained by the rotation and rescaling of the stationary driving function spectrum. It is illustrated by 5.14 (a) that due to the local increase of perceived angular frequency in front of the moving source the mirror spectra are more likely to alias: in the current example in front of the moving source even a second order aliasing component is present ($\eta = 2$ component is present in the baseband propagation region), while behind the source due to the local decrease of the perceived frequency, no aliasing component is present at all (i.e. from these parts of the SSD no aliasing echoes originate).

Also it is clear from the spectral representation that aliasing components are present in the radiated wavefield with a reversed k_x sign, thus aliasing waves emerging from secondary sources in front of the moving virtual source will propagate backwards, opposed to the source motion direction. As a direct consequence in a fixed receiver position strong frequency distortion may occur, that has been reported and investigated in numerous previous studies [Fra+07; Ahr12]. The phenomenon is illustrated

(a)

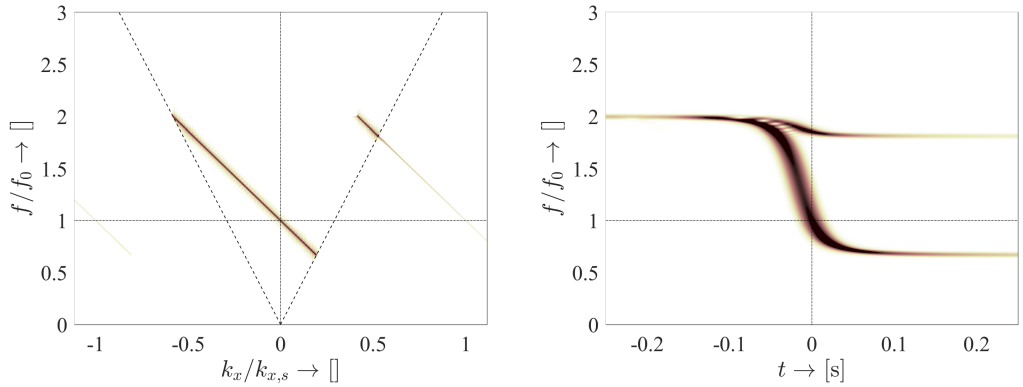

Figure 5.15. Wavenumber-frequency representation of the synthesized field of a harmonic moving source, applying a linear SSD (a) and the corresponding spectogram (b). The source is located at $\mathbf{x}_\mathrm{s} = [v \cdot t,\ -2,\ 0]^\mathrm{T}$ with $v = \frac{c}{2}$, radiating at $f_0 = 1\mathrm{kHz}$. The spectrum of the synthesized field is measured along the reference line, set to $y_\mathrm{ref} = 1.5\ \mathrm{m}$, while the spectogram of the pass-by is measured at $x = 0\ \mathrm{m}$, on the reference line.

via the example of a harmonic source excitation in Figure 5.15, depicting the spectral representation of the synthesis scenario, presented in Figure 5.14 (a). As a result of the SSD discretization after the virtual source pass-by aliasing waves are present in a given receiver position, propagating laterally backwards, with the frequency determined by the measured frequency at the aliasing SSD positions. Hence, besides the ideal perceived frequency, after the virtual source pass-by an undesired frequency component is also present in the synthesized field. With increasing source frequency (or at larger SSD sampling distance) also higher order aliasing components are present in the radiated field, resulting in multiple undesired frequency components. Furthermore, in the case when the perceived frequency behind the virtual source gets above the aliasing frequency, undesired frequency components are present before the virtual source pass-by.

For the special case of a harmonic moving source the frequency content of the synthesized field can be expressed analytically. Substituting the 2.5D SDM driving function (5.67) into (5.79), taking its spatial inverse Fourier transform and exploiting the sifting property of the Dirac-delta in order to evaluate the Fourier integral results in

$$P(x,y,z,\omega) = D(x,\omega,\omega_0) \sum_{\eta=-\infty}^{\infty} \tilde{G}\left(\frac{\omega-\omega_0}{v} + \eta\frac{2\pi}{\Delta x}, y, z, \omega\right) \mathrm{e}^{-\mathrm{j}\eta\frac{2\pi}{\Delta x}x}. \tag{5.80}$$

Obviously, $\eta = 0$ yields the unaltered, ideal synthesized field without aliasing. This formulation allows the analytical description of the undesired frequency components, stemming from the poles of the translated Green's function $\tilde{G}(\frac{\omega-\omega_0}{v} + \eta\frac{2\pi}{\Delta x}, y, z, \omega)$. As the poles are found where $|\frac{\omega-\omega_0}{v} + \eta\frac{2\pi}{\Delta x}| = |\frac{v}{c}| = |M|$ holds, therefore the actual frequency of the aliasing waves before and after the virtual source pass-by is given by

$$\omega = \frac{1}{1 \pm M}\left(\omega_0 + \eta\frac{2\pi v}{\Delta x}\right), \tag{5.81}$$

with for $\eta > 0$ taking the lower, for $\eta < 0$ taking the higher frequency into consideration. A more detailed treatise on these undesired frequency components can be found in [FF16a].

Avoiding spectral overlapping

The above description highlighted that spatial aliasing may result in clearly audible, serious artifacts due the different Doppler-shifts between the intended and the aliasing wavefronts. Hence, proper anti-aliasing strategy is crucial in the aspect of synthesizing moving sources. As a first step, the proper choice of the SSD shape is an important question: the strong contribution of undesired frequency components is the result of the theoretically infinite, linear SSD, with high contribution of lateral waves. In the aspect of avoiding aliasing a smooth, enclosing SSD shape should be chosen, at which the virtual wavefront arrives dominantly with a normal local propagation direction. The optimal choice, fulfilling this requirement (and due to further reasons, explained in the following) for an arbitrary source trajectory, is applying a circular SSD.

In order to avoid further aliasing artifacts the same anti-aliasing filtering strategy may be applied, as given for a stationary virtual field in Section 4.4. From investigating Figure 5.14 it is clear that by spatial bandlimiting the linear driving function to the Nyquist wavenumber $k_{x,\mathrm{Nyq}} = \frac{\pi}{\Delta x}$ i.e. as long as

$$\tilde{D}(k_x, \omega) = 0, \quad \text{for} \quad |k_x| > \frac{\pi}{\Delta x} \tag{5.82}$$

holds, the spectral overlapping after discretization could be entirely avoided. Similarly to the stationary case—as a generalization towards time variant sound field—, the spectrum of the linear driving function at a given wavenumber component k_x and at a given frequency ω is dominated by that part of the SSD, where $k_x^P(\mathbf{x}_0, t) = k_x$ and $\omega(\mathbf{x}_0, t) = \omega$ is satisfied, with $\omega(\mathbf{x}_0, t)$ being the perceived, Doppler shifted angular frequency. Since the two quantities are connected through (5.20), in the spatial domain the anti-aliasing condition can be formulated as

$$D(x_0, \omega) = 0, \quad \text{for} \quad k_x^P(\mathbf{x}_0, t_0) = \frac{\omega(\mathbf{x}_0, t_0)}{c} \cdot |\hat{k}_x^P(\mathbf{x}_0, t_0)| > \frac{\pi}{\Delta x}, \tag{5.83}$$

where $\hat{k}_x^P(\mathbf{x}_0, t_0)$ is the x-component of the normalized local wavenumber vector. Finally, within the validity of the Kirchhoff approximation an arbitrary smooth SSD can be considered locally linear. In this case the above anti-aliasing criterion holds, with the role of k_x^P interchanged to the tangential wavenumber component k_t^P, resulting in

$$D(\mathbf{x}_0, \omega) = 0, \quad \text{for} \quad \omega(\mathbf{x}_0, t_0) > \frac{\pi}{\Delta x} \frac{c}{|\hat{k}_t^P(\mathbf{x}_0, t_0)|}. \tag{5.84}$$

According to (5.21), for a moving source the normalized local wavenumber vector is a unit vector pointing into the receiver position from the source position at the emission

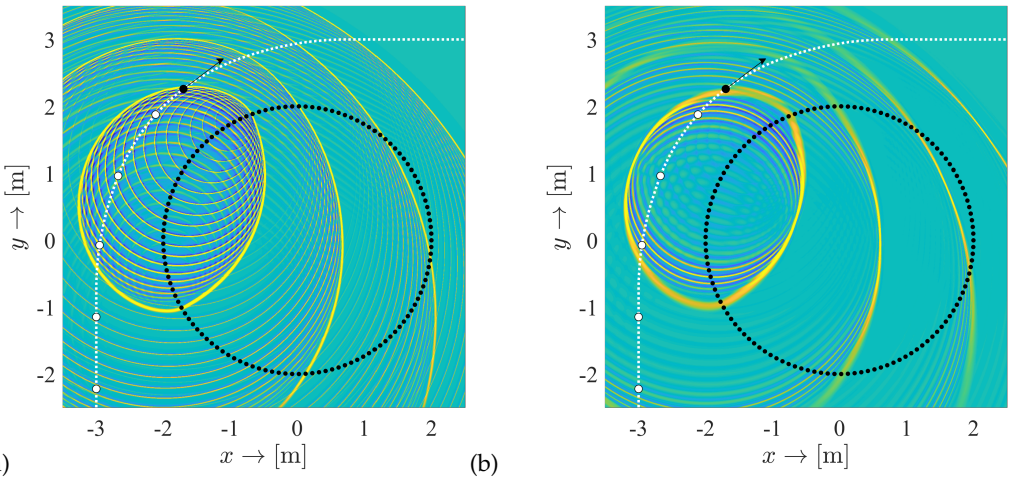

Figure 5.16. Synthesis of a moving source on an arbitrary trajectory, applying a circular SSD, with the radius of $R_{\mathrm{SSD}} = 2$ m, sampled at $\Delta x = 10$ cm. The source, traveling with a constant velocity of $|\mathbf{v}| = \frac{3}{4}c$. Figure (a) shows the effects of source discretization with clearly visible aliasing echoes with the strongest contribution emerging from front of the virtual source, where the local perceived frequency is increased by the Doppler effect. Figure (b) shows the effect of ideal anti-aliasing filtering. Time variant low-pass filtering of the driving function below the instantaneous cut-off frequency (5.85) is performed in the short-time Fourier transform domain with properly chosen window and hop sizes. The white dots on the trajectory denote the source position at the time instant, when the impulses were emitted.

time. Denoting the tangent vector of the secondary sources by $\mathbf{t}(\mathbf{x}_0)$ this leads to the final anti-aliasing condition for a moving point source:

Moving source anti-aliasing condition

$$D(\mathbf{x}_0, \omega) = 0, \quad \text{for} \quad \omega(\mathbf{x}_0, t_0) > \frac{\pi c}{\Delta x} \frac{|\mathbf{x}_0 - \mathbf{x}_\mathrm{s}(t_0 - \tau(\mathbf{x}_0, t_0))|}{|\langle \mathbf{x}_0 - \mathbf{x}_\mathrm{s}(t_0 - \tau(\mathbf{x}_0, t_0)) \cdot \mathbf{t}(\mathbf{x}_0) \rangle|}. \tag{5.85}$$

This means that anti-aliasing requires the implementation of a time variant low-pass filter with the cut-off frequency given above.

As in the stationary case, full-band synthesis is achieved only on those parts of the synthesized field, for which the stationary SSD element's normal vector coincides with the local propagation direction of the virtual field. At that position the denominator in 5.85 is zero, and the cut-off frequency $\omega(\mathbf{x}_0, t_0) = \infty$.

For the special case of a circular SSD the normal vector is always pointing towards the center of the array. Hence, due to the geometry at the center of the SSD the existence of a nearly full-band stationary SSD element is inherently ensured. This is again an important advantage of applying circular loudspeaker arrays. Terminology nearly full-band synthesis refers to the fact that due to the discretization of the SSD, full-band synthesis is only possible when at the stationary SSD position an actual SSD element is located. In practice when the moving source is located between two actual secondary sources even at the center of the array the synthesized field is slightly bandlimited (depending on the distance of the virtual source from the SSD), which may cause audible artifacts if the source is close to the SSD.

The result of the proposed anti-aliasing approach with applying a circular SSD is illustrated in Figure 5.16. In the simulation the source is traveling along an arbitrary trajectory defined by a discrete set of points, with the trajectory and the propagation

time delay calculated iteratively, as it was discussed in the previous subsections. The simulation results verify the nearly full-band synthesis in the center of the secondary array.

5.4.4 Choosing the referencing scheme

In practical applications the evaluation of the 2.5D WFS driving function, given by (5.51) requires the definition of a reference position $\mathbf{x}_{\mathrm{ref}}(\mathbf{x}_0, t_0)$ for each SSD element at each time instant. In case of a moving source, for general referencing curves with arbitrary shaped SSDs this point is found at the intersection of a straight line—connecting the actual SSD element $\mathbf{x}_0$ with the corresponding source position at the emission time $\mathbf{x}_{\mathrm{s}}(t_0 - \tau(\mathbf{x}_0, t_0))$—and a polyline, defining the reference curve. Obviously, the direct solution for the reference position is of great computational cost, making real-time applications infeasible, therefore geometries with analytical solutions are preferred. As a possible solution specific reference curve shapes may be used for which the analytical solution for the reference position is available. As an example, in case of circular SSDs the choice of a concentric circle for the reference curve may be feasible, for which geometry the intersection of a parametric line and a circle is well-known [Ebe03, Ch.7.3.2]. However, as a result amplitude correct synthesis at a given time instant is ensured only over an arc, for which part of the reference curve a stationary SSD element exist.

Alternatively, as the simplest solution, synthesis may be optimized to a given reference point $\mathbf{x}_{\mathrm{ref}}$ independently from the actual SSD position, e.g. to the center of the SSD in case of a circular secondary ensemble. Since ideal anti-aliasing can also be achieved only at a given listening position, this simple choice may be feasible in the aspect of practical implementation.

Furthermore, amplitude correct synthesis may be achieved over those parts of the reference curve, for which a stationary SSD element can be found, depending on the virtual source position. As the simplest referencing strategy in case of a circular geometry, amplitude correct synthesis may be achieved at the center of the secondary array independently on the virtual source trajectory.

6 Conclusion

The present thesis discussed a unified Wave Field Synthesis theory, giving an asymptotic, ray-tracing solution for the general sound field synthesis problems. As the central result of the present treatise, general 2.5 dimensional WFS loudspeaker driving function was introduced, allowing the synthesis of arbitrary virtual sound fields by applying arbitrary shaped SSD contours, with ensuring an optimal synthesis along a prescribed reference curve.

The central concept of the presented results is the stationary phase method, yielding an asymptotic approximation of integral formulas. Adapted from classic ray-tracing theory, the local wavenumber vector and the local wavefront curvature were introduced, as local attributes of sound fields. These quantities allow a simple, elegant physical interpretation of asymptotic evaluation of integrals, describing radiation problems: it was demonstrated via numerous examples, how boundary integrals and spatial Fourier transforms can be evaluated around their stationary points, and how the stationary points for these problems can be found in a simple geometric manner. All the involved concepts give a fair approximation for radiation problems under high frequency conditions.

By applying the introduced local wavenumber concept it was demonstrated that the stationary phase approximation of boundary integrals, with the integral kernel being the Green's function, basically realizes a wavefront matching between the target field and the surface point sources, regarding both propagation direction and wavefront curvature. For a contour of secondary source elements this wavefront matching is possible in amplitude only at a single receiver point per secondary source element. The ensemble of these individual reference positions form the reference curve, whose shape can be controlled with a simple amplitude term in the boundary integral kernel. From the stationary phase evaluation of the Kirchhoff approximation the unified 2.5D Wave Field Synthesis driving function was extracted, inherently containing the above referencing concept. The introduced generalized theoretical framework contains previous WFS approaches as special cases, as it was demonstrated via examples.

Alternatively to WFS an explicit solution exists for the general sound field synthesis scenario, solving the problem by mode-matching in the spectral domain. For an infinite linear secondary source distribution the approach yields the driving function in the form of a spectral integral, while for enclosing arrays (e.g. circular, spherical distributions) the solution is an infinite spectral sum. By applying the stationary phase

approximation for the evaluation of the explicit spectral driving function for a linear SSD, a novel, purely spatial domain explicit driving function was introduced: the new driving function requires the description of the target sound field measured along the reference curve, opposed to the WFS solution, which requires the target field properties on the secondary source array. It was verified that this new solution also realizes the wavefront matching of the target wavefront and the secondary sources' wavefronts of a prescribed reference curve. Hence, the global mode-matching solution can be transformed into a local wavefront matching approach under high frequency conditions. This solution may be generalized towards the synthesis with arbitrary shaped secondary source distributions, as long as the loudspeaker array can be considered locally linear. Finally it was also demonstrated that the explicit spatial driving function is equivalent with the unified WFS solution.

The presented equivalence of the spatial explicit and implicit solutions can be exploited in order to discuss phenomena concerning WFS in a unified manner. As an example, the effects of the secondary source discretization—modeling real-life loudspeaker arrays— can be analytically described in the wavenumber domain, by using the explicit solution. By utilizing the introduced local wavenumber concept a simple anti-aliasing strategy, that can be realized by simple low-pass filtering of the driving signals was presented, in order to avoid the resulting aliasing wavefronts. As a result anti-aliased synthesis may be achieved along certain directions over the listening region.

Finally, as a complex application example for the foregoing, the synthesis of a moving point source was discussed within the context of the introduced unified WFS framework. In this case the proper reproduction of the Doppler effect is of central importance, which is inherently ensured once an appropriate analytical model is applied. It was presented how the local attributes of wavefronts can be extended for moving sources and it was demonstrated how the introduced WFS framework can be adapted to this dynamic scenario. For the special case of sources under uniform motion the explicit driving function was introduced in the wavenumber and in the spatial domain for 3D synthesis, applying a planar SSD and for 2.5D synthesis, applying a linear SSD. Similarly to the stationary case, the explicit driving function was found to coincide with the WFS solution under high frequency assumptions. Based on the wavenumber domain representation the effects of secondary source discretization was discussed, and the anti-aliasing strategy introduced for stationary fields was extended for the synthesis of moving sources.

An aim of the present thesis was to give a complete, self-contained discussion on the questions, concerning Wave Field Synthesis. However, several aspects were out of the scope of the present treatise. As the most important example only diverging fields were discussed, i.e. the target wavefronts would originate from a sound source, outside of the listening region. Under several restrictions Wave Field Synthesis is capable of synthesizing focused sources, in which case the synthesized wavefront converges towards a focal point inside the listening area. The synthesis of such converging sound fields needs the proper manipulation of the stationary phase approximation. Although hints were given, how to adapt the unified framework to focused sources,

the exact study of this focused case—even involving focused moving sources— is the subject of future work.

Appendices

Appendix A

A

A.1 Definition and properties of Fourier transform and the Dirac delta

Temporal Fourier transform:

Given a four dimensional function $f(\mathbf{x}, t)$, depending on both time and the spatial position. The forward and inverse temporal Fourier transform, leading to the angular frequency domain, is defined as

$$F(\mathbf{x}, \omega) = \mathcal{F}_t \{f(\mathbf{x}, t)\} = \int_{-\infty}^{\infty} f(\mathbf{x}, t) \mathrm{e}^{-\mathrm{j}\omega t} \mathrm{d}t, \tag{A.1}$$

$$f(\mathbf{x}, t) = \mathcal{F}_\omega^{-1} \{F(\mathbf{x}, \omega)\} = \frac{1}{2\pi} \int_{-\infty}^{\infty} F(\mathbf{x}, \omega) \mathrm{e}^{\mathrm{j}\omega t} \mathrm{d}\omega. \tag{A.2}$$

Note that capital letter indicates that the function is taken in the angular frequency domain.

Spatial Fourier transforms:

Following the convention, given in e.g. [Ahr12] the spatial Fourier transform, leading to the wavenumber domain, is defined as follows:

- in one dimension:

$$\tilde{F}(k_x, y, z, \omega) = \mathcal{F}_x \{F(\mathbf{x}, \omega)\} = \int_{-\infty}^{\infty} F(\mathbf{x}, \omega) \, \mathrm{e}^{\mathrm{j}k_x x} \, \mathrm{d}x, \tag{A.3}$$

$$F(\mathbf{x}, \omega) = \mathcal{F}_{k_x}^{-1} \left\{ \hat{F}(k_x, y, z, \omega) \right\} = \frac{1}{2\pi} \int_{-\infty}^{\infty} \tilde{F}(k_x, y, z, \omega) \, \mathrm{e}^{-\mathrm{j}k_x x} \mathrm{d}k_x, \tag{A.4}$$

- in two dimensions:

$$\tilde{F}(k_x, y, k_z, \omega) = \iint_{-\infty}^{\infty} F(\mathbf{x}, \omega) \mathrm{e}^{\mathrm{j}(k_x x + k_z z)} \mathrm{d}x \, \mathrm{d}z, \tag{A.5}$$

$$F(\mathbf{x}, \omega) = \frac{1}{(2\pi)^2} \iint_{-\infty}^{\infty} \tilde{F}(k_x, y, k_z, \omega) \, \mathrm{e}^{-\mathrm{j}(k_x x + k_z z)} \mathrm{d}k_x \, \mathrm{d}k_z, \tag{A.6}$$

- in three dimensions:

$$\tilde{F}(\mathbf{k},\omega) = \iiint_{-\infty}^{\infty} F(\mathbf{x},\omega)\mathrm{e}^{\mathrm{j}\langle\mathbf{k}\cdot\mathbf{x}\rangle}\mathrm{d}x\,\mathrm{d}y\,\mathrm{d}z, \tag{A.7}$$

$$F(\mathbf{x},\omega) = \frac{1}{(2\pi)^3}\iiint_{-\infty}^{\infty} \tilde{F}(\mathbf{k},\omega)\mathrm{e}^{-\mathrm{j}\langle\mathbf{k}\cdot\mathbf{x}\rangle}\mathrm{d}k_x\,\mathrm{d}k_y\,\mathrm{d}k_z. \tag{A.8}$$

Hence, hat over the function symbol indicates that the function is taken in the wavenumber domain. Note that the exponent of the spatial Fourier transform is taken with a reversed sign, compared to the temporal transform. Writing an arbitrary function in the form of a spatio-temporal inverse Fourier transform

$$f(\mathbf{x},t) = \frac{1}{(2\pi)^4}\iiiint_{-\infty}^{\infty} \hat{F}(\mathbf{k},\omega)\mathrm{e}^{\mathrm{j}(\omega t-\langle\mathbf{k}\cdot\mathbf{x}\rangle)}\mathrm{d}k_x\,\mathrm{d}k_y\,\mathrm{d}k_z\mathrm{d}\omega \tag{A.9}$$

basically describes the expansion of an arbitrary function into the linear combination of plane waves, propagating to direction $\mathbf{k}$. The reversed sign therefore ensures that this simple physical interpretation can be assigned to the Fourier transform.

Fourier transform properties:

Several important properties of the Fourier transform, applied frequently in the present thesis are the following.

- Shift theorem:

$$\int_{-\infty}^{\infty} f(x-x_0)\mathrm{e}^{\mathrm{j}k_x x}\mathrm{d}x = \mathcal{F}_x\left\{f(x-x_0)\right\} = \hat{F}(k_x)\mathrm{e}^{\mathrm{j}k_x x_0}. \tag{A.10}$$

  In case of temporal Fourier transform the right side is with reversed exponent.

- Convolution theorem:

$$\int_{-\infty}^{\infty} f(x-x_0)g(x_0)\mathrm{d}x_0\,\mathrm{e}^{\mathrm{j}k_x x}\mathrm{d}x = \mathcal{F}_x\left\{f(x)*_x g(x)\right\} = \hat{F}(k_x)\cdot\hat{G}(k_x). \tag{A.11}$$

- Differentiation property:

$$\int_{-\infty}^{\infty} \frac{\partial}{\partial x}f(x)\mathrm{e}^{\mathrm{j}k_x x} = \mathcal{F}_x\left\{\frac{\partial}{\partial x}f(x)\right\} = -\mathrm{j}k_x\hat{F}(k_x). \tag{A.12}$$

  In case of temporal Fourier transform the right side is with reversed sign.

- Scaling property:

$$\int_{-\infty}^{\infty} f(ax)\mathrm{e}^{\mathrm{j}k_x x} = \mathcal{F}_x\left\{f(ax)\right\} = \frac{1}{|a|}\hat{F}(\frac{k_x}{a}). \tag{A.13}$$

  In case of temporal Fourier transform the right side is with reversed sign.

Properties of Dirac delta:

The Dirac delta is a generalized function (or distribution) applied frequently in modeling acoustic phenomena, defined as

$$\delta(x) = \begin{cases} \infty, & x = 0 \\ 0, & x \neq 0 \end{cases}, \qquad \text{with} \qquad \int_{-\infty}^{\infty} \delta(x)\mathrm{d}x = 1. \tag{A.14}$$

Several important properties of the Dirac delta, applied frequently in the present thesis are the following.

- Forward Fourier transform:

$$\mathcal{F}_x\left\{\delta(x - x_0)\right\} = \int_{-\infty}^{\infty} \delta(x - x_0)\mathrm{e}^{\mathrm{j}k_x x}\mathrm{d}x = \mathrm{e}^{\mathrm{j}k_x x_0}. \tag{A.15}$$

- Inverse Fourier transform:

$$\delta(x - x_0) = \frac{1}{2\pi}\int_{-\infty}^{\infty} \mathrm{e}^{-\mathrm{j}k_x(x-x_0)}\mathrm{d}k_x = \mathcal{F}_{k_x}^{-1}\left\{\mathrm{e}^{\mathrm{j}k_x x_0}\right\}. \tag{A.16}$$

- Sifting property:

$$\int_{-\infty}^{\infty} \delta(x - x_0)f(x)\mathrm{d}x = f(x_0). \tag{A.17}$$

- Generalized sifting property:

$$\int_{-\infty}^{\infty} f(x)\delta(g(x))\mathrm{d}x = \sum_i \frac{f(x_i)}{\left|\frac{\partial}{\partial x}g(x)\right|_{x=x_i}}, \qquad \text{where} \quad g(x_i) = 0. \tag{A.18}$$

Appendix B

B

B.1 Notes on the Hessian of the phase function

B.1.1 Definition of the principal curvatures and principal directions

Assume a wavefield, described by the general polar form $P(\mathbf{x},\omega) = A^P(\mathbf{x},\omega)\mathrm{e}^{\mathrm{j}\phi^P(\mathbf{x},\omega)}$. Supposing that the amplitude changes slowly compared to the phase function, the local dispersion relation $|\nabla\phi(\mathbf{x},\omega)| = \frac{\omega}{c} = k$ holds and the equation describing an arbitrary wavefront, i.e. $\phi^P(\mathbf{x},\omega) - C = 0$ is the *normalform* of the given surface [Har99; Har01]. The Hessian matrix of the function is given by the symmetric matrix

$$\mathbf{H}^P(\mathbf{x}) = \frac{\partial^2}{\partial x_i \partial x_j}\phi^P(\mathbf{x},\omega) = \begin{bmatrix} \phi^{P\prime\prime}_{xx}(\mathbf{x},\omega) & \phi^{P\prime\prime}_{xy}(\mathbf{x},\omega) & \phi^{P\prime\prime}_{xz}(\mathbf{x},\omega) \\ \phi^{P\prime\prime}_{xy}(\mathbf{x},\omega) & \phi^{P\prime\prime}_{yy}(\mathbf{x},\omega) & \phi^{P\prime\prime}_{yz}(\mathbf{x},\omega) \\ \phi^{P\prime\prime}_{xz}(\mathbf{x},\omega) & \phi^{P\prime\prime}_{yz}(\mathbf{x},\omega) & \phi^{P\prime\prime}_{zz}(\mathbf{x},\omega) \end{bmatrix}, \quad i,j = 1,2,3. \tag{B.1}$$

with the eigenvalues $\lambda_1, \lambda_2, \lambda_3$ and the corresponding eigenvectors $\mathbf{v}_1, \mathbf{v}_2, \mathbf{v}_3$. Since the function under consideration is a normalform, therefore the following properties hold

- $\lambda_3 = 0$ with the eigenvector $\mathbf{v}_3 = -\frac{1}{k}\nabla\phi^P(\mathbf{x},\omega) = \hat{\mathbf{k}}^P(\mathbf{x})$, i.e. being the normal of the wavefront
- $\lambda_1 = -k \cdot \kappa_1^P(\mathbf{x})$ and $\lambda_2 = -k \cdot \kappa_2^P(\mathbf{x})$ are proportional to the *main or principal curvatures* of the wavefront, where $\rho_1^P(\mathbf{x}) = \frac{1}{\kappa_1^P(\mathbf{x})}$ and $\rho_2^P(\mathbf{x}) = \frac{1}{\kappa_2^P(\mathbf{x})}$ are the *principal radii*. The principal curvatures and radii are defined as the following: Consider all the planes containing the normal of the surface at the point of investigation, defined by the surface normal and vector $\mathbf{v}$, being the tangent of the surface. The curvature is defined as the quadratic form

$$\kappa = \mathbf{v}^{\mathrm{T}}\mathbf{H}^P\mathbf{v}. \tag{B.2}$$

  The main curvatures are then defined as the minimum and maximum values of curvature, i.e. the reciprocal of the osculating circles' radii (the principal radii). The corresponding eigenvectors $\mathbf{v}_1$ and $\mathbf{v}_2$ are the tangential, orthogonal unit

vectors pointing into the direction of the maximal and minimal curvatures. For an illustration refer to Figure 3.2.

Finally, as the general case the Hessian matrix of an arbitrary wavefront can be written in terms of the principal curvatures and the corresponding eigenvectors as

$$\mathbf{H}^P = -k\left(\kappa_1 \mathbf{v}_1 \mathbf{v}_1^{\mathrm{T}} + \kappa_2 \mathbf{v}_2 \mathbf{v}_2^{\mathrm{T}}\right) = -k\mathbf{V}\mathbf{K}\mathbf{V}^{\mathrm{T}}, \tag{B.3}$$

where $\mathbf{V} = \begin{bmatrix}\mathbf{v}_1 & \mathbf{v}_2\end{bmatrix}$ and $\mathbf{K} = \begin{bmatrix}\kappa_1 & 0 \\ 0 & \kappa_2\end{bmatrix}$ are the matrices of the eigenvectors and the curvatures.

For the special case of the three-dimensional Green's function positioned at the origin, the Hessian matrix is given as

$$\mathbf{H}^G(\mathbf{x}) = -\frac{k}{|\mathbf{x}|}\begin{bmatrix}\left(1-\frac{x^2}{|\mathbf{x}|^2}\right) & \frac{xy}{|\mathbf{x}|^2} & \frac{xz}{|\mathbf{x}|^2} \\ \frac{yx}{|\mathbf{x}|^2} & \left(1-\frac{y^2}{|\mathbf{x}|^2}\right) & \frac{yz}{|\mathbf{x}|^2} \\ \frac{zx}{|\mathbf{x}|^2} & \frac{zy}{|\mathbf{x}|^2} & \left(1-\frac{z^2}{|\mathbf{x}|^2}\right)\end{bmatrix} \tag{B.4}$$

For this matrix only the eigenvector corresponding to λ_3 is well-defined over the spherical /*umbilical* wavefront, being a radial directed normal vector. Eigenvectors λ_1 and λ_2 may be arbitrary orthogonal vectors in the plane, tangent to the surface in the point of investigation $\mathbf{x}$, with the corresponding principal curvatures being $\kappa_1^G(\mathbf{x}) = \kappa_2^G(\mathbf{x}) = \frac{1}{|\mathbf{x}|}$.

In the present treatise when dealing with 2.5D problems it is a standard prerequisition, that in the plane of investigation ($z = 0$) all the involved wavefields propagate along the horizontal direction ($k_z(x, y, 0) \equiv 0$). In this special case the Hessian of the phase function becomes

$$\mathbf{H}^P(\mathbf{x}) = \begin{bmatrix}\phi_{xx}^{P''}(\mathbf{x},\omega) & \phi_{xy}^{P''}(\mathbf{x},\omega) & 0 \\ \phi_{xy}^{P''}(\mathbf{x},\omega) & \phi_{yy}^{P''}(\mathbf{x},\omega) & 0 \\ 0 & 0 & \phi_{zz}^{P''}(\mathbf{x},\omega)\end{bmatrix}, \tag{B.5}$$

with the trivial eigenvector/principal direction $\mathbf{v_2} = [0,\ 0,\ 1]^{\mathrm{T}}$ and the corresponding principal curvature $\kappa_2^P(\mathbf{x}) = -\frac{1}{k}\phi_{zz}^{P''}(\mathbf{x},\omega)$. Furthermore, considering that the eigenvector with a zero eigenvalue is given by $\mathbf{v}_3 = \hat{\mathbf{k}}^P(\mathbf{x}) = [\hat{k}_x^P(\mathbf{x}),\ \hat{k}_y^P(\mathbf{x}),\ 0]^{\mathrm{T}}$ and $\mathbf{v}_1$ is orthogonal to $\mathbf{v}_2$ and $\mathbf{v}_3$, therefore $\mathbf{v}_1 = [\hat{k}_y^P(\mathbf{x}),\ \hat{k}_x^P(\mathbf{x}),\ 0]^{\mathrm{T}}$ holds. Applying (B.3) the elements of the Hessian matrix can be expressed as

$$\mathbf{H}^P(\mathbf{x}) = -k\begin{bmatrix}\hat{k}_y^P(\mathbf{x})^2\kappa_1^P(\mathbf{x}) & \hat{k}_x^P(\mathbf{x})\hat{k}_y^P(\mathbf{x})\kappa_1^P(\mathbf{x}) & 0 \\ \hat{k}_x^P(\mathbf{x})\hat{k}_y^P(\mathbf{x})\kappa_1^P(\mathbf{x}) & \hat{k}_x^P(\mathbf{x})^2\kappa_1^P(\mathbf{x}) & 0 \\ 0 & 0 & \kappa_2^P(\mathbf{x})\end{bmatrix}. \tag{B.6}$$

In the aspect of the present treatise the signature and the determinant of the Hessian in the stationary position is of importance. In the followings these properties will be discussed when the SPA is applied for the Rayleigh integral.

B.1.2 Hessian for the SPA applied for the Rayleigh integral

Consider the Rayleigh integral written on the plane $y = 0$, with the high frequency gradient approximation applied:

$$P(\mathbf{x}, \omega) = 2 \int_{-\infty}^{\infty} \mathrm{j} k_y^P(\mathbf{x}_0) P(\mathbf{x}_0, \omega) G(\mathbf{x} - \mathbf{x}_0, \omega) \mathrm{d}x_0 \mathrm{d}z_0. \tag{B.7}$$

By definition the stationary position for the integral is found where

$$\nabla_{\mathbf{x}_0} \phi^P(\mathbf{x}_0, \omega) = -\nabla_{\mathbf{x}_0} \phi^G(\mathbf{x} - \mathbf{x}_0, \omega). \tag{B.8}$$

Geometrically the stationary position $\mathbf{x}_0^*(\mathbf{x})$ is found where the normals of the involved wavefronts coincide on the Rayleigh plane, i.e. where the wavefront of P is tangential with the spherical wavefront of the Green's function. Around the stationary point the phase function (B.8) gives the phase of sound field P measured at $\mathbf{x}$

$$\phi^P(\mathbf{x}, \omega) = \phi^P(\mathbf{x}_0^*(\mathbf{x}), \omega) + \phi^G(\mathbf{x} - \mathbf{x}_0^*(\mathbf{x}), \omega). \tag{B.9}$$

The 3x3 Hessian of the integrand's phase function, for the sake of brevity by suppressing its space dependency is defined as

$$H_{kl} = H_{kl}^P + H_{kl}^G = \frac{\partial^2}{\partial x_{0k} \partial x_{0l}} \left(\phi^P(\mathbf{x}_0, \omega) + \phi^G(\mathbf{x} - \mathbf{x}_0, \omega) \right), \quad k, l = 1, 2, 3. \tag{B.10}$$

The eigenvalues of H_{kl}^P and H_{kl}^G are the principal curvatures of the target field and the Green's function measured at the stationary position $\mathbf{x}_0^*(\mathbf{x})$. Since the principal directions for the Green's function's wavefront are arbitrary perpendicular unit vectors in the tangent plane, they can be chosen to coincide with the principal directions of H^P. Therefore at the stationary point the eigenvectors of $\mathbf{H}^P$ and $\mathbf{H}^G$ coincide and their eigenvalues are additive. The eigenvalues of the resultant matrix are therefore simply given as

$$\lambda_1(\mathbf{x}) = \lambda_1^P(\mathbf{x}_0^*(\mathbf{x})) + \lambda_1^G(\mathbf{x} - \mathbf{x}_0^*(\mathbf{x})) = -k \left(\kappa_1^P(\mathbf{x}_0^*(\mathbf{x})) + \kappa_1^G(\mathbf{x} - \mathbf{x}_0^*(\mathbf{x})) \right), \tag{B.11}$$

$$\lambda_2(\mathbf{x}) = \lambda_2^P(\mathbf{x}_0^*(\mathbf{x})) + \lambda_2^G(\mathbf{x} - \mathbf{x}_0^*(\mathbf{x})) = -k \left(\kappa_2^P(\mathbf{x}_0^*(\mathbf{x})) + \kappa_2^G(\mathbf{x} - \mathbf{x}_0^*(\mathbf{x})) \right). \tag{B.12}$$

$$\lambda_3(\mathbf{x}) = \lambda_3^P(\mathbf{x}_0^*(\mathbf{x})) + \lambda_3^G(\mathbf{x} - \mathbf{x}_0^*(\mathbf{x})) = 0. \tag{B.13}$$

In the aspect of the present thesis it is important to investigate the local principal curvatures and the principal radii of the wavefront of P at the evaluation point $\mathbf{x}$,

i.e. how these quantities change over the propagation from the Rayleigh plane. The curvatures are defined as the eigenvalues (normalized by $-k$) of the Hessian

$$H_{ij}^P = \frac{\partial^2}{\partial x_i \partial x_j}\phi^P(\mathbf{x},\omega) = \frac{\partial^2}{\partial x_i \partial x_j}\left(\phi^P(\mathbf{x}_0^*(\mathbf{x}),\omega) + \phi^G(\mathbf{x}-\mathbf{x}_0^*(\mathbf{x}),\omega)\right) \tag{B.14}$$

measured at $\mathbf{x}$. By applying the chain rule the derivative is expressed as

$$\begin{aligned} H_{ij}^P = \frac{\partial}{\partial x_j}\left(\frac{\partial x_{0k}}{\partial x_i}\frac{\partial \phi^P(x_{0k},\omega)}{\partial x_{0k}} + \frac{\partial (x_k - x_{0k})}{\partial x_i}\frac{\partial \phi^G(x_k - x_{0k},\omega)}{\partial (x_k - x_{0k})}\right) = \\ \frac{\partial^2 x_{0k}}{\partial x_i \partial x_j}\underbrace{\left(\frac{\partial \phi^P(x_{0k},\omega)}{\partial x_{0k}} + \frac{\partial \phi^G(x_{kl}-x_{0kl},\omega)}{\partial (x_k - x_{0k})}\right)}_{=0} + \\ \frac{\partial x_{0k}}{\partial x_i}\frac{\partial x_{0l}}{\partial x_j}\underbrace{\frac{\partial^2 \phi^P(x_{0k},\omega)}{\partial x_{0k}\partial x_{0l}}}_{H_{kl}^P} + \frac{\partial (x_k - x_{0k})}{\partial x_i}\frac{\partial (x_l - x_{0l})}{\partial x_j}\underbrace{\frac{\partial^2 \phi^G(x_{kl}-x_{0kl},\omega)}{\partial (x_k - x_{0k})\partial (x_l - x_{0l})}}_{H_{kl}^G} \end{aligned} \tag{B.15}$$

where the first underbraced part equals zero by the definition of the stationary position. By introducing the matrix $\nabla_{\mathbf{x}}\,\mathbf{x}_0$ for the rate of change of the stationary position with respect to the change in any coordinate of the evaluation point, defined as

$$[\nabla_{\mathbf{x}}\,\mathbf{x}_0]_{lj} = \frac{\partial x_{0l}}{\partial x_j} = \left[\frac{\partial \mathbf{x}_0^*(\mathbf{x})}{\partial x}\,\middle|\,\frac{\partial \mathbf{x}_0^*(\mathbf{x})}{\partial y}\,\middle|\,\frac{\partial \mathbf{x}_0^*(\mathbf{x})}{\partial z}\right], \tag{B.16}$$

the Hessian under consideration can be written in a matrix form

$$H_{ij}^P = (\nabla_{\mathbf{x}}\,\mathbf{x}_0)^{\mathrm{T}} H_{kl}^P (\nabla_{\mathbf{x}}\,\mathbf{x}_0) + (\mathbf{I} - \nabla_{\mathbf{x}}\,\mathbf{x}_0)^{\mathrm{T}} H_{kl}^G (\mathbf{I} - \nabla_{\mathbf{x}}\,\mathbf{x}_0). \tag{B.17}$$

In order to express this gradient of the stationary position its definition (B.8) is reconsidered:

$$\frac{\partial}{\partial x_{0k}}\phi^P(\mathbf{x}_0^*(\mathbf{x}),\omega) - \frac{\partial}{\partial x_{0k}}\phi^G(\mathbf{x}-\mathbf{x}_0^*(\mathbf{x}),\omega) = 0 \tag{B.18}$$

Taking a further derivative with respect to x_j results in

$$\frac{\partial^2}{\partial x_{0l}\partial x_{0k}}\phi^P(\mathbf{x}_0^*(\mathbf{x}),\omega)\frac{\partial x_{0l}}{\partial x_j} - \frac{\partial^2}{\partial x_{0l}\partial x_{0k}}\phi^G(\mathbf{x}-\mathbf{x}_0^*(\mathbf{x}),\omega)\frac{\partial}{\partial x_j}(x_l - x_{0l})) = 0, \tag{B.19}$$

or written in a matrix form

$$H_{kl}^P\,\nabla_{\mathbf{x}}\,\mathbf{x}_0 - H_{kl}^G\,(\mathbf{I} - \nabla_{\mathbf{x}}\,\mathbf{x}_0) = 0 \;\rightarrow\; \left(H_{kl}^P + H_{kl}^G\right)\nabla_{\mathbf{x}}\,\mathbf{x}_0 = H_{kl}^G. \tag{B.20}$$

In order to invert the matrix $H_{kl}^P + H_{kl}^G$ the involved matrices are expressed in the form, given in (B.3), i.e. by transforming it into its eigenspace:

$$\mathbf{V}\left(\mathbf{K}^P + \mathbf{K}^G\right)\mathbf{V}^{\mathrm{T}} \cdot \nabla_{\mathbf{x}}\,\mathbf{x}_0 = \mathbf{V}\mathbf{K}^G\mathbf{V}^{\mathrm{T}}, \tag{B.21}$$

where $\mathbf{K}^P$ and $\mathbf{K}^G$ are 2x2 diagonal matrices of the curvatures of P and G at the stationary point, and $\mathbf{V}$ is a 3x2 matrix consisting of the two corresponding eigenvectors.

Since the two columns of $\mathbf{V}$ are orthonormal, and the inverse of a 2x2 diagonal matrix can be calculated easily, therefore the gradient of the stationary position reads as

$$\nabla_{\mathbf{x}}\,\mathbf{x}_0 = \mathbf{V}\frac{\mathbf{K}^G}{\mathbf{K}^P+\mathbf{K}^G}\mathbf{V}^{\mathrm{T}} = \mathbf{V}\begin{bmatrix} \frac{\kappa_1^G}{\kappa_1^P+\kappa_1^G} & 0 \\ 0 & \frac{\kappa_2^G}{\kappa_2^P+\kappa_2^G} \end{bmatrix}\mathbf{V}^{\mathrm{T}}, \tag{B.22}$$

and obviously

$$\mathbf{I} - \nabla_{\mathbf{x}}\,\mathbf{x}_0 = \mathbf{V}\frac{\mathbf{K}^P}{\mathbf{K}^P+\mathbf{K}^G}\mathbf{V}^{\mathrm{T}} \tag{B.23}$$

holds.

Finally, the Hessian at the evaluation point, given by (B.17) is expressed in the same eigenspace with $H_{kl}^P = -k\mathbf{V}\mathbf{K}^P\mathbf{V}^{\mathrm{T}}$ and $H_{kl}^G = -k\mathbf{V}\mathbf{K}^G\mathbf{V}^{\mathrm{T}}$. Exploiting that $\mathbf{V}^{\mathrm{T}}\mathbf{V} = \mathbf{I}$ leads to

$$H_{ij}^P = -k\mathbf{V}\frac{\mathbf{K}^P\mathbf{K}^G}{\mathbf{K}^P+\mathbf{K}^G}\mathbf{V}^{\mathrm{T}} = -k\mathbf{V}\begin{bmatrix} \frac{\kappa_1^P\kappa_1^G}{\kappa_1^P+\kappa_1^G} & 0 \\ 0 & \frac{\kappa_2^P\kappa_2^G}{\kappa_2^P+\kappa_2^G} \end{bmatrix}\mathbf{V}^{\mathrm{T}} = -k\mathbf{V}\begin{bmatrix} \frac{1}{\rho_1^P+\rho_1^G} & 0 \\ 0 & \frac{1}{\rho_2^P+\rho_2^G} \end{bmatrix}\mathbf{V}^{\mathrm{T}} \tag{B.24}$$

This result states, that if the Rayleigh integral describes a sound field at $\mathbf{x}$, then the principal curvatures and radii of the field can be written in terms of that, measured on the Rayleigh boundary, as

Curvature change over propagation

$$\begin{aligned} \kappa^P(\mathbf{x}) &= \frac{\kappa^P(\mathbf{x}_0^*(\mathbf{x}))\kappa^G(\mathbf{x}-\mathbf{x}_0^*(\mathbf{x}))}{\kappa^P(\mathbf{x}_0^*(\mathbf{x}))+\kappa^G(\mathbf{x}-\mathbf{x}_0^*(\mathbf{x})}, \\ \rho^P(\mathbf{x}) &= \rho^P(\mathbf{x}_0^*(\mathbf{x}))+\rho^G(\mathbf{x}-\mathbf{x}_0^*(\mathbf{x})). \end{aligned} \tag{B.25}$$

Furthermore, the corresponding eigenvectors, i.e the direction of the largest and smallest curvature on the wavefront does not change along the direction of propagation.

Evaluation of the Rayleigh integral along xz-dimensions: In the case of approximating the integral with respect to both x and z direction the Hessian of the SPA may be formed from the 3x3 Hessian of the phase function by removing the rows and columns containing the y derivatives, hence by forming its 2x2 principal submatrix. Based on (B.3) the Hessian for the SPA can be expressed in terms of the principal curvatures and the corresponding eigenvectors. With also exploiting, that in the stationary point (B.11) holds the Hessian for the 2D SPA reads as

$$H = -k\begin{bmatrix} v_{1x}^2\left(\kappa_1^P+\kappa_1^G\right)+v_{2x}^2\left(\kappa_2^P+\kappa_2^G\right) & v_{1x}v_{1z}\left(\kappa_1^P+\kappa_1^G\right)+v_{2x}v_{2z}\left(\kappa_2^P+\kappa_2^G\right) \\ v_{1x}v_{1z}\left(\kappa_1^P+\kappa_1^G\right)+v_{2x}v_{2z}\left(\kappa_2^P+\kappa_2^G\right) & v_{1z}^2\left(\kappa_1^P+\kappa_1^G\right)+v_{2z}^2\left(\kappa_2^P+\kappa_2^G\right) \end{bmatrix}, \tag{B.26}$$

with $\mathbf{v}_1 = [v_{1x},\ v_{1y},\ v_{1z}]^{\mathrm{T}}$, $\mathbf{v}_2 = [v_{2x},\ v_{2y},\ v_{2z}]^{\mathrm{T}}$, $\kappa^P = \kappa^P(\mathbf{x}_0^*(\mathbf{x}))$, $\kappa^G = \kappa^G(\mathbf{x}-\mathbf{x}_0^*(\mathbf{x}))$.

The eigenvalues of this submatrix cannot be expressed in a general way, however the *interlacing inequalities of principal submatrices* ensures that they have the same sign as λ_2 and λ_3. The signature of the Hessian is therefore

- assuming a divergent sound field, the eigenvalues of the Hessian are negative (the curvatures are positive) and the signature is given by factor -2.
- assuming a convergent sound field with both principal curvature being negative *on the Rayleigh plane*, the signature of the Hessian depends on the evaluation position $\mathbf{x}$. On the parts of the space where the curvature of wavefront P is greater in magnitude than that of the Green's function the eigenvalues of the Hessian positive and it signature is 2. On other parts of the space the signature is -2.

In practice it means, that if the Rayleigh integral describes a sound field propagating toward a point, then the signature for an evaluation point between the Rayleigh plane and the focus point is given by 2, and in other parts of the space, where the waves already diverge after passing the focus point, the signature is -2.

The determinant of of the Hessian is given by

$$\det\mathbf{H}^P = -k\left(\kappa_1^P + \kappa_1^G\right)\left(\kappa_2^P + \kappa_2^G\right)\left(v_{2x}v_{1_z} - v_{1x}v_{2z}\right)^2. \tag{B.27}$$

By the definition of cross product of vectors the term $(v_{2x}v_{1_z} - v_{1x}v_{2z})$ is the second coordinate of the vector, being perpendicular to $\mathbf{v}_1$ and $\mathbf{v}_2$, i.e. of the normalized local wavenumber vector:

$$\det\mathbf{H}^P = -k\left(\kappa_1^P(\mathbf{x}_0^*(\mathbf{x})) + \kappa_1^G(\mathbf{x}-\mathbf{x}_0^*(\mathbf{x}))\right)\left(\kappa_2^P(\mathbf{x}_0^*(\mathbf{x})) + \kappa_2^G(\mathbf{x}-\mathbf{x}_0^*(\mathbf{x}))\right)\hat{k}_y^P(\mathbf{x}_0^*(\mathbf{x}))^2. \tag{B.28}$$

Note, that the description above is not limited for the Rayleigh integral: if the Kirchhoff-Helmholtz integral is written onto a smooth convex surface with the surface's curvature being significantly smaller than the wavefront curvature, than the surface can be considered locally plane, and the above given description holds with the substitution $\hat{k}_y^P(\mathbf{x}_0^*(\mathbf{x})) \rightarrow \hat{k}_{\mathrm{n}}^P(\mathbf{x}_0^*(\mathbf{x}))$ being the normal component of the local wavenumber vector. This statement is a consequence of the invariance of the determinant with respect to a linear transform.

The same formulation holds for evaluation of a 2D Fourier integral. In this case the determinant reads as

$$\det\mathbf{H}^P = -\frac{1}{k}\kappa_1^P(\mathbf{x}_0^*(k_x,k_z))\kappa_2^P(\mathbf{x}_0^*(k_x,k_z))k_y^2. \tag{B.29}$$

Evaluation of the Rayleigh integral along z-dimension: In the special case of the derivation of the 2.5D Rayleigh integral only the integration along the z-dimension is approximated and the Hessian is simply given by $\phi''_{zz}(\mathbf{x}_0) = \phi^{P''}_{zz}(\mathbf{x}_0) + \phi^{G''}_{zz}(\mathbf{x}-\mathbf{x}_0)$. Requiring, that in the horizontal plane of investigation $k_z(\mathbf{x}) \equiv 0$ guarantees, that the second derivative is the principal curvature itself, thus around the stationary position reads as

$$\phi''_{zz}(\mathbf{x}_0) = -k\left(\kappa_2^P(\mathbf{x}_0^*(\mathbf{x})) + \kappa_2^G(\mathbf{x}-\mathbf{x}_0^*(\mathbf{x}))\right). \tag{B.30}$$

Obviously for the sign of the second derivative the description given for the 2D SPA case holds.

Appendix C

C.1 Wavenumber vector of a point source pair

Given a point source pair positioned symmetrically to the y-axis $\mathbf{x}_1 = [x_1,\ y_1,\ 0]^{\mathrm{T}}$, $\mathbf{x}_2 = [-x_1,\ y_1,\ 0]^{\mathrm{T}}$ the radiated field reads

$$P(\mathbf{x},\omega) = \frac{A_1}{4\pi}\frac{\mathrm{e}^{-\mathrm{j}\frac{\omega}{c}|\mathbf{x}-\mathbf{x}_1|}}{|\mathbf{x}-\mathbf{x}_1|} + \frac{A_2}{4\pi}\frac{\mathrm{e}^{-\mathrm{j}\frac{\omega}{c}|\mathbf{x}-\mathbf{x}_2|}}{|\mathbf{x}-\mathbf{x}_2|}, \tag{C.1}$$

with the amplitude factors denoted by A_1 and A_2. Applying Euler's formula the phase function of the resultant field becomes

$$-\phi^P(\mathbf{x},\omega) = \arctan\frac{\frac{A_1}{r_1}\sin\left(\frac{\omega}{c}|\mathbf{x}-\mathbf{x}_1|\right) + \frac{A_1}{r_2}\sin\left(\frac{\omega}{c}|\mathbf{x}-\mathbf{x}_2|\right)}{\frac{A_1}{r_1}\cos\left(\frac{\omega}{c}|\mathbf{x}-\mathbf{x}_1|\right) + \frac{A_2}{r_1}\cos\left(\frac{\omega}{c}|\mathbf{x}-\mathbf{x}_2|\right)}. \tag{C.2}$$

The local wavenumber vector, i.e. the gradient of the expression can be calculated by using that

$$\left(\arctan\frac{f}{g}\right)' = \frac{f'g - fg'}{f^2+g^2}, \tag{C.3}$$

with the derivatives given by

$$f' = A_1 r_1' \frac{kr_1\cos(kr_1) - \sin(kr_1)}{r_1^2} + A_2 r_2' \frac{kr_2\cos(kr_2) - \sin(kr_2)}{r_2^2} \tag{C.4}$$

$$g' = A_1 r_1' \frac{-kr_1\sin(kr_1) - \cos(kr_1)}{r_1^2} + A_2 r_2' \frac{-kr_2\sin(kr_2) - \cos(kr_2)}{r_2^2}, \tag{C.5}$$

denoting $r_1 = |\mathbf{x}-\mathbf{x}_1|$ and $r_2 = |\mathbf{x}-\mathbf{x}_2|$ and $k = \frac{\omega}{c}$. Several simplifications lead to the gradient

$$\phi^{P'} = \frac{k\left(r_1' A_1^2 r_2^2 + r_2' A_2^2 r_1^2 + A_1 A_2 r_1 r_2 (r_1' + r_2')\cos(k\Delta r)\right) - A_1 A_2 (r_1' r_2 - r_2' r_1)\sin(k\Delta r)}{r_1^2 r_2^2 A^P(\mathbf{x},\omega)^2}, \tag{C.6}$$

with $\Delta r = r_1 - r_2$ and where $A^P(\mathbf{x},\omega)$ is the amplitude of the resulting field omitting the normalizing factor $1/4\pi$

$$A^P(\mathbf{x},\omega) = \frac{\sqrt{A_1^2 r_2^2 + A_2^2 r_1^2 + 2A_1 A_2 r_1 r_2\cos(k\Delta r)}}{r_1 r_2}. \tag{C.7}$$

These expressions describe the interference pattern of the point source pair over the whole listening area: due to destructive interference the denominator of the phase gradient vanishes over the zeros of $A^P(\mathbf{x}, \omega)$. At these positions the phase changes rapidly resulting in infinitely large local wavenumber vector lengths.

From the aspect of stereophonic application only the stereo axis is of interest, where $r_1 = r_2$ holds. Due to the symmetry of the geometry along that axis $\frac{\partial}{\partial x} r_1 = -\frac{\partial}{\partial x} r_2$, $\frac{\partial}{\partial y} r_1 = \frac{\partial}{\partial y} r_2$ and $\frac{\partial}{\partial z} r_1 = \frac{\partial}{\partial z} r_2$ holds, and the derivatives of the phase function are given as

$$-\phi_x^{P'} = k r'_x \frac{A_1 - A_2}{A_1 + A_2} \tag{C.8}$$

$$-\phi_y^{P'} = k r'_y, \tag{C.9}$$

and the amplitude factor reads

$$A^P(0, y, z, \omega) = \frac{A_1 + A_2}{r}. \tag{C.10}$$

Appendix D

D.1 Asymptotic approximation of the explicit driving function

Asymptotic spectral driving function: The derivation starts from the 2.5D explicit driving function in the wavenumber domain given by (4.45),

$$\tilde{D}(k_x, y, 0, \omega) = \frac{\tilde{P}(k_x, y, 0, \omega)}{\tilde{G}(k_x, y, 0, \omega)}, \tag{D.1}$$

ensuring perfect synthesis along a line with fixed y-coordinate. In the followings for the sake of brevity and transparency ω and z dependencies are suppressed, the latter since the driving function is defined at $z = 0$. By definition the wavenumber content of the involved quantities are obtained via a forward Fourier transform, with the involved sound fields expressed by their polar form

$$\tilde{P}(k_x, y) = \int_{-\infty}^{\infty} A^P(x, y)\, \mathrm{e}^{\mathrm{j}\phi^P(x,y)}\, \mathrm{e}^{\mathrm{j}k_x x} \mathrm{d}x, \tag{D.2}$$

$$\tilde{G}(k_x, y) = \int_{-\infty}^{\infty} A^G(x, y)\, \mathrm{e}^{\mathrm{j}\phi^G(x,y)}\, \mathrm{e}^{\mathrm{j}k_x x} \mathrm{d}x. \tag{D.3}$$

The involved spectra can be approximated by using the SPA: under high frequency assumptions the Fourier integrals may be approximated by evaluation around their stationary point $x_P^*(k_x)$ and $x_G^*(k_x)$ where their phase derivatives vanish. The stationary positions are defined as

$$\begin{aligned} \frac{\partial}{\partial x}\left(\phi^P(x, y) + k_x x\right)\Big|_{x=x_P^*(k_x)} &= 0 \quad \rightarrow \quad k_x^P(x_P^*(k_x), y) = k_x \\ \frac{\partial}{\partial x}\left(\phi^G(x, y) + k_x x\right)\Big|_{x=x_G^*(k_x)} &= 0 \quad \rightarrow \quad k_x^G(x_G^*(k_x), y) = k_x. \end{aligned} \tag{D.4}$$

Since it is assumed that $k_z^P(x, y) = k_z^G(x, y) = k_z = 0$ holds in the plane of investigation, therefore the stationary positions are found along a given y, where the local propagation direction of the virtual field and the Green's function matches to that of a plane wave, defined by k_x. The properties of the involved wavefields at these positions will dominate the corresponding Fourier integrals. Hence, the forward

transform defines two particular positions in the space, linked together via the actual spectral wavenumber.

Having defined the stationary positions, the forward Fourier transforms can be evaluated by the SPA. With accounting for the negative second phase-derivatives—since both the virtual sound field and the Green's function are diverging—their spectra can be approximated as [Tra+14, Ch. 5]

$$\tilde{P}(k_x, y) \approx \sqrt{\frac{2\pi}{\mathrm{j}\,|\phi^{P''}_{xx}(x^*_P(k_x), y)|}}\, A^P(x^*_P(k_x), y)\, \mathrm{e}^{\mathrm{j}\phi^P(x^*_P(k_x), y)}\, \mathrm{e}^{\mathrm{j}k_x \cdot x^*_P(k_x)}, \tag{D.5}$$

$$\tilde{G}(k_x, y) \approx \sqrt{\frac{2\pi}{\mathrm{j}\,|\phi^{G''}_{xx}(x^*_G(k_x), y)|}}\, A^G(x^*_G(k_x), y)\, \mathrm{e}^{\mathrm{j}\phi^G(x^*_G(k_x), y)}\, \mathrm{e}^{\mathrm{j}k_x \cdot x^*_G(k_x)}, \tag{D.6}$$

and the asymptotic approximation of the explicit driving function on a given spectral component yields

Asymptotic spectral driving function

$$\tilde{D}(k_x, y) \approx \sqrt{\frac{\phi^{G''}_{xx}(x^*_G(k_x), y)}{\phi^{P''}_{xx}(x^*_P(k_x), y)}}\, \frac{P(x^*_P(k_x), y)}{G(x^*_G(k_x), y)}\, \mathrm{e}^{\mathrm{j}k_x\left(x^*_P(k_x) - x^*_G(k_x)\right)}. \tag{D.7}$$

Hence, the spectrum can be be expressed by evaluating the target pressure and the Green's function at evaluation points, where the local propagation direction of the involved fields coincides with that of the actual spectral plane wave.

SPA of the inverse Fourier transform: In order to express the driving function in the spatial domain the inverse Fourier transform of the asymptotic spectrum (D.7), reading

$$D(x_0, y) = \frac{1}{2\pi} \int_{-\infty}^{\infty} \sqrt{\frac{\phi^{G''}_{xx}(x^*_G(k_x), y)}{\phi^{P''}_{xx}(x^*_P(k_x), y)}}\, \frac{P(x^*_P(k_x), y)}{G(x^*_G(k_x), y)}\, \mathrm{e}^{\mathrm{j}k_x\left(x^*_P(k_x) - x^*_G(k_x)\right)}\, \mathrm{e}^{-\mathrm{j}k_x x_0}\, \mathrm{d}k_x \tag{D.8}$$

is approximated by the stationary phase method, with the phase function under investigation given by

$$\Phi(k_x) = \phi^P(x^*_P(k_x), y) - \phi^G(x^*_G(k_x), y) + k_x\, x^*_P(k_x) - k_x\, x^*_G(k_x) - k_x x_0. \tag{D.9}$$

As it was discussed in Section 3.3.3, in the spatial inverse Fourier transform of an arbitrary wavefield spectrum $\tilde{P}$ each wavenumber component k_x will dominate one spatial position x_0, where the actual wavenumber component $k_x(x_0)$ coincides with the local wavenumber of the sound field $k^P_x(x_0)$. For the present case this wavenumber is found as the stationary phase wavenumber $k^*_x(x_0)$ of the integral (D.8) [Tra+14].

The derivative of the spectral phase function (D.9) can be evaluated by applying the chain rule, resulting in

$$\begin{aligned}\frac{\partial}{\partial k_x}\Phi(k_x) = x^{*'}_{P,k_x}(k_x) \underbrace{\left(\phi^{P'}_x(x^*_P(k_x), y) + k_x\right)}_{=0} - \\ - x^{*'}_{G,k_x}(k_x) \underbrace{\left(\phi^{G'}_x(x^*_G(k_x), y) + k_x\right)}_{=0} + x^*_P(k_x) - x^*_G(k_x) - x_0,\end{aligned} \tag{D.10}$$

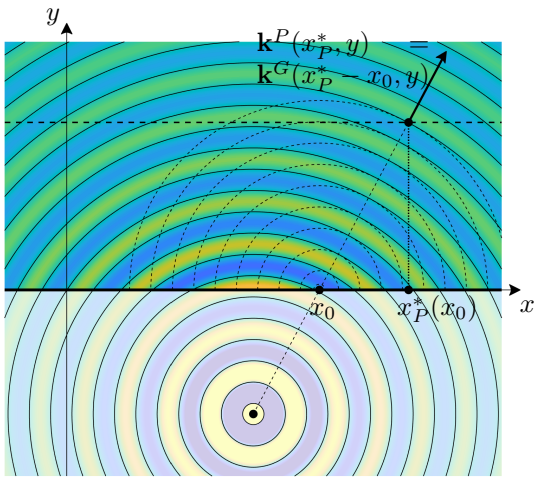

Figure D.1. Illustration of the evaluation position $x_P^*(x_0)$ (and $x_G^*(x_0)$) as the function of x_0. For a given SSD position x_0 the stationary position is found on a given reference line $y =$ const, where the virtual field propagation direction coincides with that of the Green's function, translated into x_0. Furthermore, at $x_P^*(x_0)$ the local principle radii of the Green's function positioned at $y = 0$, is always smaller, than that of a field, generated by a source distribution at $y < 0$, i.e. that of the virtual field.

where $x_{k_x}^{*'}(k_x)$ is the rate of change of the forward transform stationary positions with respect to the change of the spectral wavenumber. The bracketed terms cancel out due to the definition of the stationary points for the forward transform (D.4). The stationary wavenumber $k_x^*(x_0)$ is then found where

$$\frac{\partial}{\partial k_x}\Phi(k_x)\bigg|_{k_x=k_x^*(x_0)} = x_P^*(k_x^*(x_0)) - x_G^*(k_x^*(x_0)) - x_0 = 0 \tag{D.11}$$

holds. This definition relates the evaluation points x_P^* and x_G^* directly to the actual SSD coordinate x_0, therefore the dependency on the intermediate stationary wavenumber k_x^* may be omitted (i.e., $x_P^*(k_x^*(x_0)) \rightarrow x_P^*(x_0)$ and $x_G^*(k_x^*(x_0)) \rightarrow x_G^*(x_0)$ may be written).

The definitions for the forward and inverse transform stationary points completely define the evaluation points x_P^*, x_G^* for a given SSD position x_0 independently of the spectral wavenumber: combining (D.4) with (D.11), for an arbitrary position x_0 the evaluation points along a fixed y are found, where

2.5D SDM evaluation position

$$k_x^P(x_P^*(x_0), y) = k_x^G(x_P^*(x_0) - x_0, y) \tag{D.12}$$

is satisfied.

This result states that for a given SSD coordinate x_0 the evaluation point x_P^* is found on the reference line, where the local propagation direction of the target field P coincides with that of a point source positioned at $[x_0,\ 0,\ 0]^{\mathrm{T}}$. This principle is depicted in Figure D.1.

Having found the stationary position for (D.8) one still needs the phase function's second derivative and its sign around the stationary position in order to apply the SPA.

The second derivative is obtained by a further differentiation of (D.10) with respect to k_x

$$\begin{aligned}\frac{\partial^2}{\partial k_x^2}\Phi(k_x) = \\ x^{*''}_{P,k_xk_x}(k_x)\cdot\underbrace{\left(\phi_x^{P'}(x_P^*(k_x),y)+k_x\right)}_{=0}+x^{*'}_{P,k_x}(k_x)\cdot\left(x^{*'}_{P,k_x}(k_x)\,\phi_{xx}^{P''}(x_P^*(k_x),y)+2\right)- \\ x^{*''}_{G,k_xk_x}(k_x)\cdot\underbrace{\left(\phi_x^{G'}(x_G^*(k_x),y)+k_x\right)}_{=0}-x^{*'}_{G,k_x}(k_x)\cdot\left(x^{*'}_{G,k_x}(k_x)\,\phi_{xx}^{G''}(x_G^*(k_x),y)+2\right).\end{aligned} \tag{D.13}$$

The required rate of change of the stationary positions $x^{*'}_{P,k_x}(k_x)$ and $x^{*'}_{G,k_x}(k_x)$ can be obtained by differentiating their definition (D.4) with respect to k_x, yielding

$$x^{*'}_{P,k_x}(k_x) = -\frac{1}{\phi_{xx}^{P''}(x_P^*(k_x),y)}, \qquad x^{*'}_{G,k_x}(k_x) = -\frac{1}{\phi_{xx}^{G''}(x_G^*(k_x),y)}. \tag{D.14}$$

Thus the required second derivative is given by

$$\frac{\partial^2}{\partial k_x^2}\Phi(k_x) = \frac{\phi_{xx}^{P''}(x_P^*(k_x),y)-\phi_{xx}^{G''}(x_G^*(k_x),y)}{\phi_{xx}^{P''}(x_P^*(k_x),y)\cdot\phi_{xx}^{G''}(x_G^*(k_x),y)} = \frac{\rho_{\mathrm{h}}^P(x_P^*(k_x),y)-\rho_{\mathrm{h}}^G(x_G^*(k_x),y)}{k\,\hat{k}_y^{P2}(x_P^*(k_x),y)}, \tag{D.15}$$

with ρ_{h}^P and ρ_{h}^G being the horizontal principal radii of the target field and the Green's function, expressed by applying (B.6). Obviously, for any source distribution behind the SSD its horizontal principal radius is larger at position $y > 0$, than that of the stationary secondary point source and the sign of (D.15) is positive.

These results now may be substituted back into the SPA (3.27) of the inverse transform (D.8). For the sake of brevity in the following the evaluation point is denoted by $x_P^* \to x^*$. Denoting the stationary position by $\mathbf{x}_{\mathrm{ref}}(\mathbf{x}_0) = [x^*(x_0),\ y,\ 0]^{\mathrm{T}}$ the resulting driving function is formulated as

$$D(x_0,\omega) \approx \sqrt{\frac{\left|\phi_{xx}^{G''}(\mathbf{x}_{\mathrm{ref}}(\mathbf{x}_0)-\mathbf{x}_0,\omega)\right|^2}{\left|\phi_{xx}^{P''}(\mathbf{x}_{\mathrm{ref}}(\mathbf{x}_0),\omega)-\phi_{xx}^{G''}(\mathbf{x}_{\mathrm{ref}}(\mathbf{x}_0)-\mathbf{x}_0,\omega)\right|}}\sqrt{\frac{\mathrm{j}}{2\pi}}\frac{P(\mathbf{x}_{\mathrm{ref}}(\mathbf{x}_0),\omega)}{G(\mathbf{x}_{\mathrm{ref}}(\mathbf{x}_0)-\mathbf{x}_0,\omega)}, \tag{D.16}$$

where $k_x^P(\mathbf{x}_{\mathrm{ref}}(\mathbf{x}_0)) = k_x^G(\mathbf{x}_{\mathrm{ref}}(\mathbf{x}_0)-\mathbf{x}_0)$ holds.

Appendix E

E.1 Farfield approximation of planar radiators

Assume an infinite, rigid surface, located along the $y = 0$ plane. Over the surface only a small extent $\partial\Omega_p$ moves/vibrates with a pre-defined normal velocity profile $V_y(x, 0, z, \omega)$, while in remaining parts of the plane the surface velocity is identically zero. This geometry is termed as a baffled radiator, whose radiated field at an arbitrary receiver position $\mathbf{x} = [x,\ y > 0,\ z]^{\mathrm{T}}$ is given by the Rayleigh I integral 2.65 written in terms of the normal velocity

$$P(\mathbf{x}, \omega) = \iint_{-\infty}^{\infty} 2\mathrm{j}\omega\rho_0 V_y(\mathbf{x}_0, \omega) G(\mathbf{x} - \mathbf{x}_0, \omega)\, \mathrm{d}x_0\, \mathrm{d}z_0, \tag{E.1}$$

with the surface point being $\mathbf{x}_0 = [x_0,\ 0,\ z_0]^{\mathrm{T}}$.

Let $\mathbf{x}_\mathrm{c}$ be the geometric center of the radiator, and approximate the Green's function by it's local plane wave approximation around this center, as introduced by (3.14). The asymptotic approximation of the Green's function reads as

$$G(\mathbf{x} - \mathbf{x}_0, \omega) \approx G(\mathbf{x} - \mathbf{x}_\mathrm{c}, \omega) \mathrm{e}^{-\mathrm{j}\left\langle \mathbf{k}^G(\mathbf{x}-\mathbf{x}_\mathrm{c})\cdot(\mathbf{x}_0-\mathbf{x}_\mathrm{c})\right\rangle}. \tag{E.2}$$

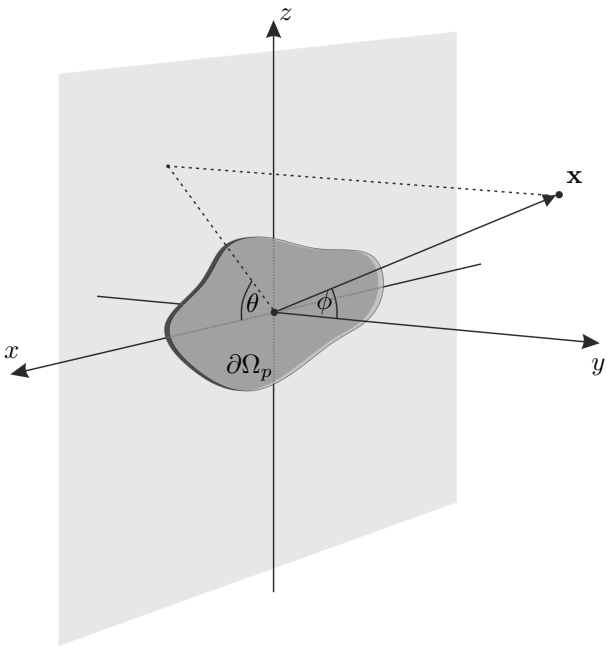

Figure E.1. Geometry for the derivation of the field, generated by a baffled radiator. A small extent of the radiator vibrates with a prescribed normal velocity, given by $V_y(x, 0, z, \omega)$. The center of the radiator is chosen to be the origin.

After substitution into the Rayleigh integral the Green's function can be collected from the integral

$$P(\mathbf{x},\omega) = G(\mathbf{x}-\mathbf{x}_\mathrm{c},\omega)\iint_{-\infty}^{\infty} 2\mathrm{j}\omega\rho_0 V_y(\mathbf{x}_0,\omega)\mathrm{e}^{-\mathrm{j}\left\langle\mathbf{k}^G(\mathbf{x}-\mathbf{x}_\mathrm{c})\cdot(\mathbf{x}_0-\mathbf{x}_\mathrm{c})\right\rangle}\,\mathrm{d}x_0\,\mathrm{d}z_0. \tag{E.3}$$

For the sake of simplicity the center of the radiator is chosen to be the origin ($\mathbf{x}_\mathrm{c} = [0,\ 0,\ 0]^\mathrm{T}$). By expanding the inner product the integral simplifies to

$$P(\mathbf{x},\omega) = 2\mathrm{j}\omega\rho_0 G(\mathbf{x},\omega)\iint_{-\infty}^{\infty} V_y(\mathbf{x}_0,\omega)\mathrm{e}^{-\mathrm{j}\left(k_x^G(\mathbf{x})\cdot x_0 + k_z^G(\mathbf{x})\cdot z_0\right)}\,\mathrm{d}x_0\,\mathrm{d}z_0. \tag{E.4}$$

The right side is a double Fourier integral of the surface velocity distribution, multiplied by the field of a point source at the center of the radiator, hence the radiated field can be written as

$$P(\mathbf{x},\omega) = 2\mathrm{j}\omega\rho_0 \cdot \tilde{V}_y(k_x^G(\mathbf{x}),0,k_z^G(\mathbf{x}),\omega)\cdot G(\mathbf{x},\omega) \tag{E.5}$$

Hence, the planar radiator can be modeled in its farfield as a directive point source, and once the 2D spectrum of the velocity distribution is known, the directivity characteristics can be obtained by evaluating the spectrum at the local wavenumber vector of the point source at the given receiver point.

The local wavenumber vector of the point source in Descartes and spherical coordinates are given as

$$\mathbf{k}^G(\mathbf{x}) = k\cdot\begin{bmatrix}\frac{x}{|\mathbf{x}|}\\ \frac{y}{|\mathbf{x}|}\\ \frac{z}{|\mathbf{x}|}\end{bmatrix} = k\cdot\begin{bmatrix}\sin\phi\cos\theta\\ \cos\phi\\ \sin\phi\sin\theta\end{bmatrix}, \tag{E.6}$$

with the spherical angles shown in Figure E.1 and the spherical form of the planar radiator's field reads as

$$P(r,\phi,\theta,\omega) = 2\mathrm{j}\omega\rho_0 \cdot \underbrace{\tilde{V}_y(k\sin\phi\cos\theta,0,k\sin\phi\sin\theta,\omega)}_{\Theta(\phi,\theta,\omega)}\cdot G(r,\phi,\theta,\omega) \tag{E.7}$$

where $\Theta(\phi,\theta,\omega)$ is termed the directivity function.

As a simple example, dynamic loudspeakers are often modeled as baffled circular pistons, whose velocity distribution is given as

$$V_y(x,0,z,\omega) = \begin{cases} V_0 & \text{if}\quad x^2+z^2 \le r_0^2\\ 0 & \text{everywhere else,}\end{cases} \tag{E.8}$$

with r_0 being the radius of the piston. Hence, each point over the rigid piston's surface moves in-phase, which is a fair approximation for loudspeakers at frequencies, at

which the modal behaviour of the membrane is negligible [1]. The 2D Fourier transform of this unit circular disk with radius r_0 is given by

$$\tilde{V}_y(k_x, 0, k_z, \omega) = 2\frac{J_1\left(r_0\sqrt{k_x^2 + k_z^2}\right)}{r_0\sqrt{k_x^2 + k_z^2}}, \tag{E.9}$$

with $J_1(\cdot)$ being the first order Bessel function. The field generated by the circular piston is then approximated by the formula:

$$P(r, \phi, \theta, \omega) = 2\mathrm{j}\omega\rho_0 \cdot \underbrace{2\frac{J_1\left(kr_0 \sin\phi\right)}{kr_0 \sin\phi}}_{\Theta(\phi,\omega)} G(r, \phi, \theta, \omega). \tag{E.10}$$

In the aspect of sound field synthesis the directivity function in the horizontal plane, containing the directive point source (i.e. at $\theta = 0$) is of special interest. In this plane the directivity yields

$$\Theta(\phi, \omega) = \tilde{V}_y(k_x^G(\mathbf{x}), 0, k_z^G(\mathbf{x}) \equiv 0, \omega) = \mathcal{F}_x\left\{\int_{-\infty}^{\infty} V_y(x, 0, z, \omega)\mathrm{d}z\right\}_{k_x = k\sin\phi}, \tag{E.11}$$

hence a horizontal „strength function" may be defined as $\int_{-\infty}^{\infty} V_y(x, 0, z, \omega)\mathrm{d}z$, which characterizes the directivtiy in the horizontal plane. This fact has been exploited in order to design spatial low-pass filters in previous studies [Ver97].

[1] At high frequencies mode shapes of a circular membrane can be expanded into a Fourier-Bessel series, from which the directivity function can be directly expressed. The present result is the zeroth order term of this expansion [Wil99].

Appendix F

F.1 Spectral representation of non-stationary convolutions

Assume the following non-stationary convolution

$$g(t) = \int_{-\infty}^{\infty} h(t_0, t - t_0) f(t_0) \mathrm{d}t_0, \tag{F.1}$$

with $h(t_0, t - t_0)$ denoting the time-variant convolution kernel. Terms $f(t_0)$ and $h(t_0, t - t_0)$ can be expressed by means of the inverse transform of its spectrum given as

$$f(t_0) = \frac{1}{2\pi} \int_{-\infty}^{\infty} F(\omega_0) \mathrm{e}^{\mathrm{j}\omega_0 t_0} \mathrm{d}\omega_0, \tag{F.2}$$

$$h(t_0, t - t_0) = \frac{1}{2\pi} \int_{-\infty}^{\infty} H(t_0, \omega_1) \mathrm{e}^{\mathrm{j}\omega_1 (t - t_0)} \mathrm{d}\omega_1. \tag{F.3}$$

Applying the above formulations the non-stationary convolution can be cast into the form

$$g(t) = \frac{1}{2\pi} \iint_{-\infty}^{\infty} H(t_0, \omega_1) \mathrm{e}^{\mathrm{j}\omega_1 (t - t_0)} \mathrm{d}\omega_1 f(t_0) \mathrm{d}t_0, \tag{F.4}$$

$$g(t) = \frac{1}{(2\pi)^2} \iiint_{-\infty}^{\infty} H(t_0, \omega_1) \mathrm{e}^{\mathrm{j}\omega_1 (t - t_0)} \mathrm{d}\omega_1 F(\omega_0) \mathrm{e}^{\mathrm{j}\omega_0 t_0} \mathrm{d}\omega_0 \mathrm{d}t_0. \tag{F.5}$$

Taking the Fourier transform of the latter expression:

$$G(\omega) = \frac{1}{(2\pi)^2} \iiint_{-\infty}^{\infty} H(t_0, \omega_1) \mathrm{e}^{\mathrm{j}\omega_1 (t - t_0)} \mathrm{d}\omega_1 \int_{-\infty}^{\infty} F(\omega_0) \mathrm{e}^{\mathrm{j}\omega_0 t_0} \mathrm{d}\omega_0 \mathrm{d}t_0 \mathrm{e}^{-\mathrm{j}\omega t} \mathrm{d}t. \tag{F.6}$$

Reversing the order of integration and rearrangement results in

$$G(\omega) = \frac{1}{(2\pi)^2} \iiint_{-\infty}^{\infty} H(t_0, \omega_1) F(\omega_0) \mathrm{e}^{-\mathrm{j}(\omega_1 - \omega_0) t_0} \underbrace{\int_{-\infty}^{\infty} \mathrm{e}^{-\mathrm{j}(\omega - \omega_1) t} \mathrm{d}t}_{2\pi\delta(\omega - \omega_1)} \mathrm{d}\omega_1 \, \mathrm{d}\omega_0 \, \mathrm{d}t_0. \tag{F.7}$$

Integration along ω_1 sifts out $\omega_1 = \omega$:

$$G(\omega) = \iint_{-\infty}^{\infty} H(t_0, \omega) F(\omega_0) \mathrm{e}^{-\mathrm{j}(\omega - \omega_0) t_0} \mathrm{d}\omega_0 \, \mathrm{d}t_0. \tag{F.8}$$

Finally it can be exploited that

$$\tilde{H}(\omega - \omega_0) = \int_{-\infty}^{\infty} H(t_0, \omega) \mathrm{e}^{-\mathrm{j}(\omega-\omega_0)t_0} \mathrm{d}t_0 \tag{F.9}$$

holds, yielding the final result

$$G(\omega) = \int_{-\infty}^{\infty} H(\omega - \omega_0, \omega) F(\omega_0) \mathrm{d}\omega_0. \tag{F.10}$$

Hence, a non-stationary convolution in the second variable of a time domain function yields a non-stationary convolution in the first variable of its spectral representation.

Appendix G

G

G.1 Representation of sources, moving on straight trajectories

For the sound field, generated by sources moving uniformly along arbitrary directed straight trajectories, closed form expression may be found either in the spatio-temporal, time-frequency or in the wavenumber domain. All the formulations utilize the analytical expression for a source, moving parallel with the x-axis and a corresponding coordinate transform.

Assume a source, with the location time history given by $\mathbf{x}_\mathrm{s}(t) = [v \cdot t,\ 0,\ 0]^\mathrm{T}$, i.e. moving along the x-axis, located at the origin at $t = 0$. The point source oscillates harmonically at the angular frequency ω_0 The generated sound field in the spatio-temporal domain reads as

$$P_\mathrm{m}(\mathbf{x}, t, \omega_0) = \frac{1}{4\pi} \frac{\mathrm{e}^{\mathrm{j}\omega_0(t-\tau(\mathbf{x},t))}}{\Delta(\mathbf{x}, t)}, \tag{G.1}$$

with

$$\Delta(\mathbf{x}, t) = \sqrt{(x - v \cdot t)^2 + (y^2 + z^2)(1 - M^2)}, \tag{G.2}$$

$$\tau(\mathbf{x}, t) = \frac{1}{c} \frac{M(x - v \cdot t) + \Delta(\mathbf{x}, t)}{(1 - M^2)}. \tag{G.3}$$

The angular frequency content of the radiated field is given by (5.58), reading

$$P_\mathrm{m}(\mathbf{x}, \omega, \omega_0) = \frac{1}{v} \tilde{G}(\frac{\omega - \omega_0}{v}, y, z, \omega) \mathrm{e}^{-\mathrm{j}\frac{\omega-\omega_0}{v}x}. \tag{G.4}$$

These formulations can be applied in order to express the corresponding representations for sources moving parallel with the $z = 0$ plane and arriving to the x-axis under an angle of inclination φ. This is performed by rotation of the receiver coordinate system, so that the new coordinate system $\mathbf{x}' = [x',\ y',\ z']^\mathrm{T}$ is defined by the transform

$$\mathbf{x}' = \begin{bmatrix} x' \\ y' \\ z' \end{bmatrix} = \begin{bmatrix} \cos\varphi & \sin\varphi & 0 \\ -\sin\varphi & \cos\varphi & 0 \\ 0 & 0 & 1 \end{bmatrix} \begin{bmatrix} x - x_\mathrm{s} \\ y - y_\mathrm{s} \\ z - z_s \end{bmatrix}. \tag{G.5}$$

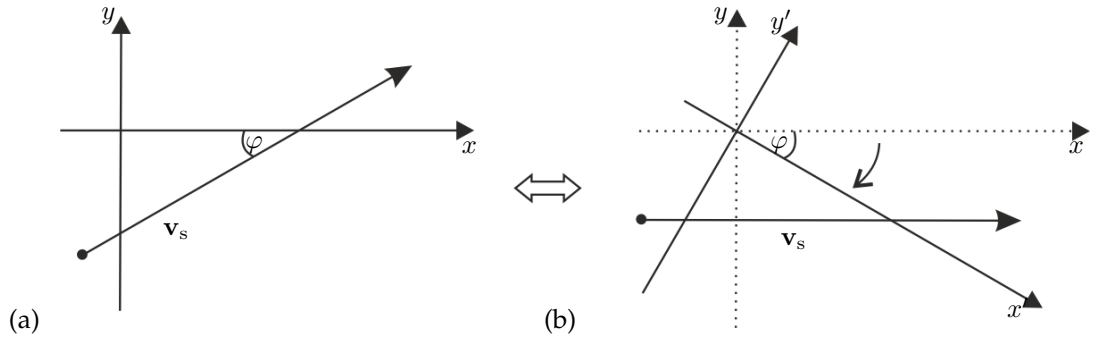

Figure G.1. Receiver coordinate transform in order to derive the field of a point source moving along an arbitrary directed straight trajectory.

As it is illustrated in Figure G.1 in the shifted and rotated coordinate system the source is located in the origin at $t = 0$ and travels parallel to the x'-axis, thus the radiated field is written in time time domain as

$$P_{\mathrm{m}}(\mathbf{x}, t, \omega_0) = \frac{1}{4\pi} \frac{\mathrm{e}^{\mathrm{j}\omega_0(t-\tau(\mathbf{x}',t))}}{\Delta(\mathbf{x}', t)}. \tag{G.6}$$

Note, that this description of sources with arbitrary linear trajectories is equivalent with the approach proposed in [AS08c]. The corresponding frequency domain formulation is obtained as

$$P_{\mathrm{m}}(\mathbf{x}, \omega, \omega_0) = \frac{1}{v} \tilde{G}(\frac{\omega - \omega_0}{v}, y', z', \omega) \mathrm{e}^{-\mathrm{j}\frac{\omega-\omega_0}{v}x'}. \tag{G.7}$$

The wavenumber domain representation is obtained by the spatial Fourier transform of (G.7) along the x-axis. According to the convolution theorem the wavenumber content is written as a spectral convolution

$$\tilde{P}_{\mathrm{m}}(k_x, y, z, \omega, \omega_0) = \frac{1}{v} \mathcal{F}_x \left\{ \tilde{G}(\frac{\omega - \omega_0}{v}, y', z', \omega) \right\} *_{k_x} \mathcal{F}_x \left\{ \mathrm{e}^{-\mathrm{j}\frac{\omega-\omega_0}{v}x'} \right\}, \tag{G.8}$$

with the explicit dependencies with respect to the x-coordinate given by (G.5). For the sake of simplicity the spectrum is only investigated in the most relevant plane, at $z = 0$. The first term on the right-hand side may be either evaluated by making use of the expression [GR07, (6.677,9.)] or applying directly the angular spectrum representation of the Green's function given in (2.1) together with applying the Fourier similarity and shift theorem

$$\mathcal{F}_x \left\{ \tilde{G}(\frac{\omega - \omega_0}{v}, y', z', \omega) \right\} = \frac{1}{|\sin\varphi|} \tilde{G}(\frac{\omega - \omega_0}{v}, -\frac{k_x}{\sin\varphi}, z) \mathrm{e}^{\mathrm{j}k_x \frac{\sin\varphi x_s + \cos\varphi(y - y_s)}{\sin\varphi}}. \tag{G.9}$$

The right term in the spectral convolution is again obtained from the spectrum of an exponential using the shifting theorem, yielding

$$\mathcal{F}_x \left\{ \mathrm{e}^{-\mathrm{j}\frac{\omega-\omega_0}{v}x'(x)} \right\} = 2\pi\delta(k_x - \cos\varphi\frac{\omega - \omega_0}{v}) \mathrm{e}^{-\mathrm{j}\frac{\omega-\omega_0}{v}(\sin\varphi(y-y_s) - \cos\varphi x_s)}. \tag{G.10}$$

The convolution of the two expressions sifts out $k_x = k_x - \cos\varphi\frac{\omega-\omega_0}{v}$, resulting in the final expression for the wavenumber content of the moving source

$$\tilde{P}_{\mathrm{m}}(k_x, y, z, \omega, \omega_0) = \\ = \frac{2\pi}{v|\sin\varphi|}\tilde{G}(\frac{\omega-\omega_0}{v}, \frac{\cos\varphi\frac{\omega-\omega_0}{v} - k_x}{\sin\varphi}, z)\mathrm{e}^{\mathrm{j}k_x\frac{\sin\varphi x_s+\cos\varphi(y-y_s)}{\sin\varphi}}\mathrm{e}^{-\mathrm{j}\frac{\omega-\omega_0}{v}\frac{y-y_s}{\sin\varphi}}, \quad \text{(G.11)}$$

while, the angular spectrum representation reads as a further Fourier transform of the Green's function with respect to the z-dimension

$$\tilde{P}_{\mathrm{m}}(k_x, y, k_z, \omega, \omega_0) = \\ = \frac{2\pi}{v|\sin\varphi|}\tilde{G}(\frac{\omega-\omega_0}{v}, \frac{\cos\varphi\frac{\omega-\omega_0}{v} - k_x}{\sin\varphi}, k_z)\mathrm{e}^{\mathrm{j}k_x\frac{\sin\varphi x_s+\cos\varphi(y-y_s)}{\sin\varphi}}\mathrm{e}^{-\mathrm{j}\frac{\omega-\omega_0}{v}\frac{y-y_s}{\sin\varphi}}. \quad \text{(G.12)}$$

These latter two wavenumber representations can be proven to converge into a Dirac-delta distribution in k_x as the inclination angle converges to zero $\varphi \to 0$, as given by (5.60) and (5.61).

Bibliography

[AG10] T. D. Abhayapala and A. Gupta. "Spherical Harmonic Analysis of Wavefields Using Multiple Circular Sensor Arrays". In: *IEEE Transactions on Audio, Speech, and Language Processing* 18.6 (Aug. 2010), pp. 1655–1666 (cit. on p. 3).

[Ahr] J. Ahrens. *Comments on Simulating Moving Sound Sources*. `http://www.sound-fieldsynthesis.org/moving-sound-sources`. Accessed: 2015-05-28 (cit. on p. 92).

[Ahr+13] J. Ahrens, M. R. P. Thomas, and I. Tashev. "Efficient Implementation of the Spectral Division Method for Arbitrary Virtual Sound Fields". In: *IEEE Workshop on Applications of Signal Processing to Audio and Acoustics (WASPAA)*. New Paltz, NY, USA, Oct. 2013 (cit. on p. 71).

[Ahr10] J. Ahrens. "The Single-layer Potentital Approach Applied to Sound Field Synthesis Including of Non-enclosing Distributions of Secondary Sources". PhD thesis. Technische Universitat Berlin, 2010 (cit. on pp. 3, 4, 18, 53, 67, 70).

[Ahr12] J. Ahrens. *Analytic Methods of Sound Field Synthesis*. 1st. Berlin: Springer, 2012 (cit. on pp. 4, 8, 11, 18, 19, 21, 53, 67, 79, 81, 90, 91, 115, 127).

[Ale00] R. C. Alexander. *The Inventor of Stereo: The Life and Works of Alan Dower Blumlein*. Focal Press, 2000 (cit. on p. 1).

[Arn86] J. M. Arnold. "Geometrical theories of wave propagation: a contemporary review". In: *IEE Proceedings J - Optoelectronics* 133.2 (Apr. 1986), pp. 165–188 (cit. on p. 34).

[Arn95] J. M. Arnold. "Phase-space localization and discrete representations of wave fields". In: *Journal of Optical Society of America* 12.1 (1995), pp. 111–123 (cit. on pp. 47, 48).

[AS08a] J. Ahrens and S. Spors. "An Analytical Approach to Sound Field Reproduction Using Circular and Spherical Loudspeaker Distributions". In: *Acta Acustica United with Acustica* 94 (2008), pp. 988–999 (cit. on pp. 4, 65, 67).

[AS08b] J. Ahrens and S. Spors. "Analytical driving functions for higher order Ambisonics". In: *2008 IEEE International Conference on Acoustics, Speech and Signal Processing*. Mar. 2008, pp. 373–376 (cit. on p. 3).

[AS08c] J. Ahrens and S. Spors. "Reproduction of Moving Virtual Sound Sources with Special Attention to the Doppler Effect". In: *Audio Engineering Society Convention 124*. Amsterdam, May 2008 (cit. on pp. 7, 8, 150).

[AS08d] J. Ahrens and S. Spors. "Reproduction of Virtual Sound Sources Moving at Supersonic Speeds in Wave Field Synthesis". In: *Audio Engineering Society Convention 125*. 7557. San Francisco, Oct. 2008 (cit. on pp. 7, 8, 91).

[AS09a] J. Ahrens and S. Spors. "An analytical approach to 2.5D sound field reproduction employing circular distributions of non-omnidirectional loudspeakers". In: *IEEE 17th European Signal Processing Conference*. Glasgow, Aug. 2009 (cit. on pp. 65, 67).

[AS09b] J. Ahrens and S. Spors. "On the Secondary Source Type Mismatch in Wave Field Synthesis Employing Circular Distributions of Loudspeakers". In: *Audio Engineering Society Convention 127*. New York, Oct. 2009 (cit. on pp. 65, 67).

[AS10a] J. Ahrens and S. Spors. "Applying the Ambisonics Approach on Planar and Linear Arrays of Loudspeakers". In: *2nd International Symposium on Ambisonics and Spherical Acoustics*. Paris, France, May 2010 (cit. on p. 68).

[AS10b] J. Ahrens and S. Spors. "Local Sound Field Synthesis by Virtual Secondary Sources". In: *Audio Engineering Society Conference: 40th International Conference: Spatial Audio: Sense the Sound of Space*. Oct. 2010 (cit. on p. 85).

[AS10c] J. Ahrens and S. Spors. "Sound Field Reproduction Using Planar and Linear Arrays of Loudspeakers". In: *IEEE Transactions on Audio, Speech, and Language Processing* 18.8 (Nov. 2010), pp. 2038–2050 (cit. on pp. 4, 21, 68).

[AS11a] J. Ahrens and S. Spors. "An analytical approach to local sound field synthesis using linear arrays of loudspeakers". In: *IEEE International Conference on Acoustics, Speech and Signal Processing (ICASSP)*. 2011 (cit. on pp. 4, 68).

[AS11b] J. Ahrens and S. Spors. "An analytical approach to local sound field synthesis using linear arrays of loudspeakers". In: *2011 IEEE International Conference on Acoustics, Speech and Signal Processing (ICASSP)*. May 2011, pp. 65–68 (cit. on p. 85).

[AS11c] J. Ahrens and S. Spors. "Wave field synthesis of moving virtual sound sources with complex radiation properties". In: *Journal of the Acoustical Society of America* 130.5 (Nov. 2011), pp. 2807–2816 (cit. on pp. 7, 89).

[AS12] J. Ahrens and S. Spors. "Applying the Ambisonics Approach to Planar and Linear Distributions of Secondary Sources and Combinations Thereof". In: *Acta Acustica United with Acustica* 98 (2012), pp. 28–36 (cit. on pp. 4, 68).

[Atm] *Dolby Atmos Next-Generation Audio for Cinema* (cit. on pp. 1, 5).

[AW02] T. D. Abhayapala and D. B. Ward. "Theory and design of high order sound field microphones using spherical microphone array". In: *2002 IEEE International Conference on Acoustics, Speech, and Signal Processing*. Vol. 2. May 2002, pp. II–1949–II–1952 (cit. on p. 3).

[AW05] G. B. Arfken and H. J. Weber. *Mathematical Methods for Physicists*. Elsevier, 2005 (cit. on pp. 12, 67).

[Baa08] M. A. J. Baalman. "On Wave Field Synthesis and electro-acoustic music, with particular focus on the reproduction of arbitrarily shaped sound sources". PhD thesis. Technische Universitat Berlin, 2008 (cit. on p. 7).

[Bai92] M. R. Bai. "Application of BEM (boundary element method)-based acoustic holography to radiation analysis of sound sources with arbitrarily shaped geometries". In: *Journal of the Acoustical Society of America* 92.1 (July 1992) (cit. on p. 24).

[Bau61] B. B. Bauer. "Phasor Analysis of Some Stereophonic Phenomena". In: *Journal of the Acoustical Society of America* 33.11 (1961), pp. 1536–1539 (cit. on p. 2).

[Ben+08] J. Benesty, M. M. Sondhi, and Y. Huang, eds. *Springer Handbook of Speech Processing*. Springer, 2008 (cit. on p. 37).

[Ben+85] J. C. Bennett, K. Barker, and F. O. Edeko. "A New Approach to the Assessment of Stereophonic Sound System Performance". In: *Journal of Audio Engineering Society* 33.5 (May 1985), pp. 314–321 (cit. on pp. 2, 37).

[Ber+92] A. J. Berkhout, D. de Vries, and P. Vogel. "Wave Front Synthesis: A New Direction in Electroacoustics". In: *Audio Engineering Society Convention 93*. Oct. 1992 (cit. on p. 7).

[Ber+93] A. J. Berkhout, D. de Vries, and P. Vogel. "Acoustic Control by wave field synthesis". In: *Journal of the Acoustical Society of America* 93.5 (1993), pp. 2764–2778 (cit. on pp. 4, 6, 63).

[Ber84] A. J. Berkhout. *Seismic Migration: Imaging of Acoustic Energy by Wavefield Extrapolation*. 2nd edition. Elsevier, 1984 (cit. on p. 30).

[Ber88] A. J. Berkhout. "A Holographic Approach to Acoustic Control". In: *Journal of Audio Engineering Society* 36.12 (Dec. 1988), pp. 977–995 (cit. on pp. 6, 63).

[Ber92] A. J. Berkhout. "Wave front synthesis: A new direction in electroacoustics". In: *Journal of the Acoustical Society of America* 92.4 (1992), pp. 2396–2396 (cit. on pp. 6, 7).

[Ber93] L. L. Beranek. *Acoustics*. Acoustical Society of America, 1993 (cit. on p. 12).

[BG04] T. D. Carozzi A. M. Buckley and M. P. Gough. "Instantaneous local wave vector estimation from multi-spacecraft measurements using few spatial points". In: *Annales Geophysicae* 22 (2004), pp. 2633–2641 (cit. on p. 31).

[BH75] N. Bleistein and R. A. Handelsman. *Asymptotic Expansions of Integrals*. 1st. Dover Publications, 1975 (cit. on pp. 40–42).

[BL56] F. H. Brittain and D. M. Leakey. "Two Channel Stereophonic Sound Systems". In: *Wireless World* 62.5 (1956), pp. 206–210 (cit. on p. 2).

[Bla00] D. T. Blackstock. *Fundamentals of Physical Acoustics*. John Wiley & Sons, 2000 (cit. on pp. 12, 14).

[Bla83] J. Blauert. *Spatial Hearing: The Psychophysics of Human Sound Localization*. MIT Press, 1983 (cit. on p. 1).

[Ble+00] N. Bleistein, J. K. Cohen, and J. W. Stockwell Jr. *Mathematics of Multidimensional Seismic Imaging, Migration, and Inversion*. Springer, 2000 (cit. on pp. 39, 42, 48).

[Ble84] N. Bleistein. *Mathematical Methods for Wave Phenomena*. Academic Press, 1984 (cit. on pp. 34, 39, 41).

[Blu32] A. D. Blumlein. "Improvements in and relating to sound-transmission, sound-recording and sound-reproducing systems". Pat. 394 325. 1932-1933 (cit. on p. 1).

[Boe40] K. de Boer. "Stereophonic Sound Reproduction". In: *Philips Technical Review* 5.4 (Apr. 1940), pp. 107–114 (cit. on p. 2).

[Bou+97] D. Bouche, F. Molinet, and R. Mittra. *Asymptotic Methods in Electromagnetics*. Springer, 1997 (cit. on p. 45).

[Bru04] W. de Brujin. "Application of Wave Field Synthesis in Videoconferencing". PhD thesis. Delft University of Technology, 2004 (cit. on p. 6).

[Buc+04] H. Buchner, S. Spors, and R. Rabenstein. "Efficient Active Listening Room Compensation for Wave Field Synthesis". In: *Audio Engineering Society Convention 116*. May 2004 (cit. on p. 7).

[BW70] M. Born and E. Wolf. *Principles of Optics - Electromagnetic Theory of Propagation, Interference and Diffraction of Light*. Fourth Edition. Pergamon Press, 1970 (cit. on p. 45).

[Cec+18] S. Cecchi, A. Carini, and S. Spors. "Room Response Equalization—A Review". In: *Applied Sciences* 8.1 (2018) (cit. on p. 54).

[CH62] R. Courant and D. Hilbert. *Methods of Mathematical Physics Volume II*. Wiley, 1962 (cit. on p. 27).

[CN03] E. Corteel and R. Nicol. "Listening Room Compensation for Wave Field Synthesis. What Can Be Done?" In: *Audio Engineering Society Conference: 23rd International Conference: Signal Processing in Audio Recording and Reproduction*. May 2003 (cit. on p. 7).

[Cop68] L. G. Copley. "Fundamental Results Concerning Integral Representations in Acoustic Radiation". In: *Journal of the Acoustical Society of America* 44.1 (1968), pp. 28–32 (cit. on p. 26).

[Cor06] E. Corteel. "Caractérisation et Extensions de la Wave Field Synthesis en conditions réelles". PhD thesis. University of Paris 6, 2006 (cit. on p. 7).

[Cor07] E. Corteel. "Synthesis of Directional Sources Using Wave Field Synthesis, Possibilities, and Limitations". In: *EURASIP Journal on Advances in Signal Processing* 2007.1 (Feb. 2007), p. 090509 (cit. on p. 7).

[Cri+92] D. G. Crighton, A. P. Dowling, J. E. Ffowcs Williams, M. Heckl, and F. G. Leppington. *Modern Methods in Analyitcal Acoustics - Lecture Notes*. Springer-Verlag, 1992 (cit. on p. 90).

[Dan+03] J. Daniel, R. Nicol, and S. Moreau. "Further Investigations of High Order Ambisonics and Wavefield Synthesis for Holophonic Sound Imaging". In: *Audio Engineering Society Convention 114*. Amsterdam, The Netherlands, Mar. 2003, pp. 1–18 (cit. on p. 3).

[Dan00] J. Daniel. "Représentation de champs acoustiques, application à la transmission et à la reproduction de scènes sonores complexes dans un contexte multimédia". PhD thesis. University of Paris 6, 2000 (cit. on p. 3).

[Dan03] J. Daniel. "Spatial Sound Encoding Including Near Field Effect: Introducing Distance Coding Filters and a Viable, New Ambisonic Format". In: *Audio Engineering Society Conference: 23rd International Conference: Signal Processing in Audio Recording and Reproduction*. Copenhagen, Denmark, May 2003, pp. 1–15 (cit. on pp. 3, 4).

[DB83] S.M. Deregowski and S.M. Brown. "A Theory of Acoustic Diffractors Applied to 2-D Models". In: *Geophysical Prospecting* 31.2A (Apr. 1983), pp. 293–333 (cit. on pp. 51, 65).

[DeS92] J. A. DeSanto. *Scalar Wave Theory: Green's Functions and Applications*. 1st. Berlin: Springer, 1992 (cit. on p. 21).

[Dev12] A. J. Devaney. *Mathematical Foundations of Imaging, Tomography and Wavefield Inversion*. Cambridge University Press, 2012 (cit. on pp. 16, 21).

[Duf01] D. G. Duffy. *Green's Functions with Applications*. Chapman and Hall, 2001 (cit. on p. 21).

[DW83] A. P. Dowling and J. E. Ffowcs Williams. *Sound and Sources of Sound*. Ellis Horwood Publishers, 1983 (cit. on pp. 89, 90).

[Ebe03] P. J. Schneider D. H. Eberly. *Geometric Tools for Computer Graphics*. Elsevier, 2003 (cit. on p. 119).

[EG04] T. M. Elfouhaily and C. A. Guerin. "A critical survey of approximate scattering wave theories from random rough surfaces". In: *Waves in Random Media* 14.4 (2004) (cit. on p. 39).

[F.S16] F.Schultz. "Sound Field Synthesis for Line Source Array Applications in Large-Scale Sound Reinforcement". PhD thesis. University of Rostock, 2016 (cit. on pp. 64, 65, 73).

[Faz+08] F. M. Fazi, P. Nelson, J. E. Christensen, and J. Seo. "Surround System Based on Three-Dimensional Sound Field Reconstruction". In: *Audio Engineering Society Convention 125*. Oct. 2008 (cit. on p. 4).

[Faz10] F. M. Fazi. "Sound Field Reproduction". PhD thesis. University of Southampton, 2010 (cit. on pp. 4, 19, 28, 53, 67).

[FF12] G. Firtha and P. Fiala. "Prefiltering the wave field synthesis operators - anti-aliasing and source directivity". In: *ISMA 2012, International Conference on Noise and Vibration Engineering*. Leuven, Belgium, Sept. 2012, pp. 1–15 (cit. on pp. 7, 81).

[FF13a] G. Firtha and P. Fiala. "Sound Field Reproduction Applying Stochastic Secondary Sources". In: *AIA-DAGA 2013, 39th Annual Conference on Acoustics*. Merano, Italy, Mar. 2013, pp. 1–4 (cit. on p. 7).

[FF13b] G. Firtha and P. Fiala. "Sound field reproduction with stochastic secondary sources". In: *Internoise 2013, 42nd International Congress and Exposition on Noise Control Engineering*. Innsbruck, Austria, Sept. 2013, pp. 1–11 (cit. on p. 7).

[FF14a] G. Firtha and P. Fiala. "Sound field synthesis of a moving virtual sound source applying the Spectral Division Method". In: *ISMA 2014, International Conference on Noise and Vibration Engineering*. Leuven, Belgium, Sept. 2014, pp. 1–15 (cit. on p. 9).

[FF14b] G. Firtha and P. Fiala. "Synthesis of a moving virtual sound source applying the spectral division method". In: *DAGA 2014, 40th German Annual Conference on Acoustics*. Oldenburg, Germany, Mar. 2014, pp. 1–2 (cit. on p. 9).

[FF15a] G. Firtha and P. Fiala. "Sound Field Synthesis of Uniformly Moving Virtual Monopoles". In: *Journal of Audio Engineering Society* 63.1/2 (Jan. 2015), pp. 46–53 (cit. on pp. 9, 92, 108, 111).

[FF15b] G. Firtha and P. Fiala. "Synthesis of a moving virtual sources with Wave Field Synthesis". In: *DAGA 2015, 41st German Annual Conference on Acoustics*. Nürnberg, Germany, Mar. 2015, pp. 1–4 (cit. on p. 9).

[FF16a] G. Firtha and P. Fiala. "Investigation of Spatial Aliasing Artifacts of Wave Field Synthesis for the Reproduction of Moving Virtual Point Sources". In: *DAGA 2016, 42nd German Annual Conference on Acoustics*. Aachen, Germany, Mar. 2016, pp. 1008–1011 (cit. on pp. 9, 117).

[FF16b] G. Firtha and P. Fiala. "Wave Field Synthesis of Moving Sources with Retarded Stationary Phase Approximation". In: *Journal of Audio Engineering Society* 63.12 (Jan. 2016), pp. 958–965 (cit. on pp. 9, 92, 105).

[FF17a] G. Firtha and P. Fiala. "Explicit Sound Field Synthesis Driving Functions in the Spatial Domain". In: *DAGA 2017, 43rd Annual Conference on Acoustics*. Kiel, Germany, Mar. 2017, pp. 1–4 (cit. on p. 8).

[FF17b] G. Firtha and P. Fiala. "Wave Field Synthesis of moving sources with arbitrary trajectory and velocity profile". In: *Journal of the Acoustical Society of America* 142.2 (2017), pp. 551–560 (cit. on pp. 9, 113).

[FF18a] G. Firtha and P. Fiala. "Spatial Aliasing and Loudspeaker Directivity in Unified Wave Field Synthesis Theory". In: *DAGA 2018, 44th German Annual Conference on Acoustics*. München, Germany, Mar. 2018, pp. 1314–1317 (cit. on p. 9).

[FF18b] G. Firtha and P. Fiala. "Theory and Implementation of 2.5D WFS of moving sources with arbitrary trajectory". In: *DAGA 2018, 44th German Annual Conference on Acoustics*. München, Germany, Mar. 2018, pp. 1318–1321 (cit. on pp. 9, 112).

[Fir+17] G. Firtha, P. Fiala, F. Schultz, and S. Spors. "Improved Referencing Schemes for 2.5D Wave Field Synthesis Driving Functions". In: *IEEE/ACM Transactions on Audio, Speech, and Language Processing* 25.5 (May 2017), pp. 1117–1127 (cit. on pp. 8, 59, 73).

[Fir+18] G. Firtha, P. Fiala, F. Schultz, and S. Spors. "On the General Relation of Wave Field Synthesis and Spectral Division Method for Linear Arrays". In: *IEEE/ACM Transactions on Audio, Speech, and Language Processing* 26.12 (Dec. 2018), pp. 2393–2403 (cit. on p. 9).

[FN13] F. M. Fazi and P. A. Nelson. "Sound field reproduction as an equivalent acoustical scattering problem". In: *Journal of the Acoustical Society of America* 134.5 (2013), pp. 3721–3729 (cit. on p. 28).

[FR14] P. Fiala and P. Rucz. "NiHu: An open source C++ BEM library". In: *Advances in Engineering Software* 75 (2014), pp. 101–112 (cit. on p. 27).

[Fra+07] A. Franck, A. Graefe, K. Thomas, and M. Strauss. "Reproduction of Moving Sound Sources by Wave Field Synthesis: An Analysis of Artifacts". In: *Audio Engineering Society Conference: 32nd International Conference: DSP for Loudspeakers*. Hillerod, Sept. 2007 (cit. on pp. 8, 115).

[GD04] N. A. Gumerov and R. Duraiswami. *Fast Multipole Methods for the Helmholtz Equation in Three Dimensions*. Elsevier, 2004 (cit. on pp. 11, 20).

[Ger73] M. A. Gerzon. "Periphony: With-Height Sound Reproduction". In: *Journal of Audio Engineering Society* 21.1 (1973), pp. 2–10 (cit. on p. 3).

[Ger75] M. A. Gerzon. "The Design of Precisely Coincident Microphone Arrays for Stereo and Surround Sound". In: *Audio Engineering Society Convention 50*. Mar. 1975 (cit. on p. 3).

[Ger85] M. A. Gerzon. "Ambisonics in Multichannel Broadcasting and Video". In: *Journal of Audio Engineering Society* 33.11 (1985), pp. 859–871 (cit. on p. 3).

[Ger92] M. A. Gerzon. "General Metatheory of Auditory Localisation". In: *Audio Engineering Society Convention 92*. Mar. 1992 (cit. on p. 3).

[Gib08] W. C. Gibson. *The Method of Moments in Electromagnetics*. Chapman & Hall, 2008 (cit. on p. 21).

[Gir+01] B. Girod, R. Rabenstein, and A. Stenger. *Signals and Systems*. Wiley, 2001 (cit. on pp. 68, 79, 90).

[Gol05] R. Goldman. "Curvature formulas for implicit curves and surfaces". In: *Computer Aided Geometric Design* 22.7 (Oct. 2005), pp. 632–658 (cit. on pp. 34, 95).

[Goo05] J. W. Goodman. *Introduction to Fourier Optics*. 3rd edition. Greenwood Village: Roberts & Co Publ, 2005 (cit. on p. 18).

[GR07] I. S. Gradshteyn and I. M. Ryzhik. *Table of Integrals, Series, and Products*. 7th. Academic Press, 2007 (cit. on p. 150).

[Hah+16] N. Hahn, F. Winter, and S. Spors. "Local Wave Field Synthesis by Spatial Bandlimitation in the Circular/Spherical Harmonics Domain". In: *Audio Engineering Society Convention 140*. Paris, France, June 2016 (cit. on p. 85).

[Hah+17] N. Hahn, F. Winter, and S. Spors. "Synthesis of a Spatially Band-Limited Plane Wave in the Time-Domain using Wave Field Synthesis". In: *25th European Signal Processing Conference (EUSIPCO)*. Kos Island, Greece, Aug. 2017, pp. 673–677 (cit. on p. 85).

[Ham+05] K. Hamasaki, K. Hiyama, and R. Okumura. "The 22.2 Multichannel Sound System and Its Application". In: *Audio Engineering Society Convention 118*. May 2005 (cit. on p. 1).

[Ham+11] K. Hamasaki, K. Matsui, I. Sawaya, and H. Okubo. "The 22.2 Multichannel Sounds and its Reproduction at Home and Personal Enviroment". In: *Audio Engineering Society Conference: 43rd International Conference: Audio for Wirelessly Networked Personal Devices*. Sept. 2011 (cit. on p. 1).

[Har01] E. Hartmann. "The normalform of a space curve and its application to surface design". In: *The Visual Computer* 17.7 (2001), pp. 445–456 (cit. on pp. 34, 131).

[Har99] E. Hartmann. "On the curvature of curves and surfaces defined by normalforms". In: *Computer Aided Geometric Design* 16.5 (June 1999), pp. 355–376 (cit. on pp. 34, 131).

[Hav+08] D. Havelock, S. Kuwano, and M. Vorländer, eds. *Handbook of Signal Processing in Acoustics*. Vol. Volume 1. Springer, 2008 (cit. on p. 36).

[Her+03] D. W. Herrin, F. Martinus, T. W. Wu, and A. F. Seybert. "A New Look at the High Frequency Boundary Element and Rayleigh Integral Approximations". In: *SAE Technical Paper*. SAE International, May 2003 (cit. on p. 39).

[Her+15a] J. Herre, J. Hilpert, A. Kuntz, and J. Plogsties. "MPEG-H 3D Audio: The New Standard for Coding of Immersive Spatial Audio". In: *IEEE Journal of Selected Topics in Signal Processing* 9.5 (Aug. 2015), pp. 770–779 (cit. on p. 5).

[Her+15b] J. Herre, J. Hilpert, A. Kuntz, and J. Plogsties. "MPEG-H Audio—The New Standard for Universal Spatial/3D Audio Coding". In: *Journal of Audio Engineering Society* 62.12 (2015), pp. 821–830 (cit. on p. 5).

[Hoo05] A. T. de Hoop. "Fields and waves excited by impulsive point sources in motion—The general 3D time-domain Doppler effect". In: *Wave Motion* 43.2 (Dec. 2005), pp. 116–122 (cit. on pp. 89, 91).

[How07] M. S. Howe. *Hydrodynamics and Sound*. Cambridge University Press, 2007 (cit. on pp. 14, 22).

[Hul04] E. Hulsebos. "Auralization using Wave Field Synthesis". PhD thesis. Delft University of Technology, 2004 (cit. on p. 7).

[Huy90] C. Huygens. *Treatise on Light (Traité de la Lumière))*. Leyden by Van der Aa, 1690 (cit. on p. 6).

[HW97] C. Hugonnet and P. Walder. *Stereophonic Sound Recording: Theory and Practice*. John Wiley & Sons, 1997 (cit. on p. 2).

[Jac99] J. D. Jackson. *Classical Electrodynamics*. Third. Wiley, 1999 (cit. on p. 90).

[Jen+07] F. B. Jensen, W. A. Kuperman, M. B. Porter, and H. Schmidt. *Computational Ocean Acoustics*. Ed. by William H. Hartmann. Springer, 2007 (cit. on p. 14).

[Kel67] O. D. Kellogg. *Foundations of Potential Theory*. Frederick Ungar Publishing Company, 1967 (cit. on p. 27).

[Kin+00] L. E. Kinsler, A. R. Frey, and A. B. Coppens. *Fundamentals of Acoustics*. 4th. Wiley and Sons, 2000 (cit. on pp. 14, 33).

[Kir07] S. Kirkup. *The Boundary Element Method in Acoustics*. Journal of Computational Acoustics, 2007 (cit. on p. 24).

[Koy+14] S. Koyama, K. Furuya, Y. Hiwasaki, Y. Haneda, and Y. Suzuki. "Wave Field Reconstruction Filtering in Cylindrical Harmonic Domain for With-Height Recording and Reproduction". In: *IEEE/ACM Transactions on Audio, Speech, and Language Processing* 22.10 (Oct. 2014), pp. 1546–1557 (cit. on p. 67).

[Koy14] S. Koyama. "Boundary Integral Approach to Sound Field Transform and Reproduction". PhD thesis. University of Tokyo, 2014 (cit. on pp. 19, 67).

[Lal68] É. Lalor. "Inverse Wave Propagator". In: *Journal of Mathematical Physics* 9.12 (1968), pp. 2001–2006 (cit. on p. 69).

[Lea60] D. M. Leakey. "Further thoughts on stereophonic sound systems". In: *Wireless World* 66 (1960), pp. 154–160 (cit. on p. 2).

[LF47] M. Lax and H. Feshbach. "On the Radiation Problem at High Frequencies". In: *Journal of the Acoustical Society of America* 19.4 (1947), pp. 682–690 (cit. on p. 38).

[Lig52] M. J. Lighthill. "On sound generated aerodynamically I. General theory". In: *Proceedings of the Royal Society A* 211.1107 (Mar. 1952), pp. 564–587 (cit. on p. 14).

[Lig54] M. J. Lighthill. "On sound generated aerodynamically II. Turbulence as a source of sound". In: *Proceedings of the Royal Society A* 222.1148 (Feb. 1954), pp. 1–32 (cit. on p. 14).

[Lip85] S. P. Lipshitz. "Stereo Microphone Techniques: Are the Purists Wrong?" In: *Audio Engineering Society Convention 78*. May 1985 (cit. on p. 2).

[Mar98] G. F. Margrave. "Theory of nonstationary linear filtering in the Fourier domain with application to time-variant filtering". In: *Geophysics* 63.1 (Jan. 1998), pp. 244–259 (cit. on p. 90).

[ME02] J. Meyer and G. Elko. "A highly scalable spherical microphone array based on an orthonormal decomposition of the soundfield". In: *2002 IEEE International Conference on Acoustics, Speech, and Signal Processing*. Vol. 2. May 2002, pp. II–1781–II–1784 (cit. on p. 3).

[MF53] P. M. Morse and H. Feshbach. *Methods of Theoretical Physics*. Vol. Vol.I. McGraw-Hill Book Company Inc., 1953 (cit. on p. 67).

[MI68] P. M. Morse and K. U. Ingard. *Theoretical Acoustics*. 1st. New York, NY: McGraw-Hill Book Company, 1968 (cit. on pp. 12, 94).

[MN08] S. Marburg and B. Nolte, eds. *Computational Acoustics of Noise Propagation in Fluids - Finite and Boundary Element Methods*. Springer, 2008 (cit. on p. 24).

[Moo90] F. R. Moore. *Elements of Computer Music*. Prentice-Hall,Inc., 1990 (cit. on p. 37).

[NE99] R. Nicol and M. Emerit. "3D-Sound Reproduction Over an Extensive Listening Area: A Hybrid Method Derived from Holophony and Ambisonic". In: *Audio Engineering Society Conference: 16th International Conference: Spatial Sound Reproduction*. Mar. 1999 (cit. on p. 55).

[NV06] M. Nieto-Vesperinas. *Scattering And Diffraction in Physical Optics*. 2nd edition. Singapore: World Scientific, 2006 (cit. on p. 18).

[Olv+10] F. W. J. Olver, D. W. Lozier, R. F. Boisvert, and C. W. Clark, eds. *NIST Handbook of Mathematical Functions*. New York, NY: Cambridge University Press, 2010 (cit. on pp. 21, 49).

[Par12] R. Parent. *Computer Animation*. 3rd. Morgan Kaufmann, 2012 (cit. on p. 112).

[Pet+05] S. Petrausch, R. Rabenstein, and S. Spors. "Simulation and Visualization of Room Compensation for Wave Field Synthesis with the Functional Transformation Method". In: *Audio Engineering Society Convention 119*. Oct. 2005 (cit. on p. 7).

[Pie91] A. D. Pierce. *Acoustics, An Introduction to its Physical Principles and Applications*. Acoustical Society of America, 1991 (cit. on pp. 14, 33).

[Pig+15] N. J. Pignier, C. J. O'Reilly, and S. Boij. "A Kirchhoff approximation-based numerical method to compute multiple acoustic scattering of a moving source". In: *Applied Acoustics* 96 (2015), pp. 108–117 (cit. on p. 39).

[Pol05] M. A. Poletti. "Three-Dimensional Surround Sound Systems Based on Spherical Harmonics". In: *Journal of Audio Engineering Society* 53.11 (2005), pp. 1004–1025 (cit. on p. 4).

[Pol77] H. F. Pollard. *Sound Waves in Solids*. Law Book Co of Australasia, 1977 (cit. on p. 32).

[PS02] R. Pike and P. Sabatier, eds. *Scattering: Scattering and Inverse Scattering in Pure and Applied Science*. Academic Press, 2002 (cit. on p. 39).

[PT92] A. D. Pierce and R. N. Thurston, eds. *High Frequency and Pulse Scattering*. Vol. XXI. Physical Acoustics. Academic Press, 1992 (cit. on p. 34).

[Pul01a] V. Pulkki. "Localization of Amplitude-Panned Virtual Sources I: Stereophonic Panning". In: *Journal of Audio Engineering Society* 49.9 (Sept. 2001), pp. 739–752 (cit. on pp. 2, 37).

[Pul01b] V. Pulkki. "Localization of Amplitude-Panned Virtual Sources II: Two- and Three-Dimensional Panning". In: *Journal of Audio Engineering Society* 49.9 (Sept. 2001), pp. 753–767 (cit. on p. 2).

[Pul01c] V. Pulkki. "Spatial Sound Generation and Perception by Amplitude Panning Techniques". PhD thesis. Helsinki University of Technology, 2001 (cit. on p. 37).

[Pul97] V. Pulkki. "Virtual Sound Source Positioning Using Vector Base Amplitude Panning". In: *Journal of Audio Engineering Society* 45.6 (June 1997), pp. 456–466 (cit. on pp. 3, 37).

[Roe05] H. Roemer. *Theoretical Optics: An introduction*. Wiley, 2005 (cit. on p. 31).

[RS07] R. Rabenstein and S. Spors. "Springer Handbook of Speech Processing". In: ed. by J. Benesty, M. Sondhi, and Y. Huang. Springer, 2007. Chap. Chapter 53, Sound Field reproduction, pp. 1095–1114 (cit. on pp. 2, 7).

[Rum01] F. Rumsey. *Spatial Audio*. Focal Press, 2001 (cit. on pp. 2, 37).

[SA09a] S. Spors and J. Ahrens. "Spatial Sampling Artifacts of Focused Sources in Wave Field Synthesis". In: *NAG/DAGA 2009, 35th Annual Conference on Acoustics*. Rotterdam, 2009 (cit. on p. 78).

[SA09b] S. Spors and J. Ahrens. "Spatial Sampling Artifacts of Wave Field Synthesis for the Reproduction of Virtual Point Sources". In: *Audio Engineering Society Convention 126*. May 2009 (cit. on pp. 78, 80).

[SA10] S. Spors and J. Ahrens. "Analysis and Improvement of Pre-equalization in 2.5-Dimensoinal Wave Field Synthesis". In: *Audio Engineering Society Convention 128*. London, May 2010 (cit. on pp. 8, 64).

[Sch+13] F. Schultz, V. Erbes, S. Spors, and S. Weinzierl. "Derivation of IIR prefilters for soundfield synthesis using linear secondary source distributions". In: *AIA-DAGA 2013, 39th Annual Conference on Acoustics*. Merano, Italy, 2013 (cit. on pp. 51, 65).

[Sch+17] F. Schultz, G. Firtha, P. Fiala, and S. Spors. "Wave Field Synthesis Driving Functions for Large-Scale Sound Reinforcement Using Line Source Arrays". In: *Audio Engineering Society Convention 142*. May 2017 (cit. on p. 8).

[Sch92] S. H. Schot. "Eighty Years of Sommerfeld's Radiation Condition". In: *Historia Mathematica* 19 (1992), pp. 385–401 (cit. on p. 15).

[SH11] I. Stakgold and M. Holst. *Green's Function and Boundary Value Problems*. Third. Wiley, 2011 (cit. on p. 20).

[SM93] B. Z. Steinberg and J. J. McCoy. "Marching acoustic fields in a phase space". In: *Journal of the Acoustical Society of America* 93.1 (1993), pp. 188–204 (cit. on p. 48).

[Sno53] W. B. Snow. "Basic Principles of Stereophonic Sound". In: *Journal of the Society of Motion Picture and Television Engineers* 61.5 (Nov. 1953), pp. 567–589 (cit. on p. 6).

[Son+98] J. J. Sonke, J. Labeeuw, and D. de Vries. "Variable Acoustics by Wavefield Synthesis: A Closer Look at Amplitude Effects". In: *Audio Engineering Society Convention 104*. May 1998 (cit. on p. 7).

[Spo+01] T. Sporer, J. Plogsties, and S. Brix. "CARROUSO - An European Approach to 3D-Audio". In: *Audio Engineering Society Convention 110*. May 2001 (cit. on p. 7).

[Spo+03] S. Spors, A. Kuntz, and R. Rabenstein. "An Approach to Listening Room Compensation with Wave Field Synthesis". In: *Audio Engineering Society Conference: 24th International Conference: Multichannel Audio, The New Reality*. June 2003 (cit. on p. 7).

[Spo+04] S. Spors, H. Buchner, and R. Rabenstien. "A novel approach to active listening room compensation for wave field synthesis using wave-domain adaptive filtering". In: *2004 IEEE International Conference on Acoustics, Speech, and Signal Processing*. Vol. 4. May 2004, iv–29–iv–32 vol.4 (cit. on p. 7).

[Spo+08] S. Spors, R. Rabenstein, and J. Ahrens. "The Theory of Wave Field Synthesis Revisited". In: *Audio Engineering Society Convention 124*. Amsterdam, May 2008 (cit. on pp. 7, 56).

[Spo+11] S. Spors, J. Ahrens, and K. Helwani. "Local Sound Field Synthesis by Virtual Acoustic Scattering and Time-Reversal". In: *Audio Engineering Society Convention 131*. Oct. 2011 (cit. on p. 85).

[Spo+13] S. Spors, H. Wierstorf, A. Raake, et al. “Spatial Sound With Loudspeakers and It’s Perception: A Review of the Current State”. In: *Proceedings of the IEEE* 101.9 (Sept. 2013), pp. 1920–1938 (cit. on pp. 4, 5).

[Spo05] S. Spors. “Active Listening Room Compensation for Spatial Sound Reproduction Systems”. PhD thesis. Friedrich-Alexander-Universitat Erlangen-Nurnberg, 2005 (cit. on pp. 18, 24, 54).

[Spo07a] S. Spors. “An Analytic Secondary Source Selection Criterion for Wavefield Synthesis”. In: *DAGA 2007, 33rd German Annual Conference on Acoustics*. 2007 (cit. on p. 55).

[Spo07b] S. Spors. “Extension of an Analytic Secondary Source Selection Criterion for Wave Field Synthesis”. In: *Audio Engineering Society Convention 123*. New York, Oct. 2007 (cit. on p. 55).

[SS14] F. Schultz and S. Spors. “Comparing Approaches to the Spherical and Planar Single Layer Potentials for Interior Sound FIeld Synthesis”. In: *Acta Acustica United with Acustica* 100 (2014), pp. 900–911 (cit. on pp. 28, 53, 67, 69).

[SS16] F. Schultz and S. Spors. “On the Connections of Wave Field Synthesis and Spectral Division Method Plane Wave Driving Functions”. In: *DAGA 2016, 42nd German Annual Conference on Acoustics*. Aachen, Germany, 2016 (cit. on pp. 8, 73).

[SS34] J. C. Steinberg and W. B. Snow. “Symposium on Wire Transmission of Symphonic Music and Its Reproduction in Auditory Perspective: Physical Factors”. In: *Electrical Engineering* 13.2 (1934), 245–258 (cit. on p. 6).

[Sta96] E. W. Start. “Application of Curved Arrays in Wave Field Synthesis”. In: *Audio Engineering Society Convention 100*. May 1996 (cit. on p. 7).

[Sta97] E. W. Start. “Direct sound enhancement by wave field synthesis”. PhD thesis. Delft University of Technology, 1997 (cit. on pp. 6, 7, 63, 64, 83, 105).

[Str+04] M. Strauss, A. Wagner, A. Walther, and F. Melchior. “Generation of Highly Immersive Atmospheres for Wave Field Synthesis Reproduction”. In: *Audio Engineering Society Convention 116*. May 2004 (cit. on p. 7).

[TM05] I. Tinkelman and T. Melamed. “Local spectrum analysis of field propagation in an anisotropic medium. Part I. Time-harmonic fields”. In: *Journal of Optical Society of America* 22.6 (2005), pp. 1200–1207 (cit. on pp. 47, 48).

[Tra+14] E. R. Tracy, A. J. Brizard, A. S. Richardson, and A. N. Kaufman. *Ray tracing and beyond: Phase Space Methods in Plasma Wave Theory*. Cambridge University Press, 2014 (cit. on p. 140).

[Tsa+00] L. Tsang, J. A. Kong, and K. Ding. *Scattering of Electromagnetic Waves: Theory and Applications*. Wiley and Sons, 2000 (cit. on p. 38).

[Ver97] E.N.C. Verheijen. “Sound Reproduction by Wave Field Synthesis”. PhD thesis. Delft University of Technology, 1997 (cit. on pp. 4, 6, 63, 64, 86, 105, 145).

[VF12] F. Voelk and H. Fastl. “Wave Field Synthesis with Primary Source Correction: Theory, Simulation Results, and Comparison to Earlier Approaches”. In: *Audio Engineering Society Convention 133*. San Francisco, USA, 2012 (cit. on p. 62).

[Vog93] P. Vogel. “Application of Wave Field Synthesis in Room Acoustics”. PhD thesis. Delft University of Technology, 1993 (cit. on p. 6).

[Vor07] A. G. Voronich. “Tangent Plane Approximation and Some of Its Generalizations”. In: *Acoustical Physics* 53.3 (2007), pp. 298–304 (cit. on p. 39).

[Vor99] A. G. Voronich. *Wave Scattering from Rough Surfaces*. 2nd. Vol. Springer Series on Wave Phenomea. Springer, 1999 (cit. on p. 38).

[Vri+94] D. de Vries, E. W. Start, and V. G. Valstar. “The Wave-Field Synthesis Concept Applied to Sound Reinforcement Restriction and Solutions”. In: *Audio Engineering Society Convention 96*. Feb. 1994 (cit. on p. 6).

[Vri96] D. de Vries. “Sound Reinforcement by Wavefield Synthesis: Adaptation of the Synthesis Operator to the Loudspeaker Directivity Characteristics”. In: *Journal of Audio Engineering Society* 44.12 (1996), pp. 1120–1131 (cit. on p. 7).

[WA01] D. B. Ward and T. D. Abhayapala. “Reproduction of a plane-wave sound field using an array of loudspeakers”. In: *IEEE Transactions on Speech and Audio Processing* 9.6 (Sept. 2001), pp. 697–707 (cit. on p. 4).

[Wan16] Y. Wang. *Seismic Inversion: Theory and Applications*. Wiley-Blackwell, 2016 (cit. on p. 51).

[War76] C. H. E. Warren. “A note on moving multipole sources of sound”. In: *Journal of Sound and Vibration* 44.1 (1976), pp. 3–13 (cit. on p. 89).

[Wat15] K. Watanabe. *Integral Transform Techniques for Green’s Function*. Second Edition. Springer, 2015 (cit. on p. 21).

[WB89] C. P.1A. Wapenaar and A. J. Berkhout. *Elastic Wave Field Extrapolation*. 2nd edition. Elsevier, 1989 (cit. on p. 26).

[WD99] M. Williams and G. Le Du. “Microphone Array Analysis for Multichannel Sound Recording”. In: *Audio Engineering Society Convention 107*. 1999 (cit. on p. 2).

[Wie14] H. Wierstorf. “Perceptual Assessment of Sound Field Synthesis”. PhD thesis. Technischen Universitat Berlin, 2014 (cit. on p. 53).

[Wil99] E. G. Williams. *Fourier Acoustics: Sound Radiation and Nearfield Acoustical Holography*. 1st. London: Academic Press, 1999 (cit. on pp. 12, 15, 18–20, 24, 25, 27, 41, 50, 69, 145).

[Win+16] F. Winter, J. Ahrens, and S. Spors. “On Analytic Methods for 2.5-D Local Sound Field Synthesis Using Circular Distributions of Secondary Sources”. In: *IEEE/ACM Transactions on Audio, Speech, and Language Processing* 24.5 (2016), pp. 914–926 (cit. on p. 85).

[Win+18a] F. Winter, J. Ahrens, and S. Spors. “A Geometric Model for Spatial Aliasing in Wave Field Synthesis”. In: *DAGA 2018, 44th German Annual Conference on Acoustics*. DAGA. Mar. 2018, pp. 1310–1313 (cit. on pp. 79, 85).

[Win+18b] F. Winter, H. Wierstorf, C. Hold, et al. “Colouration in Local Wave Field Synthesis”. In: *IEEE/ACM Transactions on Audio, Speech, and Language Processing* 26.10 (Oct. 2018), pp. 1913–1924 (cit. on p. 79).

[Wit+04] H. Wittek, S. Kerber, F. Rumsey, and G. Theile. “Spatial Perception in Wave Field Synthesis Rendered Sound Fields: Distance of Real and Virtual Nearby Sources”. In: *Audio Engineering Society Convention 116*. May 2004 (cit. on p. 7).

[Wit07] H. Wittek. “Perceptual differences between wavefield synthesis and stereophony”. PhD thesis. University of Surrey, 2007 (cit. on p. 7).

[WR09] Y. Wang and Y. Rao. "Reflection Seismic Wavefront Tomography". In: *Journal of Geophysical Research* 114.B3 (2009), pp. 1–12 (cit. on p. 51).

[WS15a] F. Winter and S. Spors. "Physical Properties of Local Wave Field Synthesis using Circular Loudspeaker Arrays". In: *EuroNoise 2015, 10th European Congress and Exposition on Noise Control Engineering*. Maastricht, The Netherlands, May 2015 (cit. on p. 85).

[WS15b] F. Winter and S. Spors. "Physical Properties of Local Wave Field Sythesis using Linear Loudspeaker Arrays". In: *Audio Engineering Society Convention 138*. Warsaw, Poland, May 2015 (cit. on p. 85).

[WT17] H. Wittek and G. Theile. "Development and Application of a Stereophonic Multichannel Recording Technique for 3D Audio and VR". In: *Audio Engineering Society Convention 143*. Oct. 2017 (cit. on p. 2).

[Wu10] S. F. Wu. "Techniques for Implementing Near-Field Acoustical Holograph". In: *Journal of Sound and Vibration* 44.2 (Feb. 2010), pp. 12–16 (cit. on p. 24).

[ZF12] F. Zotter and M. Frank. "All-Round Ambisonic Panning and Decoding". In: *Journal of Audio Engineering Society* 60.10 (2012), pp. 807–820 (cit. on p. 3).

[Zha+17] W. Zhang, P. N. Samarasinghe, H. Chen, and T. D. Abhayapala. "Surround by Sound: A Review of Spatial Audio Recording and Reproduction". In: *Applied Sciences* 7.5 (2017) (cit. on pp. 1, 4).

[Zio95] L. J. Ziomek. *Fundamentals of Acoustic Field Theory and Space-Time Signal Processing*. Boca Raton, 1995 (cit. on p. 14).

[Zot+12] F. Zotter, H. Pomberger, and M. Noisternig. "Energy-preserving Ambisonics decoding". In: *Acta Acustica United with Acustica* 98.1 (2012). cote interne IRCAM: Zotter12b, pp. 37–47 (cit. on p. 3).

[Zot09] F. Zotter. "Analysis and Synthesis of Sound-Radiation with Spherical Arrays". PhD thesis. Institute of Electronic Music, Acoustics University of Music, and Performing Arts, 2009 (cit. on pp. 19, 67).

[ZS13] F. Zotter and S. Spors. "Is sound field control determined at all frequencies? How it is related to numerical acoustics?" In: *Audio Engineering Society Conference: 52nd International Conference: Sound Field Control*. Guildford, UK, Sept. 2013 (cit. on pp. 28, 55, 56, 67).